

A Hero Revealed:

targeting the AHR for treatment of inflammatory skin diseases

N.J.M. van den Brink

A Hero Revealed: targeting the AHR for treatment of inflammatory skin diseases

Noa van den Brink

Radboud Dissertation Series

ISSN: 2950-2772 (Online); 2950-2780 (Print)

Published by RADBOUD UNIVERSITY PRESS Postbus 9100, 6500 HA Nijmegen, The Netherlands www.radbouduniversitypress.nl

Design: Proefschrift AIO | Annelies Lips Cover: Proefschrift AIO | Guntra Laivacuma

Printing: DPN Rikken/Pumbo

ISBN: 9789465151557

DOI: 10.54195/9789465151557

Free download at: https://doi.org/10.54195/9789465151557

© 2025 Noa van den Brink

RADBOUD UNIVERSITY PRESS

This is an Open Access book published under the terms of Creative Commons Attribution-Noncommercial-NoDerivatives International license (CC BY-NC-ND 4.0). This license allows reusers to copy and distribute the material in any medium or format in unadapted form only, for noncommercial purposes only, and only so long as attribution is given to the creator, see http://creativecommons.org/licenses/by-nc-nd/4.0/.

A Hero Revealed:

targeting the AHR for treatment of inflammatory skin diseases

Proefschrift ter verkrijging van de graad van doctor
aan de Radboud Universiteit Nijmegen
op gezag van de rector magnificus prof. dr. J.M. Sanders,
volgens besluit van het college voor promoties
in het openbaar te verdedigen op

woensdag 22 oktober 2025 om 12.30 uur precies

door

Noa Johanna Maria van den Brink

geboren op 25 januari 1996 te Venray

Promotor:

Prof. dr. Ellen van den Bogaard

Copromotoren:

Dr. Jos Smits

Dr. Patrick Zeeuwen

Manuscriptcommissie:

Prof. dr. Annemiek van Spriel (voorzitter)

Prof. dr. Dirk Jan Hijnen

Dr. Thomas Haarmann-Stemmann (Heinrich-Heine-Universität Düsseldorf, Duitsland)

Table of contents

ls 31
63
ig 67
111
141 ction
167
185
191
203
228 233 235 237 244 245 246



Chapter 1

Introduction and thesis outline

The skin: morphology and composition

The skin is known as the largest barrier organ of the body. It has a protective role in preventing excessive water loss and preventing harmful microbiota and chemicals from entering the body. The skin is also able to sense warmth and cold, and plays a role in the thermoregulation of the body. Moreover, the skin has a complex and dynamic immune system, aiding in defense against microbes and repair in case of wound healing. The skin consists of three main layers, from inside to outside: the subcutaneous adipose tissue, the dermis and the epidermis. Each layer consists of its own cell types and has specific roles in maintenance of the well-being of the organism. In my thesis, I will focus mostly on the outside layer of the skin, the epidermis.

The epidermis is mainly composed of keratinocytes and is divided in several layers, also called strata, based on the proliferation and differentiation status of the keratinocytes (Figure 1). These different layers are easily distinguished, both in morphology as well as in specific gene expression patterns. In the stratum basale, keratinocytes are in a proliferative state, renewing the cell pool at the base of the epidermis. Morphologically, these cells are cuboid shaped and express keratin 5 and 14 [1]. Keratins are structural components of the epidermis and are part of the cytoskeleton of keratinocytes [2]. When keratinocytes divide, some are pushed upwards exiting their proliferative state and embarking on the terminal differentiation program that commences in the stratum spinosum. Herein, keratinocytes become more flattened and express the typical marker proteins keratin 1 and 10 [1]. When differentiating cells are pushed more upward, they form the last living cell layers, the stratum granulosum, where the cells are characterized by keratohyalin granules containing keratins, profilaggrin, loricrin and trichohyalin proteins [3]. Keratohyalin granules play a major role in the keratinization process in promoting dehydration of the cells. Moreover, profilaggrin is a key component of keratohyalin granules that functions in cross-linking keratin filaments and providing a structural skeleton of protein aggregates in the keratinocytes, causing them to flatten [3]. Granular keratinocytes express a variety of proteins involved in the formation of the skin barrier, including but not limited to the proteins mentioned above, which will be more extensively discussed below.

After differentiation in the granular layer, keratinocytes undergo a special form of programmed cell death, termed cornification. During this process, cells become more flattened, and lose their organelles and nuclei. Enucleation is the degradation and clearance of the nucleus from the cells and is mediated by DNA-degrading enzymes and nucleophagy [4]. Flattened, enucleated cells are now called

corneocytes. Through crosslinking of several proteins involved in differentiation, such as involucrin and loricrin, and envelopment in lipids, the cornified envelope is formed [5, 6]. Here, filaggrin is processed further by proteases, such as caspase 14, to form natural moisturizing factors (NMFs), having a major contribution to *stratum corneum* hydration [7]. NMFs are composed of free amino acids such as histidine, 2-pyrrolidone-5-carboxylic acid (PCA) and urocanic acid (UCA), as well as inorganic salts such as chlorides and phosphates [8]. They are stored within the corneocytes and can bind water from the atmosphere in the corneocytes, aiding in skin hydration. Finally, corneocytes are shed from the skin in a process called desquamation.

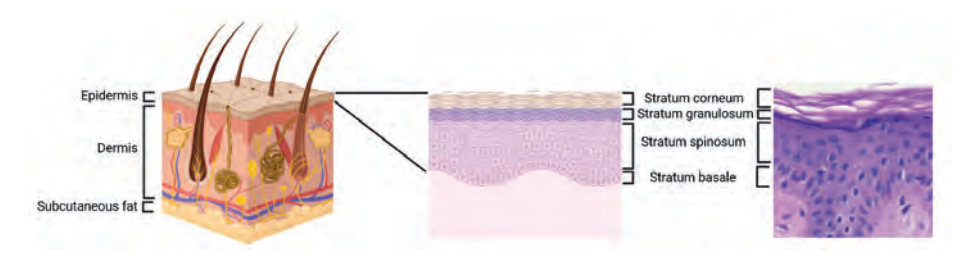


Figure 1. Schematic overview of the structures in the skin. Left: the skin is composed of three layers, the epidermis, dermis and subcutaneous fat. The dermis contains multiple structures, including blood vessels and hair follicles. Middle: schematic overview of the epidermis. The epidermis consists of several *strata*. Right: hematoxylin and eosin staining of healthy human skin, showing the different *strata* of the epidermis.

Processes involved in keratinocyte proliferation, differentiation, cornification and desquamation are tightly controlled and orchestrated by key transcription factors that drive gene transcription, leading to protein translation and thereby facilitate cell function. These transcription factors do not act on their own, but function in interactive networks and allow for compensatory regulation. Many transcription factors and signaling pathways have been described being important regulators of epidermal homeostasis, amongst others, p63, AP1 transcription factors, grainyhead-like transcription factors, Krüppel-like factor 4 (KLF4) and the aryl hydrocarbon receptor (AHR) [9-12]. The AHR is the main subject of this thesis and will be further introduced in the next paragraphs of this chapter.

The skin barrier

The skin has an important role as a barrier, keeping harmful toxic substances and pathogens outside and preventing excessive water loss and loss of nutrients from the body. The skin barrier is effectuated by a quadruple function: the physical, chemical, immunological and microbial skin barrier (Figure 2).

The physical skin barrier is generally considered to be formed by adhesions between keratinocytes in the granular and spinous layers. These adhesions, also called tight junctions or adherence junctions, are protein complexes between cells, mostly present in the stratum granulosum [13]. Additionally, a matrix of lipids consisting of ceramides and fatty acids is present between the corneocytes giving the stratum corneum a hydrophobic character and, together with tight junctions, prevent excessive water loss and extensive dehydration of the epidermis [14].

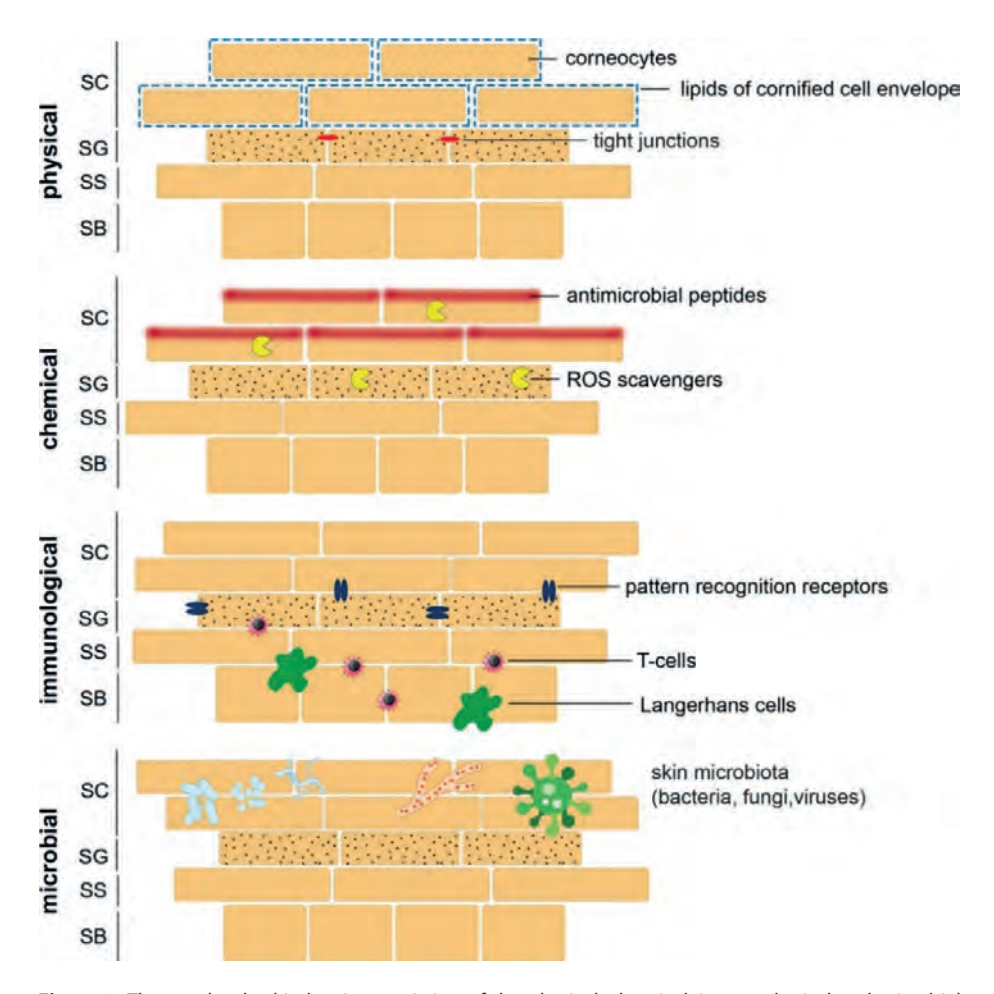


Figure 2. The quadruple skin barrier consisting of the physical, chemical, immunological and microbial skin barrier. The physical skin barrier consists of lipids in the stratum corneum as well as cell-cell connections. The chemical skin barrier consists of antimicrobial peptides protecting against pathogens and ROS scavengers preventing oxidative damage. The immunological barrier consists of various parts of the immune system, such as adaptive immune cells such as T-cells, tissue-resident Langerhans cells and pattern recognition receptors on for example keratinocytes. The microbial barrier consists of resident bacteria, fungi and viruses. Figure is reprinted with permission from Niehues et al [19].

The **chemical skin barrier** is mainly composed of antimicrobial peptides (AMPs) that are expressed by keratinocytes in the granular layer of the epidermis [15]. AMPs have a role in the formation and composition of the skin microbiome and have a protective role in prevention of infection by pathogens [16]. Several AMPs expressed in human skin include the human β-defensins, psoriasin, calprotectin, SKALP/elafin and the LCE proteins [17, 18].

Additionally, reactive oxygen species (ROS) are considered to be part of the chemical skin barrier, ROS have a role in protection of the host against microbes by causing oxidative stress in microbial cells as well as increasing ROS-induced cytokine production like tumor necrosis factor (TNF) and interleukin 6 (IL-6) in host cells [17]. However, elevated levels of ROS result in DNA damage of the cell and eventually to apoptosis. To protect against these high levels of ROS, expression of the NF-E2 p45-related factor 2 (NRF2) pathway is induced upon oxidative stress. NRF2 is a transcription factor, and its activation leads to increased expression of antioxidative enzymes [20]. ROS are byproducts of normal oxygen metabolism by cells, but also formed upon Cytochrome P450 (P450)-mediated phase 1 xenobiotic metabolism [21, 22] of toxic agents and pollutants [21, 22]. Herein, the AHR plays a key regulatory role which will be further discussed below.

The **immunological skin barrier** is composed of innate and adaptive immune cells present in the dermis and epidermis of the skin. In the epidermis, tissue-resident Langerhans cells as well as keratinocytes can detect presence of microbes or microbial substances through their receptors, when the skin barrier is breached. In response, keratinocytes are able to secrete AMPs, cytokines and chemokines, inducing an inflammatory response and attracting immune cells, such as T-cells and neutrophils, from the circulation [23, 24]. Langerhans cells are part of the innate immune system and play a pivotal role in antigen presentation to cells of the adaptive immune system, making their response to intruding microbes more efficient [25]. A larger group of immune cells is present in the dermis. This includes cells of the innate immune system such as dendritic cells and macrophages, as well as cells from the adaptive immune system such as the B- and T-cells. Adaptive immune cells are activated upon registering presence of antigens and play an active role in removing pathogenic microbes. Activated T-helper cells are also able to excrete cytokines, dependent on their maturation type (e.g., Th1, Th2, Th17 or Th22) and plasticity [26]. Excreted cytokines have further signaling functions and can activate keratinocytes to produce AMPs, further aiding the skin barrier function [24].

Lastly, the microbial skin barrier is made up of a large number of bacteria and fungi that are present on human skin. These microbes are harmless when on the outside of the skin and are called the commensals of our microbiome. Their presence on the skin prevents colonization by more pathogenic species through a battle for resources such as space and nutrients [27]. Commensal microbes generally include bacteria from the genera Cutibacterium, Corynebacterium and Staphylococcus and fungi from the Malassezia species [27]. The composition of the microbiome is highly diverse between different body sites and differs between individuals [28, 29]. Recently, an additional mechanism of defense of the microbial barrier was described for gram-positive anaerobic cocci (GPACs). These GPACs are commensals on human skin and through, as thus far unknown, secreted factors stimulate keratinocytes to produce AMPs, which prevent pathogenic growth of Staphylococcus aureus. Additionally, GPACs stimulate cytokine-production, which activates immune cells and further hampers the growth of pathogenic species [30].

Inflammatory skin diseases - from pathogenesis to therapeutics

Healthy skin barrier is pivotal for water balance and prevention of infection, however in several inflammatory skin diseases the skin barrier is disrupted [31, 32]. Inflammatory skin diseases like atopic dermatitis (AD) and psoriasis are nowadays highly prevalent in Western populations [33]. For example, a disease such as AD affects up to 20% of children and up to 4% of the adult population [34]. Psoriasis affects 2% of adults worldwide, with a higher prevalence in Western population [35]. Both inflammatory skin diseases are characterized by a distinct clinical representation, morphological features of the skin, and underlying cytokine signaling pathways, which will be discussed in more detail below (Figure 3).

Atopic dermatitis

AD usually presents early in life and is characterized by red, scaly patches of skin accompanied by intense itch (pruritis). Itch is often the main discomfort in patients, as it can cause sleep deprivation and a reduced quality of life. AD often precedes the development of other allergic diseases, including asthma. This phenomenon is known as atopic march. The mechanism behind this is sought in the impaired barrier function in these patients, leading to sensitization against other allergens [36]. Several factors have been associated with the risk of developing AD. Risk factors

include genetic predispositions, environmental and dietary components. Exposure to pollution and tobacco smoke increases risk of development of AD, fresh fruit consumption poses a protective effect [37]. However, loss-of-function variants of the skin barrier filaggrin gene (FLG) confer the main risk for developing AD [38]. Next to the heterozygous loss-of-function variants of the FLG gene, expression of filaggrin protein is also targeted by the dominant Th2 cytokine environment (see Figure 3) in lesional skin, that downregulates expression of epidermal differentiation genes [39]. Reduction of filaggrin expression directly correlates to reduced NMF levels causing dehydration of the stratum corneum and changing corneocyte topography [40]. Whether reduced filaggrin levels are the sole cause of impaired barrier function in AD has been under debate [41]. Yet, restoration of filaggrin protein in AD skin is considered an important therapeutic strategy [42]. Genetic variations of other genes involved in epidermal differentiation have been identified, including variations in hornerin (HRNR) [43]. Additionally, variants of immune-related genes have been identified as risk factors for developing AD. These are found in various immune components, like variants in Langerin (CD207), important for Langerhans cell function. Additionally, genetic variants of components of the Janus kinase/signal transducer and activator of transcription (JAK-STAT) signaling pathway are considered a risk factor [44, 45].

The inflammatory process in AD is dominated by increased levels of Th2 cells and cytokines. Th2 cytokines are produced by CD4 positive T-cells that are abundantly present in lesional AD skin [46]. Th2 cytokines include several pro-inflammatory interleukins (IL), e.q., IL-4, IL-13, and IL-5, as well as IL-10, which elicits a more anti-inflammatory response [47]. Increased Th2 immune response is believed to be triggered by a compromised skin barrier and allergens, with keratinocytes producing alarmins (e.g., IL-33 and thymic stromal lymphopoietin (TSLP)) which then provoke a Th2-mediated immune response [48]. Cytokines such as IL-4 and IL-13 are able to bind their common receptor, IL-4 receptor alpha (IL4RA), and activate downstream signaling cascades [49]. In this process, activation of the JAK-STAT signaling pathway is pivotal [50]. Binding of IL-4 or IL-13 to its receptor causes phosphorylation of JAK and subsequent phosphorylation of STAT proteins, which then dimerize and move to the nucleus to act as transcription factors. STAT6 binding to DNA in the nucleus results in decreased filaggrin expression and subsequent skin barrier dysfunction whereas binding of STAT3 induces transduction of pruritis [51], further exaggerating patient discomfort.

The disrupted skin barrier in AD patients results in increased transepidermal water loss (TEWL) which negatively correlates to disease severity [52]. Next to the biophysical measurements (erythema, TEWL, hydration, pH), characteristic morphological features are observed at the microscopic level. Epidermal thickening (acanthosis) due to keratinocyte hyperproliferation and hypertrophy, intercellular oedema (spongiosis) and apoptosis can be noted. The decreased presence of keratohyalin granules or even absence of the granular layer [53] is often accompanied by reduced expression of keratinocyte differentiation markers, including filaggrin, loricrin and several keratins (keratin 2) [54]. Many of these epidermal hallmarks can be attributed to the presence of the disease-specific inflammatory cytokine milieu [55].

Psoriasis

Psoriasis can both have a childhood onset as well as onset in adults and is characterized by sharply demarcated red, scaly plagues. It is often associated with other comorbidities, including an increased body mass index as well as systemic inflammation (metabolic syndrome) and local inflammation at other body sites. Psoriatic arthritis (inflammation in the joints) is strongly associated with moderate to severe psoriasis [35].

Genetic background plays a major role in the development of psoriasis. Most notably, genetic variants of HLA-Cw6, which has a role in regulation of the immune system, are associated with the development of psoriasis [56]. Other genetic risk factors for psoriasis include genes important in the epidermis, with a deletion of the LCE3B/C region being associated with possible impaired barrier response to exogenous agents [57, 58]. Increased copy numbers of human beta defensin 2 have also been associated with individuals with psoriasis as compared to healthy controls [59]. Beta defensins exercise anti-microbial effects in the skin [60]. Besides genetic variations related to epidermal differentiation and defensins, gene variants related to the immune response are associated with the risk of developing psoriasis. Some genes are associated with regulation of the NF-kB pathway, such as CARD14 and IL36RN, possibly facilitating increased immune cell signaling [61]. Besides genetic risk factors, lifestyle factors, such as smoking, confer a higher risks of developing psoriasis [62].

Psoriasis is mediated by Thelper (Th)1 and Th17 cells, which excrete associated cytokines including the pro-inflammatory cytokines TNFα, IFNg, IL-1β, IL-17, IL-21, IL-22 and IL-26 [63-65]. IL-17 affects keratinocytes, leading to increased expression of chemokines, resulting in a positive feedback loop for inflammation in the skin. In addition, IL-22 also affects keratinocytes, inducing the STAT3 pathway and leading to keratinocyte swelling and acanthosis, unrelated to the keratinocyte proliferation rate [55, 66].

Morphologically, lesional psoriasis skin is characterized by a thickened epidermal layer (acanthosis), elongated rete ridges, and extensive parakeratosis. In the dermis, an increased immune cell infiltrate is present [35]. Keratinocytes in lesional psoriatic skin show aberrant differentiation as well as hyperproliferation. In addition, connections between keratinocytes, such as tight- and adherencejunctions, are abnormally regulated in psoriasis, leading to barrier defects [32]. Aberrant differentiation includes dysregulated expression of keratins 14 and 10 and a keratin switch to keratin 16. Moreover, expression of keratinocyte terminal differentiation genes, such as loricrin and filaggrin is reduced in psoriasis. On the contrary, expression of transglutaminases 1 and 3, which have a role in crosslinking proteins and consequent stratum corneum formation, is increased in psoriatic lesions [32], potentially relating to the extensive scaling of the skin.

Therapeutic strategies for AD and psoriasis

Nowadays, even though inflammatory skin diseases cannot be cured, several treatment options enable the management of the disease and its symptoms. Mild-to-moderate disease phenotype can be treated by application of emollients, with or without corticosteroids, as well as UVB-light therapy. Emollients are a generic treatment, focusing on keeping the skin moist and therefore alleviating disease symptoms. However, emollients lack active therapeutic components and therefore do not treat the underlying cause of the disease [67]. Corticosteroids are an effective anti-inflammatory drug and a relatively cheap treatment option, however prolonged use has been associated with the development of adverse effects including atrophy [68]. This makes corticosteroids an effective treatment option during disease flares, but unsuitable for long-term disease management. For more severe disease presentations, nowadays several biologicals are available for treatment [69, 70]. Biologicals are antibodies that can be systemically administered and target various parts of the immune response involved in inflammatory skin diseases. An overview of biologicals used in the treatment of AD and psoriasis, as well as targeted pathways, is presented in Table 1. Treatment with biologicals is expensive and therefore often used as a last option in case of severe disease. For example, treatment with dupilumab has an annual cost of 30,000 USD per patient in 2020 while a substantial proportion of patients do not respond to treatment or discontinue due to side effects [71-74]. This underlines the need for new treatment options, especially topical medications, to be discovered for use in a larger patient population with less systemic side effects.

One of the oldest treatment options for inflammatory skin diseases is coal tar. For a long time, it was unknown how coal tar functioned in the treatment of these diseases. However, recently our group discovered that coal tar exerts its therapeutic mechanism through activation of the aryl hydrocarbon receptor [75] and subsequent epidermal differentiation [76], elevated AMP production [77], and that it is safe for prolonged topical use [78]. I will elaborate more in detail on the biological functions and signaling pathways in which AHR is involved in the skin.

Table 1. Approved biologicals and targeted pathways for treatment of atopic dermatitis and psoriasis

Biological name	Disease	Targeted molecule	Mechanism
Dupilumab	Atopic dermatitis	IL-4/IL-13	Receptor blocking
Tralokinumab	Atopic dermatitis	IL-13	Cytokine binding
Adalimumab	Psoriasis	Tumor necrosis factor (TNF)	Cytokine binding
Etanercept	Psoriasis	Tumor necrosis factor (TNF)	Cytokine binding
Certolizumab	Psoriasis	Tumor necrosis factor (TNF)	Cytokine binding
Infliximab	Psoriasis	Tumor necrosis factor (TNF)	Cytokine binding
Golimumab	Psoriasis	Tumor necrosis factor (TNF)	Cytokine binding
Ustekinumab	Psoriasis	IL-12/IL-23	Cytokine binding
Guselkumab	Psoriasis	IL-23	Cytokine binding
Risankizumab	Psoriasis	IL-23	Cytokine binding
Tildrakizumab	Psoriasis	IL-23	Cytokine binding
Secukinumab	Psoriasis	IL-17	Cytokine binding
Ixekizumab	Psoriasis	IL-17	Cytokine binding
Brodalumab	Psoriasis	IL-17	Receptor blocking
Bimekizumab	Psoriasis	IL-17	Cytokine binding
Spesolimab	Psoriasis	IL-36	Receptor blocking

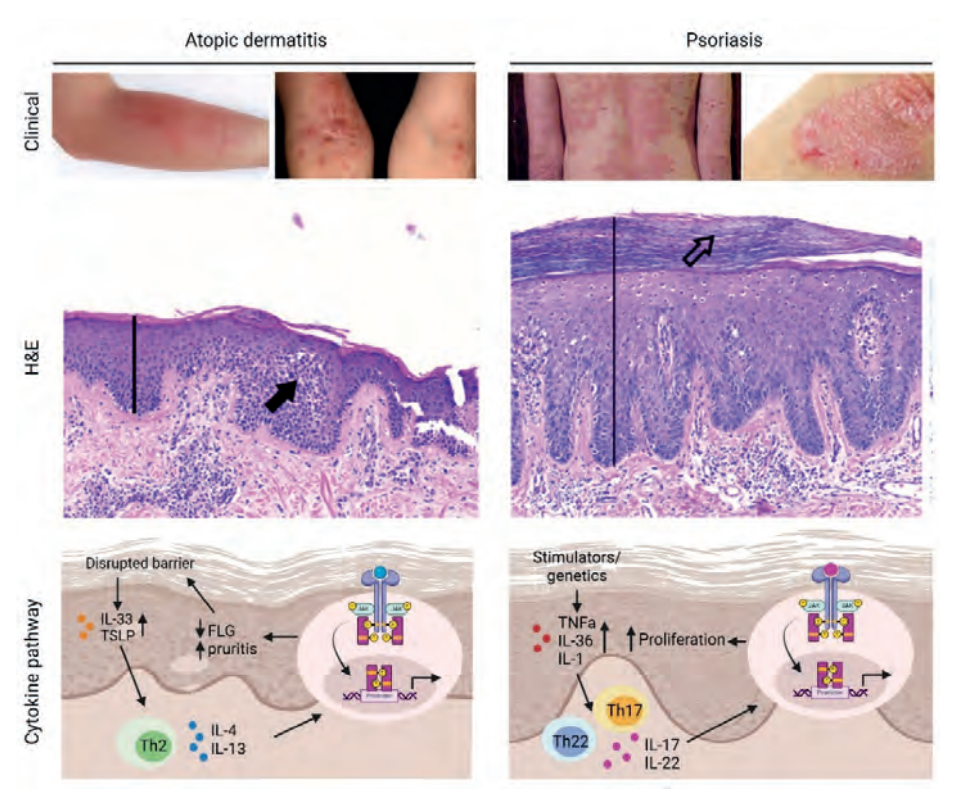


Figure 3. Clinical representation, morphology on hematoxylin and eosin staining of atopic dermatitis (left) and psoriasis (right). In the H&E pictures, increased epidermal thickness (line), spongiosis (solid arrow) and parakeratosis (open arrow) are shown. Also, a schematic overview of part of the signaling mechanism underlying disease development is shown. However, the full mechanism underlying development of these diseases is far more complex and involves complex interplay between various parts of the skin and the immune system.

The aryl hydrocarbon receptor and signaling events

The aryl hydrocarbon receptor (AHR) was initially discovered in the 1950s as an environmental sensor for exogenous xenobiotic chemicals [79]. In an inactive state, the AHR resides in the cytoplasm in complex with its chaperone proteins heat shock protein 90 (Hsp90), p23, X-associated protein 2 (XAP2) and cellular SRC kinase (c-SRC). AHR can be activated by a wide variety of both exogenous and endogenous ligands and functions as a transcription factor, regulating target gene expression [80-82]. The AHR is activated upon ligand binding and then translocates to the nucleus. Here, heterodimerization of the AHR with the aryl hydrocarbon nuclear translocator (ARNT) displaces the chaperone proteins [83]. The DNA recognition motif of the AHR/ARNT complex is referred to as dioxin-responsive elements (DRE) or xenobiotic response

elements (XRE), which consists of the core consensus sequence 5'-GCGTGA-'3 [84]. Binding of the AHR/ARNT complex to these DREs drives expression of a wide variety of genes and hence modulated important signaling pathways, including xenobiotic metabolism, immune response and intestinal homeostasis [85, 86] (Figure 4).

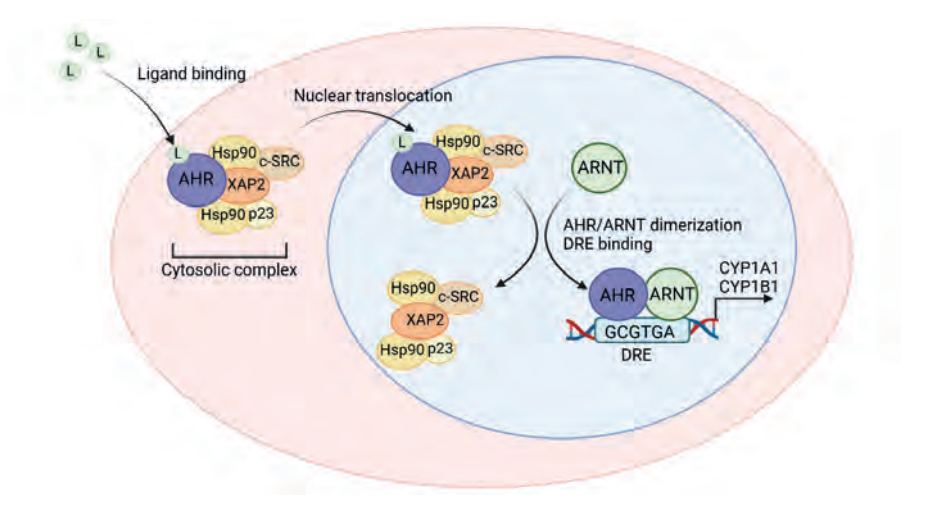


Figure 4. Schematic overview of the canonical AHR signaling pathway. AHR resides in the cytosol in complex with Hsp90, c-SRC, XAP2 and p23. Upon binding of a ligand to AHR, the complex translocates to the nucleus. Here, ARNT binds to AHR and displaces the complex partners. In complex with ARNT, AHR can bind DREs in the DNA and influence gene transcription, amongst other members of the CYP family. Figure adapted from Murray et al [87].

Gene regulation by AHR/ARNT is known as the canonical signaling pathway. Canonical AHR signaling leads to gene transcription of a variety of genes including members of the cytochrome P450 (CYP) family of genes. The CYP family consists of monooxygenases, that have a role in metabolizing xenobiotics. Members of the cytochrome P450 family include CYP1A1 and CYP1B1, of which transcription was shown to be regulated by the AHR and expression of these genes is widely used as an indicator of AHR-activation [88]. The most well-known activators of canonical AHR signaling are several environmental pollutants, including dioxins (e.q., biphenyls and dibenzofurans) [89], 2,3,7,8-tetrachlorodibenzo-p-dioxin (TCDD) and polycyclic aromatic hydrocarbons (PAHs) [90, 91]. Activation of the AHR by these ligands leads to subsequent transcription of genes with a DRE-binding motif. Amongst these genes are CYP enzymes that oxidize environmental pollutants to produce less hazardous products, which are finally excreted. CYP expression was shown to prevent spreading of environmental pollutants past the liver and therefore aid in their excretion [92]. However, the detoxification process can also lead to

formation of mutagenic metabolites and reactive oxygen species (ROS), which can have mutagenic effects on DNA [93]. Additionally, research showing lack of TCDDinduced carcinogenesis in Ahr knockout mice proves involvement of the AHR in development of cancer induced by TCDD [94]. Due to these toxic and carcinogenic effects associated with AHR activation, pharmaceutical companies have long been hesitant to develop drugs with AHR activating properties. Recently though, after our initial finding on the coal tar-mediated AHR-driven therapeutic effects in AD [74], pharmaceuticals targeting the AHR have become available on the market [95].

Table 2. Ligands binding the AHR

Ligand	Source	Effect
Dioxins (TCDD)	Chemical	Chloracne, carcinogenic [100], keratinization, induction of inflammation [101-103]
PAHs (BaP)	Environmental (exhaust, tobacco smoke, smoked foods)	Carcinogenic [104], formation of DNA adducts, induction of inflammation, induced skin ageing, disruption of skin barrier [105]
6-Formylindolo(3,2-b) carbazole (FICZ)	Tryptophan photoproduct	Induce skin differentiation, homeostasis of skin inflammation [106], and photosensitization of the skin [107]
Tryptophan metabolites (Kynurenine, Idole-3- Aldehyde)	Metabolites formed by the host or microbiome	Decrease inflammation in skin disease [108], protection against UVB damage, enhance skin barrier [109]
Tryptophan metabolites (Indole-3-carbinol)	Diet (cruciferous vegetables)	Reduce inflammation in skin disease, reduced proliferation [110, 111]
Coal tar, Tapinarof, Leflunomide, Omeprazol (indirect)	Pharmaceutical	Therapeutic for inflammatory diseases [75, 95], induced keratinocyte differentiation, reduced proliferation, decreased inflammatory response

The AHR is a highly conserved receptor and genes encoding AHR are even found in invertebrate species. However, invertebrate AHR does not bind the typical ligands for mammalian AHR, pointing to a conserved role of AHR that goes beyond sensing the xenobiotic environment [96]. Additionally, AHR function has existed in humans long before the large increase in pollutants in our environment, indicating core physiological functions of the AHR in humans. Mammalian AHR has been found to bind a wide variety of ligands. Next to the already mentioned environmental pollutants, endogenous ligands have also been discovered. These endogenous ligands include UVB radiation-induced tryptophan metabolites (FICZ), metabolites formed by the microbiota of the skin and intestine (ICZ, indoles), and dietary plant constituents (flavonoids, phenols) [75, 97-99]. Additionally, several pharmaceuticals activate the AHR pathway [75, 95]. In Table 2, an (non-exhaustive) overview of several different ligands and their effects in the human body is presented to illustrate the variety in ligands, sources and effect sizes. The increasing amount of literature on AHR-mediated effects and interactions with different signaling pathways clearly highlights important roles for the AHR in human physiology and tissue homeostasis.

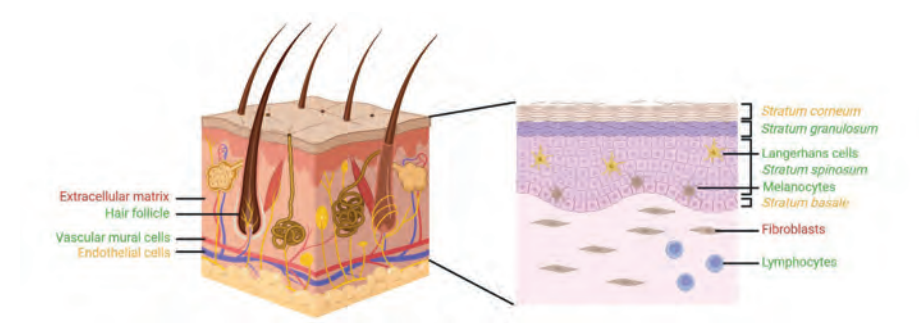


Figure 5. Overview of AHR protein expression in the skin. Green represents medium to high expression, yellow low expression and red no expression in the indicated cell layers and cell types. These expression data are based on human protein atlas [121].

The interaction of the AHR with other binding partners besides ARNT is termed the non-canonical AHR signaling pathway which has important functions in regulating cell proliferation (amongst others in the gut and reproductive cells [112, 113]), differentiation, cell migration, and cellular stress response [114-116]. Effects of AHR signaling were found to be highly ligand specific, as well as cell type specific and dependent on the micro-environment of the tissue. This ligand promiscuity as well as the resulting downstream signaling remains poorly understood, also due to the lack of studies on AHR ligand bound crystal structure. Excitingly, the ligand-bound cytosolic AHR complex was recently elucidated by crystallography. AHR was able to bind indole rings from ligands, providing important information about ligand structure able to activate the AHR [117]. Additionally, this crystallography structure provided insight into ligand binding differences of the AHR. Ligands such as PAHs formed strong bonds with the receptor to activate the AHR. On the contrary, hydrophilic compounds such as indoles were able to form hydrogen bonds, which are more easily broken than those formed by PAHs. This could explain differences in effects of AHR activation based on which ligand binds the AHR and how long the duration of binding lasts, being either carcinogenic (in case of PAHs) or beneficial (in case of indoles). This provides a structural basis for the development of novel AHR activating therapeutics. In my thesis, novel AHR ligands and their AHR binding potential, as well as therapeutic effects, will be discussed in **chapter 2** and **3**.

Increasing research on AHR function has provided insight into the role and importance of the AHR in development and maintenance in various fields, including neurobiology, embryonic development, and cardiovascular physiology [118-120]. An important role for the AHR has also been described for skin homeostasis. In the skin, the AHR is expressed in a wide variety of cells in both the epidermis and the dermis, including keratinocytes, Langerhans cells, endothelial cells, sebaceous glands, and various immune cells (Figure 5). In this thesis, I will focus on the physiological role of the AHR in keratinocytes, which I will further introduce below.

AHR influences proliferation in the skin

Keratinocytes in the basal layer proliferate and renew the skin cell pool. Proliferation in keratinocytes is a tightly regulated process that can be disturbed in inflammatory skin diseases, where often an increase in proliferation rate is noted. In healthy state, as well as in treatment of inflammatory skin disease, the AHR has a role in regulating proliferation rate. Although evidence suggests a physiological role for the AHR in regulation of keratinocyte proliferation, the effects are highly ligand- and contextspecific and differ between healthy skin and an induced proliferative state in case of inflammatory skin diseases [122].

In healthy individuals, activation of the AHR with TCDD leads to increased proliferation of epithelial cells, by inducing phosphorylation of the epidermal growth factor receptor (EGFR) pathway [123]. Additionally, knockdown of AHR by siRNAs in HaCaT cells reduced proliferation rate, indicating a role for the AHR in cell cycle progression in absence of a ligand [124]. In contrast, Tapinarof, which has been FDA-approved for the treatment of psoriasis and is known to exert its function through AHR activation, has been shown to reduce proliferation rate in HaCaT cells and enhancing the proportion of cells remaining in G0/G1-phase of the cell cycle [125]. This underlines the ligand-specific effects of AHR activation, leading to either an increase or decrease in keratinocyte proliferation.

In inflammatory skin diseases, such as AD and psoriasis, keratinocyte proliferation rates are increased as compared to healthy individuals [55]. AHR activating ligands, such as Tapinarof, were able to restore keratinocyte proliferation rate in an imiguimod mice model for psoriasis [126]. This effect was possibly mediated through reduced expression of mini-chromosome maintenance protein 6 (MCM6) and phosphorylated signal transducer and activator of transcription 3 (pSTAT3), which are both involved in regulating keratinocyte proliferation [125]. Additionally, coal tar treatment has been shown to reduce cell proliferation [127]. However, the molecular mechanism through which AHR regulates keratinocyte proliferation in healthy and diseased conditions remains to be elucidated.

Epidermal differentiation is induced by AHR signaling

The AHR has a role in epidermal differentiation and modulation of the AHR influences keratinocyte differentiation and cutaneous development. AHR levels are increased in differentiating keratinocytes as compared to proliferating keratinocytes. This indicates a state-specific expression level of AHR [128]. Additionally, when comparing the transcriptome of $Ahr^{+/+}$ and $Ahr^{/-}$ mice, a significantly decreased expression of epidermal differentiation genes was found in Ahr/- mice. This indicates a physiological role for endogenous AHR signaling in regulation of epidermal differentiation [76]. Primary murine Ahr/- keratinocytes showed impaired gene and protein expression of for example keratin 1, involucrin and loricrin. Inhibition of the human AHR with pharmacological antagonists led to impaired keratinocyte differentiation, marked by reduced expression of filaggrin and hornerin, and to impaired epidermal stratification in human epidermal equivalents [76].

Ligand-activated AHR (e.g., with TCDD) facilitates accelerated differentiation and increased expression of filaggrin in normal human epidermal keratinocytes. Stimulation with TCDD showed increased expression of several genes located in the epidermal differentiation complex on chromosome 1 [76] and in utero exposure by TCDD accelerated skin barrier formation during fetal development [129]. Activation of the AHR by coal tar also induced epidermal differentiation [75]. Coal tar consists of a wide range of polycyclic aromatic hydrocarbons (PAHs) that are able to activate the AHR [130]. In organotypic epidermal models from AD patient keratinocytes, treatment with coal tar restored expression levels of skin barrier proteins filaggrin and hornerin. This was confirmed by skin biopsies from AD patients that received coal tar treatment. AHR knockdown completely abrogated restoration of epidermal differentiation, indicating an AHR-dependent mechanism in coal tar induced epidermal differentiation [75]. Although this indicates a role of AHR in regulating keratinocyte differentiation, the mechanisms by which AHR induces and regulates keratinocyte differentiation are still largely unknown. However, several pathways of regulation have been elucidated, namely by direct binding, by activating other transcription factors, or through effects from byproducts of xenobiotic metabolism [131-133]. More recently, an AHR-induced decrease in glycolysis was reported to relate to enhanced keratinocyte differentiation, indicating the importance of metabolic activity of keratinocytes in AHR-induced keratinocyte differentiation [134].

Besides direct binding, AHR was shown to induce expression of other transcription factors involved in keratinocyte differentiation. For example, AHR restores filaggrin

expression in AD via ovo like transcriptional repressor 1 (OVOL1) [132]. OVOL1 is expressed in cells in human skin and it can redirect cell proliferation towards cell differentiation [135, 136]. The promoter of OVOL1 was shown to contain a xenobiotic response element. Levels of OVOL1 in normal human epidermal keratinocytes correlated with transcriptional levels of FLG. AHR-dependent upregulation of FLG was completely abolished in cells lacking OVOL1, indicating an interplay between OVOL1 and AHR in the regulation of FLG expression. Moreover, in skin of AD patients, nuclear translocation of OVOL1 was inhibited, which could be responsible for lowered FLG levels in AD skin [132].

Lastly, a mechanism involving ROS was found through which AHR activation leads to increased induction of differentiation in normal human epidermal keratinocytes. A group of these ROS, reactive nitrogen species (RNS), are formed through reactions mediated by nitric oxide synthases (NOS). The isoform NOS3 was shown to be significantly induced after stimulation of TCDD. Inhibition of NOS3 showed reduced terminal differentiation upon stimulation with TCDD, indicating an interplay between AHR-mediated differentiation and the ROS signaling pathway [133]. Induced by this oxidative stress is the transcription factor nuclear factor erythroid 2-related factor 2 (NRF2). NRF2 and AHR increase each other's expression in the presence of xenobiotics, by binding each other's promotor elements. Nrf2 knockout mice showed severely impaired skin barrier function, similar to Ahr knockout mice [137]. This further underlines the interplay between xenobiotic metabolism and the non-canonical signaling pathway to induce keratinocyte differentiation.

In my thesis, the anti-proliferative effect of AHR ligands in skin diseases is investigated in chapters 2 and 3. Additionally, chapters 2 and 3 of my thesis therapeutic effects of novel AHR ligands on keratinocyte differentiation are described. In **chapter 5**, novel regulatory pathways by which the AHR is involved in terminal differentiation are investigated to get a better insight into the molecular effects downstream of AHR activation. Finally, in chapter 7 the effect of AHR stimulation on proliferation in healthy human skin is further studied.

AHR signaling is required for maintenance of skin barrier function

As described above, the AHR plays a role in keratinocyte proliferation and differentiation. However, this is not equal to having a role in the actual skin barrier, as this barrier function is dependent on many factors. The epidermis, particularly the stratum corneum, plays a crucial role in maintaining the skin's barrier function, effectively preventing excessive water loss in healthy skin. Transepidermal water loss (TEWL) can be measured and correlated to impairment of the skin barrier. In healthy individuals, water loss through the skin is low, and increases sharply in case of inflammatory skin disease or wound infliction. In in vitro settings, impairment of the skin barrier can be measured by several techniques, such as permeation of hydrophilic dyes (e.g., lucifer yellow, biotin), transepithelial electrical resistance (TEER) and TEWL [138-140]. However, permeation of dyes requires the experiment to be terminated and common electrical resistance measurements such as the chopstick-based TEER measurements are biased by lack of standardization. To study the *in vitro* skin barrier properties we used a novel technique called electrical impedance spectroscopy (EIS), quantitatively estimate the epidermal barrier function using a fixed electrode system (chapter 6). This allowed us to measure the effects of AHR activation on epidermal barrier function.

Until recently it was unclear whether the AHR actually has a role in skin barrier function. It was discovered that in Ahr deficient mice, TEWL is increased compared to wild type animals. Removing AHR ligands from the diet of wild type mice mimicked the Ahr-deficient phenotype in terms of impaired barrier, and addition of an AHR agonist rescued this phenotype, even in aged mice [141]. This clearly shows a role for the AHR in maintenance of the epidermal barrier function. Moreover, the role of AHR in barrier function was shown by treatment of mice suffering from mite-induced dermatitis with the AHR agonist FICZ (see Table 2). Mice showed a reduced dermatitis score as well as reduced TEWL after 2 weeks of treatment with FICZ. In these mice, filaggrin was also upregulated in an AHR-dependent fashion as compared to nontreated mice [142]. This provides evidence that activating the AHR actually plays a role in improving the barrier function of the skin and can thus be used for the treatment of human skin diseases. These investigations clearly point towards a role for the AHR in maintenance of the skin barrier. However, the mechanism behind AHR signaling and skin barrier maintenance is still unclear. Therefore, in **chapter 7** of my thesis we investigated the ability of coal tar to repair skin barrier defects in healthy human volunteers, or to prime the skin for repair before skin damage is applied.

The AHR functions as a moderator of the inflammatory response in skin

Inflammation is an important aspect of the immune response and is controlled and mediated by a variety of factors, including cytokines and various soluble mediators such as prostaglandins. Classical symptoms of inflammation include pain, redness, and swelling of affected tissues. Even though the immune response has an important function in host defense, the reaction itself is also detrimental to surrounding tissues and must therefore be orchestrated accordingly and stopped after clearance of the causative trigger. In the skin, the immune response has an important role in protection as the skin is in direct contact with harmful microbes, chemicals and continuously under fire by UVB radiation. The AHR has been shown to play a role in orchestrating the immune response adding to its role as a drug target in skin inflammatory diseases, which will be discussed below.

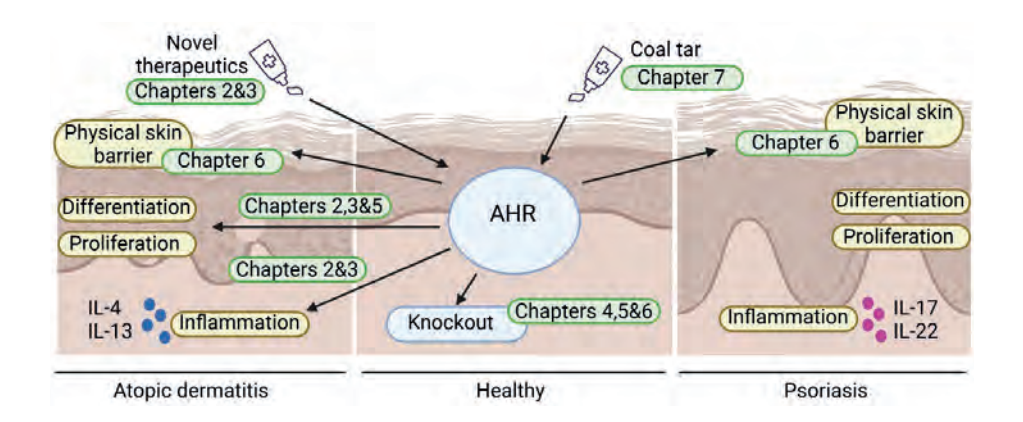
The AHR was initially found to regulate a balance between T-regulatory (Treg) and Th 17 subsets, dependent on specific ligand activation. Activation with TCDD induced the development of Treg cells and was able to reduce symptoms in an autoimmune encephalomyelitis mice model, but exacerbating symptoms when activated with a different ligand, namely FICZ [143]. This indicated involvement of the AHR in immune cell lineage development, but with a ligand-dependent effect. This study propelled investigations in the role of AHR in immune cell development, finding a role for the AHR in many immune cell subsets, including innate lymphoid cell lines, as well as tissue resident and circulating T-cell lineages, and epidermal Langerhans cells [144, 145].

Studies into regulation of inflammation through AHR signaling also involved psoriasis-like mouse models induced by topical application of imiguimod (IMQ) on mice skin [146]. Disease development in these mice is shown to be dependent on the IL-23/IL-17/IL-22 axis [147] and is exaggerated in Ahr/- mice, whilst attenuated by the AHR agonist FICZ in wildtype mice [148]. Ex vivo skin cultures from psoriasis lesional skin biopsies when treated with FICZ showed reduced expression of psoriasis marker genes [148]. In contrast, constitutive expression of AHR induces dermatitis-like lesions and immunological imbalance resembling AD in mice [149]. Similarly, air pollutant exposure in mice results in epidermal hyper-innervation, causing pruritus, as well as inflammation [150]. This underlines the importance of balanced AHR signaling as well as ligand-specific signaling via the AHR in the development of AHR-targeting drugs.

In recent years, the AHR gained major attention in dermatology after our studies indicating the AHR-dependent therapeutic efficacy of coal tar and the FDA approval of Tapinarof for the treatment of psoriasis [151]. Tapinarof (or Benvitimod) is a compound derived from a group of bacterial symbionts, the entomopathogenic nematodes, and was already shown to display anti-inflammatory activity and inhibit allergic contact dermatitis [152]. Tapinarof binds directly to the AHR and functions as an agonist of the AHR signaling pathway. In ex vivo human skin, treatment with Tapinarof reduced expression of IL-17A. In the IMQ treated mice model, treatment with Tapinarof led to decreased tissue cytokine expression of both IL-17A and IL-22 [153]. Activation of the AHR with natural agonists was therefore shown to moderate the immune response, both in mouse and human skin. However, common side effects of treatment with Tapinarof included folliculitis and contact dermatitis, similar to coal tar, once again underlining the importance of well-balanced AHR signaling and ligand turnover [95].

AHR agonists are a valuable addition to the therapeutic arsenal for the treatment of chronic inflammatory skin diseases, however studies into repressing and stimulating effects of AHR activation on the inflammatory response in both health and disease skin are needed to better understand the side effects and potential long term adverse events of deregulated AHR signaling in human. In my thesis we took studies from the laboratory to the bedside by coal tar treatment in a human in vivo tape stripping model to study skin barrier disruption and repair mechanisms (chapter 7).

Graphical thesis outline



Summary of thesis outline

The main aim of my thesis was to increase our understanding of the role of AHR signaling in the formation and maintenance of the epidermal barrier. I focused on the regulation of keratinocyte proliferation and differentiation and investigated the potential of novel ligands as therapeutics to restore epidermal homeostasis in inflammatory skin diseases.

Novel therapeutic ligands were analyzed in vitro and in vivo as described in chapters 2 and 3. We studied the capability of these AHR ligands in inflammatory skin models to restore aberrant keratinocyte differentiation and proliferation as well as dampen inflammatory signaling. To discover novel AHR-targeting therapeutics it is important to understand the mechanism behind AHR signaling. In chapter 5 we studied the mechanism of AHR-driven keratinocyte differentiation and elucidated novel interaction partners through which the AHR directs terminal differentiation. To further investigate the role of AHR in organotypic skin models, we developed a method to knock out genes in a keratinocyte cell line using CRISPR/Cas9 (chapter 4) as well as a novel method to measure skin barrier function (chapter 6). To assess the importance of AHR signaling in the inflammatory response of keratinocyte towards diseaseassociated cytokines, the effects of AHR activation upon experimental skin barrier defects in healthy human volunteers were investigated and described in **chapter 7**.

The experimental studies in my thesis that point towards new molecular insights into AHR's function in skin biology and underscore the potential of AHR ligands as a therapeutic modality in the treatment of inflammatory skin diseases, are presented in the following chapters:

Chapter 2 | Lead optimization of aryl hydrocarbon receptor ligands for treatment of inflammatory skin disorders

A novel class of AHR ligands, the SGA compounds, were studied for their therapeutic potential in in vitro human models of atopic dermatitis and murine models of inflammation

Chapter 3 | Carboxamide derivatives are potential therapeutic AHR ligands for restoring IL-4 mediated repression of epidermal differentiation proteins

Carboxamide derivatives were shown to be AHR activating ligands and their potential in improving keratinocyte proliferation and differentiation was studied in in vitro human models of atopic dermatitis.

Chapter 4 | Investigations into the FLG null phenotype: Showcasing the methodology for CRISPR/Cas9 editing of human keratinocytes

CRISPR/Cas9 was used in human keratinocytes to knock out and subsequently rescue the expression of filaggrin. This study highlights the potential of using CRISPR/Cas9 in editing human keratinocytes. In later chapters, the technology and methods described in this study were used to knock out AHR to investigate its role in the human skin barrier.

Chapter 5 | The aryl hydrocarbon receptor regulates epidermal differentiation through transient activation of TFAP2A

Genome-wide AHR binding and transcriptome analysis revealed possible mechanisms behind AHR-induced keratinocyte differentiation and identified other transcription factors with which the AHR is able to influence these pathways.

Chapter 6 | Electrical impedance spectroscopy analysis quantifies organotypic epidermis formation and skin barrier function in vitro

A novel technique enabling electrical impedance measurements of human epidermal equivalent in a multi-well format was found to be non-harmful for equivalents and provided novel insights in barrier function in inflammatory diseases models as well the response of AHR activation in keratinocytes.

Chapter 7 | Coal tar attenuates acute experimentally-induced dermatitis: insights into AHR-targeting therapies for inflammatory skin diseases

Healthy volunteers were tape-stripped and treated with the AHR agonist coal tar to provide insights in the protective roles of AHR signaling in the inflammatory response.

Chapter 8/9 Summary and discussion

Finally, the experimental data described in this thesis are summarized and discussed.



Chapter 2

Lead optimization of aryl hydrocarbon receptor ligands for treatment of inflammatory skin disorders

Gijs Rikken^{1*}, Kayla J. Smith^{2*}, Noa J.M. van den Brink^{1*}, Jos P.H. Smits¹, Krishne Gowda³, Angela Alnemri², Gulsum E. Kuzu², Iain A. Murray², Jyh-Ming Lin⁴, Jos G.A. Smits⁵, Ivonne M. van Vlijmen-Willems¹, Shantu G. Amin³, Gary H. Perdew^{2#} and Ellen H. van den Bogaard^{1#}

¹Department of Dermatology, Radboud University Medical Center, Radboud Institute for Molecular Life Sciences, Nijmegen, The Netherlands;

²Department of Veterinary and Biomedical Sciences, and Center for Molecular Toxicology and Carcinogenesis, Penn State University, University Park, Pennsylvania, USA;

³Department of Pharmacology, Penn State College of Medicine, Hershey, Pennsylvania, USA;

⁴Department of Biochemistry and Molecular Biology, Penn State College of Medicine, Hershey, Pennsylvania, USA; Metabolomics Facility, The Huck Institutes of the Life Sciences, The Pennsylvania State University, University Park, Pennsylvania, USA;

⁵Department of Molecular Developmental Biology, Faculty of Science, Radboud Institute for Molecular Life Sciences, Radboud University, Nijmegen, The Netherlands.

^{*} Shared first authorship; # Shared senior authorship

Abstract

Therapeutic aryl hydrocarbon receptor (AHR) modulating agents gained attention in dermatology as non-steroidal anti-inflammatory drugs that improve skin barrier properties. By exploiting AHR's known ligand promiscuity, we generated novel AHR modulating agents by lead optimization of a selective AHR modulator (SAhRM; SGA360). Twenty-two newly synthesized compounds were screened yielding two novel derivatives, SGA360f and SGA388, in which agonist activity led to enhanced keratinocyte terminal differentiation. SGA388 showed the highest agonist activity with potent normalization of keratinocyte hyperproliferation, restored expression of skin barrier proteins and dampening of chemokine expression by keratinocytes upon Th2-mediated inflammation in vitro. The topical application of SGA360f and SGA388 reduced acute skin inflammation in vivo by reducing cyclooxygenase levels, resulting in less neutrophilic dermal infiltrates. The minimal induction of cytochrome P450 enzyme activity, lack of cellular toxicity and mutagenicity classifies SGA360f and SGA388 as novel potential therapeutic AHR ligands and illustrates the potential of medicinal chemistry to fine-tune AHR signaling for the development of targeted therapies in dermatology and beyond.

Introduction

The bHLH/PAS (basic-Helix-Loop-Helix/Per-Arnt-Sim) family of transcription factors are considered sensors of both endogenous and exogenous stimuli [154]. The aryl hydrocarbon receptor (AHR) is the only known vertebrate member of this family that is capable of binding low molecular weight molecules (e.g. MW150-400) and inducing a transcriptional response, hence acting as a ligand-activated transcription factor [155]. The AHR is increasingly considered as an important receptor for physiological functions in barrier tissues (e.g., lung, skin and intestine) that is capable of sensing exogenous and endogenous chemicals [156]. AHR binds a wide array of chemicals from simple two-ring compounds (e.g., indole) to much larger compounds with multiple ring structures (e.g., benzo(a)pyrene) [157, 158]. There are three distinct classes of AHR ligands: agonists, antagonists, and selective AHR modulators (SAhRMs), these ligand vary in both affinity or occupancy potential and intrinsic efficacy, the latter referring to the ability to activate the AHR to mediate gene transcription [87, 159, 160]. Furthermore, agonists can vary in AHR activation potential based not only on their affinity for the AHR but also on the ability to be metabolized and their inherent hydrophobicity, which influences tissue distribution and half-life in vivo. 2,3,7,8-tetrachlorodibenzo-p-dioxin (TCDD), often considered a prototypic AHR ligand, is poorly metabolized, exhibits a half-life in mice of 11 days, and thus is atypical compared to most other AHR ligands [161]. Importantly, a weak agonist can also exhibit SAhRM or antagonist activity dependent on the cellular context, and SAhRMs can act as an AHR antagonist [76]. These classes of ligands have allowed the various functions of this enigmatic receptor to be dissected and underscore the potential to modulate the AHR and explore its use as a therapeutic target. There is a growing list of endogenous and dietary compounds known to activate the AHR [158]. In particular, mammalian host tissues or microbiota can metabolize tryptophan to AHR ligands. For example, the indoleamine 2,3-dioxygenase pathway present in immune cells degrades tryptophan to AHR ligands such as kynurenine and kynurenic acid [162, 163]. Exposure to sunlight or oxidants can catalyze the formation of the endogenous AHR agonist 6-formylindolo[3,2-b]carbazole, thus linking sun exposure to the generation of AHR ligands in the skin [164]. Gut and skin commensal bacterial metabolites can activate host AHR signaling and mediate tissue homeostasis [158, 165]. In addition, yeasts, like the Malassezia species, abundant on human skin, can generate several high-affinity AHR ligands (e.g., indolo[3,2b] carbazole) from tryptophan [166]. Furthermore, the array of compounds that activate the AHR appears to be expanded in humans relative to rodents, suggesting an evolutionary expansion of AHR sensitivity [158].

Within the skin, the AHR is expressed in a variety of cell types and plays a role in innate and adaptive immunity, keratinocyte differentiation, and melanocyte pigmentation (reviewed in [167]). AHR expression levels [76] and nuclear levels of AHR [168] correlate with the differentiation status of keratinocytes and agonistmediated AHR activation, which leads to increased expression of key genes involved in epidermal differentiation [75, 76, 169, 170] and accelerates skin barrier formation in vivo [171]. Furthermore, Ahr null keratinocytes fail to differentiate in vitro, and inhibition of endogenous AHR signaling in 3D human skin equivalents hampers epidermal differentiation and stratification [76].

The first evidence of the therapeutic potential of AHR-targeted therapies in skin diseases with deprived barrier function came from our discovery of the mechanism of action of coal tar therapy. For centuries, coal tar has been used as an effective treatment in dermatological practice, predominantly for the treatment of atopic dermatitis (AD) and psoriasis, two highly prevalent chronic inflammatory skin diseases characterized by impaired skin barrier function. Coal tar, rich in polycyclic aromatic hydrocarbons, mediates an AHR-dependent increase in skin barrier protein expression in human skin models and dampens the IL-4-mediated inflammatory signaling cascade [75]. Later, other AHR ligands (e.g. Chinese herbal extracts [172-174] and Henna constituents [170]) were also reported to induce therapeutic effects similar to coal tar. It was also found in psoriasis that AHR signaling actively dampens inflammation [148, 175], and the first therapeutic single AHR ligand, Tapinarof [153], has been approved by the FDA for topical treatment after finalizing phase 3 trials in psoriasis [95]. We are, however, in need of a greater variety of structurally diverse AHR ligand classes given the ligand-dependent variation in downstream (side) effects of AHR activation [176], which is also influenced by the specific tissue microenvironment [122].

In the current study we aimed for the coupling of SAhRM activity to partial AHR agonist activity to breach pro-inflammatory processes in the skin and improve skin barrier function by targeting keratinocyte terminal differentiation.

Results

Lead optimization and synthesis of SGA indazole derivatives

Previous studies established that SGA360 is devoid of AHR agonist activity, while having anti-inflammatory effects [159]. We thus attempted to generate derivatives based on SGA360 that would exhibit varying degrees of AHR agonist activity to additionally foster the expression of skin barrier-related proteins. Twentytwo 7-(trifluoromethyl)-1H-indazole derivatives were synthesized of which the chemical structures are shown in Figure 1A. The structure of each compound was confirmed by a combination of nuclear magnetic resonance spectroscopy and mass spectrometry analysis. Briefly, two basic variations in the structure of SGA360 were made: a number of functional groups were added to indazole at the 3rd position, or an allyl group was added to either N1 or N2 (see core structure Figure 1A).

SGA derivatives vary in AHR agonist mediated activity

All new SGA derivatives, and the previously described SGA360 and SGA315 [159], were screened for agonist activity in a Hepa 1.1 dioxin response element (DRE)driven stable reporter mouse cell line (Figure 1B-C). Eight of the compounds tested at a 10 mM concentration induced a significant level of AHR transcriptional activity between 15-85% of the response obtained with a saturating dose of TCDD. As expected, SGA360 did not exhibit agonist activity. SGA377, SGA385, and SGA387 all showed agonist activity, while moving the allyl group from N1 to N2 lowered agonist activity in SGA378, SGA386, and SGA388. In contrast, SGA390 exhibited considerable activity with the allyl group in the N2 position but failed to exhibit agonist activity in the N1 position (SGA389). This is likely due to the conformation of the functional group at position 3. A comparison of SGA360a to SGA360f revealed that SGA360f had considerably more agonist activity, yet the only difference in the structure is the positions of the hydroxyl and methoxyl group switched in the ortho and para position on the functional group at the 3rd position of the indazole. These results underscore the potential of designing ligands that vary in AHR agonist activity. Due to the known differences in ligand binding affinity between murine and human AHR, we completed our discovery studies with the human (HepG2 40/6) DRE-driven reporter cell line (Figure 1D-E). This screen identified additional SGA compounds with stronger agonist activity in the human reporter cells, such as SGA388, SGA360a, and SGA360f. Next, we compared the ability of a subset of SGA derivatives to induce both DRE-driven reporter activity and Cyp1a1 mRNA levels in the murine hepatocyte cell line. In contrast to TCDD, the SGA derivatives show a dramatic difference in the level of induction of reporter activity (Figure 1B-C) versus Cyp1a1 mRNA (Figure 1F), hence the need for additional screening of AHR target gene expression levels in primary skin cells of murine and human origin to minimize false-negative results.

SGA derivatives are direct AHR ligands and agonists in primary keratinocytes and dermal fibroblasts

Based on the results of the initial screen, selected SGA derivatives were first tested in primary mouse keratinocytes. SGA360f, SGA315, SGA385 and SGA388 (10 mM) exhibited weak agonist activity by a 2-10 fold induction of *Cyp1a1* mRNA levels and increased *Cyp1b1* expression levels (Figure 2A-B). SGA derivatives were found to also activate the AHR in other skin-related cell types, as primary dermal mouse fibroblasts showed a similar expression pattern upon stimulation, albeit less pronounced than in keratinocytes (Figure 2A-B). Next, primary adult human keratinocytes cultures were exposed to SGA360, SGA360f, SGA315, SGA388, and TCDD. SGA360f and SGA388 showed agonist activity (20% and 55% of TCDD response, Figure 2C).

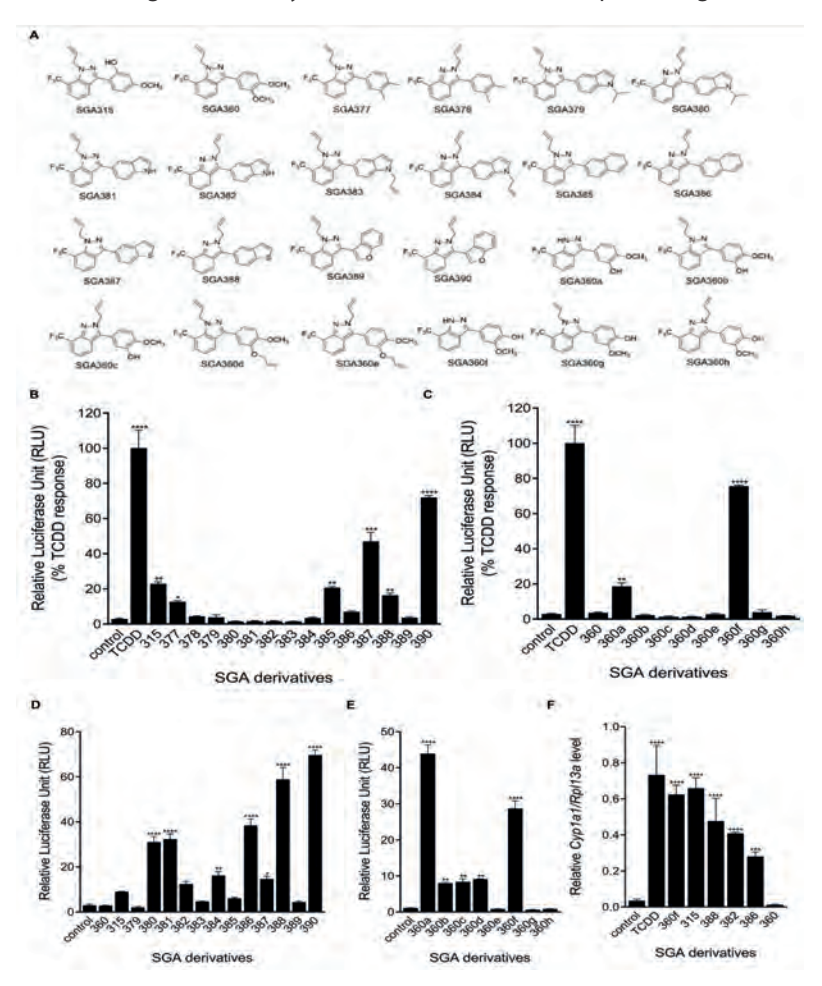


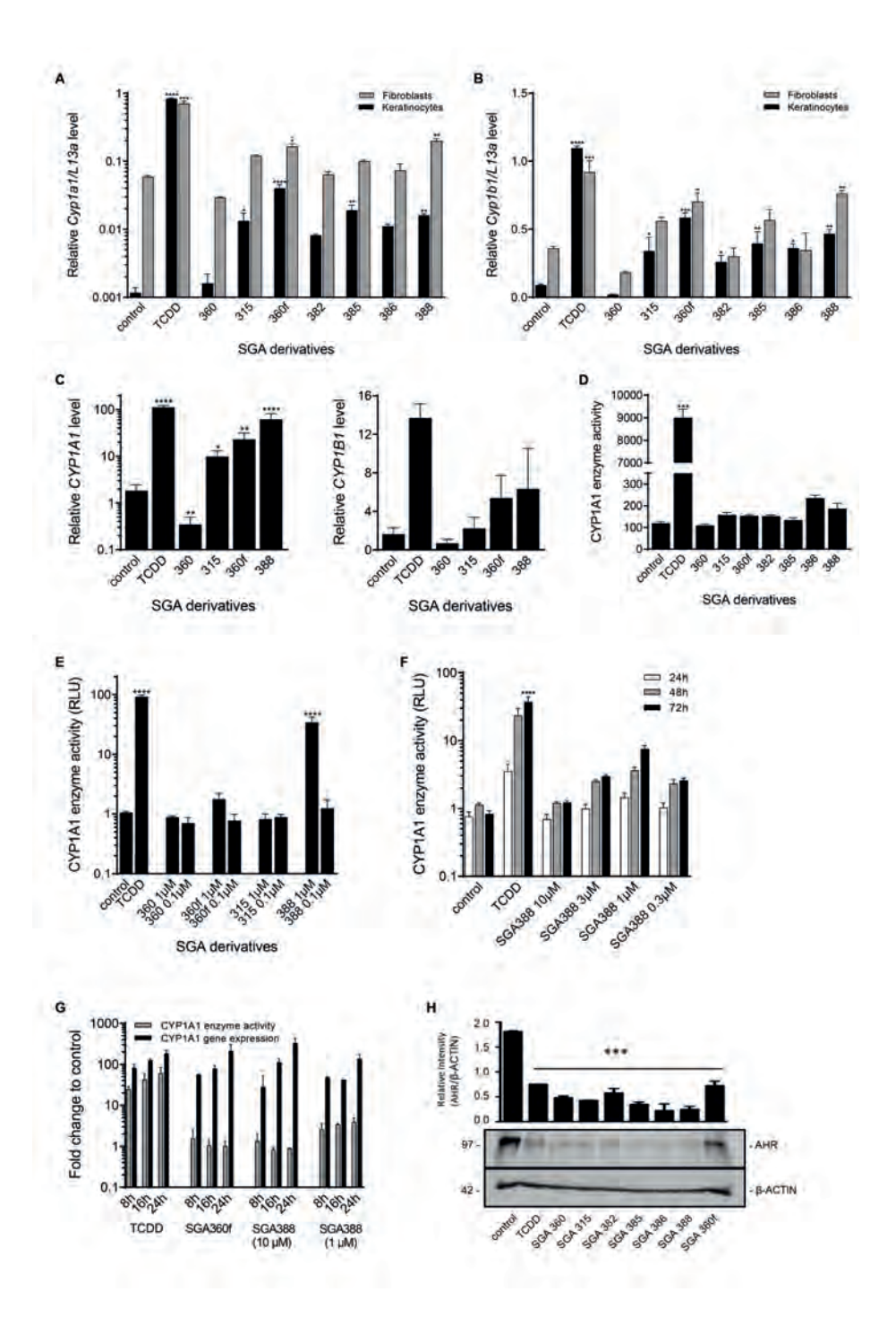
Figure 1. AHR agonist activity in mouse and HepG2 40/6 human reporter cell lines. **A)** SGA core structure and structures of the compounds. **B,C)** Hepa 1.1 DRE-driven stable reporter mouse cell line stimulated with SGA derivatives (10 μ M) and TCDD (10 nM) for 4 h after which the luciferase activity was measured (TCDD response set at 100%), N=3. **D,E)** HepG2 40/6 human reporter cell line stimulated with SGA derivatives (10 μ M) for 4 h after which the luciferase activity was measured, N=3. **F)** *Cyp1a1* mRNA expression analysis of selected SGA compounds after 4 h stimulation of the Hepa 1.1 reporter cell line, N=3. *P < 0.05, **P < 0.01, ****P < 0.001, *****P < 0.0001. Mean +/- SEM.

Since elevated CYP1A1 enzyme levels were recently implicated to exaggerate inflammation [175], and are important for phase I biotransformation, we assessed the capability of SGA derivatives to elevate CYP1A1 enzyme activity levels in primary keratinocytes. In sharp contrast to the strongly induced enzyme activity levels by TCDD, no significant increase in SGA360 derivative mediated CYP1A1 enzyme activity in murine keratinocytes was observed (Figure 2D).

However, in human keratinocytes, SGA388 at 1 µM concentration elevated CYP1A1 enzymatic levels after 48 h of stimulation (Figure 2E). Further examinations revealed SGA388 effects on CYP1A1 enzymatic levels were time and concentrationdependent in keratinocytes (Figure 2F). Yet, induction levels were significantly lower than for TCDD exposure, while CYP1A1 mRNA levels were similar to the effects of TCDD (Figure 2G). This may be due to the ability of SGA compounds at micromolar levels to actually inhibit CYP1A1 activity. In a cell-based radioactive photoaffinity ligand competition assay, SGAs significantly blocked the binding of the radioligand to the murine AHR (Figure 2H), indicating direct binding of the SGA derivatives to the AHR. Considering these results, SGA388 and SGA360f were subjected to extensive characterization based on exhibiting similar AHR agonist activity in both mouse and human keratinocytes. Furthermore, the parent SAhRM, SGA360, and SGA315 were selected for evaluating the effect of AHR activation since they exhibited essentially no or weaker agonist activity compared to SGA388 and SGA360f.

In vitro toxicity of SGA derivatives

Often biotransformation of mutagens is required to form reactive intermediates that lead to DNA damage through phase I xenobiotic metabolism. For example, CYP1A1 enzymatic activity can lead to carcinogenicity (as with benzo(a)pyrene), and we therefore examined the toxicity potential of SGA derivatives. We screened for in vitro cellular toxicity (lactate dehydrogenase release assay) and mutagenicity (Ames II fluctuation assay) of SGA derivatives. No signs of cellular toxicity were observed (Figure 3A) and none of the SGA derivatives (SGA360, SGA360f, SGA315 and SGA388) reached the mutagenic threshold in any of the conditions and concentrations tested, with or without cytochrome-mediated biotransformation (+S9 fraction) (Figure 3B).



< Figure 2. AHR agonist activity in primary keratinocytes and dermal fibroblasts. A) Cyp1a1 and B) Cyp1b1 mRNA expression analysis of selected SGA derivatives (10 μM) and TCDD (10 nM) in primary mouse keratinocytes and dermal fibroblasts after 4 h of stimulation and normalized for the murine household gene L31a, N=3. C) CYP1A1 and CYP1B1 mRNA expression patterns of primary human keratinocytes stimulated for 48 h (re-stimulation after 24 h) with 10 µM of selected SGA compounds and 10 nM TCDD, N=3. CYP1A1 enzyme activity measured in D) mouse and E,F,G) human primary keratinocytes. Mouse keratinocytes were stimulated for 36 h with 10 µM of the SGA derivates and 10 nM TCDD, N=3. For the human keratinocytes, time and concentration series were performed with selected SGA derivatives and TCDD (10 nM). E) 48 h stimulation (re-stimulation after 24 h), N=3. F) SGA388 time and concentration series, N=3, statistics performed for each time point separately. G) CYP1A1 enzyme activity in comparison to CYP1A1 mRNA levels for TCDD, SGA360f and SGA388, controls set at 1, N=2 (no statistics). H) A murine Hepa 1.1 cell-based radioactive photoaffinity ligand competition assay (1 h stimulation). * p < 0.05, *** p < 0.01, **** p < 0.001, **** p < 0.0001. Mean +/- SEM.

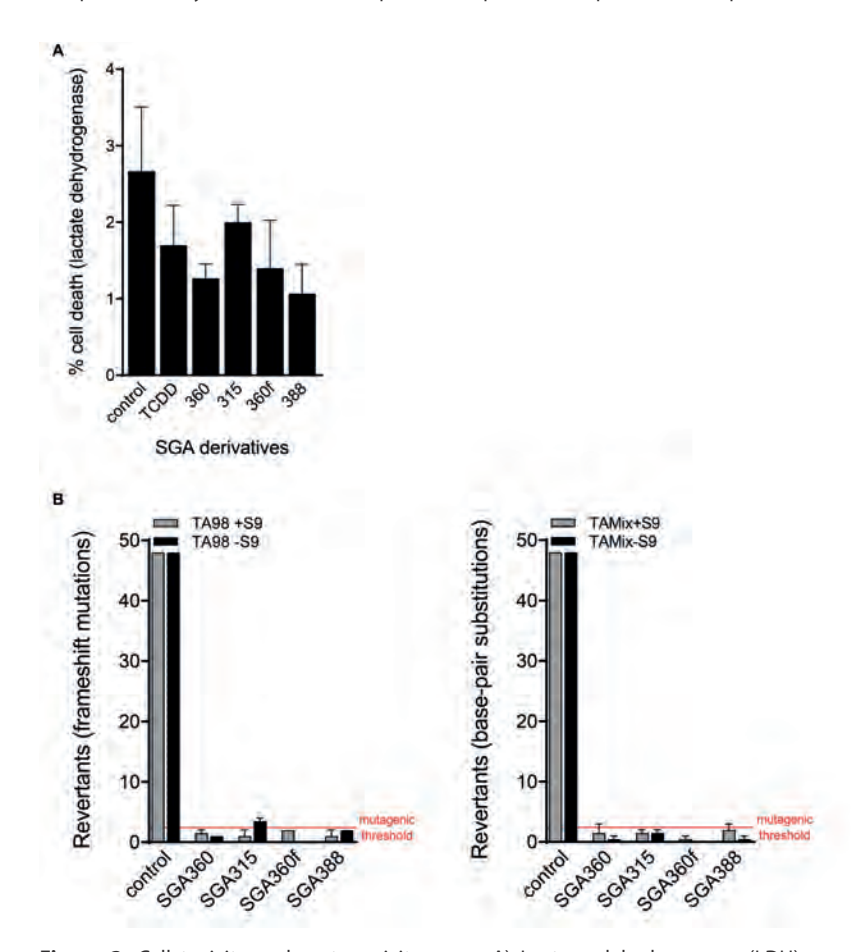


Figure 3. Cell toxicity and mutagenicity assay. A) Lactase dehydrogenase (LDH) measurement of monolayer primary human keratinocytes stimulated with the SGA compounds (10 µM) and TCDD (10 nM) for 24 h, N=3. B) SGA derivatives tested in the Ames mutagenicity assay using the strains TA98 (frameshift mutations) and TAMix (base-pair substitutions), with and without the addition of the rat liver S9 microsomal fraction (for cytochrome-mediated biotransformation), performed in duplicates.

AHR-dependent epidermal differentiation, stratification and skin barrier protein expression by SGA derivatives

The ability of SGA derivatives to enhance epidermal differentiation was investigated in mouse and human keratinocyte monolayer cultures. SGA360, having no AHR agonist activity, failed to induce terminal differentiation gene expression. SGA360f and SGA388 exhibited the greatest induction rate for filaggrin (Flg), hornerin (Hrnr) and loricrin (Lor) in murine primary keratinocytes (Figure 4A) which was AHRdependent, as Ahr/- keratinocytes failed to differentiate upon treatment with SGAs (Figure 4B). Although it is important to keep in mind that the calcium-induced differentiation culture system will differ from the *in vivo* situation. In human primary keratinocytes, SGA388 and SGA360f were also relatively potent compounds, given the early rise in gene expression levels at 12 h that preceded the response of SGA315 for which increased expression levels were only observed after 36 h of stimulation (Figure 4C). Interestingly, the early stratum spinosum marker cytokeratin 10 (KRT10) which normally precedes the expression of stratum granulosum terminal differentiation markers, including FLG and HRNR upon normal keratinocyte differentiation in vitro in absence of any ligand stimulation (Figure 4D), was not induced by SGA360f and SGA388. Canonical AHR signaling appeared essential for SGA-mediated epidermal differentiation as GNF-351 (selective AHR antagonist) completely abolished SGA effects (Figure 4F). Next, we validated whether the induction of epidermal differentiation seen in monolayer cultures would be sufficient to positively contribute to epidermal development in organotypic human epidermal equivalents (HEEs) (Figure 5A). Treatment with SGA360 resulted in less layers of stratum granulosum (SG) and stratum corneum (SC) while SGA315 did not induce major changes when compared to the untreated (control) HEEs. HEEs treated with TCDD, SGA360f and SGA388 showed more layers of stratum granulosum and stratum corneum with concomitant higher levels of CYP1A1 and filaggrin protein (Figure 5B). CYP1A1 gene expression levels followed similar trends as the monolayer cultures with a correlating dose response for HRNR gene expression (Figure 5C). Similar to filaggrin and hornerin, loricrin protein expression was also induced by SGA388 (Figure 5D), while proliferation rates remained unaffected (Figure 5E).

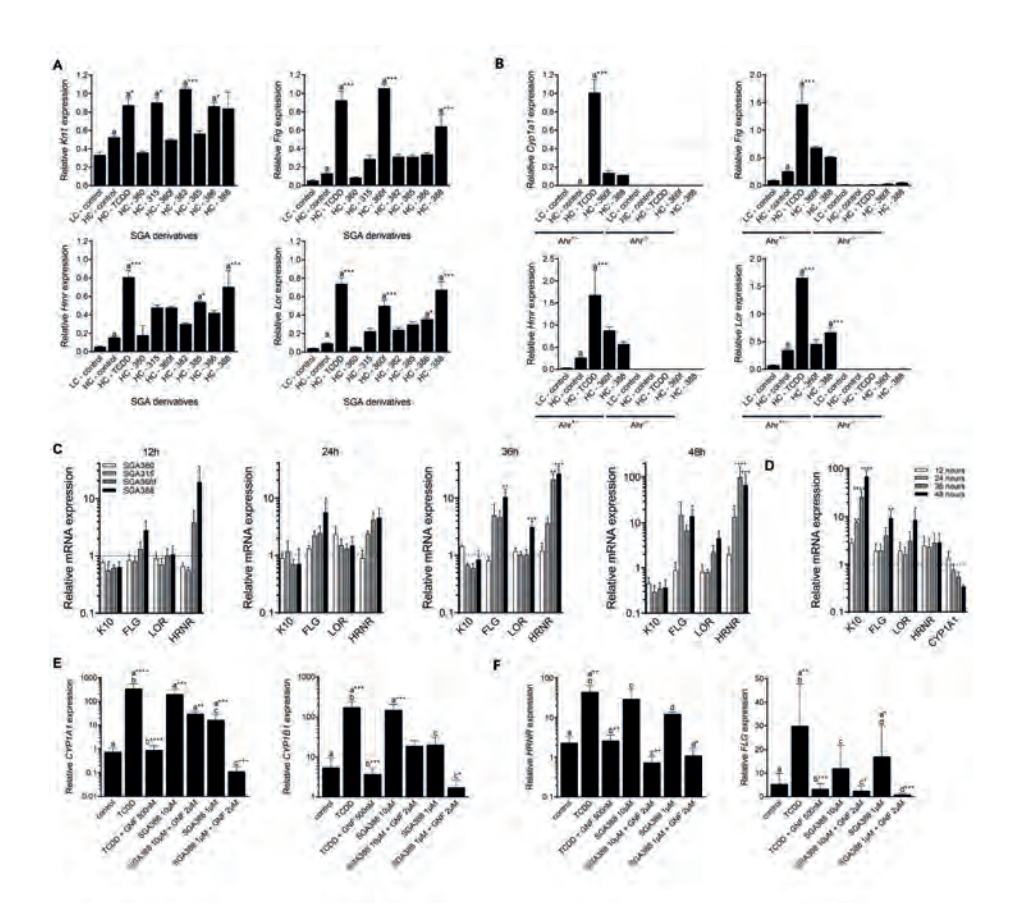


Figure 4. Epidermal differentiation gene expression analysis. LC, low calcium (0.05 mM); HC, high calcium (0.12 mM). A) Expression of the terminal differentiation genes Krt1, Flq, Hrnr and Lor in murine keratinocytes after 24 h of stimulation with SGA derivatives, N=3. B) Ahr+/+ and Ahr/- monolayer murine keratinocytes stimulated with SGA compounds followed by gene expression analysis; Ahr activity (Cyp1a1) and epidermal differentiation (Fla, Hrnr, Lor), N=3. C) Expression analysis of terminal differentiation genes (KRT10 (K10), FLG, HRNR, LOR) in monolayer primary human keratinocytes stimulated with SGA derivatives and harvested in a time series, N=4 (24 h data N=3), statistical analysis for each time point and gene separately. D) Primary human keratinocytes harvested after different time points of differentiation and analyzed for AHR activity (CYP1A1) and terminal differentiation (K10, FLG, LOR, HRNR), start of differentiation (0 h) was set at 1, N=4 (24 h data N=3). E) Expression analysis of AHR target genes CYP1A1 and CYP1B1 and F) differentiation genes HRNR and FLG of monolayer cultures stimulated with GNF-351 prior to the addition of TCDD (10 nM) and SGA388 (10 and 1 μ M) for 48 h (re-stimulation after 24 h), N=3.*p < 0.05, ***p < 0.01, ****p < 0.001, ****p < 0.0001. Mean +/- SEM.

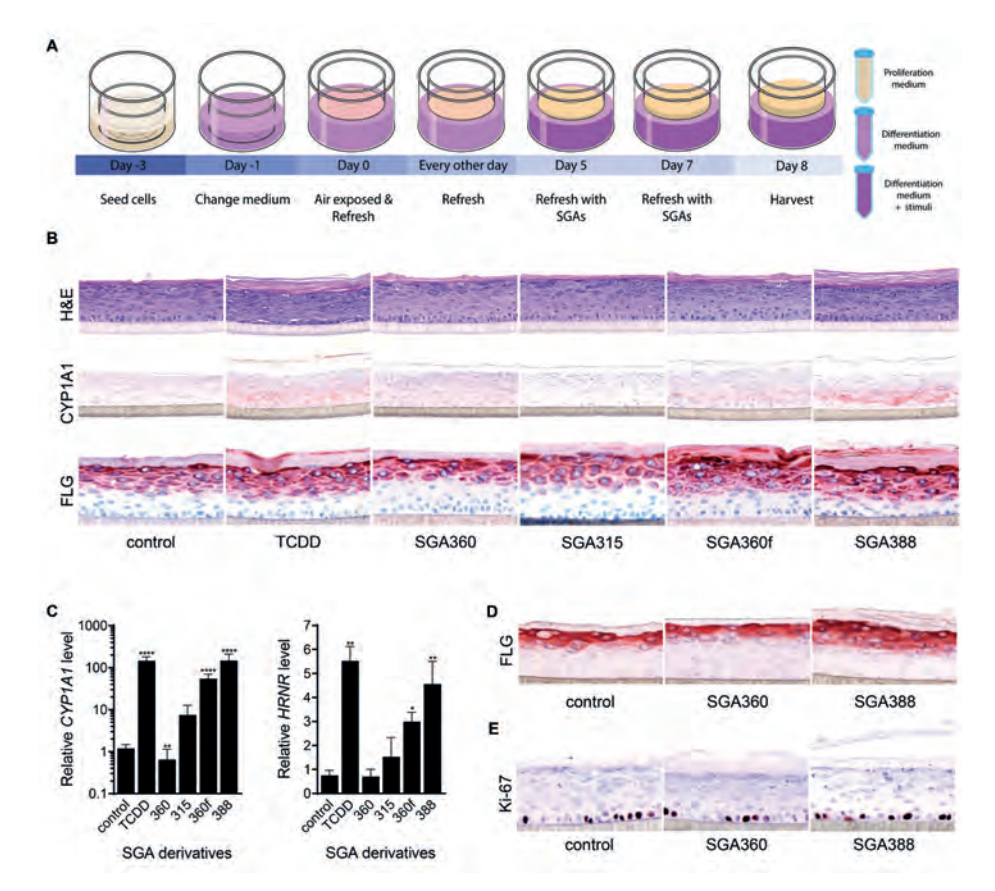
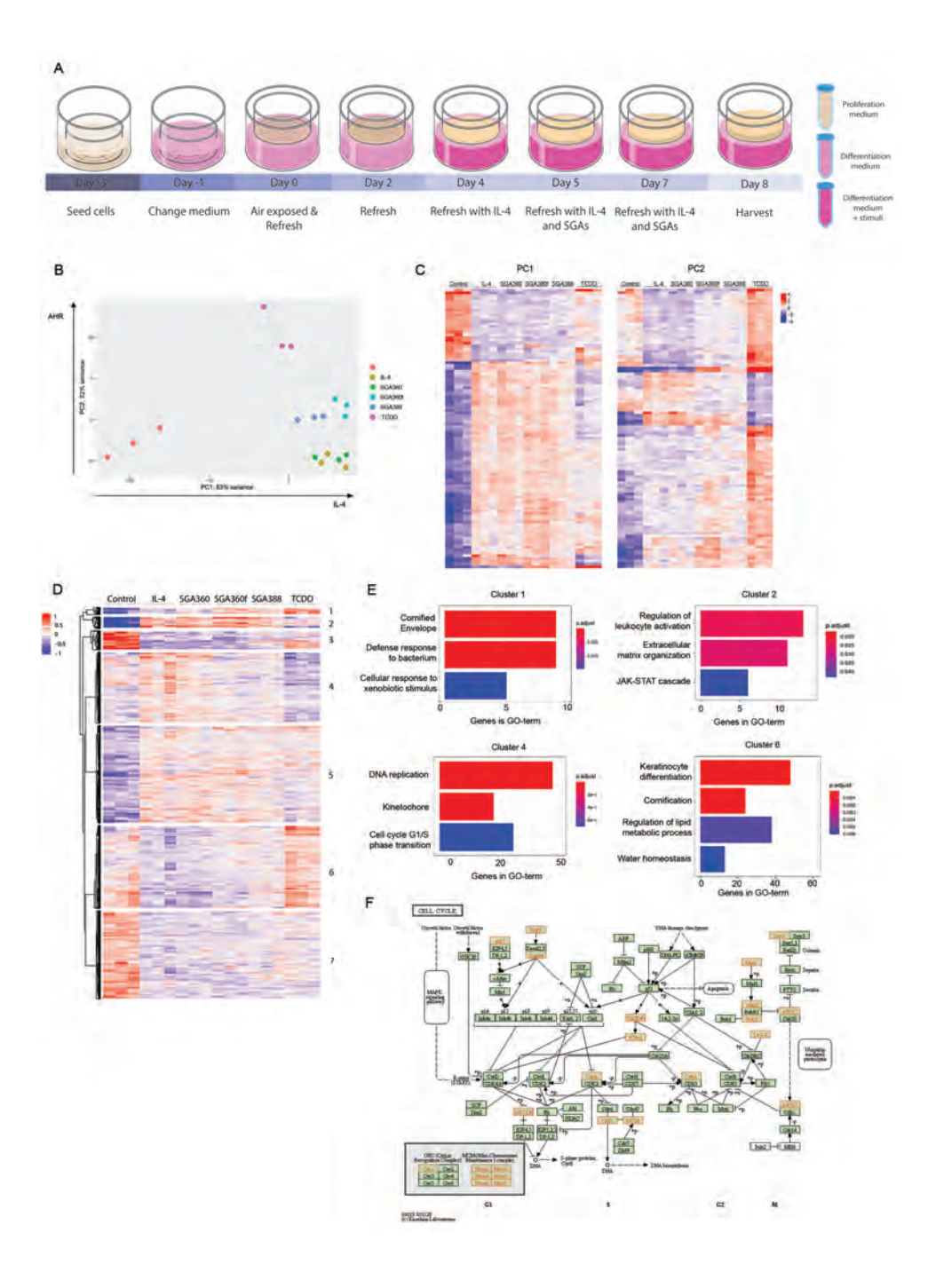


Figure 5. AHR activation and induction of epidermal differentiation in human epidermal equivalents. **A)** schematic presentation of 3D culture schedule for normal human epidermal equivalents (HEEs) stimulated with SGA compounds at day 5 of the air-liquid interface. **B)** H&E, filaggrin (FLG) and CYP1A1 staining, **C)** *CYP1A1* and *HRNR* mRNA expression analysis (N=5), **D)** loricrin (LOR), **E)** Ki-67 staining of HEEs stimulated with 10 μ M of SGA derivatives and 10 nM TCDD for 72 h (re-stimulated after 48 h). SC = *Stratum corneum*, SG = *Stratum granulosum*, SS = *Stratum spinosum*, SB = *Stratum basale*. * p < 0.05, ** p < 0.01, **** p < 0.0001. Mean +/- SEM. Scale bar = 100 μ m.

Genome-wide effects of SGA derivatives upon IL-4 mediated inflammation in vitro

Next, we guestioned whether SGA derivatives can restore the disturbed epidermal differentiation processes that are known for the key AD-associated Thelper-2 cytokine, interleukin-4 (IL-4). We performed genome-wide transcriptomic analysis by bulk RNAsequencing after co-stimulation of HEEs with interleukin-4 (IL-4; atopic dermatitis (AD)-like HEE (AD-HEE)) and SGA360 (SAhRM activity), SGA360f or SGA388 (coupling of SAhRM to agonist activity), or TCDD (full AHR agonist) (Figure 6A). We and others have demonstrated that this setup enables the verification of AHR-mediated therapeutic effects on skin inflammation [132, 177]. Principal component analysis (PCA, Figure 6B) and heatmap analysis of the top 500 most variable genes (Figure 6C) indicated that PC1 accounted for 62% of the variance between the top 500 most variable genes that could be attributed to IL-4 treatment. In PC2, 22% of the variance was attributed to AHR activation by TCDD, SGA388 and SGA360f, clearly showing a dose effect of AHR agonist activity. Next, pairwise comparisons between all conditions versus IL-4 treatment alone were filtered (P<0.05 and FC>1.5) resulting in 4182 differentially expressed genes to be included for heatmap analysis and unsupervised K-means clustering on pre-defined experimental conditions (GSE212539). Seven hierarchical clusters were generated based on gene expression dynamics upon treatment between experimental conditions (Figure 6D). Gene ontology analysis for each cluster identified specific biological processes that relate to differentially expressed genes (Figure 6E). Smaller clusters 1, 2 and 3 include genes involved in xenobiotic metabolism, antimicrobial response and cornified envelope formation (C1), regulation of leukocyte activation, extracellular matrix organization and JAK-STAT cascade (C2), and mostly extracellular matrix organization in C3. Genes in C1 are strongly regulated only by AHR agonist activity, while C2 and C3 are strongly controlled by IL-4 treatment and only rescued by the full AHR agonist, TCDD. The most interesting clusters were considered C4 and C6, in which genes are up- or downregulated by IL-4, respectively, and restored by AHR agonist activity in a dose-dependent manner. In C4 almost all genes are involved in cell cycle processes corresponding to the mitogenic effects of IL-4 [55]. This process can clearly be controlled by canonical AHR signaling. Subsequent KEGG analysis indicated key genes (e.g. MCM genes for G1) that are targeted by AHR agonists in every phase of the cell cycle (Figure 6F). C6 genes relate to processes involved in skin development and skin barrier function that are downregulated by IL-4 and reinstated by AHR agonists. In general, SAhRM activity alone (SGA360) was not sufficient to cause major transcriptomic changes related to any of these processes. The final clusters, C5 and C7, included genes annotated to processes including initiation of translation or actin binding but were not affected by any of the AHR ligands.

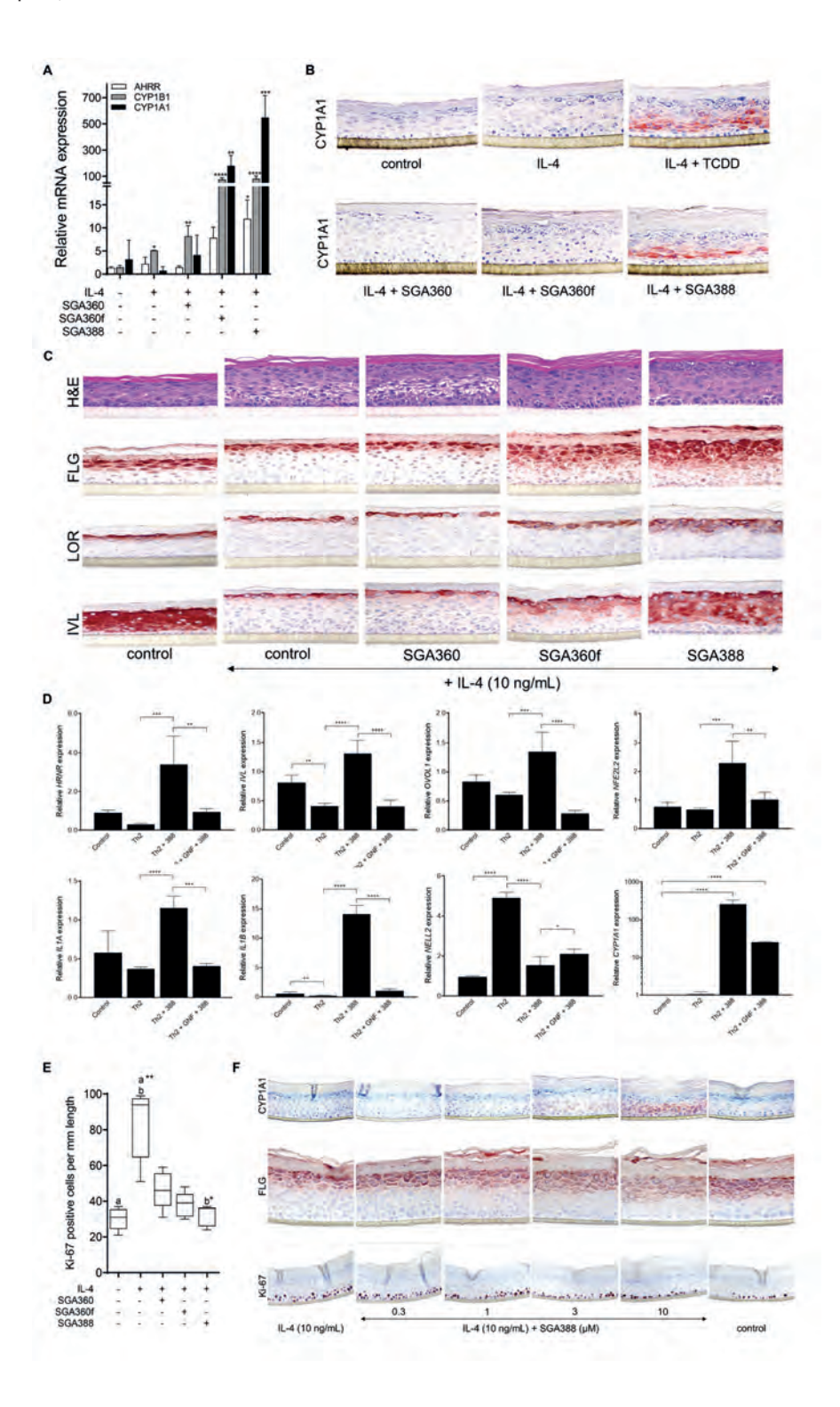


< Figure 6. Transcriptome analysis of SGA treatment upon IL-4 mediated inflammation in vitro. A) Schematic representation of experimental setup. B) Principal component analysis of top 500 most variable genes. PC1 and PC2 are shown in the plot. Different treatments are indicated with different colors. **C)** Heatmap of top 100 contributing genes to principal components from the PCA analysis. D) Heatmap of differentially expressed (DE) genes received from pairwise comparisons between conditions. Heatmap was generated using k-means clustering, columns were sorted on treatment. E) Visualization of GO-term analysis of selected cluster from heatmap in figure 4C. GO-terms are indicated in front of bars. Bar color indicates P adjusted-value and length of the bar indicates number of genes in specified GO-term. F) KEGG analysis for genes in cluster 4 of heatmap in figure 4C.

Verification of SGA-mediated 'therapeutic' effects in vitro

Next, we investigated the biological consequences of the transcriptomic changes as described above. AHR activation and downstream transcriptional regulation of target genes CYP1A1, CYP1B1, AHRR and CYP1A1 protein expression by the SGA derivatives was similar in the AD-HEEs (Figure 7A-B), as seen before with the normal HEEs. To differentiate between the effects of SAhRM versus coupled agonist activity, we first compared SGA360 to SGA388, respectively, and found striking differences. In contrast to SGA360, SGA388 was able to reduce the Th2-cytokine mediated epidermal spongiosis and counteract the strong reduction of filaggrin, loricrin and involucrin expression by Th2 cytokines (Figure 7C), even beyond the expression levels for the unstimulated control. SGA effects were AHR-dependent considering that co-stimulation with the AHR antagonist GNF-351 abolished the SGA388 induced expression levels of CYP1A1, HRNR and IVL, including known transcription factors, and AHR interacting proteins that mediate terminal differentiation, OVOL1 and NFE2L2. In addition, IL-4 mediated differential expression of host defenserelated genes IL1B, IL1A, and the AD signature gene NELL2 was rescued by SGA388 in an AHR-dependent fashion (Figure 7D).

Epidermal hyperproliferation is a key hallmark of inflammatory skin diseases like AD and psoriasis and leads to acanthosis. We previously found that IL-4 and IL-13 are potent mitogens in HEEs [55]. This IL-4-induced hyperproliferation of basal keratinocytes in AD-HEEs was completely abolished by SGA388 and SGA306f. Interestingly, SAhRM activity alone by SGA360 could also reduce proliferation rates, albeit to a lesser extent (Figure 7E). In a dose tapering study, SGA388 could be titrated to 1 µM for effective normalization of proliferation and terminal differentiation in AD-HEEs, and thereby minimize CYP1A1 protein induction (Figure 7F).



< Figure 7. Validation of SGA derivatives efficacy in AD-HEE model. A) Expression analysis of the AHR target genes CYP1A1, CYP1B1 and AHRR (N=4), B) analysis of AHR activity via immunostaining of CYP1A1 and C) H&E staining and the expression of epidermal differentiation proteins via immunostainings for filaggrin (FLG), loricrin (LOR) and involucrin (IVL) of HEEs stimulated with IL-4 (10 ng/mL) for 24 h prior to co-stimulation with SGA derivatives for 72 h. D) Gene expression levels in monolayer keratinocyte cultures stimulated with Th2 cytokines (IL-4 and IL-13, both 50 ng/mL) in combination with GNF-351 (2 μM, 30 min pre-incubation) and SGA388 (10 μM) for 48 h, technical N=4 using one human keratinocyte donor. E) Quantification of the proliferation marker Ki-67 of HEEs stimulated with 10 ng/mL IL-4 for 24 h, followed by co-stimulation with the SGA compounds for another 72 h, N=5. F) CYP1A1, FLG and Ki-67 protein staining of HEEs stimulated with 10 ng/mL IL-4 for 24 h followed by co-stimulation with a concentration series of SGA388 for another 72 h. SC = Stratum corneum, SG = Stratumqranulosum, SS = Stratum spinosum, SB = Stratum basale. * p < 0.05, ** p < 0.01, *** p < 0.001, **** p < 0.0001. Mean +/- SEM. Scale bar = 100 μ m.

Treatment of acute skin inflammation with SGA derivatives in vivo

Besides the targeting of skin inflammation-related epidermal proliferation and differentiation processes, SGA derivatives may possess important anti-inflammatory properties by SAhRM activity. To test if SGA360f and SGA388 retained in vivo anti-inflammatory SAhRM activity [159] along with the agonist effects targeting epidermal proliferation and differentiation, the 12-O-tetradecanoylphorbol-13-acetate (TPA)-induced mouse ear edema model was employed in $Ahr^{+/+}$ and Ahr'- mice. In this well-established model for in vivo skin inflammation, TPA induces an acute inflammatory reaction consisting of erythema, edema and polymorphonuclear leukocyte infiltration due to the release of prostaglandins, leukotrienes and pro-inflammatory cytokines by epidermal and innate immune cells. Ear swelling, a parameter for edema and inflammation, was strikingly reduced upon treatment with SGA360f and SGA388 in C57BL/6J (Ahr+/+) mice, similar to SGA360 (Figure 8A). Treatment in Ahr/mice was ineffective, indicating that the observed therapeutic effects were solely AHR-dependent (Figure 8B-D). Since TPA induces a neutrophilic inflammatory response, mouse ears were stained for the neutrophil marker Ly6q. In the dermis of $Ahr^{+/+}$ mice that were treated with SGA360f, less Ly6g positive cells were observed (a similar trend was seen for SGA388). In Ahr/- mice, SGA treatment did not reduce the number of neutrophils by TPA treatment (Figure 8E-F). Investigation into the expression of inflammatory signaling molecules by quantitative RT-PCR revealed most significant downregulation of Ptsq2 (COX2) and S100a9 by SGA360f and SGA388 in the TPA model (Figure 8G), which relate to the known SAhRM-activity of the parent compound SGA360 in this model [159].

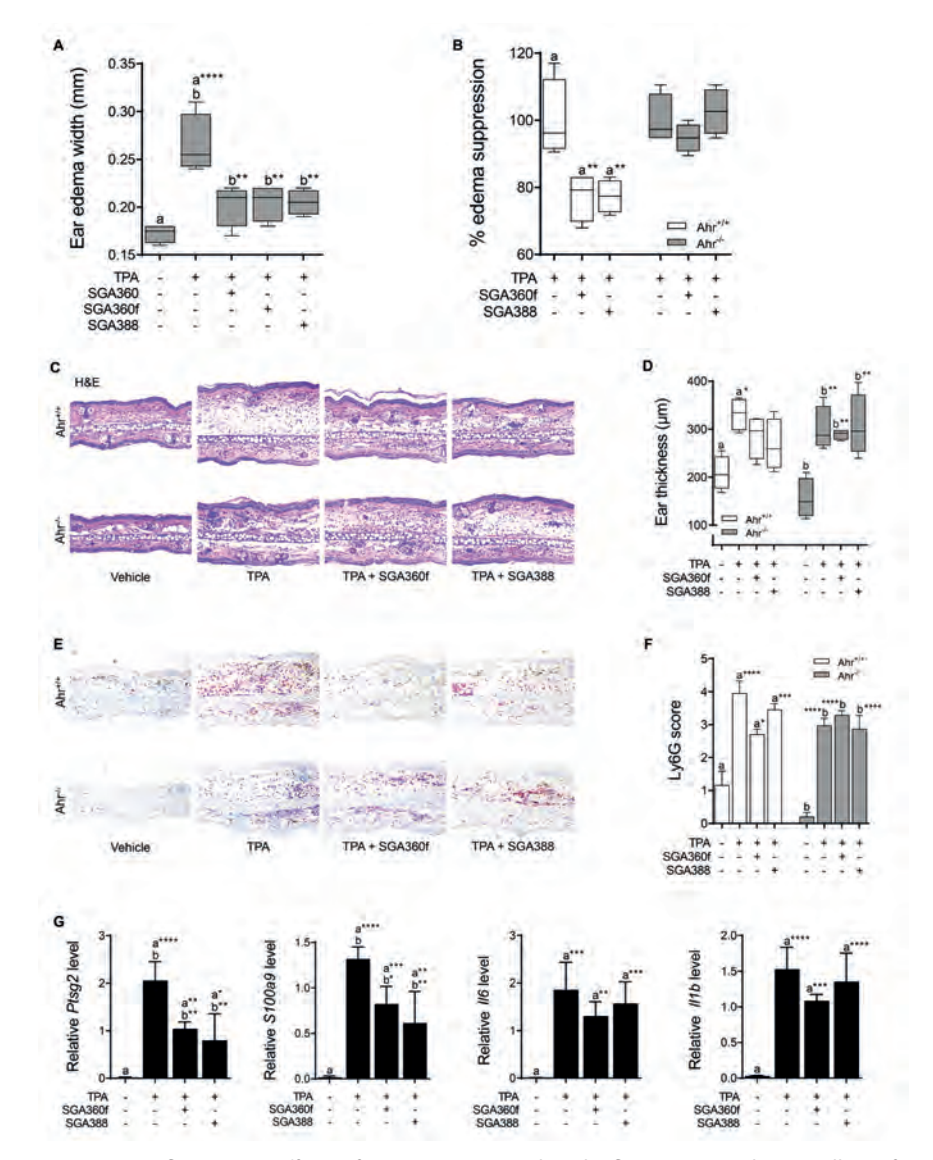


Figure 8. Anti-inflammatory effects of SGAs *in vivo*. **A)** Induced inflammation and ear swelling of TPA treated mice and the therapeutic effect after SGA treatment, N=4 mice per group. **B)** Percentage of edema suppression in $Ahr^{+/+}$ and $Ahr^{/-}$ mouse ears treated with TPA and SGA360f and SGA388 for 6 h, N=4 mice per group. **C)** H&E staining and **D)** microscopic measurement of ear thickness of $Ahr^{+/+}$ mouse ears stimulated with TPA, SGA360, SGA360f and SGA388, N=4. Ear thickness was measured at three locations of the total H&E image, and the average was calculated. **E)** The influx of peripheral neutrophils, monocytes and granulocytes is visualized by Ly6G marker staining in $Ahr^{+/+}$ and $Ahr^{-/-}$ mice. **F)** Semi-quantitative analysis (double-blinded by two independent investigators) of the Ly6G staining, N=4. Three images per slide were chosen as representative for the whole staining, after which the average score was calculated. **G)** Gene expression analysis for inflammation marker genes: *Ptgs2*, *s100a9*, *ll6* and *ll1b* in the mouse ears, N=4. * p < 0.05, ** p < 0.01, *** p < 0.001, **** p < 0.0001. Mean +/- SEM. Scale bar = 100 μm.

Discussion

Phenotypical outcomes upon AHR activation range from extreme toxicity to physiologically important processes and therapeutic effects. This spectrum of downstream effects depends on ligand affinity, receptor promiscuity, cell-specific transcriptional programs and the local tissue microenvironment. Our study provides compelling evidence of the possibility of fine-tuning the intricate balance between detrimental and beneficial receptor activation through lead optimization of the SAhRM molecule, SGA360. We hereby developed a novel AHR ligand class that is characterized by controlled agonist activity while maintaining AHR-dependent anti-inflammatory SAhRM activity. This is of particular importance in barrier organs such as the lung, gut, and skin where the AHR plays a pivotal role in barrier integrity maintenance. Here, treatment of inflammatory disorders by SAhRM only, could cause detrimental barrier defects due to blocked canonical AHR signaling that is required for epithelial differentiation. Chronic inflammatory diseases of barrier organs, including atopic dermatitis, psoriasis, inflammatory bowel disease or asthma may therefore specifically benefit from treatment with AHR modulators, such as SGA360f and SGA388, through combined targeting of the inflammatory process while fostering epithelial homeostasis and barrier function.

As a barrier and sensory organ, the skin is highly capable of sensing both the external and internal environment and reacting to chemical stimuli of exogenous, microbial, or endogenous origin [87, 178]. Virtually all skin cell types express the AHR [122, 157, 179, 180] and at high levels similar to cells of the lung and the gut [156, 181]. In the skin, the AHR can therefore fulfill a pivotal role in the regulation of skin integrity, the skin barrier and skin immunity [76, 122, 157, 169]. Targeting the AHR in skin diseases is more likely to have a positive outcome when compared to internal barrier organs given the possibility of obtaining only local effects, thus circumventing potential adverse effects due to systemic AHR ligands. The interest in topical treatment with AHR ligands was heightened after the finding that the therapeutic effects of coal tar are AHR-mediated [75]. Considering the appearance of coal tar (brown color, strong odor) and its complex chemical composition, including many potentially hazardous (polycyclic) aromatic hydrocarbons, single well-defined molecules that target the AHR would be preferable for therapeutic use. The first example of such a drug reaching the clinic is the natural agonist, Tapinarof [153]. The recent FDA approval for Tapinarof in psoriasis treatment, however, should not stop the development of alternative AHR ligands given the clear ligand-dependent biological effects downstream of AHR activation and hence the possibility for improving therapeutic efficacy whilst minimizing adverse effects. The SGA derivatives we describe here may have a favorable safety profile for topical administration given that they are relatively weak agonists resulting in very low levels of cytochrome P450 enzyme activity in keratinocytes. The recently proposed detrimental effects of sustained elevated CYP1A1 levels which could deplete natural AHR ligands present in the tissue [175], underscores the importance of low CYP1A1 enzymatic levels in keratinocytes after treatment with SGAs.

The synthesis of SGA360 was based on the structure of WAY-169916, which is a selective estrogen receptor modulator or partial ER agonist [182, 183]. WAY-169916 has been shown to exhibit anti-inflammatory activity through ER-mediated transrepression of NFkB transcriptional activity and attenuate inflammation in disease models [184-186]. We established that WAY-169916 exhibits partial AHR agonist activity as well and is capable of repressing the acute phase gene SAA1 in an AHR-dependent fashion [187]. Employing structure-activity analysis was used to generate WAY-169916 analogs that bind the AHR without activating the ER [159], studies were initiated to develop a compound that exhibited anti-inflammatory activity mediated through binding to the AHR and yet did not exhibit agonist activity. These compounds (e.g., SGA360) were designated selective Ah receptor modulators (SAhRM), a term originally proposed by Dr. Steve Safe's laboratory to characterize weak or partial AHR agonist that exhibited anti-carcinogenic activity [188]. SGA360mediated AHR binding and the subsequent anti-inflammatory effects [159, 187, 189, 190] suggests that in part, the anti-inflammatory activities of AHR activation are dissociated from canonical DRE-mediated transcription. However, the latter is vital when targeting skin barrier defects in inflammatory skin diseases, like AD and psoriasis, as the AHR/ARNT canonical pathway has a physiological role in driving the transcription of epidermal barrier genes [76]. Loss of canonical AHR signaling in our case through SAhRM activity by SGA360, indeed appeared to reinforce the disease-associated downregulation of terminal differentiation and could potentially worsen barrier defects in patients. Leveraging dissociated anti-inflammatory effects of SAhRMs while retaining residual canonical AHR signaling would provide dual efficacy regarding the beneficial suppression of inflammation combined with keratinocyte differentiation. It is likely that the retention of both aspects of AHR signaling associated with SAhRMs mirrors the non-pathological patterns of AHR activation and multi-faceted signaling elicited by endogenous AHR ligands.

Rapid alleviation of inflammation by SGAs in the TPA model illustrates a potential broad therapeutic applicability for the treatment of inflammatory dermatoses. TPA activates the protein kinase C pathway resulting in the elevated synthesis of potent eicosanoid chemoattractants such as prostaglandin E2 and leukotrienes from arachidonic acid through cyclooxygenase (COX) [191]. Lower levels of prostaglandins and leukotrienes resulting from COX2 inhibition may explain the decline in neutrophil influx and hence reduced inflammation by SGA treatment and provides a novel approach to the current knowledge on AHR-mediated therapeutic effects. SAhRMs may thus exert in part similar molecular effects as steroids in skin by lowering COX2 levels and reducing prostaglandin synthesis, as reported in lung epithelial cells [192]. However, in contrast to the negative sideeffects of corticosteroid use on the skin barrier [193], SAhRMs could improve skin barrier function through the AHR-mediated control of cornified envelope protein expression and lipid biosynthesis.

Besides the known differentiation-promoting effects of AHR agonist activity, we observed almost complete normalization of IL-4 mediated keratinocyte hyperproliferation by SGA derivatives. Expression of the AHR plays a role in normal epithelial proliferation, mostly directing pro-proliferative signaling [76, 124, 194], and anti-apoptotic effects [195], at least in cell lines derived from keratinocytes and in primary keratinocyte cultures. Our observation that keratinocyte hyperproliferation can already be counteracted by SGA360 and thus through SAhRM activity that lacks AHR agonist activity, suggests a potential AHR-independent mode of action, or implies the importance of non-canonical signaling routes. This could be of interest for the regulation of keratinocyte proliferation by SAhRMs in other hyperproliferative skin conditions, including psoriasis or malignancies where keratinocyte turnover is elevated and causing health problems and will be a subject for future investigations. Studies modeling other pro-inflammatory skin conditions such as psoriasis can furthermore identify commonly or distinctly regulated pathways by AHR signaling in skin and the molecular mechanisms that underpin the ambiguous effects of AHR signaling that are directed by the local tissue-microenvironment.

In conclusion, our lead optimization strategy provides key information on AHR SAhRM structure facilitating the clinically beneficial incomplete functional dissociation of AHR-mediated anti-inflammatory activity from overt and sustained initiation of canonical DRE-dependent transcription. SGA360f and SGA388 are identified as restricted AHR agonists effective in suppressing Th2 cytokine-mediated inflammation and restoring barrier function in a human 3D, full thickness model of atopic dermatitis. As such, SAhRMs mimic the action of currently available, FDAapproved AHR-driven therapeutics such as, Tapinarof and the old king coal (tar). These findings provide a novel avenue for the development of additional SAhRMs for the amelioration of hyperproliferative inflammatory skin diseases.

Materials and Methods

Animals. C57BL/6J mice were obtained from Jackson Laboratories (Bar Harbor, ME, USA), C57BL6/J Ahr+/- and Ahr/- were kindly provided by Dr Christopher Bradfield (University of Wisconsin-Madison). Mice were bred at Penn State University. All studies using mice were conducted with protocols approved under the auspices of The Pennsylvania State University Institutional Animal Care and Use Committee (IACUC).

Chemicals, laboratory chemicals and culture medium. All general buffers, culture media and supplements were purchased from major vendors including Sigma-Aldrich and Thermo Fisher Scientific (Gibco, Hyclone), unless stated otherwise.

Organic chemistry. For the synthesis of the SGA compounds utilized in this study all chemicals and solvents were purchased from major vendors. Anhydrous solvents were used as received. Reactions were carried out using dried glassware and under an atmosphere of nitrogen. Reaction progress was monitored with analytical thinlayer chromatography (TLC) on aluminum-backed precoated silica gel 60 F254 plates (E. Merck KG, Darmstadt, Germany), Column chromatography was carried out using silica gel 60 (230–400 mesh, E. Merck KG) with the solvent system indicated in the individual procedures. NMR spectra were recorded using a Bruker Avance 500 MHz spectrometer. Chemical shifts (d) were reported in parts per million downfield from the internal standard. The signals are quoted as s (singlet), d (doublet), t (triplet), m (multiplet). High-resolution mass spectra (HRMS) were determined in 5600 (QTOF) TripleTOF using a Duospray™ ion source (Sciex, Framingham, MA, USA). The capillary voltage was set at 5.5 kV in positive ion mode with a declustering potential of 80 V. The mass spectrometer was scanned from 50 to 1000 m/z in operating mode with a 250 ms scan from 50 to 1000 m/z. Melting points were determined on a Fischer–Johns melting point apparatus and are uncorrected.

Cell based AHR ligand binding competition assay. 2-azido-3-[1251]iodo-7,8dibromodibenzo-p-dioxin (photoaffinity ligand) was synthesized as previously described [196]. Mouse keratinocytes in 12 well plates were treated with either 10 mM of the indicated SGA compound or 10 nM TCDD in the presence of 1.0 pmol of photoaffinity ligand for 1 h. Dr. Steve Safe (Texas A&M University) kindly provided 2,3,7,8-tetrachlorodibenzo-p-dioxin (TCDD). Cells were washed with Dulbecco's phosphate-buffered saline, then exposed to UV light from two 15-watt lamps (UV products, >302 nM) at a distance of 8 cm for 4 min. Cells were homogenized in lysis buffer containing 25 mM MOPS, 2 mM EDTA, 0.02%, 20 mM sodium molybdate, pH 7.5 + 10% glycerol using a Dura-Grind tissue grinder (Wheaton Instruments,

Millville, NJ, USA). Samples were then subjected to SDS-PAGE, transferred to PVDF membrane and the amount of radioactivity determined by phosphor imaging. This data was normalized to ß-actin quantitated on the PVDF membrane using a mouse anti-actin antibody (Santa Cruz Biotechnology, Inc., Dallas, TX, USA), a biotinylated goat antibody mouse secondary antibody (Jackson ImmunoResearch, West Grove, PA, USA) and streptavidin [190].

Cell based luciferase reporter assay. The stable dioxin responsive element (DRE)driven luciferase reporter cell lines H1L1.1c2 (Hepa 1.1) and HepG2(40/6) were kindly provided by the late Mike Denison (University of CA, Davis) and generated in the Perdew laboratory, respectively [191, 197]. Both lines were maintained in aMEM (Sigma) supplemented with 10% (v/v) fetal bovine serum (Hyclone) and antibiotic cocktail comprising 100 IU/mL penicillin and 0.1 mg/mL streptomycin (Sigma) and cultured at 37°C in a humidified 5% CO₂/95% air atmosphere. Cells were treated with indicated AHR ligands for 4 h and the carrier solvent DMSO was present at 0.1% (v/v) in each assay. Cells were lysed in 0.2 mL lysis buffer [25 mM Tris-phosphate pH 7.4, 2 mM DTT, 2 mM CDTA, 10% (v/v) glycerol and 1% (v/v) Triton X-100] and subjected to a single freeze-thaw cycle. Luciferase reporter activity was quantified utilizing the Promega Luciferase Assay system (Madison, WI, USA). Briefly, 80 mL reconstituted luciferase substrate was added to 20 ml cell lysate, mixed and relative luciferase units were determined using a luminometer.

Isolation and culture of mouse primary keratinocytes and fibroblasts. Primary $Ahr^{+/+}$ keratinocyte and fibroblast cultures were obtained from neonatal (1-4 days old, hairless) littermates derived from C57BL6/J matings, as previously described [198]. Briefly, mice were euthanized by CO₂-asphyxiation, soaked in Betadine, washed twice with 70% (v/v) ethanol and kept on ice. Aseptically, limbs and tail were removed, and the skin peeled away from a ventral cranial-caudal incision. Skins were stored dermisside down at 4°C in culture plates. Skins (epidermis-side up) were floated on 0.25% (w/v) trypsin overnight at 4°C. Using forceps, the epidermal and dermal layers were separated with the dermal layer retained for subsequent fibroblast isolation. The epidermis was diced and stirred into calcium-free Eagle's minimum essential medium (EMEM; Gibco) supplemented with 1X non-essential amino acids, 2 mM L-glutamine, 8% (v/v) Chelex-Ca²⁺-depleted FBS, and 100 IU/ml penicillin and 0.1 mg/ml streptomycin. Prior to addition to cells, the calcium concentration of the media was adjusted to 1.4 mM. Dissociated keratinocytes were filtered through 100 mm nylon cell strainer and seeded at a density of 2-4x10⁵ cells/cm² in EMEM media with calcium adjusted to 0.2 mM. After 24 h incubation, keratinocytes were washed with Ca²⁺/Mg²⁺-free PBS and EMEM media with calcium adjusted to 0.05 mM was added.

Dermal fibroblasts were isolated from the dermal layer following keratinocyte isolation. Briefly, the dermal layer was incubated in media supplemented with 0.35% (w/v) collagenase I. Dermal layers were combined, diced and incubated at 37°C for 30 min while shaking, 200 U/dermis DNase were added from a 100X stock prepared in sterile PBS. After swirling to mix, DMEM supplemented with 10% (v/v) FBS and antibiotic cocktail comprising 100 IU/ml penicillin and 0.1 mg/ml streptomycin were added. The cell suspensions were incubated a room temperature for further 10 min without shaking. Cells were filtered through a 100 mm nylon cell strainer and centrifuged at 200 x g for 5 min. Cell pellets were suspended in DMEM supplemented with 10% (v/v) FBS and antibiotic cocktail and centrifuged at 100 x g for 5 min. Fibroblast-containing supernatants were transferred to fresh tubes and recentrifuged at 100 x g for 5 min. Fibroblast were seeded into plates and cultured at 37°C in a humidified 5% air/95% CO₂ atmosphere. Primary Ahr -/- keratinocyte and fibroblast cultures were obtained from neonatal littermates derived from female Ahr -/+ x male Ahr -/- matings. Littermates were genotyped regarding Ahr status from tail clip genomic DNA isolated using the Wizard SV genomic isolation kit (Promega) and subsequent PCR using 5'CAGTGGGAATAAGGCAAGAGT-3' and 5'-AGGGAGATGAAGTATGTATGTA-3' primers. Following Ahr genotype verification, primary keratinocyte and fibroblast were isolated as described for Ahr +/+ neonates. In all cases, primary keratinocytes and dermal fibroblast cultures were exposed to indicated AHR ligands after initial seeding and not passaged prior to treatment.

Isolation and culture of primary human keratinocytes. 3T3-J2 mouse embryonic fibroblast cells (kind gift from Dr. J. Rheinwald, Harvard University) were cultured in Dulbecco's modified Eagle's medium (DMEM) supplemented with 1% (v/v) penicillin/streptomycin and 10% (v/v) fetal bovine serum. Human surplus skin was obtained from plastic surgery in line with the principles and guidelines of the Declaration of Helsinki. Keratinocytes were cultured in medium (2:1 [v/v] DMEM:Ham's F12 (both Gibco) supplemented with 10% (v/v) fetal bovine serum (Hyclone), I-glutamine (4 mM), 1% penicillin/streptomycin, adenine (24.3 µg/mL), insulin (5 µg/mL), hydrocortisone (0.4 µg/mL), triiodothyronine (1.36 ng/mL), and cholera toxin (1-11 U/mL) in the presence of irradiated 3T3-J2 feeder cells. After 3 days, the medium was replaced by medium containing epidermal growth factor (EGF, 10 ng/mL) and refreshed every 2-3 days. At 90-100% confluency, feeder cell remnants were removed by EDTA (0.05 mM) and subsequent trypsinization with 0.05% (v/v) trypsin-EDTA after which the keratinocytes were harvested and stored in liquid nitrogen. Monolayer keratinocytes were cultured in 24-well plates at 37 °C with 5% CO₂ using keratinocyte growth medium with required growth factors and supplements (KGM, Lonza, Basel, Switzerland) without antibiotics until reaching

100% confluency. The keratinocytes were stimulated with TCDD (10 nM) and the SGA compounds using different concentrations (ranging from 0.1 to 10 µM) and harvested at various time points of exposure (8 h to 72 h) as indicated. The AHR antagonist GNF-351 (Sigma, 500 nM or 2 µM) was incubated for 30 minutes prior to the addition of TCDD (10 nM) or SGA388 (1 or 10 µM). For Th2 cytokine stimulation, keratinocytes were grown to 100% confluency and exposed to IL-4 and IL-13 (both 50 ng/mL, PeproTech, Cranbury, NJ, USA) in the presence or absence of AHR ligands for a total period of 48 h, including a restimulation at 24 h.

Quantitation of mRNA levels. For murine cells, total RNA was isolated using TRI Reagent (Sigma-Aldrich), then converted to cDNA using a High-Capacity cDNA Reverse Transcription Kit (Applied Biosystems, Thermo Fisher Scientific). Quantitative real-time PCR was conducted using PerfeCTa SYBR Green Supermix for iQ (Quanta Biosciences, Beverly, MA) on a CFX Connect Real-Time PCR Detection System (Bio-Rad, Hercules, CA, USA). Sequences of quantitative PCR primers for murine gene expression are listed in Table 1, using the L31a as housekeeping gene.

For the primary human keratinocytes, RNA was isolated with the Tissue Total RNA Kit (Favorgen, Vienna, Austria) or the E.Z.N.A. Total RNA Kit I (OMEGA Bio-Tek, Norcross, GA, USA). RNA was treated with DNAsel (Invitrogen, Waltham, MA, USA) and used for cDNA synthesis using SuperScript IV VILO Master Mix (Invitrogen) or UltraScript 2.0 (PCR Biosystems, London, UK). RT-qPCR analysis was performed using SYBR Green (Bio-Rad). Target gene expression was normalized to the expression of the housekeeping gene human acidic ribosomal phosphoprotein P0 (RPLP0). The $\Delta\Delta$ Ct method was used to calculate relative mRNA expression levels. Primer sequences (Biolegio, Nijmegen, The Netherlands) for human genes are depicted in Table 2.

CYP1A1 activity assay. CYP1A1 activity was assessed utilizing the P450-Glo[™] CYP1A1 assay following the manufacturer's instructions (Promega). Primary mouse keratinocytes were cultured in a 12-well plate in EMEM media with calcium adjusted to 0.2 mM for 24 h, then treated with indicated AHR ligands for 36 h prior to the addition of Luc-CEE at 1:100 v/v for 4 h. Medium was removed and 150 mL of lysis buffer was added to the cells, chemiluminescence was determined by mixing 50 mL of cell lysate with 50 mL of luciferase substrate and measured in a luminometer [165]. Human primary keratinocytes were cultured until confluency was reached and treated with indicated AHR ligands for 8, 16, 24, 48 and 72h (refreshed every 24h), prior to the addition of Luc-CEE at 1:75 for 3 h.

Table 1. Primers Used in Real-Time PCR for murine genes

Gene	Forward Primer (5'-3')	Reverse Complement Primer (5'-3')				
Control Gene						
Rpl13a	TTCGGCTGAAGCCTACCAGAAAGT	GCATCTTGGCCTTTTTCCGTT				
Known Ta	arget Genes					
Ahrr	CAGAAGCGGAGGCTTACCAT	CTCTGTATTGAGGCGGTCCC				
Cyp1a1	CTCTTCCCTGGATGCCTTCAA	GGATGTGGCCCTTCTCAAATG				
Cyp1b1	GCTAGCCAGCAGTGTGATGATATT	GGTTAGCCTTGAAATTGCACTGAT				
Epiderma	al Differentiation Genes					
Dsc1	GATGGCTATGCCCCAGACTAC	TATGGCAGTCACTTGTCCCAC				
Flg	GGACAACTACAGGCAGTCTTGAAGA	CATTTGCATGAAGACTTCAGCG				
Hrnr	TCTCAACGGTTTGGATCTGGCTCA	TGTTGACTGCCTTCTGTCTGTCCA				
Invol	CCCTCCTGTGAGTTTGTTTGGTCT	ACCTGGCATTGTGTAGGATGTGGA				
Krt1	ACATGCAAGACCTGGTGGAGGAGT	TGGTCACGAACTCATTCTCTGCGT				
Lor	TGGGTTGTGGAAAGACCTCTGGT	AGCTGGAACCACCTCCATAGGAA				
Inflamma	atory Genes					
Cd14	TTCAGAATCTACCGACCATGGAGC	CAATTGAAAGCGCTGGACCAA				
Cox2	CTGACCCCAAGGCTCAAAT	ACCTCTCCACCAATGACCTGA				
Cxcl1	GCTGGGATTCACCTCAAGAA	TCTCCGTTACTTGGGGACAC				
Cxcl2	AGACAGAAGTCATAGCCACTCTCAAG	CCTCCTTTCCAGGTCAGTTAGC				
Cxcl5	TGCCCTACGGTGGAAGTCAT	AGCTTTCTTTTGTCACTGCCC				
II1b	AGCTTCCTTGTGCAAGTGTCT	GACAGCCCAGGTCAAAGGTT				
S100a9	TCATCGACACCCTCCATCAA	TTACTTCCCACAGCCTTTGC				

Table 2. Primers Used in Real-Time PCR for human genes

Gene	Forward Primer (5'-3')	Reverse Complement Primer (5'-3')				
Housekeeping Gene						
RPLP0	CACCATTGAAATCCTGAGTGATGT	TGACCAGCCCAAAGGAGAAG				
AHR targ	et Genes					
CYP1A1	CTGGAGACCTTCCGACACTCTT	GTAAAAGCCTTTCAAACTTGTGTCTCT				
CYP1B1	TGGCTGCTCCTCTTCAC	CCACGACCTGATCCAATTCTG				
Epiderma	al Differentiation Genes					
FLG	ACTTCACTGAGTTTCTTCTGATGGTATT	TCCAGACTTGAGGGTCTTTTTCTG				
HRNR	TACAAGGCGTCATCACTGTCATC	ATCTGGATCGTTTGGATTCTTCAG				
IVL	ACTTATTTCGGGTCCGCTAGGT	GAGACATGTAGAGGGACAGAGTCAAG				
LOR	AGGTTAAGACATGAAGGATTTGCAA	GGCACCGATGGGCTTAGAG				
KRT10	TGGTTCAATGAAAAGAGCAAGGA	GGGATTGTTTCAAGGCCAGTT				
Inflamma	atory Genes					
CCL2	GAAGAATCACCAGCAGCAAGTG	GATCTCCTTGGCCACAATGG				
CCL26	CCTGGGTGCGAAGCTATGAA	TTGCCTCTTTTGGTAGTGAATATCAC				

Lactate Dehydrogenase (LDH) Assay. The supernatant of monolayer cultures that were stimulated for 24 h with SGA derivatives (10 µM) and TCDD (10 nM) was collected, after which LDH activity was measured using a cytotoxicity detection kit (Roche, Basel, Switzerland) according to the manufacturer's protocol. Absorbance was read at 490 nm with a microplate reader. Keratinocytes treated with 1% Triton X-100 in KGM were used as a positive control for 100% cell death.

Ames mutagenicity assay. Genotoxicity was evaluated with a mutagenicity assay according to the manufacturers' protocol (Xenometrix, Ames II Microplate Format Mutagenicity Assay, Allschwil, Switzerland), Briefly, Salmonella Typhimurium strains TA98 (frameshift mutations) and TAMix (base-pair substitutions) were used with or without metabolic activation by the liver fraction S9. 1% DMSO, carrier solvent, was used as a negative control and 2-nitrofluorene and 4-nitroguinoline N-oxide (assay without S9) and 2-aminoanthracene (assay with S9) as positive controls. SGA360, SGA360f and SGA388 were examined at three concentrations (250, 125 and 62.5 µg/mL) in duplicate with a final DMSO concentration of 1%. The plates were incubated at 37°C and the number of wells with a purple to yellow color shift (indicative of bacterial growth) were counted after 48 h. Calculations were based on the 'fold induction over baseline' (according to the manufacturers' specifications), which is the ratio of the mean number of positive wells for the dose concentration divided by the baseline. The baseline is obtained positive wells for the dose concentration divided by the baseline (baseline = mean number of positive wells of the solvent control + 1*SD).

3D human epidermal equivalents and 3D atopic dermatitis (AD)-like model.

HEEs were generated using 24-well cell culture inserts (ThinCert, Greiner Bio-One or Nunc, Thermo Fisher Scientific) coated with rat tail collagen (100 µg/mL, Sigma) at 4°C for 1 h prior to seeding of 100.000–150.000 primary human keratinocytes in 100–150 uL CnT-prime medium (CELLnTEC, Bern, Switzerland). After 48 h, cell culture medium was switched to 3D differentiation medium for another 24 h, consisting of 60% CnT-Prime 3D Barrier medium (CELLnTEC) and 40% High Glucose Dulbecco's Modified Eagle's Medium. Thereafter, the HEEs were lifted to the air-liquid interface (ALI), with the differentiation medium refreshed every other day. In the normal skin model, HEEs were treated with the SGA derivatives (10 µM) and TCDD (10 nM) at day 5 of the ALI for 72 h (refreshed after 48 h). To generate an atopic dermatitis (AD)like (AD-HEE) model, HEEs were used in combination with the disease-associated cytokine Interleukin-4 (IL-4). AD-HEEs were first stimulated with IL-4 (10 ng/mL, PeproTech (supplemented with 0.05% bovine serum albumin, BSA (Sigma-Aldrich)) at day 4 of the ALI. After 24 h of disease initiation, HEEs were co-stimulated with the SGA derivatives (SGA360 (10 μM), SGA360f (10 μM) and SGA388 (10 μM and a concentration series)) and TCDD (10 nM) for 72 h (re-stimulation after 48 h). At day 8 of the ALI, HEEs were harvested and processed for RNA isolation (qPCR and RNA sequencing) and immunohistochemical analysis.

In vivo inflammation model. Dermal ear inflammation was induced in 8-10-weekold C57BL6/J mice through topical application of 1.5 mg 12-O-tetradecanoylphorbol-13-acetate (TPA, Sigma), administered to each ear as a 20 mL solution comprising 2 ml 0.75 mg/mL TPA (solubilized in DMSO), 2 mL DMSO and 16 mL acetone. AHR ligands were co-administered with TPA by substitution of DMSO with 2 mL indicated AHR ligand solubilized in DMSO at 15 mg/mL i.e., 30 mg/ear. Ear edema was assessed 6 h post-application and quantified using digital calipers. Mice were euthanized through carbon dioxide-mediated asphyxiation, ears removed and snap frozen in liquid nitrogen for subsequent RNA isolation and fixed in formalin for routine histology.

Immunohistochemistry. Formalin fixed-paraffin embedded HEEs and mouse ears were stained with hematoxylin and eosin (Sigma-Aldrich) or processed for immunohistochemistry using an indirect immunoperoxidase technique with avidin-biotin complex enhancement (Vectastain, Vector Laboratories, Newark, CA, USA). Detailed information on antibodies used in the study are provided in Table 3.

RNA sequencing and bioinformatics. 3D AD-like HEEs (N=3 donors) were generated and treated with SGA ligands and TCDD as described above. After total RNA isolation, RNA libraries for sequencing were generated using KAPA HyperPrep library prep kit (Roche) following manufacturer's protocol. The quality of generated libraries were checked using a Bioanalyzer (Agilent, Santa Clara, CA, USA) and KAPA library quantification (Roche). RNA libraries were sequenced on an Illumina sequencer (10X). Sequencing reads were aligned to human genome assembly hg19 (NCBI version 37) using STAR 2.5.0a [200] with default options. Data frames were generated using DEseq2 [201]. To correct for donor variation, Limma correction was applied. For PCA analysis, the top 500 genes with highest variance were included for analysis. PCA plots were generated in R by prcomp and visualized using ggplot2 package. For heatmaps, pairwise comparison of treatments to control or IL-4 only were performed. Genes were included in the analysis if differential expression fold change was lower than -1.5 or higher than 1.5 with p-value <0.05. Heatmaps were generated using z-values of included genes using ComplexHeatmap [202] with k-means clustering. GO-term analysis and KEGG pathway analysis were performed using clusterProfiler [203].

Table 3. Antibodies used for immunohistochemistry of tissues

Protein	Antibody (clone)	Dilution	Manufacturer	Antigen retrieval			
AHR target							
CYP1A1	B-4	1:50	Santa Cruz				
Differentiation							
FLG IVL LOR	FLG01 Mon150 145P-100	1:100 1:20 1:4000	Thermo Fisher van Duijnhoven et al.[204] Covance Inc.	Citrate buffer 95°C Citrate buffer 95°C			
Proliferation							
Ki67 Ki67	MIB-1 SP-6	1:50 1:200 (o/n, 4°C)	DAKO Abcam	Citrate buffer 95°C Citrate buffer 95°C			
Immune cells							
Ly6G	RB6-8C5	1:1000 (o/n, 4°C)	Abcam	Citrate buffer 95°C			

o/n = overnight

Quantification of proliferation (Ki-67 expression) in HEEs. Image acquisition of Ki-67 staining was performed by a ZEISS (Breda, The Netherlands) Axio Imager equipped with a ZEISS Axiocam 105 color Digital Camera and a 20× objective. Two images per slide were chosen as representative for the whole culture and stored in CZI format. The images were analyzed with the cell image analysis software CellProfiler [205]. A software pipeline for Ki-67 analysis was created (available up-on request) and GraphPad Prism 9.0 was used for statistical analysis and visualization of the data. The quantified data is shown as Ki-67 positive nuclei per millimeter length of the epidermis. To determine statistical significance between the multiple groups (N=5 groups) the Friedman test (paired nonparametric test) was performed. If significant, Dunn's multiple comparison post hoc test was used (*p<0.05; **p< 0.01).

Statistical analysis. Statistical significance (GraphPad Prism) between multiple groups (N≥3 groups) was determined by one-way analysis of variance (ANOVA; if there are missing values, mixed effects model for repeated measures data was used) followed by Tukey's multiple comparison post hoc test. For the RT-qPCR gene expression analysis, the raw ΔCt values were used. Each human cell culture experiment (monolayer or organotypic HEE) includes biological donor replicates, unless otherwise specified in the figure legend.

All data is displayed as the mean +/- SEM, and the level of significance is signified by: *p<0.05; **p< 0.01; ***p< 0.001; or ****p< 0.0001, and if appropriate, between experimental conditions indicated by a, b, c or d.

Acknowledgments

The research was funded in part by the National Institutes of Health (Grants ES004869, ES028244 (GHP), Dutch Research Council (VENI grant 91616054) (EHB), and Top sector Life Science & Health, The Netherlands (LSHM13013-EA) (EHB). The authors declare no competing financial interests. Sequencing was performed by the Radboud University sequencing facility. We thank the late Dr. Michael Denison for kindly providing H1L1.1c2 cells. We thank Marcia H. Perdew for excellent editorial assistance and Diana Rodijk-Olthuis for technical assistance. The content is solely the responsibility of the authors and does not necessarily represent the official views of the National Institutes of Health.

Data availability statement

The data from the RNA sequencing analysis can be found under GSE212539.

Author contributions

Funding acquisition and conceptualization: EvdB, GHP, SGA

Data curation: GR, NvdB, JPHS, JGAS, KJS

Formal Analysis: GR, NvdB, JPHS, IvV, KJS, IAM, KG, GEM Investigation and validation: GR, NvdB, JPHS, IvV, KJS

Project administration: GR, EvdB, GHP, SGA

Software: JGAS

Supervision: EvdB, GHP, IAM, SGA

Visualization: GR, NvdB, IvV

Writing – original draft: GR, EvdB, NvdB, GHP

Writing - review & editing: all authors



Chapter 3

Carboxamide derivatives are potential therapeutic AHR ligands for restoring IL-4 mediated repression of epidermal differentiation proteins

Gijs Rikken¹, Noa J.M. van den Brink¹, Ivonne M.J.J. van Vlijmen-Willems¹, Piet E.J. van Erp¹, Lars Pettersson², Jos P.H. Smits^{1,†} and Ellen H. van den Bogaard^{1,*,†}

¹ Department of Dermatology, Radboud Institute for Molecular Life Sciences (RIMLS), Radboud University Nijmegen Medical Center (Radboudumc), 6525 GA, Nijmegen, The Netherlands

² Immunahr AB, Prästasvängen 21, 224 80 Lund, Sweden

^{*} Correspondence: ellen.vandenbogaard@radboudumc.nl; Tel.: +31-24-3614093

[†] These authors contributed equally to this work.

Abstract

Atopic dermatitis (AD) is a common T-helper 2 (Th2) lymphocyte-mediated chronic inflammatory skin disease characterized by disturbed epidermal differentiation (e.g., filaggrin (FLG) expression) and diminished skin barrier function. Therapeutics targeting the aryl hydrocarbon receptor (AHR), like coal tar and tapinarof, are effective in AD, yet new receptor ligands with improved potency or bioavailability are in demand to expand the AHR-targeting therapeutic arsenal. We found that carboxamide derivatives from laquinimod, tasquinimod, and roquinimex can activate AHR signaling at low nanomolar concentrations. Tasquinimod derivative (IMA-06504) and its prodrug (IMA-07101) provided full agonist activity and were most effective to induce FLG and other epidermal differentiation proteins, and counteracted IL-4 mediated repression of terminal differentiation. Partial agonist activity by other derivatives was less efficacious. The previously reported beneficial safety profile of these novel small molecules, and the herein reported therapeutic potential of specific carboxamide derivatives, provides a solid rationale for further preclinical assertation.

Introduction

During epidermal differentiation, multiple structural proteins are expressed in the last living cell layer, the stratum granulosum. Amongst others, filament aggregating protein (filaggrin), encoded by the FLG gene, is processed into the cornified envelope, an insoluble network consisting of the debris of keratinocytes corneocytes—that are tightly crosslinked and imbedded in a matrix of lipid components ultimately forming the physical barrier of the skin: the stratum corneum. Disturbed epidermal differentiation and skin barrier function loss are key hallmarks of common chronic inflammatory skin diseases like atopic dermatitis (AD) and psoriasis (Pso). The epidermal differentiation process is affected by the disease-specific cytokine milieu (the Th2-cytokines in AD (e.g., IL-4) or the Th1/ Th17 cytokines in Pso), or due to genetic predisposition mostly associated to AD (e.g., FLG loss-of-function mutations [206, 207], FLG copy number variation [42], hornerin (HRNR)- Single-Nucleotide Polymorphism (SNP) [208, 209], small prolinerich protein 3 (SPRR3) [210]. Most therapeutic strategies are aimed at general or targeted immunosuppression combined with indifferent skin moisturizing emollients. However, the direct targeting of the epidermal differentiation process in combination with immunomodulatory effects could be an attractive therapeutic avenue by killing two birds with one stone.

Evidence for such effective therapeutics came from our studies on the molecular mechanism of coal tar. Coal tar is a viscous liquid that is obtained by burning coal and is thought to consist of at least 10,000 chemicals of which many are characterized as polycyclic aromatic hydrocarbons (PAHs). Although topical application of coal tar is an ancient treatment option for AD and Pso, its exact therapeutic mechanism of action has long been unknown, until recently. PAHs in coal tar activate the aryl hydrocarbon receptor (AHR) in keratinocytes, thereby counteracting the keratinocyte activation towards AD-related interleukins and restoring the expression levels of affected differentiation proteins, including that of FLG [75]. In addition, genes encoding antimicrobial peptides are upregulated which together with restored differentiation capability and reconstituted skin barrier properties are thought to contribute to dampening of the inflammatory processes in skin [77].

The AHR is a highly conserved receptor and member of the family of basic helixloop-helix transcription factors, that can be activated by a wide variety of both exogenous and endogenous ligands. Dioxins are a group of chemicals that are considered organic pollutants. TCDD (2,3,7,8-tetrachlorodibenzo-p-dioxin), one of the most widely used polychlorinated dioxins and considered an AHR model ligand, is often used to study AHR signaling in epidermal keratinocytes [171, 211]. As TCDD is highly toxic with prolonged half-life of several years, dioxins such as TCDD are not suited for therapeutic purposes. Short-lived AHR ligands include UVinduced endogenous tryptophan metabolites [97] (hence the postulated role for AHR-mediated therapeutic effects of UV therapy in Pso). Other metabolites can be formed by members of the skin's microbiome, and dietary plant constituents, as well as several pharmaceutics [98, 99, 212, 213] . Upon activation, AHR signaling is known to regulate a plethora of cellular processes, e.g., embryonic development [119], keratinocyte proliferation and differentiation [76], epidermal barrier formation [141, 212], immune cell development [145], angiogenesis [214], and many more [118-120, 141, 145, 215, 216]. However, studies also report contradicting outcomes depending on the tissue and disease context [122], and AHR ligand promiscuity has long been a subject of research [157].

Ever since the working mechanism of coal tar via AHR was elucidated, a search for novel AHR targeting therapeutics has been ongoing. This has led to the development of tapinarof, a natural AHR ligand that is currently in Phase 3 trials as a topical drug for AD and Pso [153, 217]. However, other immunomodulatory molecules that are investigated in clinical trials for different indications, such as quinoline-3-carboxamide derivatives, also act on the AHR signaling pathway [218]. Laguinimod (LAQ) targets the AHR and is effective in alleviating disease symptoms in experimental models of multiple sclerosis and Huntington's disease [219] and reduces IL-17 levels [220, 221]. Roquinimex (ROQ, the first clinical compound in the series) and tasquinimod (TASQ) have been investigated being potential immunomodulating drugs effective in cancer treatment and in autoimmune diseases. Interestingly, ROQ was found effective against Pso in two patients that were included in a phase 2 clinical renal cell carcinoma trial [222]. Although LAQ, TASQ and ROQ may lead to AHR activation, they do not activate AHR signaling in their original form, Instead, intracellular metabolism generates potent N-dealkylated metabolites that are capable of AHR binding, as previously described in the patent application [223]. These N-dealkylated compounds have been tested in toxicity studies in vitro [224] and as diacetyl prodrugs in vivo [225] at high doses with minor signs of adverse effects. Albeit the structural similarity to TCDD and shared theoretical receptor binding modes [224], these carboxamide derivatives are considered less metabolically resistant as compared to TCDD. The pharmacokinetic clearance of AHR ligands would be important to mitigate the adverse effects of sustained AHR signaling.

In this study, carboxamide derivatives from LAQ, TASQ and ROQ were analyzed for their AHR activating potential in human keratinocytes and in human epidermal

models. Primary read out was the expression level of epidermal differentiation genes and proteins. In addition, the ability to rescue deprived FLG expression, and other important epidermal barrier proteins in AD-like organotypic skin models, was investigated to identify new drug candidates for further preclinical testing.

Results

Structure of IMA-compounds

LAQ and TASQ are both metabolized by CYP3A4 (N-dealkylation) to form the AHRactive metabolites IMA-06201 and IMA-06504 in low concentrations (Figure 1A,B, Supplemental Table S1). These AHR-active compounds have extremely low aqueous solubility and are therefore not appropriate for in vivo or clinical use. Even though prodrugs IMA-08401 and IMA-07101 also have low aqueous solubility, they can easily be formulated (e.g., PEG-400) [225]. Furthermore, the in vivo hydrolysis of the prodrug IMA-08401 results in higher levels of IMA-06201 than corresponding levels from LAQ metabolism (unpublished). Analogously to IMA-06201 and IMA-06504, compound IMA-05101 is an AHR agonist and a metabolite of the clinical compound ROQ. IMA-01403 was synthesized by blocking the IMA-05101 4-OH with a benzyl group, which adds extra bulk and disrupts internal hydrogen bonding, expected to severely reduce the activity of the compound (Figure 1C, Supplemental Table S1).

IMA-compounds induce AHR activity in reporter cell line and primary keratinocyte

First, all newly synthesized derivatives were screened for AHR activating potential using the established human HepG2 (40/6) reporter cell line [191]. LAQ was used for comparison being a parent compound, 2,3,7,8-Tetrachlorodibenzo-p-Dioxin (TCDD) was included as a full AHR agonist at a saturating dose of 10 nM. All metabolites and prodrugs derived from LAQ, TASQ, and ROQ were able to activate AHR signaling in a clear dose dependent manner, maximally leading to 110-145% of the TCDD response. Blocking the -OH group in IMA-01403 indeed reduced the agonist activity (Figure 2A).

Next, we subjected primary human keratinocyte monolayer cultures to all derivatives. Again, clear dose dependent gene expression levels of AHR target genes, cytochrome P450 1A1 (CYP1A1) and 1B1 (CYP1B1) were observed (Figure 2B, Supplemental Figure S1A). Prodrug IMA-07101 and its active metabolite IMA-06504 (from TASQ) and prodrug IMA-08401 (from LAQ) exhibited saturated responses such as those seen after TCDD exposure.

AHRR gene expression levels indicate the activation of a negative control feedback loop to downscale prolonged AHR activation, which was most evident for TCDD and the TASQ derivatives (Supplemental Figure 1B). Only CYP1A1 mRNA expression levels reaching a 1000-fold change resulted in significantly induced enzymatic CYP1A1 activity, as observed for TCDD, IMA-06504, and IMA-07101 (all at 10 nM) (Figure 2C). Cell viability was unaffected in all cell cultures as lactate dehydrogenase (LDH) levels were comparable to control (unstimulated) keratinocyte cultures (Figure 2D)

Figure 1. Structure of IMA-compounds. **(A)** Laquinimod (LAQ) is metabolized (N-dealkylation) to form the AHR-active metabolite IMA-06201. Hydrolysis of the prodrug IMA-08401 also forms the IMA-06201 derivative. **(B)** Tasquinimod (TASQ), its AHR-active metabolite IMA-06504, and the prodrug IMA-07101. **(C)** Roquinimex (ROQ), its AHR-active metabolite IMA-05101, and the 4-O-benzyl derivative IMA-01403.

.

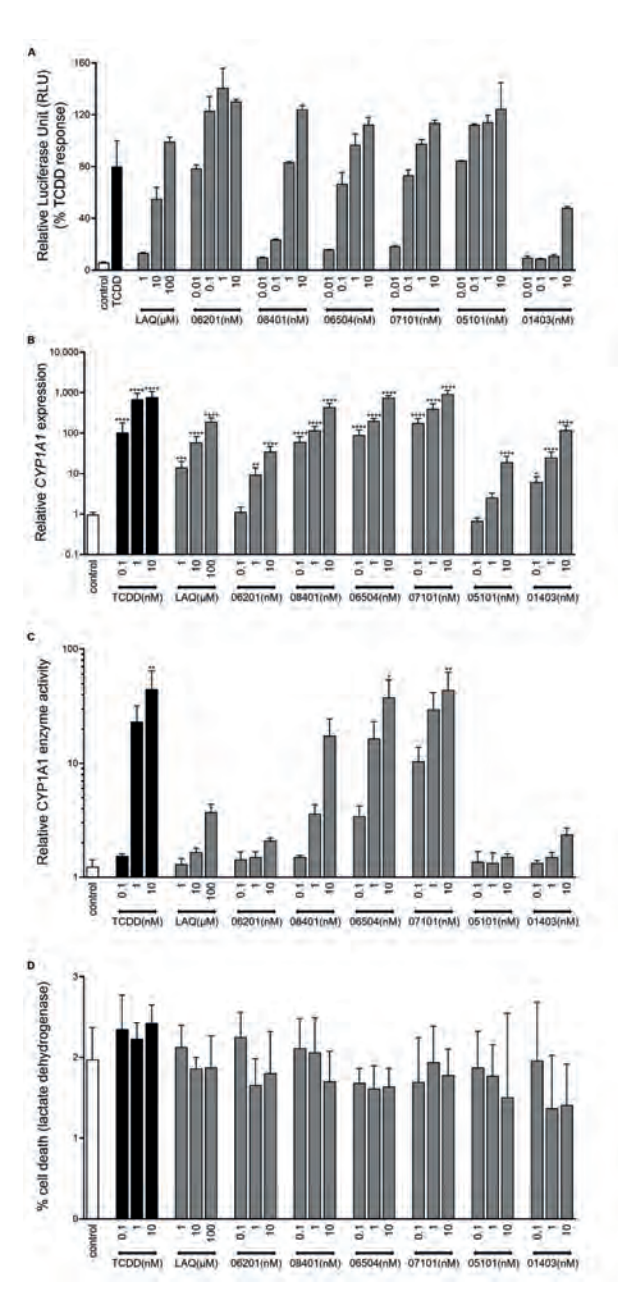


Figure 2. Induction of AHR activity by IMA-derivatives. (A) HepG2 40/6 cell cultures stimulated for 4 h with a concentration series of LAQ and IMA-compounds. TCDD (10 nM) was used as a full AHR agonist and set at 100% luminescent activity (n = 2). (B) CYP1A1 mRNA expression levels, (C) CYP1A1 enzyme activity (luminescent assay), and (D) percentage cell death (24 h measurement, lactate dehydrogenase (LDH) assay) of primary human keratinocytes (n = 3) stimulated for 48 h (re-stimulated after 24 h) with a concentration series of the IMA-compounds, LAQ, and TCDD. * p < 0.05, ** p < 0.01, *** p < 0.001, **** p < 0.0001. Mean +/- SEM.

AHR-mediated expression of epidermal differentiation

Given the stimulating effects of coal tar, TCDD, and other AHR ligands on epidermal differentiation through AHR-dependent mechanisms [75, 171, 226, 227], we analyzed the following marker levels for terminal differentiation: filagarin (FLG), hornerin (HRNR), involucrin (IVL), and loricrin (LOR) (Figure 3). Stimulation with IMA-07101 significantly and dose-dependently induced FLG, HRNR, and IVL levels, similar to TCDD. Based on these results, we subjected organotypic human epidermal equivalents (HEEs) to 1 nM IMA exposure during the final 96 h of the air-liquid interface culture. In particular, the increase in numbers of stratum granulosum layers was most apparent after IMA-06504, IMA-07101, and IMA-08401 exposure (Figure 4A) and correlated to the levels of CYP1A1 expression (Figure 4B). We also observed epidermal thickening and induction of stratum corneum layers most notably after AHR activation via TCDD and the TASQ derivatives. FLG protein expression levels were most strongly induced by TASQ derivative IMA-06504 and its prodrug IMA-07101 (Figure 4C). This finding was further substantiated by loricrin (LOR) and involucrin (IVL) immunostainings of IMA-07101 exposed HEEs (Supplemental Figure 2A), and subsequent semi-quantitative analysis (Supplemental Figure 2B). Thus, activation of AHR signaling by LAQ and TASQ derivatives resulted in similar stimulating effects on epidermal development and formation as previously described for coal tar [75].

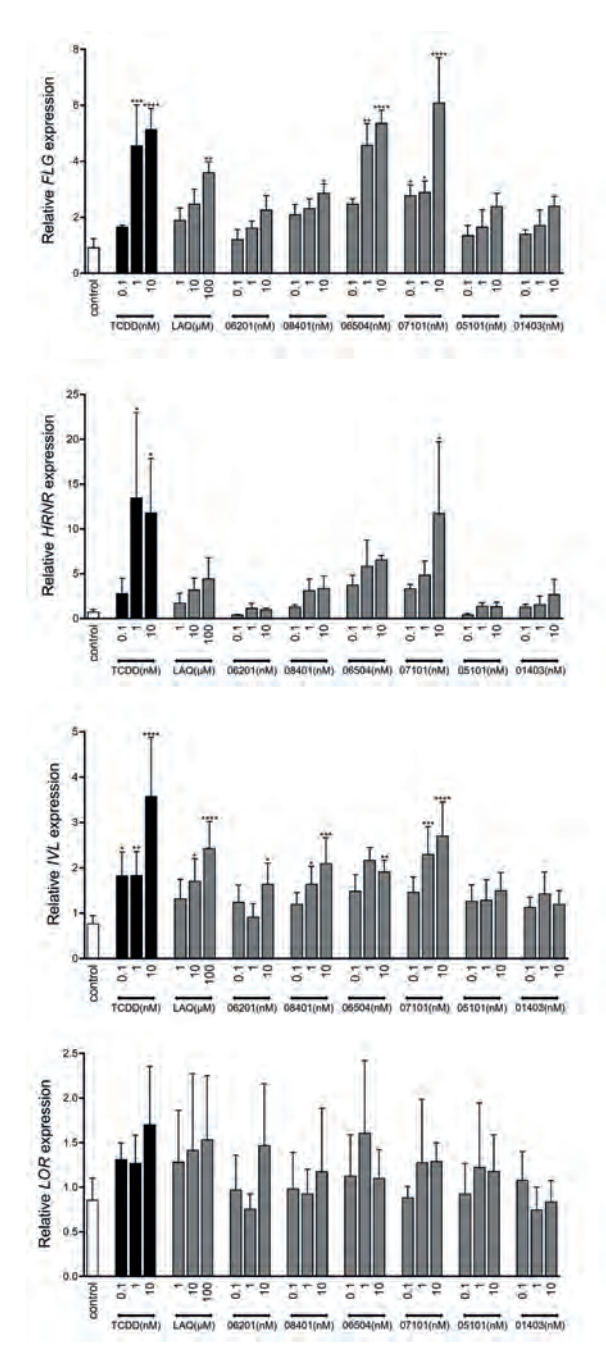


Figure 3. Upregulation of epidermal differentiation in vitro. Expression analysis of terminal differentiation genes filaggrin (FLG), hornerin (HRNR), involucrin (IVL), and loricrin (LOR) after 48 h stimulation (re-stimulation after 24 h) of monolayer primary human keratinocytes (n = 3) with a concentration series of the IMA-compounds, LAQ, and TCDD. * p < 0.05, ** p < 0.01, *** p < 0.001, **** p < 0.0001. Mean +/- SEM.

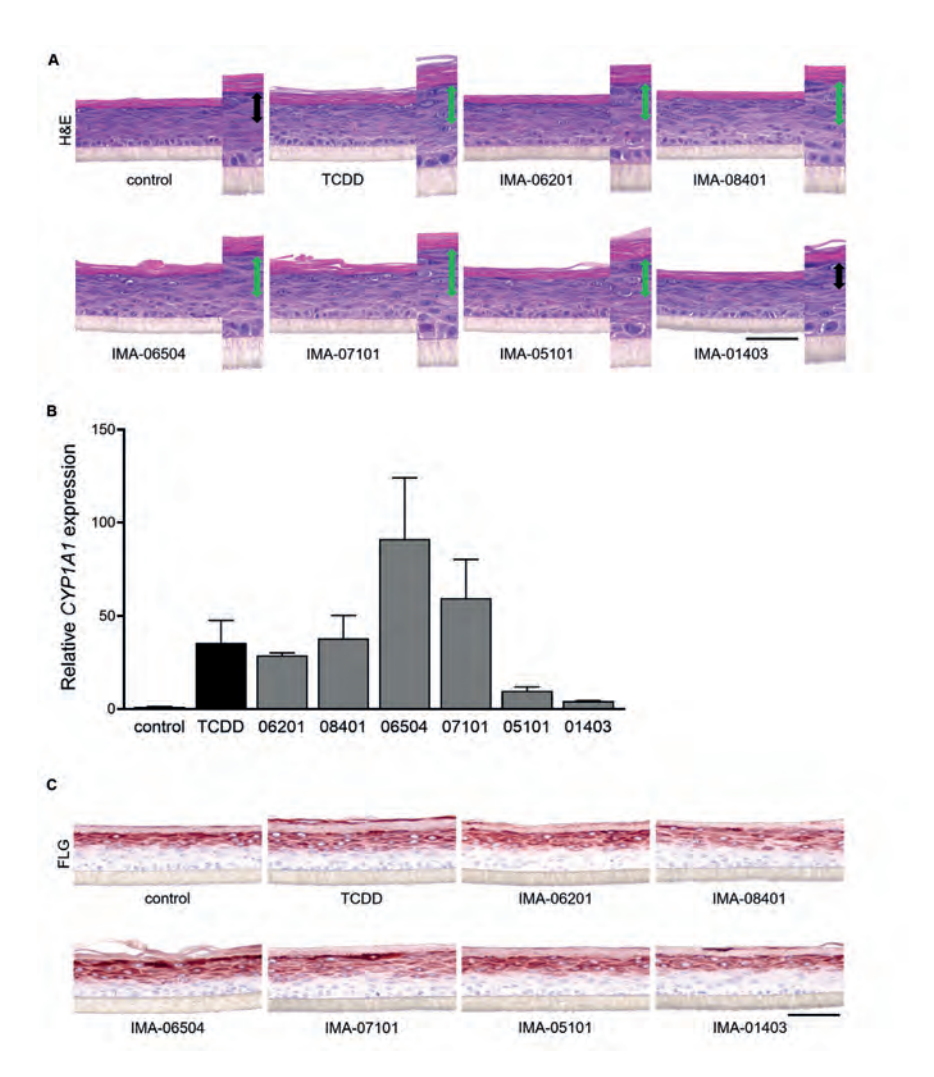


Figure 4. AHR activation and induction of epidermal differentiation in human epidermal equivalents. (A) H&E staining of human epidermal equivalents (HEEs) stimulated with 1 nM of IMA-compounds and TCDD for 96 h (re-stimulated after 48 h). Double headed arrows in magnified images indicate stratum granulosum layers (green arrows show an increase compared to the control-HEE). (B) CYP1A1 mRNA levels (n = 2), mean +/- SEM. (C) Immunostaining for filaggrin (FLG) after 96 h of stimulation with IMAcompounds. Scale bar = $100 \mu m$.

Therapeutic effect of IMA-compounds in organotypic AD-like epidermal models

The potential of IMA-compounds to counteract detrimental effects of Th2 cytokines (e.g., IL-4) on epidermal differentiation protein expression, as seen for coal tar treatment, was investigated in an AD-like disease model. Hereto, HEEs generated from human primary keratinocytes harboring a heterozygous FLG mutation (Supplemental Table 2) were exposed to 10 ng/mL IL-4 for 96 h in total. After the first 24 h (disease initiation phase), the AD-HEEs were additionally stimulated with 1 nM of IMA-06504, IMA-07101, IMA-01403 (as a negative control) and TCDD for the final 72 h (treatment phase). IL-4 treated HEEs present with a thickened epidermis with fewer granular layers. Treatment with the TASQ derivatives increased the number of granular layers (Figure 5B). AHR activation in the AD-model by the TASO derivatives and TCDD was verified by CYP1A1 protein expression detection (Supplemental Figure 2A).

The IL-4 mediated downregulation of FLG, LOR, and IVL expression, indicated by irregular staining patterns and staining of less epidermal layers, was effectively counteracted by IMA-07101 and its active metabolite IMA-06504. IMA-01403 was ineffective (Figure 5B). These findings were substantiated by semi-quantitative analysis (Supplemental Figure 2B).

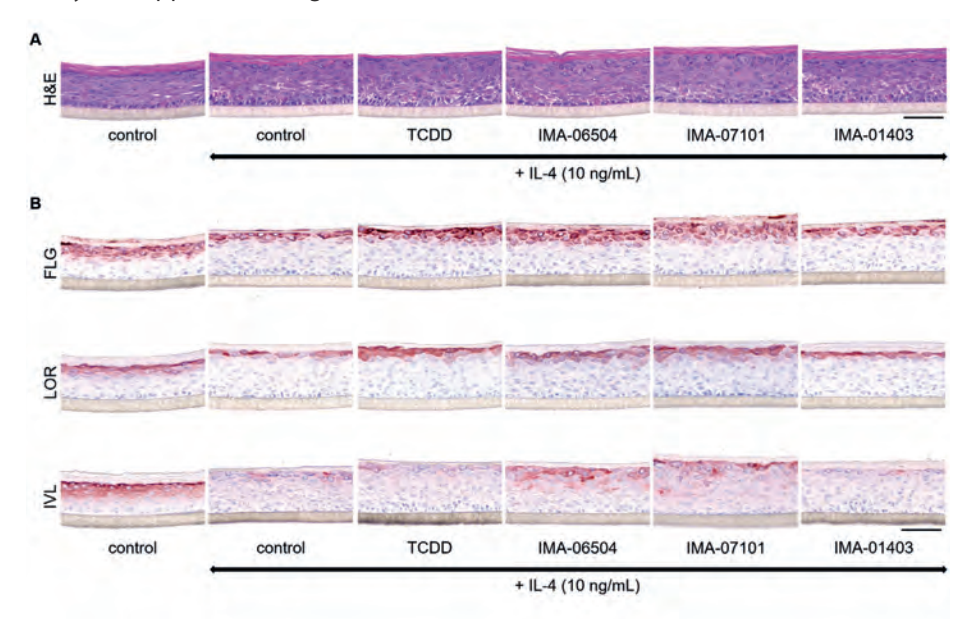


Figure 5. Therapeutic effect of TASQ derivatives in the AD-HEE model. (A) H&E staining of HEEs stimulated with 10 ng/mL IL-4 for 24 h followed by co-stimulation with the compounds for another 72 h. (B) Analysis of epidermal differentiation proteins via immunostainings for filaggrin (FLG), loricrin (LOR) and involucrin (IVL). Scale bar = $100 \mu m$.

Discussion

In search of novel therapeutic AHR ligands for the treatment of inflammatory skin diseases, we here showed that carboxamide derivates are full AHR agonists in the low nanomolar range. TASQ metabolites most effectively induce FLG and other epidermal proteins important for skin barrier function, both in normal skin conditions and in a Th2-cytokine dominated inflammatory milieu representing ADlike inflammation

The first compound from the carboxamide compound class, ROQ (drug name Linomide) was withdrawn from clinical trials due to severe drug-related adverse events in phase III trials with MS patients.[228-230]. Thereafter, LAO and TASO were developed and intended as safer derivatives [231, 232]. Phase II/III clinical trials indicate therapeutic efficacy of LAQ in patients with multiple sclerosis [233, 234], as also confirmed in recent meta-analysis [235]. Herein, a significantly higher risk of LAQ treatment was associated with back pain, headache, and vomiting [235]. Tasquinimod is intended for the oral treatment of prostate cancer, but also comes with adverse events (e.g., skeletal pain, digestive disorders, insomnia) [236, 237]. Systemic exposure of exogenous AHR ligands may modulate and disrupt physiological AHR signaling given its expression in many tissues [120, 238]. Topical application and thus local and tissue specific targeting in dermatological indications may therefore provide a better setting for the use of AHR ligands as therapeutics. Lead optimization of LAQ and TASQ resulted in increased potency of AHR activation in keratinocytes as LAQ only elevated AHR target gene levels at micromolar concentrations, whereas the IMA-metabolites induced AHR signaling already at 1 nM. This important step resulted in the first positive preclinical in vitro studies for dermatological indications herein described and provides solid ground for further preclinical development and topical formulation.

The in vivo safety aspects of the IMA-compounds have been studied in rodents, where no clinical signs of subacute toxicity were observed upon systemic exposure [225], other than generic AHR-mediated responses not relating to dioxininduced toxicity. IMA-06201 and IMA-06504 were classified as non-mutagenic in in vitro analysis [224]. Furthermore, IMA-compounds are predicted to be faster metabolized to inactive compounds as compared to TCDD, which may be supportive of an improved safety profile [224, 225]. Of note, TASQ derivatives were not rapidly metabolized and inactivated in keratinocyte monolayer cultures, as indicated by the induced AHRR expression and CYP1A1 enzyme activity after 48 h at similar levels as TCDD. These findings advocate for additional studies with prolonged culturing of keratinocytes after single dosing to determine the duration of AHR activation (e.g., CYP1A1 expression dynamics) which may indicate TASQ metabolism rates and AHR ligand half-life as compared to dioxin. Our keratinocyte studies at least did not reveal cytotoxic effects (LDH leakage) or detrimental effects on the epidermal viability and morphology after exposure to IMA-compounds up to 96 h. However, also for TCDD, no acute cellular toxicity was observed, confirming the need for data on prolonged exposure to IMA-compounds, also including topical exposure in formulations rather than supplementation of culture medium as herein used.

The induction of epidermal differentiation by TASQ derivatives (even in the presence of IL-4) appeared more efficacious than for TCDD. This enables future dose reduction strategies for at least IMA-07101. Ideally, induction of epidermal differentiation should be retained while CYP1A1 enzymatic levels are minimized. CYP1A1 is associated with phase 1 metabolism and the generation of mutagenic epoxides from certain environmental pollutants. Although in vivo, CYP450 enzymes appear more important for detoxication than their activation of carcinogens [239]. Moreover, sustained CYP1A1 activity may metabolize endogenous AHR ligands hence resulting in deprived physiological AHR signaling and skin tissue that is prone to inflammatory processes [175, 239, 240]. Besides concerns on phase 1 metabolism by CYP1A1 due to AHR activation, a specific side effect, folliculitis, is reported in patients treated with topical AHR-activating therapies, such as coal tar and tapinarof [241, 242]. The likelihood of other ligand classes, such as the IMAcompounds here investigated, causing similar side effects should be subject of further research.

TASQ derivatives IMA-06504 and IMA-07101 were most potent and effective for AHR-mediated induction of epidermal differentiation and the rescue of epidermal AD hallmarks by IL-4. The accelerated formation and development of the epidermis and skin barrier function upon AHR activation has also been shown upon in vivo TCDD treatment [171], in vitro coal tar treatment [75], and in Chinese traditional medicine [215]. Next to the regulation of terminal differentiation, AHR signaling was also reported to mediate keratinocyte proliferation [76, 124]. Considering that proliferation and differentiation processes in both AD and Pso are disturbed, and that therapeutic effects of AHR activation are not specific to AD but are also demonstrated in Pso patients [95], efficacy of IMA-compounds in psoriasiform inflammation may be expected. Further preclinical studies are recommended including topical formulations and efficacy studies using other experimental AD models or ex vivo skin biopsies.

In future years, the search for novel or existing AHR-targeting drugs with high efficacies and minimized side effects will expand the currently limited arsenal of AHR-targeting therapeutics. Lead optimization of existing drug compounds, as we showed here for quinoline-3-carboxamide derivatives, is a promising strategy for the development of novel therapeutic AHR ligands to feed pharmaceutical pipelines.

Materials and Methods

Synthesis of IMA-Compounds

Synthetic preparations of LAQ and IMA-compounds, except for IMA-01403, are described in patent application WO2012/050500A1 [223]. IMA-01403 was prepared by benzylation of N-(2,4-dimethoxybenzyl)-N-phenyl-1,2-dihydro-4-hydroxy-1methyl-2-oxo-quinoline-3-carboxamide [223] using BnBr (1,5 eg.) and K₂CO₂ (2 eg.) in DMF at 60 °C overnight, followed by concentration and conventional workup. The crude product was deprotected (cleavage of N-2,4-dimethoxybenzyl) using cerium ammonium nitrate (CAN, 3 eg., 0,1 M in 95% ag. MeCN) at room temperature for 20 min, followed by concentration conventional workup and purification by silica chromatography (CH₂Cl₂) to give IMA-01403 in 50% overall yield.

¹H NMR (400 MHz, CDCl₂) δ 3.75 (s, 3H), 5.45 (s, 2H), 7.14 (t, 1H), 7.25 (d, 1H), 7.32–7.47 (m, 8H), 7.65 (t, 1H), 7.77 (d, 2H), 8.09 (d, 1H), 10.71 (s, 1H).

HepG2 (40/6) Luciferase Reporter Assay

Human HepG2 (40/6) AHR reporter cells (hepatocellular carcinoma liver cells) were seeded in a 24-well format in Minimal Essential Medium Eagle (α-MEM, Sigma-Aldrich, St. Louis, MO, USA) supplemented with 1% penicillin/streptomycin and 8% fetal bovine serum (125.000 cells in 500 µL). After 24 h, cells were stimulated with LAQ (100, 10, or 1 µM), IMA-compounds (10, 1, 0.1, or 0.01 nM), and TCDD (10 nM) for 4 h at 37 °C with 5% CO₂. Thereafter, the cells were lysed in 200 mL lysis buffer (20 mM Tris-HCl, pH 7.8, 1% Triton X-100, 150 mM NaCl and 2 mM dithiothreitol) and stored at -80 °C. To detect luciferase activity, 20 μL cell lysate was mixed with 40 μL luciferase activity assay reagent (Promega Luciferase Assay system) and the luminescence signal measured (Synergy HT microplate reader, BioTek, Winooski, VT, USA).

Primary Keratinocyte Isolation

Surplus human skin was obtained from plastic surgery. Human primary keratinocytes were isolated as previously described and stored in liquid nitrogen (according to the principles of the Declaration of Helsinki) [243].

Monolayer Primary Keratinocyte Culture

Human primary keratinocytes were cultured submerged in 24-well plates at 37 °C with 5% CO₂ using keratinocyte growth medium with required growth factors and supplements (KGM, Lonza; without antibiotics) until confluency was reached [244]. Keratinocyte differentiation was initiated by depletion of growth factors and the cells were simultaneously stimulated with the IMA-compounds (10, 1, or 0.1 nM), TCDD (10, 1, or 0.1 nM), and LAQ (100, 10, or 1 µM). Keratinocytes were harvested after 48 h of stimulation (re-stimulated after 24 h) and processed for RNA isolation and subsequent qPCR analysis.

Lactate Dehydrogenase (LDH) Assay

The supernatant of the above-mentioned monolayer culture experiment was collected after 24 h of compound stimulation. Keratinocytes treated with 1% Triton X-100 in KGM were used as a positive control for 100% cell death. A cytotoxicity detection kit (Roche) was used to measure LDH activity according to the manufacturer's protocol and absorbance was read at 490 nm with a microplate reader (Bio-Rad).

CYP1A1 Enzyme Activity Assay

The P450-Glo™ CYP1A1 assay system (Promega, Madison, WI, USA) was used to measure CYP1A1 enzyme activity according to the manufacturer's protocol. Keratinocytes were treated as described previously (see monolayer primary keratinocyte culture). After 48 h of stimulation (refreshed after 24 h), cells were washed with PBS after which 200 µL Luc-CEE substrate solution in KGM without growth factors was added to the wells and incubated for 3 h at 37 °C with 5% CO₂. The culture medium was collected and mixed with luciferin detection reagent for detection of luminescence (Synergy HT microplate reader, BioTek, Winooski, VT, USA).

Human Epidermal Equivalent (HEE) Culture (Normal Skin and Atopic **Dermatitis Model**)

HEEs were generated according to the protocols previously described [243]. Briefly, 24-well cell culture inserts (ThinCert, Greiner Bio-One or Nunc, Thermo Fisher Scientific, Waltham, MA, USA) were coated with rat tail collagen (100 µg/mL, BD Biosciences) at 4 °C for 1 h. Then, 100.000-150.000 primary human keratinocytes were seeded submerged in 100-150 µL CnT-prime medium (CELLnTEC) After 48 h, cultures were switched to 3D differentiation medium, consisting of 60% CnT-Prime 3D Barrier medium (CELLnTEC) and 40% High Glucose Dulbecco's Modified Eagle's Medium (DMEM, Sigma-Aldrich, St. Louis, MO, USA). Then, 24 h later, the HEEs were lifted to the air-liquid interface (ALI), after which the differentiation medium was refreshed every other day.

In the normal skin model, HEEs were treated with the IMA-compounds (1 nM) and TCDD (1 nM) at day 4 of the ALI for 96 h (re-stimulation after 48 h). At day 8, HEEs were harvested and processed for qPCR and immunohistochemical analysis.

To generate an atopic dermatitis (AD)-like (AD-HEE) model [41, 55, 75, 245], human primary FLG+/- keratinocytes (Supplemental Table S2) were used in combination with the disease-associated cytokine interleukin-4 (IL-4). AD-HEEs were first stimulated with IL-4 (10 ng/mL, Peprotech (supplemented with 0.05% bovine serum albumin, BSA, Sigma-Aldrich, St. Louis, MO, USA)) at day 4 of the ALI. After 24 h of disease initiation, HEEs were co-stimulated with the TASQ derivatives (IMA-06504 and IMA-07101), IMA-01403 and TCDD at a concentration of 1 nM and harvested 72 h later (re-stimulation after 48 h) for immunohistochemical analysis.

Immunohistochemistry

HEEs were fixed in 4% formalin for 4 h and processed for routine histology. The 6 µm paraffin sections were stained with hematoxylin and eosin (Sigma-Aldrich, St. Louis, MO, USA) after deparaffinization. For immunohistochemical analysis, sections were stained using an indirect immunoperoxidase technique with avidin-biotin complex enhancement (Vectastain, Vector Laboratories) using antibodies listed in Supplemental Table S3.

RNA Isolation Real-Time Quantitative PCR (RT-gPCR)

RNA was isolated with the Tissue Total RNA Kit (Favorgen, Vienna, Austria) according to the manufacturer's protocol. RNA was treated with DNAsel (Invitrogen, Waltham, MA, USA) and used for cDNA synthesis using SuperScript IV VILO Master Mix (Invitrogen, Waltham, MA, USA) according to the manufacturer's protocol. RT-gPCR analysis was performed using SYBR Green (Bio-Rad, Hercules, CA, USA). Target gene expression was normalized to the expression of the house keeping gene human acidic ribosomal phosphoprotein P0 (RPLP0) and relative expression levels were calculated by the ΔΔCt method [246]. Primer sequences (Biolegio, Nijmegen, The Netherlands) are depicted in Supplemental Table S4.

Quantification of Differentiation Protein Expression in HEEs

Image acquisition of HEE immunostainings was performed by a ZEISS Axio Imager equipped with a ZEISS Axiocam 105 color Digital Camera and a 40x objective. The ZEISS Axiocam 105 color is a compact 5-megapixel camera (2560 \times 1920 pixels) for high resolution images with a 1/2.5" sensor. Two images per slide were chosen as representative for the whole culture and stored in CZI format. The images were analyzed with the cell image analysis software CellProfiler (Broad Institute) [205]. Software pipelines for Filaggrin (FLG), Loricrin (LOR), and Involucrin (IVL) analysis were created (available upon request) and GraphPad Prism 9.0 was used for the visualization of the data. The quantified data is shown as the protein area occupied (µm²) per millimeter length of the epidermis. Because this value does not normalize for the thickness of the epidermis (differences in epidermal thickness were observed after compound stimulation), we also calculated the area of expression as percentage of the epidermal surface for comparison.

Statistics

Statistical analyses were performed using GraphPad Prism 9.0 on experiments of at least n=3 replicates. To determine statistical significance between multiple groups for the in vitro monolayer cultures, paired one-way analysis of variance (ANOVA: mixed effects model for repeated measures data (one missing value)) was performed followed by Tukey's multiple comparison post hoc test. For the data obtained by CellProfiler software, the calculated protein area (µm²) per millimeter length was used to analyze significant differences between multiple groups by performing the Friedman test (paired nonparametric test), indicated as (p = x.xx) in the legend. If significant, Dunn's multiple comparison post hoc test was executed. Each culture experiment (monolayer or organotypic HEE) includes biological donor replicates.

Author Contributions

Conceptualization, L.P. and E.H.v.d.B.; data curation, G.R.; formal analysis, G.R.; funding acquisition, E.H.v.d.B.; investigation, G.R., N.J.M.v.d.B. and I.M.J.J.v.V.-W.; methodology, G.R.; project administration, E.H.v.d.B.; resources, L.P. and E.H.v.d.B.; software, P.E.J.v.E.; supervision, J.P.H.S. and E.H.v.d.B.; validation, G.R.; visualization, G.R.; writing—original draft, G.R., N.J.M.v.d.B., L.P. and J.P.H.S.; writing—review and editing, G.R., L.P., J.P.H.S. and E.H.v.d.B. All authors have read and agreed to the published version of the manuscript.

Supplemental tables

Supplemental Table 1. Overview of quinoline-3-carboxamide derivatives for the study on epidermal differentiation induction. The structural relationship between the parent compound (LAQ, TASQ or ROQ) and its newly developed derivatives is depicted with color codes and in the comments column.

Compound abbreviation	Chemical structure	Scientific name	Comments
Laquinimod (LAQ)	CI OH O	5-chloro- <i>N</i> -ethyl-4- hydroxy-1-methyl- 2-oxo- <i>N</i> -phenyl-1,2- dihydroquinoline- 3-carboxamide	Site of N-dealkylation indicated in structure
IMA-06201	CI OH O	N-phenyl-5-chloro-1,2- dihydro-4-hydroxy-1- methyl-2-oxo-quinoline- 3-carboxamide	N-dealkylated metabolite of LAQ (DELAQ in lit.). Intramolecular H-bonds stabilizes a planar structure
IMA-08401	CI O O Ac	N-acetyl-N-phenyl-4- acetoxy-5-chloro-1,2- dihydro-1-methyl-2-oxo- quinoline-3-carboxamide	Di-acetyl prodrug of IMA-06201
Tasquinimod (TASQ)	MeO OH O	4-hydroxy-5-methoxy- N,1-dimethyl-2-oxo-N-[4- (trifluoromethyl)phenyl] quinoline-3-carboxamide	Aimed for the treatment of prostate cancer
IMA-06504	MeO OH O	N-(4- trifluoromethylphenyl)- 1,2-dihydro-4-hydroxy-5- methoxy-1-methyl-2-oxo- quinoline-3-carboxamide	N-dealkylated metabolite of TASQ
IMA-07101	MeO O O O F F F F	N-acetyl-N-(4- trifluoromethylphenyl)- 4-acetoxy-1,2-dihydro-5- methoxy-1-methyl-2-oxo- quinoline-3-carboxamide	Di-acetyl prodrug of IMA-06504
Roquinimex (ROQ)	OH O	4-hydroxy- <i>N</i> ,1-dimethyl- 2-oxo- <i>N</i> -phenylquinoline- 3-carboxamide	First clinical compound (Linomide) in class
IMA-05101	OH O NO	<i>N</i> -phenyl-1,2-dihydro-4-hydroxy-1-methyl-2-oxo-quinoline-3-carboxamide	N-dealkylated metabolite of ROQ

Supplemental Table 1. Continued

Compound abbreviation	Chemical structure	Scientific name	Comments
IMA-01403	O O O O O O O O O O O O O O O O O O O	<i>N</i> -phenyl-4-benzyloxy-1,2-dihydro-1-methyl-2-oxo-quinoline-3-carboxamide	Low-potency ligand. 4-O-benzyl breaks H-bond
TCDD	CI CI CI	2,3,7,8-tetrachlorodibenzo- p-dioxin	The metabolically resistant compound "dioxin"

Supplemental Table 2. Human primary keratinocytes used to generate the AD-HEEs harboring a heterozygous FLG mutation leading to depicted amino acid change

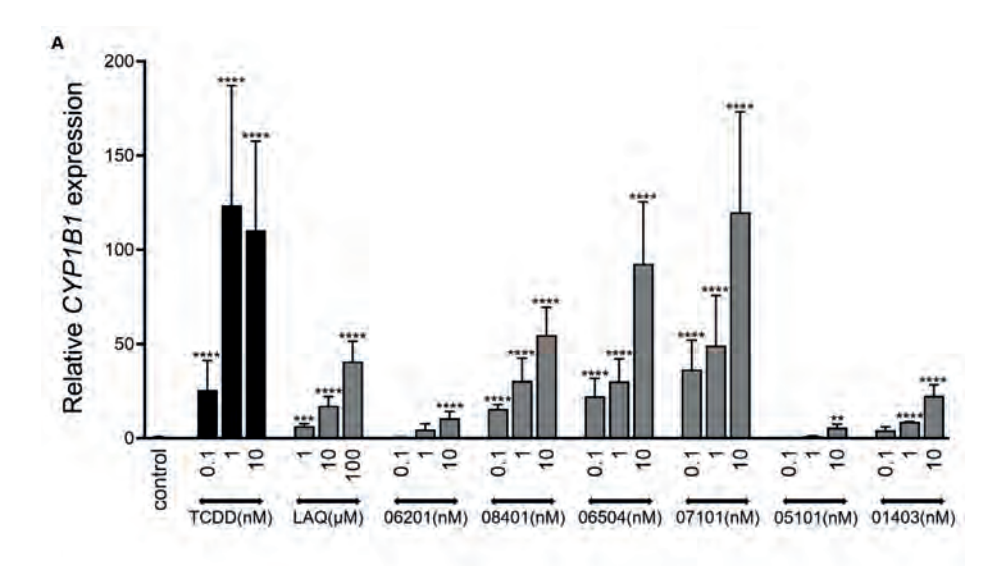
Sample ID	FLG mutation	Amino acid change
Donor#1	c.7339C>T	p.(Arg2447*)
Donor#2	c.5702del	p.(Gly1901Alafs*194)
Donor#3	c.10898C>G	p.(Ser3633*)

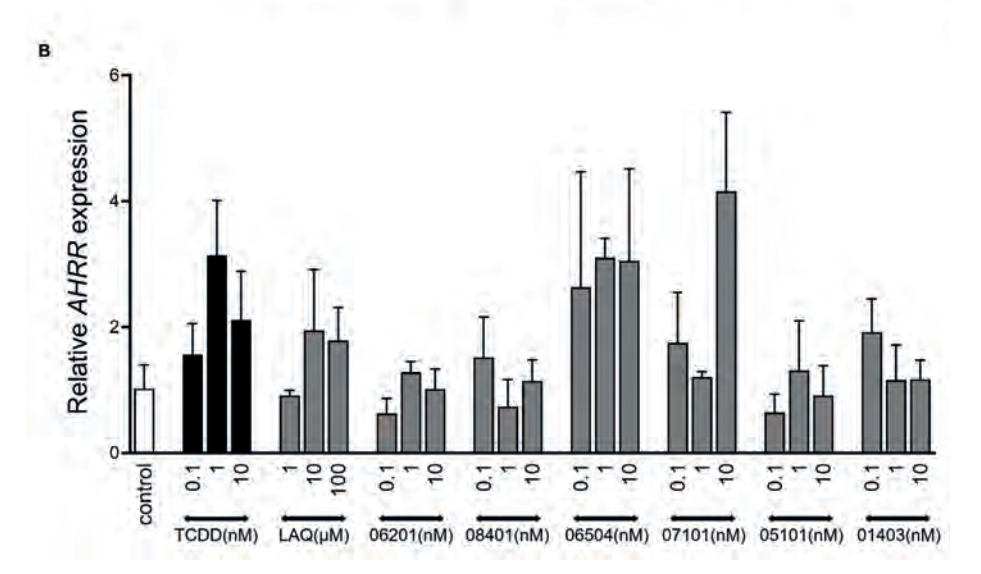
Supplemental Table 3. Antibodies used of immunohistochemical analysis.

Species	Dilution	Company
Mouse	1:100	Thermo Fisher, MA5-13440
Mouse	1:50	Santa Cruz, sc-25304
Mouse	1:20	van Duijnhoven et. al. [204]
Rabbit	1:4000	Convance 145P100
	Mouse Mouse Mouse	Mouse 1:100 Mouse 1:50 Mouse 1:20

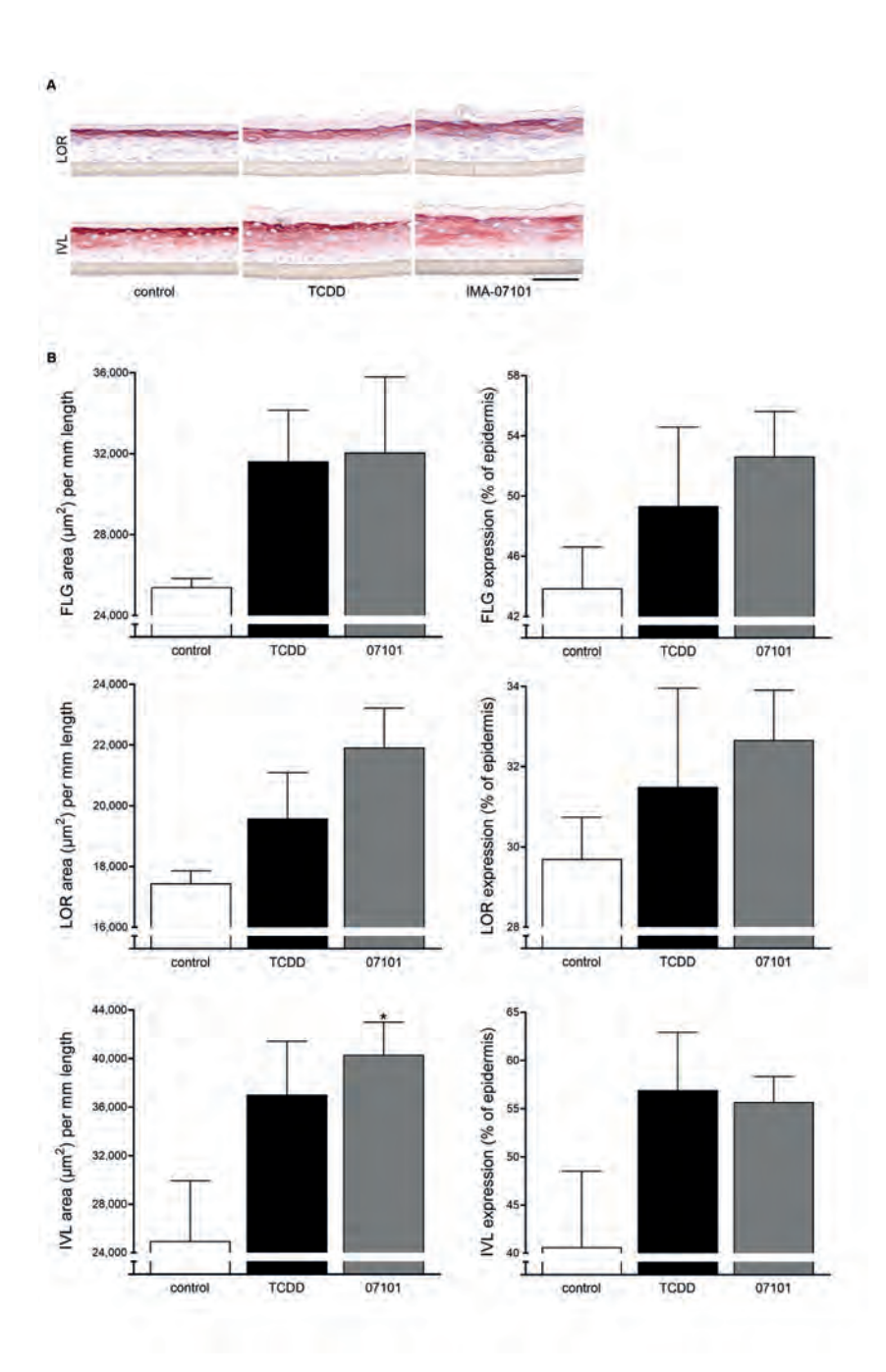
Supplemental Table 4. Primers used of RT-qPCR analysis

Gene	Forward primer (5′-3′)	Reverse primer (5'-3')
HARP	caccattgaaatcctgagtgatgt	tgaccagcccaaaggagaag
CYP1A1	ctggagaccttccgacactctt	gtaaaagcctttcaaacttgtgtctct
FLG	acttcactgagtttcttctgatggtatt	tccagacttgagggtctttttctg
HRNR	tgttcctctggtgagctaggttact	tgggtggcatattggtagaaaac
IVL	acttatttcgggtccgctaggt	gagacatgtagagggacagagtcaag
LOR	aggttaagacatgaaggatttgcaa	ggcaccgatgggcttagag

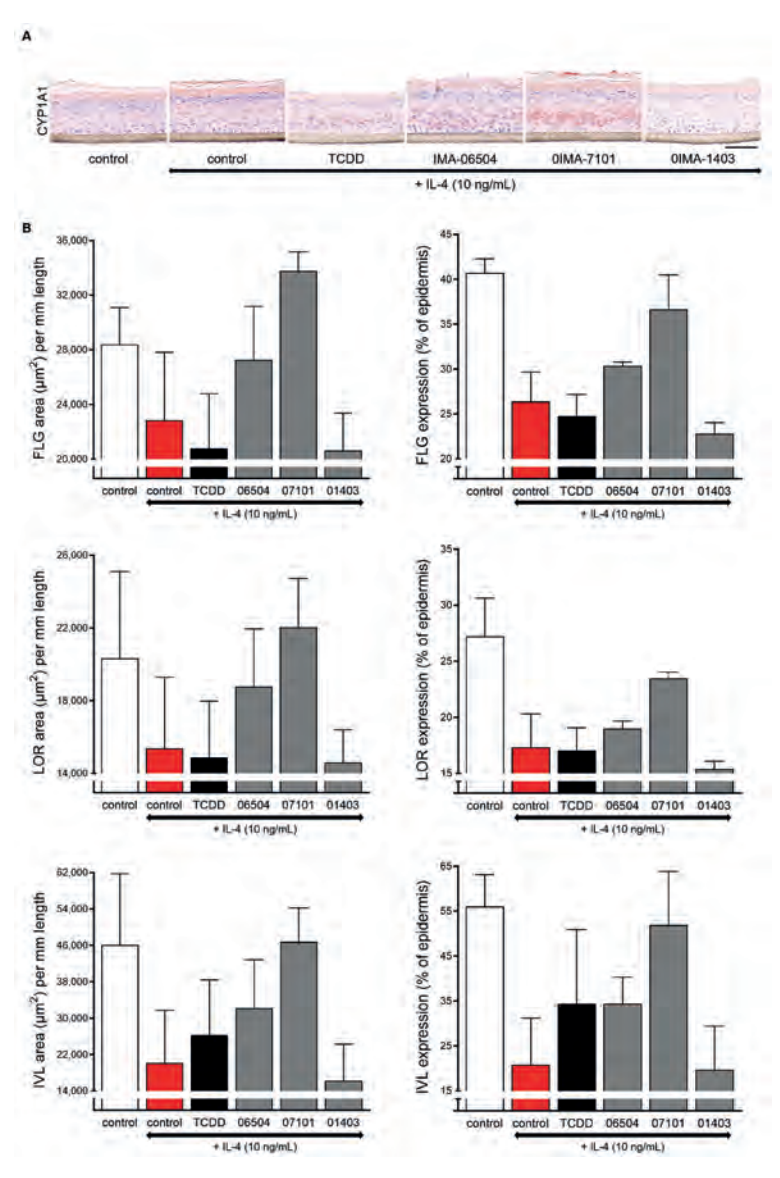




Supplemental Figure 1. Analysis of AHR target genes. mRNA expression analysis of **(A)** *CYP1B1* and **(B)** *aryl hydrocarbon receptor repressor* **(***AHRR***)** after 48 hours stimulation (re-stimulation after 24 hours) of monolayer primary human keratinocytes (N=3) with a concentration series of the IMA-compounds, LAQ and TCDD. *P<0.05, **P<0.01, ***P<0.001, ****P<0.001. Mean +/- SEM.



Supplemental Figure 2. Epidermal differentiation analysis in HEE model. (A) loricrin (LOR) and involucrin (IVL) staining of HEEs stimulated with 1 nM TCDD and IMA-07101 for 96 hours and (B) quantification thereof (µm2 per mm length of the epidermis and percentage expression of the epidermis), including filaggrin (FLG) expression (N=3). *P<0.05. Mean +/- SEM. Scale bar = 100 μ m.



Supplemental Figure 3. AHR-mediated restoration of differentiation protein expression. **(A)** immunostaining for CYP1A1 and **(B)** quantification (μ m2 per mm length of the epidermis and percentage expression of the epidermis) of protein expression for filaggrin (FLG; P = 0.032, N=3)), Loricrin (LOR) and Involucrin (IVL; P = 0.025) in HEEs stimulated with 10 ng/mL IL-4, for 24 hours followed by co-stimulation with the compounds for another 72 hours. Scale bar = 100 μ m.



Chapter 4

Investigations into the FLG null phenotype: showcasing the methodology for CRISPR/Cas9 editing of human keratinocytes

Jos P.H. Smits^{1,2}, Noa J.M. van den Brink¹, Luca D. Meesters^{1,3}, Hadia Hamdaoui¹, Hanna Niehues¹, Patrick A.M. Jansen¹, Ivonne M.J.J. van Vlijmen-Willems¹, Diana Rodijk-Olthuis¹, Céline Evrard⁴, Yves Poumay⁴, Michel van Geel^{5,6,7}, Wiljan J.A.J. Hendriks⁸, Joost Schalkwijk¹, Patrick L.J.M. Zeeuwen¹, Ellen H. van den Bogaard¹

¹Department of Dermatology, Radboud Institute for Molecular Life Sciences (RIMLS), Radboud University Medical Center (Radboudumc), Nijmegen, The Netherlands;

²Department of Dermatology, University Hospital Düsseldorf, Medical Faculty, Heinrich Heine University, Düsseldorf, Germany;

³Department of Molecular Developmental Biology, RIMLS, Radboudumc, Nijmegen, The Netherlands; ⁴Research Unit for Molecular Physiology, NARILIS, University of Namur, Namur, Belgium;

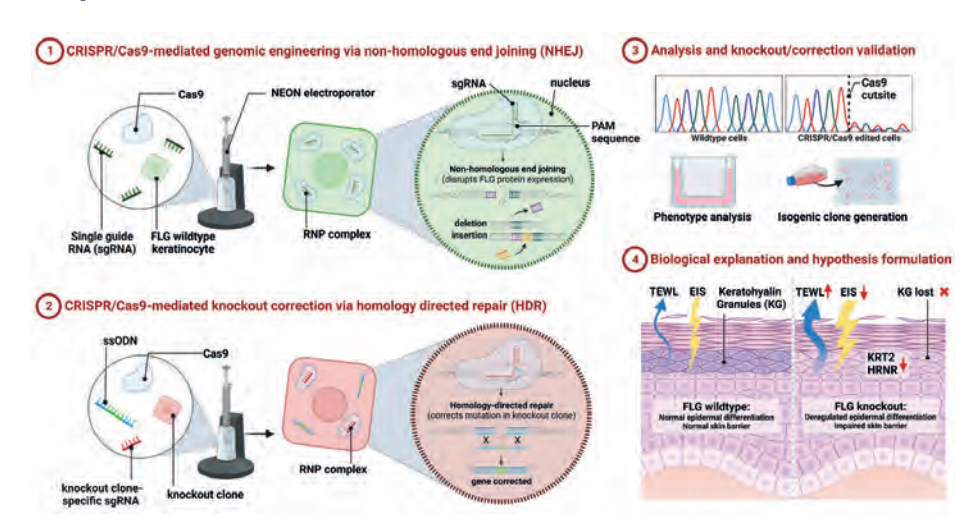
⁵Department of Dermatology, Maastricht University Medical Center+, Maastricht, The Netherlands;

⁶GROW School for Oncology and Developmental Biology, Maastricht University, Maastricht, The Netherlands;

⁷Department of Clinical Genetics, Maastricht University Medical Center+, Maastricht, The Netherlands;

⁸Department of Cell Biology, RIMLS, Radboudumc, Nijmegen, The Netherlands

Graphical abstract



Abstract

Ever since the association between filaggrin (FLG) loss-of-function variants and ichthyosis vulgaris and atopic dermatitis disease onset was identified, filaggrin's function has been under investigation. Intraindividual genomic predisposition, immunological confounders, and environmental interactions complicate the comparison between FLG genotypes and related causal effects. Using CRISPR/ Cas9, we generated human FLG knockout (ΔFLG) N/TERT-2G keratinocytes. Filaggrin deficiency was demonstrated by immunohistochemistry of human epidermal equivalent (HEE) cultures. Next to (partial) loss of structural proteins (IVL, HRNR, KRT2, and TGM1), the stratum corneum was more dense and lacked the typical basket weave appearance. In addition, electrical impedance spectroscopy and transepidermal water loss analyses highlighted a compromised epidermal barrier in ΔFLG-HEEs. Correction of FLG reinstated the presence of keratohyalin granules in the stratum granulosum, filaggrin protein expression, and expression of aforementioned proteins. The beneficial effects on stratum corneum formation were reflected by normalization of EIS and TEWL. This study demonstrates the causal phenotypical and functional consequences of filaggrin deficiency, indicating filaggrin is not only central in epidermal barrier function but also vital for epidermal differentiation by orchestrating the expression of other important epidermal proteins. These observations pave the way to fundamental investigations into the exact role of filaggrin in skin biology and disease.

Introduction

Atopic dermatitis (AD) is a common chronic inflammatory skin condition which is characterized by itchy, dry, erythematous, plaques, and an impaired skin barrier function. The pathophysiologic basis of AD is multifactorial, including genetic polymorphisms, environmental stimuli, and deregulation of innate and adaptive immunity. The seminal work from the McLean group, identifying genetic risk factors such as loss-of-function variants in the filaggrin gene (FLG) in AD [206] and ichthyosis vulgaris (IV) [247], has caused a paradigm shift indicating that epidermal biology and the skin barrier proteins themselves are of importance in complex inflammatory skin diseases like AD. The FLG gene is located at chromosome 1g21 within the epidermal differentiation complex (EDC). This gene complex encodes proteins that are typically involved in the terminal differentiation and cornification of keratinocytes. Profilaggrin protein can be proteolytically degraded into filaggrin monomers and further converted into natural moisturizing factors (NMFs)[248]. Hygroscopic NMFs maintain epidermal hydration of the skin, and reduction of NMFs directly results in dry skin [249]. Loss-of-function variants in FLG lead to reduced levels of NMFs in the stratum corneum (SC) [250]. NMF levels directly correlate to filaggrin genotype and AD severity [251] and are found to correlate with cornecyte morphology in AD patients [251]. In mouse models, filaggrin deficiency results in barrier impairment and allergen sensitization [252]. When comparing AD patients with and without FLG variants, increased water loss and skin permeability were found in both groups [253-255], while others report that FLG variants do not influence transepidermal water loss (TEWL) [41]. In experimental in vitro studies, the lack of consistency between cell sources, organotypic models, and knockdown efficiencies have yielded contradictory evidence on the consequences of filaggrin deficiency [41]. Although the importance of filaggrin for healthy skin barrier development and maintenance is widely accepted, interpatient differences complicate genotype-phenotype studies, and the short life span of primary cells in culture limits the meticulous dissection of all functional properties of (pro)filaggrin.

To overcome these limitations, genomic engineering by the Clustered Regularly Interspaced Short Palindromic Repeats (CRISPR) and CRISPR associated protein 9 (Cas9) [256-259] could be a powerful technique. Yet, the introduction of the CRISPR/Cas9 machinery into the notoriously difficult-to-transfect keratinocytes has been proven troublesome, although many options are seemingly available [260]. Some CRISPR/Cas9 related work is performed in primary keratinocytes, although most of the published research utilizes immortalized keratinocytes [261]. The immortalized human N/TERT keratinocyte cell lines (N/TERT-1 and N/TERT-2G) have been available [262] and our recent studies on their excellence as alternatives to primary keratinocytes sparked great interest in these cell lines [263]. N/ TERT keratinocytes are more amenable to transfection with foreign DNA or ribonucleoprotein complexes (RNPs) followed by clonal expansion as they are less prone to terminal differentiation than primary keratinocytes. Additionally, the N/ TERT cells are diploid [263] in contrast to other immortal lines, and thus very useful as an alternative to primary keratinocytes in genome editing experiments.

In this study, we illustrate the complementary potential of both the human N/TERT keratinocytes and a high efficiency CRISPR/Cas9 gene editing protocol for generating and functionally characterizing filaggrin knockout (ΔFLG) isogenic N/TERT-2G keratinocytes. The subsequent repair of the induced knockout in clonal cell lines of identical genomic background underlines the apparent genotypephenotype relationship. These key and to our knowledge novel aspects of profilaggrin expression and downstream regulation of epidermal biology have clear implications for our understanding of skin diseases that are characterized by the loss of filaggrin.

Methods

Culturing and freezing of human N/TERT-2G keratinocytes

Human N/TERT keratinocyte cell line N/TERT-2G, purchased from J. Rheinwald laboratory (Harvard Medical School, Boston, USA), was cultured in Epilife medium (MEPI500CA, ThermoFisher Scientific, Waltham, MA, USA), complemented with human keratinocyte growth supplement (S0015, ThermoFisher Scientific) and 1% penicillin/streptomycin (P4333, Sigma-Aldrich, Saint-Louis, MO, USA). Upon generation of the different clonal N/TERT-2G keratinocyte cell lines, they were frozen in liquid nitrogen. In short, N/TERT-2G keratinocytes were detached from culture plastic using 0.25% trypsin/EDTA (25200-072, ThermoFisher Scientific). A similar amount of DMEM containing fetal calf serum (FCS) was used to stop trypsin/EDTA activity and the cells were washed twice with DPBS (BE17-512F, Lonza Bioscience, Basel, Switzerland) before resuspension in Epilife medium. After cell counting, the cell suspension was diluted one-on-one with DMEM containing 20% FCS and 20% DMSO and slowly frozen in MrFrosty freezing containers (ThermoFisher Scientific) before moving them to liquid nitrogen storage.

N/TERT-2G human epidermal equivalent (HEE) generation

Epidermal equivalents were generated as previously described [263], with minor adjustments. Briefly, inert Nunc cell culture inserts (141002, ThermoFisher Scientific) were coated with rat tail collagen (100 µg/mL, BD Biosciences, Bedford, MA, USA) at 4°C for 1 hour. A total of 1.5 x 10⁵ N/TERT-2G keratinocytes were seeded on the transwells in 150 µL Epilife medium (ThermoFisher Scientific) supplemented with 1% penicillin/streptomycin (Sigma-Aldrich) in a 24 wells format. After 48 hours, cultures were switched to a mixture of CnT-PR-3D medium (CELLnTEC, Bern, Switzerland) and DMEM medium (60:40 (v/v)) without penicillin/streptomycin for 24 hours and then cultured at the air-liquid interface for an additional ten days. Culture medium was refreshed every other day until harvesting on day 10 of the air-exposed phase.

Single guide RNA design, single strand donor oligonucleotide and synthetic Cas9

Synthetic sgRNAs to knockout FLG gene and purified Edit-R Cas9 nuclease protein (NLS, #CAS11200) were obtained from Synthego Corporation (Menlo Park, CA, USA) and IDT Technologies (Coralville, IA, USA), respectively. Custom synthetic Alt-R sqRNAs and single strand donor oligonucleotide (ssODN) to correct FLG expression were ordered from IDT Technologies. See Supplementary Table S4 for details on the sgRNAs and ssODN used.

Electroporation of ribonucleoprotein (RNP) complexes and analysis of editing efficiency

N/TERT-2G keratinocytes were electroporated using the NEON transfection system 10 µL kit (ThermoFisher Scientific)[264]. Per electroporation condition, synthetic sqRNA (300 ng) and Cas9 (1.5 μg) were incubated with 5 μL resuspension buffer R for 20 minutes before adding 1 x 10⁵ N/TERT-2G keratinocytes. After mixing the cell suspension, the cells were electroporated using 1 pulse of 1700V for a duration of 20 ms before immediate seeding in a 6-well plate. DNA was isolated using the QIAamp DNA blood mini kit (51106, Qiagen, Hilden, Germany) according to manufacturer's protocol after reaching approximately 50% confluency and CRISPR/ Cas9 induced editing efficiency was analyzed by PCR and separation of amplicon on 2% agarose gel containing 1:10,000 GelRed nucleic acid gel stain (41003, Biotium Inc., Fremont, CA, USA). Amplicons were purified by MinElute Gel extraction kit (28606, Qiagen) using the manufacturers protocol and Sanger sequenced to assess editing efficiency. Sanger sequencing reads were analyzed using the Inference of CRISPR edits (ICE) webtool (ice.synthego.com, v2, Synthego Corporation). See Supplementary Table S5 for details on the PCR primers used.

Generation of clonal ΔFLG N/TERT keratinocytes

ΔFLG N/TERT-2G keratinocyte cell pool and FLG gene-corrected N/TERT-2G keratinocyte cell pool were diluted to 1 cell per 100 µL Epilife medium and seeded into 6 x 96-well plates, 100 µL cell suspension per well, and allowed to grow for one week before refreshing the medium. After another week of culture, cells were passaged, as described earlier, into 24-well plates, 6-wells plates, T25 flasks, and T75 flasks subsequently before freezing them into liquid nitrogen. Cell clonality was assessed by Sanger sequencing and analyzing genomic DNA at the targeted FLG locus with help of the ICE webtool (ice.synthego.com, v2, Synthego Corporation).

Results

Generation of human ΔFLG N/TERT-2G keratinocytes via CRISPR/Cas9

A single guide RNA (sqRNA) was designed to target exon 3 of the FLG gene in order to disrupt filaggrin protein expression, as schematically visualized (Figure 1a). Immortalized human keratinocyte N/TERT-2G cells were electroporated with RNP complex containing the FLG targeting sgRNA and synthetic spCas9 protein [264]. Targeted Cas9 introduced a double strand break typically repaired through nonhomologous end joining (NHEJ). This efficiently generated indels giving rise to human ΔFLG N/TERT-2G keratinocytes as analyzed by the Inference of CRISPR Edits webtool (ICE, http://ice.synthego.com, v2), showing 99% indels with 87% protein knockout prediction in the cell pool (Figure 1b). 3-dimensional human epidermal equivalents (HEEs) generated from N/TERT-2G control keratinocytes ('FLG wild type') and the ΔFLG N/TERT-2G keratinocyte cell pool ('ΔFLG pool') showed absence of keratohyalin granules in the ΔFLG pool culture. Specific filaggrin protein staining validated the partial loss of filaggrin expression (Figure 1c). We obtained clonal cell lines by seeding single cells from the ΔFLG pool into 96 well plates, one cell per well. The ΔFLG clonal line presented (Figure 1C) was further analyzed and used throughout the study.

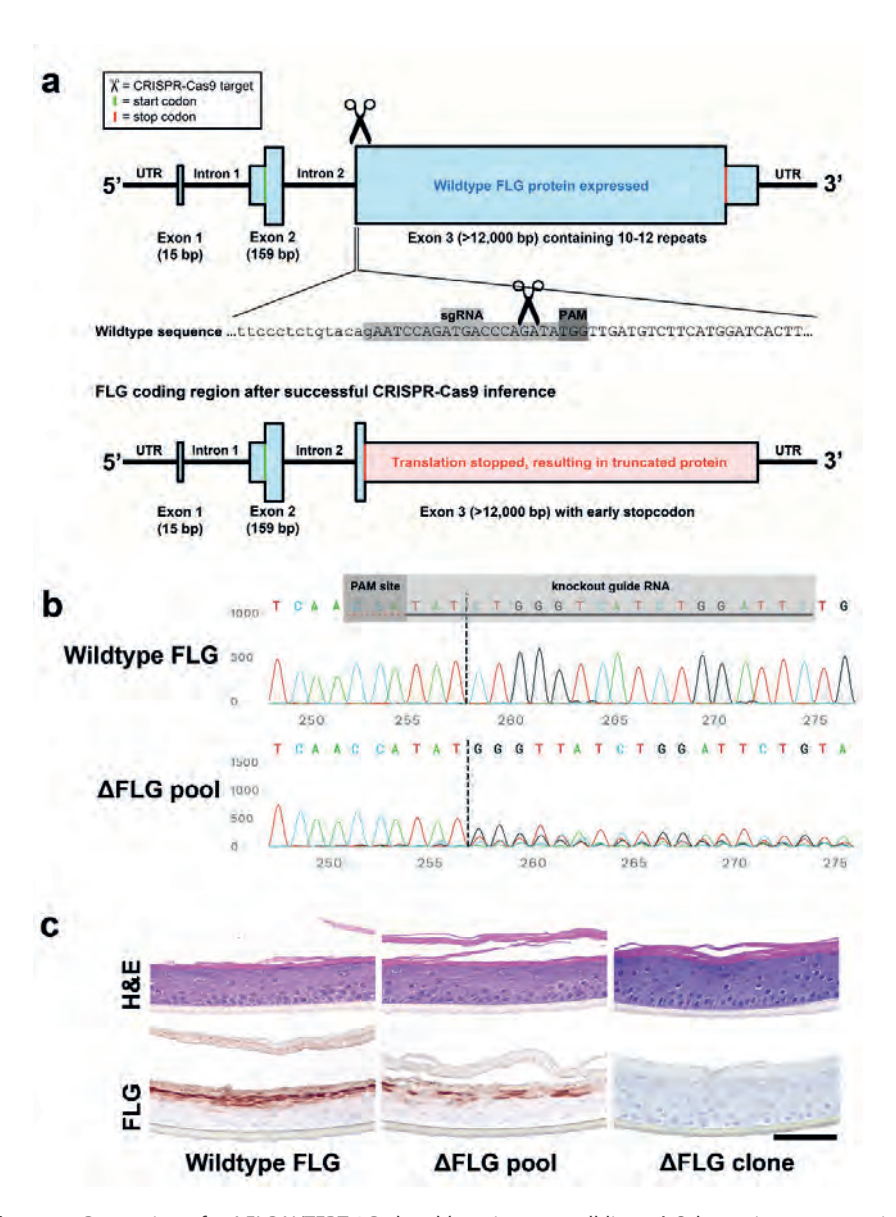


Figure 1. Generation of a ΔFLG N/TERT-2G clonal keratinocyte cell line. a) Schematic representation of the FLG knockout experiment. N/TERT-2G keratinocytes were electroporated with RNP complex containing FLG-specific gRNA and synthetic SpCas9 protein, introducing NHEJ-induced insertions and deletions leading to a frameshift mutation. b) FLG gene was analyzed after PCR amplification of the knockout locus (reverse complement sequence depicted). AFLG pool of keratinocytes show aberrant sequence reads starting 3 nucleotides 5' of the PAM site. c) ΔFLG pool was used to generate human epidermal equivalents (HEEs), showing partial loss of keratohyalin granules and filaggrin expression. After clonal expansion of ΔFLG pool, full ΔFLG clonal cells (c.152del5 encoding p.P51HfsX3) show complete absence of keratohyalin granules and filaggrin protein. Bar = $100 \mu m$.

Characterization of FLG genotype-defined clonal N/TERT-2G keratinocyte cell lines

After generating a number of single cell clones from the Δ FLG pool, we proceeded to analyze these clones for FLG variants at the sgRNA targeted Cas9 cleavage site to identify which clones were likely 100% knockout for FLG protein expression. Out of 14 clones isolated, 6 had mutations on both alleles but were heterozygous knockout (data not shown) while 3 clones were predicted and validated to be fully knockout for filaggrin protein expression (Supplementary Table S1, Supplementary Figure S1). One particular Δ FLG clone demonstrated the deletion of 5 bases (c.152del5) on both alleles, leading to a predicted p.P51HfsX3 frameshift mutation and an early stop codon (Figure 2a and 2c). This cell line was used for further experiments (' Δ FLG clone').

Genomic engineering via CRISPR/Cas9 potentially introduces off-target effects. The CRISPOR tool [265] was used to find and rank potential sgRNA specific offtarget sites based on cutting frequency determination (CFD) score (Supplementary Table S2). The top-5 potential off-target sites were amplified by PCR and the amplicons were Sanger sequenced. None of the predicted off-target mutations were found (data not shown). In addition, to prove specific genotype-phenotype correlations we engineered a N/TERT-2G keratinocyte cell line corrected for the 5 bases deletion ('FLG corrected'). Hereto, a ΔFLG clone-specific sgRNA and single strand donor oligonucleotide (ssODN) was designed. The ssODN encodes the wild type FLG sequence plus a silent variant (c.139-11C>T) 22 bases downstream of the protospacer adjacent motif (PAM) to allow identification of the rescued clone from unedited wild type cells. Through CRISPR/Cas9 induced homology directed repair (HDR), the previously induced homozygous FLG variant would be restored ultimately leading to reinstation of filaggrin protein expression, as schematically depicted (Figure 2b). HDR yielded a correction efficiency of 27% and the FLG corrected cell pool was expanded to generate FLG corrected clones. Off-target effects were screened again as described earlier (Supplementary Table S3), and none were detected (data not shown).

To validate the CRISPR/Cas9 mediated genomic engineering and clonality of our cell lines, FLG PCR amplicons were sequenced via Sanger sequencing (Figure 2c). These results indicate clonality of the Δ FLG clone and the FLG corrected clone and show the introduction of the silent intronic variant in the FLG corrected clone. The comparison of HEEs from wild type FLG keratinocytes (HEEWT) and from the Δ FLG clone (HEE $^{\Delta$ FLG}), demonstrated that knockout of FLG results in the absence of keratohyalin granules and abrogated filaggrin protein expression (Figure 2d). In the FLG corrected clone (HEE^{COR}), the presence of keratohyalin granules was reinstated together with the complete recovery of filaggrin expression, as it was expected from the protein sequences (Supplementary Table S1).

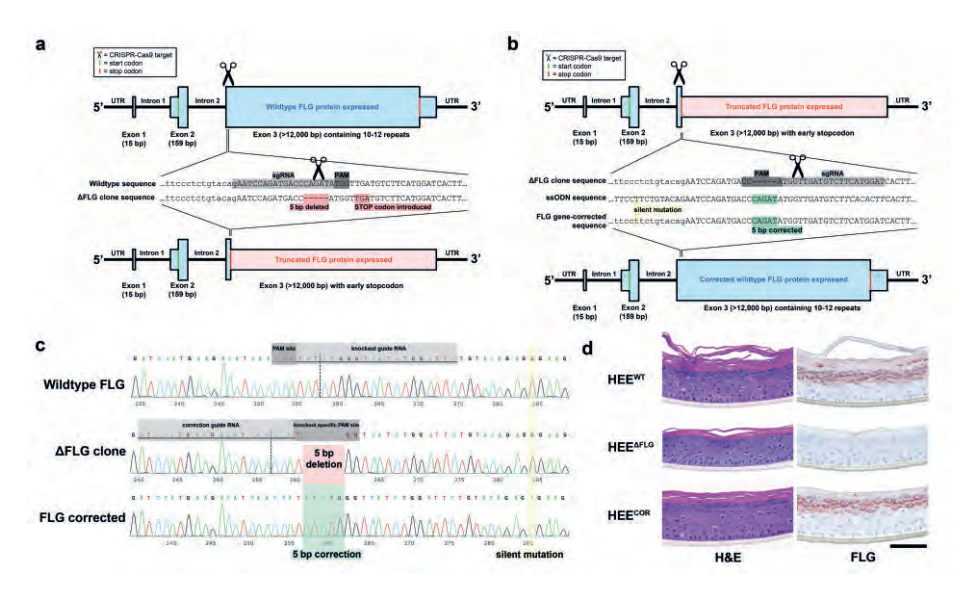


Figure 2. Validation of filaggrin expression in ΔFLG and FLG corrected cultures. a-b) Schematic representation of the genomic changes in the Δ FLG clone and FLG corrected clone, respectively. c) PCR amplified FLG sequence (reverse complement sequence depicted) indicates a 5 bp deletion (c.152del5) leading to a predicted p.P51HfsX3 frameshift mutation with an early stop codon in the ΔFLG clone and restoration of the 5bp deletion in the FLG corrected clone, d) Filaggrin protein expression is lost in HEE^{ΔFLG}, accompanied by a complete loss of keratohyalin granules, while filaggrin expression and keratohyalin granules are fully restored in HEE^{COR}. Bar = $100 \mu m$.

Filaggrin regulates epidermal differentiation gene and protein expression

Next, the expression of key epidermal marker proteins was analyzed through immunohistochemistry (Figure 3a). Interestingly, specific alterations in protein expression profiles due to the presence or absence of FLG were observed. The expression of involucrin (IVL) and transglutaminase 1 (TGM1) was partially lost in HEE^{ΔFLG} but restored in HEE^{COR}, while expression of hornerin (HRNR) and keratin 2 (KRT2) was completely abrogated in HEE^{ΔFLG} and (partially) restored in HEE^{COR}. The knockout of filaggrin expression therefore seems pivotal for the deregulated expression of other differentiation proteins. Keratin 10 (KRT10), loricrin (LOR), and late cornified envelope (LCE)2, and LCE3 were similar between HEEWT, HEEAFLG, and HEE^{COR}. To assess whether the differential expression originates from transcriptional or post-translational processes, we analyzed gene expression levels corresponding to the investigated differentially expressed proteins. These gene expression levels followed a similar pattern as for protein, with strong and significantly downregulated HRNR and KRT2 levels in the ΔFLG clone. Gene expression of KRT2 was rescued upon FLG correction, although HRNR expression remained downregulated (Figure 3b). These results indicate that loss of filaggrin can lead to (sustained) transcriptional changes in keratinocytes.

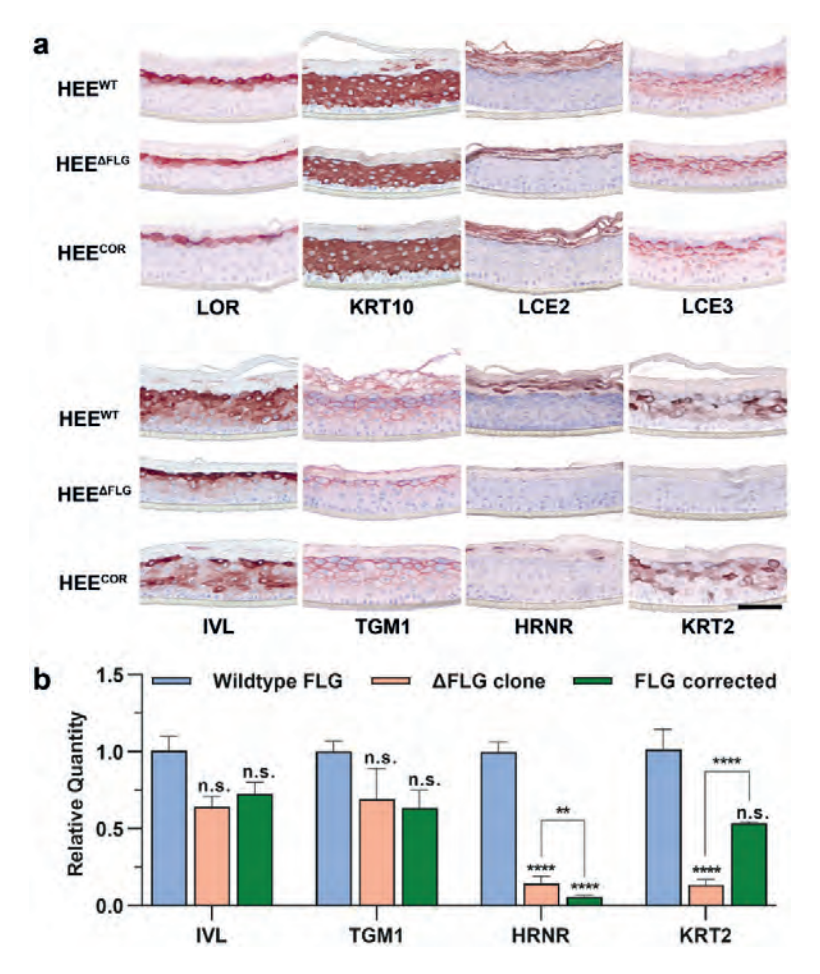


Figure 3. KRT2 and HRNR are completely abrogated as a result of FLG knockout. **a)** Immunohistochemical staining for several differentiation proteins expressions shows similarities between FLG wild type (HEE^{WT}), Δ FLG clone (HEE^{ΔFLG}) and FLG corrected clone (HEE^{COR}) (upper panel). Nevertheless, HEE^{ΔFLG} displays a downregulation of IVL and TGM1 while KRT2 and HRNR expressions were completely lost. Upon FLG correction (HEE^{COR}), the expression of IVL, TGM1, and KRT2 was completely restored, while HRNR expression is partly restored (lower panel). **b)** Quantitative PCR to analyze gene expression of differentially expressed proteins shows minor downregulation of *IVL* and *TGM1* and major downregulation of *HRNR* and *KRT2* in Δ FLG clone. FLG correction shows no effect on *IVL*, *TGM1*, and *HRNR* expression, while *KRT2* expression is partially restored to control levels. N=3 HEE cultures, ** p-value <0.01, **** p-value <0.001, n.s. non-significant. Bar = 100 μm.

Filaggrin expression is essential for epidermal barrier function

To study whether the differential gene and protein expression patterns in HEE^{ΔFLG} would have functional consequences, we first performed two qualitative microscopic analyses by small molecule permeation of lucifer yellow (for gross SC defects) and EZ-link sulfo-NHS-LC-biotin (for qualitative tight junction functioning [266, 267]).

No apparent changes in permeation of the dyes were observed (Figure 4a). Similar to what is known from in vivo studies in patients with known FLG deficiency [254], the quantitative barrier analyses by electrical impedance spectroscopy (EIS, Figure 4b) and TEWL (Figure 4c) showed a significant impairment of barrier function (lower EIS and higher TEWL) upon FLG deficiency (HEE^{ΔFLG}), while functional properties were regained upon FLG gene-correction (HEE^{COR}).

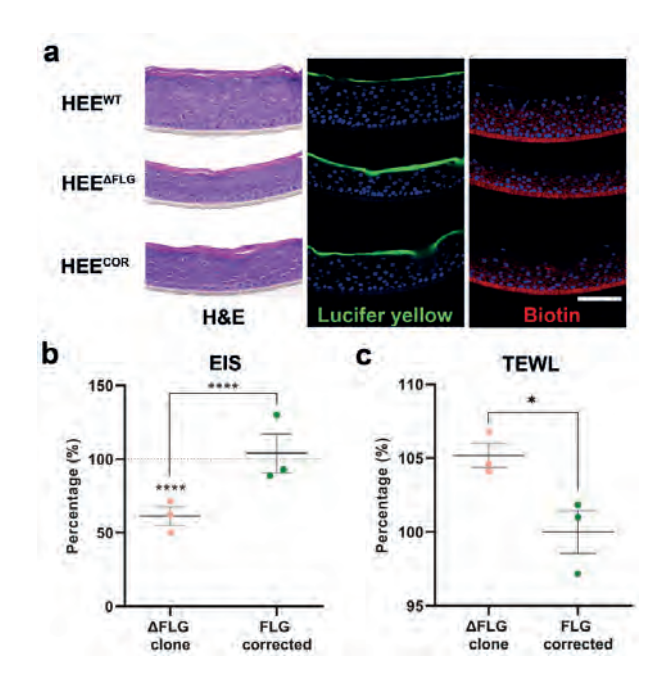


Figure 4. Knockout of FLG is accompanied by subtle changes in functional barrier properties that improve upon FLG reinstation. a) Lucifer yellow and biotin permeation assays do not display aberrant functional barrier properties of the 3D epidermal equivalent cultures. Nevertheless, b) electrical impedance spectroscopy (EIS) and c) transepidermal water loss (TEWL) analysis show significant improvement of barrier properties in FLG corrected keratinocytes compared to the Δ FLG clone. N=3 HEE, * p-value <0.05, **** p-value <0.0001. Bar = $100 \mu m$.

Discussion

In this study, we showcase straightforward RNP-based genomic editing in immortalized N/TERT keratinocytes without the use of plasmids or viral vectors that incorporate their genetic material. Because N/TERT-2G keratinocytes can be expanded in clonal (dilution) series, there is no need for antibiotic or fluorescence activated selection procedures, thereby CRISPR/Cas9 genome editing can be harnessed rather easily in many research programs and may revolutionize the investigative dermatology field. In reality, we observed that its implementation is rather slow, based on number of publications using (immortalized) keratinocytes compared to publications using any cell type [261]. Therefore, we deem it important to showcase how to disrupt (and to reinstate) the protein of interest in the immortalized N/TERT-2G keratinocyte cell line. Genome editing as we performed utilizes NHEJ, a repair mechanism that is completely stochastic and unpredictable, but suitable to generate random indels [268]. For subsequent specific corrective editing we successfully employed a HDR strategy by supplying a donor oligonucleotide carrying the desired gene-correcting DNA sequence. Given the highly intriguing, yet partly undefined, role of (pro)filaggrin in skin barrier function and the remaining knowledge gap on the therapeutic targeting of FLG deficiency, we focused on the FLG gene in this proof-of-principle study by targeting its N-terminal domain leading to a full protein knockout.

The identification of FLG loss-of-function variants and copy number variations as genetic risk factors for AD [42, 206, 207, 269] underscores the importance of the epidermal compartment in the pathogenesis of complex immune-mediated diseases. Fundamental research into the role of profilaggrin in AD pathophysiology has primarily addressed the palette of contributing profilaggrin-degrading factors [270, 271], e.g. skin-specific retroviral-like aspartic protease (SASPase) [272], kallikrein-related peptidase 5 (KLK5) [273], matriptase (MT-SP1) [274], and furin [275]. Further processing of filaggrin into NMFs can be attributed to proteases like caspase 14 (CASP14) [7] and bleomycin hydrolase (BLMH) [276]. While these studies on the breakdown and processing of profilaggrin into filaggrin monomers and amino-acids, and crosslinking to keratin intermediate filaments are abundant, studies on the N-terminal domains of profilaggrin and their functions are scarce.

Analysis of the structure and functional domains of profilaggrin showed that the N-terminal fragment of profilaggrin contains a nuclear localization signal enabling its translocation to the nucleus before onset of terminal differentiation [277-280]. It has been hypothesized that the translocated N-terminal fragment promotes keratinocyte

denucleation in apoptotic terminally differentiating keratinocytes [278]. In addition, the profilaggrin N-terminal fragment potentially regulates epidermal differentiation genes, as suggested before [281], and may halt keratinocyte proliferation upon overexpression of the profilaggrin N-terminus [280]. Similar to our experiments on ΔFLG clonal keratinocytes, siRNA-mediated knockdown studies also do not report on altered proliferation rates or epidermal thickness due to filaggrin loss [282].

The truncated profilaggrin that is expressed in AD and IV disease-associated genotypes (e.g., p.R501X, c.2282del4, p.R2447X) still has an unaffected N-terminus that potentially can translocate to the nucleus. In fact, the most predominant variants in the *filagarin* gene are situated downstream of the A and B domains, although truncating sequence variants have also been found in the A domain [283]. Whether these rare early variants are also associated with atopic disease is not clear. Early truncating variants, e.a., the deletion of 17 nucleotides (c.411del17 [284]), are located downstream of the nuclear localization signal, suggesting a great importance of the A and (partial) B domain of profilaggrin. Moreover this would imply that expression of truncated profilaggrin and downstream proteolytic processing of the N-terminal part of profilagarin – at least including the nuclear localization signal – might be intact in all of the known disease-associated FLG genotypes. The herein reported Δ FLG keratinocytes express an incomplete N-terminal fragment that harbors only part of the profilaggrin A domain (50 amino acids) and completely lacks the B domain. The B domain contains a putative nuclear localization signal. These ΔFLG keratinocytes could leverage a new cellular model to study the biological function of filaggrin in the epidermis when comparing these cells to similarly created cells harboring diseaseassociated FLG genotypes. This will be the subject of further research.

Our data indicate that the loss of profilaggrin expression results in altered differentiation gene expression, e.a., HRNR and IVL are both downregulated, as was previously shown by FLG knockdown experiments [285]. Interestingly, these genes are commonly downregulated in AD [286] and their expression is reduced upon stimulation with T-helper (Th)2 cytokines IL-4 and IL-13 in vitro [75, 287, 288]. Furthermore, parallel downregulation of HRNR and FLG has been described [288], which is in line with the data presented in this paper. The concomitant downregulation in AD may thus not be due to merely the T helper 2-cytokine milieu, as previously suggested [288], but also result from loss-offunction variants in FLG. In addition, we identified other important proteins to be largely downregulated in ΔFLG keratinocytes. Of particular interest is KRT2, the disease-causing gene in superficial epidermolytic ichthyosis (or ichthyosis bullosa of Siemens) [289, 290], a congenital skin disease, characterized by dry skin and barrier loss [291], and recently found to be differentially expressed in vesicular hand eczema patients [292]. We hypothesize that the profilaggrin N-terminal fragment can fulfill a regulatory function in the epidermis. This would explain the observed loss of specific epidermal proteins, such as KRT2, under knockout conditions, while its loss is not reported in any of the well-studied FLG loss-of-function variants that still express the N-terminal profilaggrin fragment. Besides having a potential regulatory function in the epidermis, it was reported that filaggrin might function as a structural anchoring protein in the terminally differentiating keratinocytes [6, 293]. The loss of filaggrin then implies that other differentiation proteins, e.g., IVL, are less stabilized and consequently more prone to degradation by proteasomal machinery. Although this does not explain sustained downregulation even after correction of the ΔFLG genotype, like seen for HRNR.

Microscopic qualitative analysis of lucifer yellow and biotin permeation did not indicate gross functional barrier disturbance in HEEs from Δ FLG keratinocytes, which is in line with our previous findings on patient-derived *FLG* null keratinocytes [41]. Nevertheless, the quantitative and presumably more sensitive barrier measurements we now performed (EIS and TEWL), indicate that the loss of filaggrin does affect barrier properties of HEEs, which is reversed by reinstating filaggrin expression. Whether this is directly or indirectly linked to the proposed scaffolding properties of filaggrin [294] requires further investigation, likewise the comparison of the Δ FLG-associated barrier impairment to patient-derived HEEs. Furthermore, additional analyses could be focused at the regulation of tight junction associated genes and proteins [255], and at the organization of structural intercellular lipid lamellae which are considered important for functional barrier properties of the SC [251].

For the clinical translation of our findings, next steps are aimed at the reproduction of common *FLG* variants (*e.g.*, p.R501X, c.2282del4, and p.R2447X) in N/TERT-2G immortalized keratinocytes to allow for a better comparison of genotype-phenotype differences in organotypic skin models within an otherwise identical genetic background. The subsequent exposure disease-associated inflammatory mediators or environmental factors enables the characterization of gene-environment interactions that drive multifactorial diseases, like AD. We here present the key technology and translational tools for generating unique human keratinocytes to create epidermal models with defined *FLG* variants, in which future integrative multiomics analysis can elucidate the modes of action by which profilaggrin controls terminal differentiation, and potentially finding new therapeutic options for atopic dermatitis and ichthyosis vulgaris to restore epidermal homeostasis.

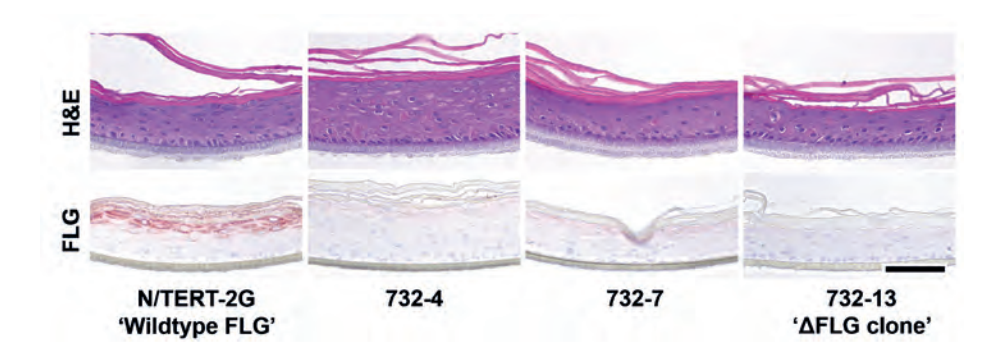
Conflict of interest

The authors declare no conflicts of interest. This publication reflects only the author's view and the JU is not responsible for any use that may be made of the information it contains.

Acknowledgements

This work was supported by a LEO foundation grant LF18068 (PZ and EB), PAST4FUTURE grant LSHM20043-HSGF (EB), and Innovative Medicines Initiative 2 Joint Undertaking (JU) grant under grant agreement no. 821511 (EB). The JU receives support from the European Union's Horizon 2020 research and innovation program and EFPIA. The Graphical abstract was created with Biorender.com.

Supplemental figures



Supplementary Figure S1. Three Δ FLG N/TERT-2G clonal keratinocyte cell lines. After clonal expansion of the Δ FLG pool, Δ FLG clonal cells were isolated (732-4, 732-7, and 732-13). Clonal cells 732-13 were renamed to ' Δ FLG clone' and used throughout the manuscript. In HEE culture, all of the Δ FLG clonal cell lines show absence of keratohyalin granules and FLG expression, whilst epidermal thickness between clonal cell lines varies. Bar = 100 μ m.

Supplemental tables

Supplementary Table S1. Genomic information on isolated clonal N/TERT-2G keratinocytes

Name in manuscript Cell line	Cell line	Zygosity	FLG expression Allele 1	Allele 1	Allele 2	Predicted FLG protein
"Wildtype FLG"	N/TERT-2G keratinocytes	Homozygous Yes	Yes	wildtype	wildtype	wildtype, 4061 amino acids
"∆FLG clone"; 732-13	ΔFLG N/TERT-2G keratinocytes	Homozygous	No	c.152_156del	c.152_156del	c.152_156del truncated, 52 amino acids
732-4	ΔFLG N/TERT-2G keratinocytes	Heterozygous	No	c.148_158del	c.151_160del	c.148_158del c.151_160del truncated, 50 amino acids and 60 amino acids
732-7	ΔFLG N/TERT-2G keratinocytes	Homozygous	No	c.153_154del	c.153_154del	c.153_154del c.153_154del truncated, 53 amino acids
"FLG corrected"	FLG corrected N/TERT-2G keratinocytes Homozygous Yes	Homozygous	Yes	c.139-11C>T	c.139-11C>T	c.139-11C>T c.139-11C>T wildtype, 4061 amino acids

Supplementary Table S2. Predicted off-target sites for guide RNA to generate FLG knockout N/TERT-2G keratinocytes (available online)

Supplementary Table 53. Predicted off-target sites for guide RNA to generate FLG gene-corrected N/TERT-2G keratinocytes (available online)

Supplementary Table 54. Sequences of the sgRNAs and ssODN.

Target	Target Name	sgRNA sequence (5′ – 3′)	PAM site	Strand
FLG	FLG FLG wildtype	GAATCCAGATGACCCAGATA	TGG	
ΔFLG	ΔFLG ΔFLG clone	ATCCATGAAGACATCAACCA	TGG	+
Target	Target ssODN name	ssODN sequence		
ΔFLG	Δ <i>FLG</i> Filaggrin correction ssODN	AATTGGCTGATAATGTGATTCTGTCTGATGCAGTCTCCCTCTGTGACTTC_CTCTGTGACAGGCTTCATGGATTCACTGAGTTTCTTCT	AAITGGCTGATAATGTGATTCTGTCTGATGCAGTCTCCCTCTGTGACTTC <u>T</u> CTCTGTACAGAATCCAGATGACCCAGATATGGTTGATGT- CTTCATGGATCACTTGGATATAGACCACAAAAAAAATTGACTTCACTGAGTTTCTTCT	AGATGACCCAGATATGGTTGATGT-

Supplementary Table S5. PCR Primer sequences

Gene	Target name	Forward primer (5' – 3')	Reverse primer (5' – 3')
FLG	FLG wildtype	TGGCTGATAATGTGATTCTGTC	CTGTTTCTCTTGGGCTCTTGG
Name	Off-target site	Forward primer (5' – 3')	Reverse primer (5' – 3')
KO_Off1	intergenic:PROM2- KCNIP3	TTGAGAAAGCTCAGGCACAC	CACTCAGGCTAGAAGCGATG
KO_Off2	intergenic:MIR873- LINC01242	CTCCAGCCAACATCAAGAAA	TTTCCAAAGGGAATTGATCC
KO_Off3	intron:ELAVL2	GGACAGACATCTGCATTCATTC	TTACCAGATTGCGTCCTGTG
KO_Off4	intergenic:GMNC- OSTN	AGAAGCAGGCTGACACCTTT	CCCAGTGATGAGGAATGGAT
KO_Off5	intergenic:Y_RNA- RP11-112L7.1	CTGTGGTTTGGTCCATTCAG	GGGAGGTCTTGTCCAGTGAT
Cor_Off1	intron:ZC3H13	CTTCTGACGCTTCATTTCCA	AACCCAACTTCCAAACAACC
Cor_Off2	intron:LINC00375	GCCAAGGTATTCAAAAGATGG	ACAACAAAGCCTCCCTGAAT
Cor_Off3	intergenic:AC090573.1- RP11-65D17.1	CGCTCCTGCAACTTCAGTAA	AGATGGCTTTGGGGAGTATG
Cor_Off4	intron:SLC16A9	TCCCACAAACATTCCATGAG	CATCTGTGAAGGCAGGCTAA
Cor_Off5	intergenic:RP11- 574O16.1-AC010887.1	GAGCCACAGAGCCTTCTTCT	AGAGCTGGGATTTGAGCCTA

Supplementary Table S6. Antibodies used for immunohistochemistry

Antibody; clone	Manufacturer	Dilution
FLG; 1957R	LifeSpan BioSciences, Inc., Seattle, WA, USA (catalog # LS-C751132)	1:200
LOR; polyclonal	Abcam, Cambridge, United Kingdom (catalog # ab85679)	1:3000
KRT10; DE-K10	Progen Biotechnik GmbH	1:100
LCE2; #74	Bergboer et al 2011 [295]	1:10000
LCE3; clone 7	Abmart, Berkeley Heights, NJ, USA	1:5000
IVL; Mon150	Van Duijnhoven et al 1992 [204]	1:20
TGM1; A-5	Santa Cruz Biotechnology Inc., Dallas, TX, USA (catalog # sc-365821)	1:100
HRNR; polyclonal	Sigma-Aldrich (catalog # HPA031469)	1:500
KRT2; Ks2.342.7.4	Progen Biotechnik GmbH, Heidelberg, Germany (catalog # 65191)	1:200

Supplementary Table S7. Quantitative PCR primer sequences

	•		
Gene	Target name	Forward primer (5' – 3')	Reverse primer (5' – 3')
hARP	Human acidic ribosomal phosphoprotein P0	CACCATTGAAATCCTGAGTGATGT	TGACCAGCCCAAAGGAGAAG
IVL	Involucrin	ACTTATTTCGGGTCCGCTAGGT	GAGACATGTAGAGGGACAGAGTCAAG
TGM1	Transglutaminase 1	CCCCGCAATGAGATCTACA	ATCCTCATGGTCCACGTACACA
HRNR	Hornerin	TACAAGGCGTCATCACTGTCATC	ATCTGGATCGTTTGGATTCTTCAG
KRT2	Keratin 2	CGCCACCTACCGCAAACT	GAAATGGTGCTGCTTGTCACA

Supplemental methods

In silico search for potential off-target effects

CRISPOR (version 4.98)[265] was used to search for potential off-target sites dependent on the *Streptococcus pyogenes* derived Cas9 (SpCas9) PAM site (5'-NGG-3'), target genome (homo sapiens GRCh38/hg38) and our specific sgRNA selection. The top-5 potential off-target sites, ranked on cutting frequency determination (CFD) score [296], were amplified by PCR and analyzed by Sanger sequencing to assure no off-target mutations occurred. See Supplementary Table S5 for details on the PCR primers used.

Protein sequence prediction

EMBOSS Transeq (https://www.ebi.ac.uk/Tools/st/emboss_transeq/), a webtool designed to predict the translation of mRNA sequence into protein amino acid sequence was used with standard settings to predict the result of the DNA mutations generated [297].

Morphological and immunohistochemical analysis

HEEs were fixed in 4% formalin solution for 4 hours and subsequently embedded in paraffin. 6 µm sections were stained with hematoxylin and eosin (H&E, Sigma-Aldrich) or processed for immunohistochemical analysis. Sections were blocked for 15 minutes with 5% serum in phosphate-buffered saline (PBS) and subsequently incubated with primary antibody against the protein of interest for 1 hour at room temperature. Next, a 30 minute incubation step with biotinylated secondary antibody (Vector Laboratories, Burlingame, CA, USA) was performed, followed by a 30 minute incubation with avidin-biotin complex (Vector laboratories). The peroxidase activity of 3-Amino-9-ethylcarbazole (AEC) was used to visualize the protein expression and the sections were mounted using glycerol gelatin (Sigma-Aldrich). See Supplementary Table S6 for details on the primary antibodies used.

Transcriptional analysis

Total RNA was isolated using the Favorprep total tissue RNA kit (Favorgen Biotech, Taiwan), according to the manufacturer's protocol. cDNA was generated after DNase treatment and used for quantitative real-time PCR (RT-qPCR) by use of the MyiQ Single-Colour Real-Time Detection System (Bio-Rad laboratories, Hercules, CA, USA) for quantification with Sybr Green and melting curve analysis. Primers (Supplementary Table S7) were obtained from Biolegio (Nijmegen, The Netherlands) and Merck KGaA (Darmstadt, Germany). Target gene expression levels were normalized to the expression of *human acidic ribosomal phosphoprotein P0*

(RPLPO). The relative expression levels of all genes of interest were measured using the 2-ΔΔCT method [246]. Two-way ANOVA with Tukey's multiple comparison tests were performed on the Δ CT values to assess statistical significance.

Lucifer yellow dye penetration assay

To study the outside-in SC barrier function, 20 µL Lucifer Yellow (1 mM, Sigma-Aldrich) was applied on top of the HEEs and was allowed to incubate for 60 minutes in the dark at room temperature. HEEs were fixed in buffered 4% formalin solution, embedded in paraffin and sectioned, 6 um sections were deparaffinized and mounted with Fluoromount-G, containing DAPI (eBioscience Inc. San Diego, CA, USA).

Biotin penetration assay

To study the inside-out SC barrier function, the HEEs were turned upside down and 20 µL EZ-link sulfo-NHS-LC-biotin (3.3 mg/mL, Thermo Fisher Scientific, Waltham, MA, USA) was applied on the bottom of the filters and allowed to incubate for 60 minutes at room temperature. HEEs were fixated in buffered 4% formalin solution, embedded in paraffin and sectioned. 6 µm sections were deparaffinized and incubated for 30 minutes, in the dark, with 1:200 Alexa Fluor 594 streptavidin (Thermo Fisher Scientific) conjugate. The sections were mounted with Fluoromount-G containing DAPI.

Electrical impedance spectroscopy (EIS) and transepidermal water loss (TEWL)

Whereas transepithelial electrical resistance (TEER) measurements are suitable for detecting barrier properties related to tight junction presence and functionality, EIS is more suitable for epidermal equivalent cultures as it is a composed measure of TEER and electrical capacity of the cell compartment. EIS was measured using the real-time impedance detector Locsense Artemis (Locsense, Enschede, The Netherlands) equipped with SmartSense lid for monitoring cells in conventional transwell plates containing inserts. After lowering of day 10 air-exposed HEE cultures to the middle position of the culture plate, 500 µL of PBS was added on top and 1100 µL PBS was added beneath the transwell filter. Following calibration, continuous impedance (Ω) was measured while sweeping frequency from 10Hz to 100.000Hz. Afterwards, measured impedance was corrected for blank impedance per electrode and corrected for culture insert size (0.47 cm²), resulting in impedance per cm² values (Ω /cm²). Subsequently, measured phase values along the same frequency reach were used to pinpoint the frequencies where contribution of cellular capacity was relatively limited. Mean impedance per cm² at these three frequencies was used to calculate relative differences between conditions. Two-way ANOVA with Tukey's multiple comparison test was performed to assess statistical significance. TEWL was measured, after equilibration of the HEE cultures to room temperature, using the Aquaflux AF200 (Biox, London, UK) on day 10 of the airexposed phase of the HEE culture, as described before [41]. Unpaired parametric t test was used to assess statistical significance.

Funding information

This work was supported by a LEO foundation grant LF18068 (PZ and EB), PAST4FUTURE grant LSHM20043-HSGF (EB), and Innovative Medicines Initiative 2 Joint Undertaking (JU) grant under grant agreement no. 821511 (EB). The JU receives support from the European Union's Horizon 2020 research and innovation program and EFPIA.



Chapter 5

The aryl hydrocarbon receptor regulates epidermal differentiation through transient activation of TFAP2A

Jos P.H. Smits^{1,2†}, Jieqiong Qu^{3†}, Felicitas Pardow^{1,3,#}, Noa J.M. van den Brink^{1#}, Diana Rodijk-Olthuis¹, Ivonne M.J.J. van Vlijmen-Willems¹, Simon J. van Heeringen³, Patrick L.J.M. Zeeuwen¹, Joost Schalkwijk¹, Huiqing Zhou^{3,4,†*}, Ellen H. van den Bogaard^{1,†*}

¹Department of Dermatology, Radboud Research Institute for Medical Innovation, Radboudumc, Nijmeaen, The Netherlands;

²Department of Dermatology, University Hospital Düsseldorf, Medical Faculty, Heinrich Heine University, Düsseldorf, Germany;

³Department of Molecular Developmental Biology, Faculty of Science, Radboud University, Nijmegen, The Netherlands:

⁴Department of Human Genetics, Radboudumc, Nijmegen, The Netherlands;

†These authors contributed equally;

#These authors contributed equally.

Abstract

The aryl hydrocarbon receptor (AHR) is an evolutionary conserved environmental sensor identified as indispensable regulator of epithelial homeostasis and barrier organ function. Molecular signaling cascade and target genes upon AHR activation and their contribution to cell and tissue function are however not fully understood. Multi-omics analyses using human skin keratinocytes revealed that, upon ligand activation, AHR binds open chromatin to induce expression of transcription factors (TFs), e.g., Transcription Factor AP-2 α (TFAP2A), as a swift response to environmental stimuli. The terminal differentiation program including upregulation of barrier genes, filaggrin and keratins, was mediated by TFAP2A as a secondary response to AHR activation. The role of AHR-TFAP2A axis in controlling keratinocyte terminal differentiation for proper barrier formation was further confirmed using CRISPR/Cas9 in human epidermal equivalents. Overall, the study provides additional insights into the molecular mechanism behind AHR-mediated barrier function and identifies potential targets for the treatment of skin barrier diseases.

Introduction

The skin, being an important barrier organ, plays a major role in protecting and fostering the life it encloses. Within the ever-renewing epidermis, keratinocytes are the predominant cell type, accounting for 95% of epidermal cells [298]. The continuous renewing of the epidermis is highly dependent on the delicate balance between keratinocyte proliferation and differentiation. During epidermal development, basal stem cells give rise to daughter cells which undergo a coordinated program of cell cycle arrest, upward migration, and terminal differentiation. Maintaining the integrity of the epidermis is essential for skin homeostasis and protection of the host against infections, allergens, UV radiation and other external threats through host defense, and physical, chemical, and immunological barrier mechanisms [299]. As such, a compromised epidermal barrier is a prominent feature of common inflammatory skin diseases, like atopic dermatitis and psoriasis [300, 301]. In healthy skin, epidermal homeostasis is tightly controlled through a set of essential transcription factors (TFs), e.a., TP63, AP1, and the aryl hydrocarbon receptor (AHR)[9, 167, 302].

AHR is a TF that is considered a sensor of environmental, microbial, metabolic, and endogenous cues. Depending on the specific activating ligand, AHR activation can cascade into a response ranging from highly toxic to therapeutic [144, 167, 303]. AHR is involved in many biological processes, from cellular proliferation and differentiation to immune responses both innate and adaptive of origin. Upon activation, AHR translocates from the cytoplasm to the nucleus, where it dimerizes with AHR nuclear transporter (ARNT) to bind to its cognate DNA consensus sequence (5¢-TNGCGTG-3¢) known as the xenobiotic response element (XRE) and regulates gene transcription [167, 304]. Certain AHR-activating ligands are highly toxic, e.g., high-affinity environmental pollutant dioxins (e.g., 2.3,7,8-Tetrachlorodibenzop-dioxin (TCDD)). TCDD has an extremely long half-life (estimated at 7.1 years in humans) resulting in prolonged and uncontrolled AHR activation [305, 306], while other AHR ligands are rapidly degraded and considered of more physiological importance, e.g., 6-formylindolo[3,2-b]carbazole (FICZ), which is generated upon UV radiation of keratinocytes [97, 307, 308].

Over the years, we have gained better understanding of the effects of AHR activation on inflammatory skin conditions since the discovery of AHR activation as the working mechanism of coal tar (CT) ointment that was used for psoriasis and atopic dermatitis treatment [75, 77, 309]. These insights sparked the global interest in therapeutics that target the AHR in skin diseases and beyond, and led to the registration of Tapinarof, an AHR ligand, for psoriasis [153, 217]. Phase 3 clinical trials in atopic dermatitis are ongoing (NCT05032859). Other AHR ligands with similar biological implications, including carboxamide and indazole derivatives, have also been studied for their therapeutic anti-inflammatory and barrier promoting potential [177, 219, 221, 222, 310].

At the molecular level, mainly four groups of genes are known to be targeted by AHR in the skin. Firstly, a battery of xenobiotic metabolizing enzymes (XMEs), including cytochrome P450 monooxygenases (P450s), e.g., *CYP1A1*[311]; secondly, genes involved in keratinocytes differentiation [211], e.g., *filaggrin* and *involucrin* [75, 132, 150, 171]; thirdly, genes related to host defense, e.g., the antimicrobial peptide (AMP) families of *S100* genes, *late cornified envelope* (*LCE*) genes, and *peptidase inhibitor* (*Pl*)3, amongst others [77, 171]; and finally, genes related to immunity, e.g., the inflammatory cytokines *Interleukin* (*IL*)-1 β , *IL*-6, *CXCL5*, *CCL20* and *IL*-10 [312-314]. Hence, AHR activation is found to increase epidermal differentiation and barrier formation [75, 76, 169, 171], and dampen skin inflammation [148]. However, the sequence and dynamics of the molecular events and other players involved through which AHR mediates these effects are poorly understood.

In this study, we aim to characterize regulatory cascade upon AHR activation in human keratinocytes. Through transcriptomic and epigenomic analyses, we identified a hitherto unrecognized AHR-TFAP2A axis that regulates epidermal keratinocyte terminal differentiation and skin barrier formation.

Results

AHR activation results in distinct early and late transcriptional programs

To characterize the gene expression pattern upon AHR activation in human primary keratinocytes, we performed RNA-sequencing on keratinocytes either treated with TCDD or coal tar (CT), two AHR model ligands, for short term (2 h) and longer exposure duration (24 h). Principle component analysis (PCA) showed transcriptome alterations in ligand treated samples already after 2 h of treatment, indicating that ligand exposure results in swift AHR activation and transcription regulation (Fig. 1a). The differences became increasingly apparent between 2 h and 24 h of ligand treatment, indicated as the major change through PC1 axis (71% variance). Differences between TCDD and CT treated samples were minor as they closely clustered in the PCA plot, indicating that regulatory events downstream of AHR activation are similar in both treatment conditions. *CYP1A1* and *CYP1B1*, target genes

in canonical AHR signaling, showed consistent up-regulation upon both ligand treatments, more significantly after 24h treatment (Fig. 1b). Their gene expression was validated with gPCR (Fig. 1c). These observations indicate that TCDD and CT treatment activate AHR signaling pathways through a similar pool of genes within 24 h, and we therefore focused on the common mechanism shared between TCDD and CT treatment in subsequent analyses, hereafter referred to as "ligand-treatment".

Next, we identified differentially expressed genes (DEGs, adjusted p value <0.05) between the control and at both 2 h and 24 h of ligand treatment. In total, 8160 DEGs were grouped into eight hierarchical clusters according to the gene expression dynamics at different time points after ligand treatment (Fig. 1d, Table 1, and Supplementary Data 1), Clusters 1 and 2 show early downregulation upon ligandtreatment, with no apparent late effects or dampened downregulation after 24 h of treatment, respectively. Cluster 3 and cluster 8 comprised the majority of DEGs but their gene expression was unrelated to AHR ligand treatment and mainly affected by the keratinocyte differentiation itself. Genes from cluster 3 are mainly associated with gene ontology (GO) term 'cell cycle' and genes from cluster 8 are involved in 'translation', Importantly, genes in cluster 4 showed up-regulated expression after 2 h ligand treatment and are involved in the processes of 'phosphorylation' and 'epithelium development', e.g., NOTCH2, JUN, TFAP2A, KRT4, and POU3F1. In contrast, genes in cluster 5 showed late up-regulated expression only after 24 h of ligand treatment and mainly contribute to 'keratinocyte differentiation', e.g., FLG and IVL, and 'oxidationreduction process', e.g., HYAL1 and CYCS. Clusters 6 contains genes that are slightly upregulated early after ligand treatment. These genes appear downregulated at 24 h in control, probably due to differentiation, while ligand treatment at this timepoint dampens the downregulation. Cluster 7 contains genes that are downregulated 24 h after treatment initiation. Interestingly, there was no distinct cluster of genes that showed continuous up-regulation or down-regulation at 2 h and 24 h after TCDD and CT treatment. This highlights the dynamics of AHR signaling in primary cells, rather than the reported continuous signaling in (cancer) cell lines [315].

To dissect the molecular events upon AHR activation, we continued to focus on clusters of 'early-responsive genes (ERGs)' (cluster 4, Fig. 1e, upregulation 2h after ligand treatment) and 'late-responsive genes (LRGs)' (cluster 5, Fig. 1f, upregulation 24h after ligand treatment). The separation of ERGs and LRGs suggests a different regulatory mechanism of AHR signaling between early and late responses. This observation led us to hypothesize that the early and late responses are potentially linked via TFs in ERGs that activate transcription of LRGs. Indeed, among the 8160 DEGs, 558 genes were classified as TFs and 76 TFs out of 791 genes (10%, hypergeometric p value = 0.001) were found in ERGs, e.g., *HES1*, *HES2*, *FOSL1*, *JUN*, *TFAP2A*, and *SOX4*. In contrast, LRGs did not show a significant enrichment of TFs (13 TFs in 633 genes, e.g., *GRHL1* and *STAT6*, hypergeometric p-value = 1.2) (Fig. 1e, f, Supplementary Data 1). This clear enrichment of TFs in ERGs in contrast to LRGs supports our hypothesis that the up-regulated TFs among ERGs regulated the expression of LRGs, including the expression of epidermal differentiation genes.

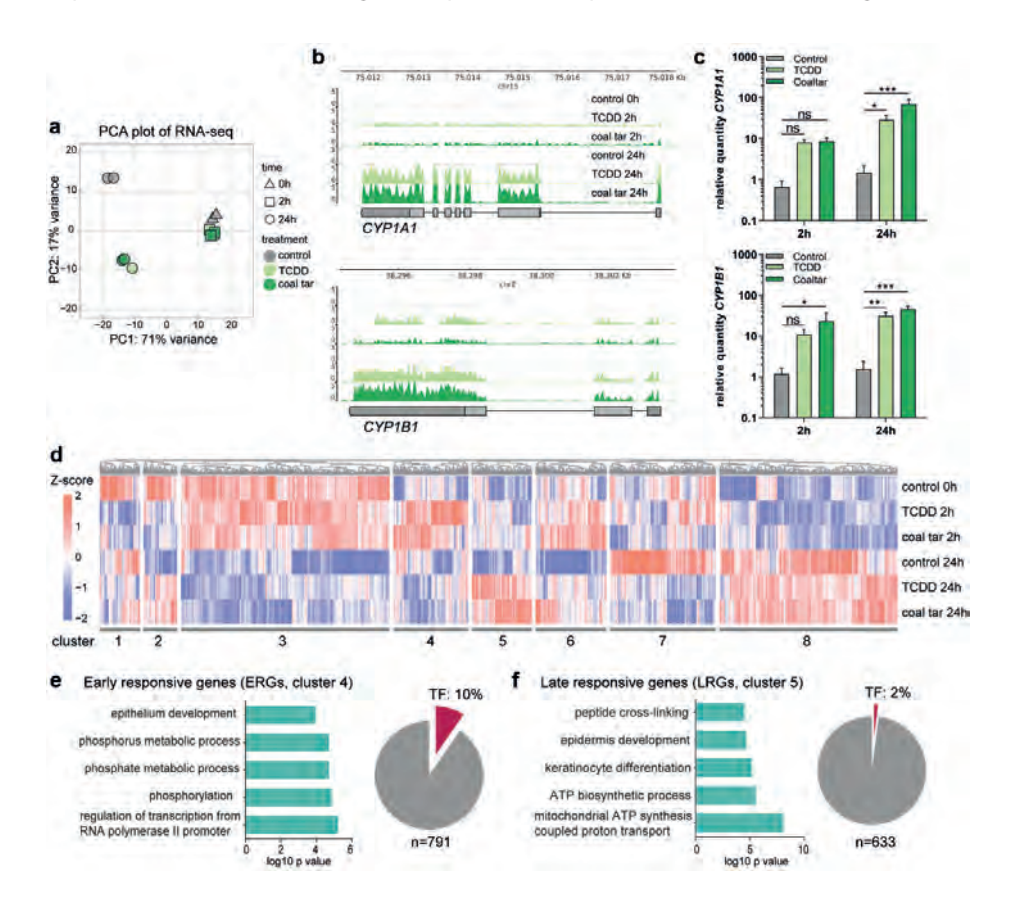


Figure 1. AHR activation results in distinct early and late response. **a)** Principal component analysis (PCA) of RNA-seq data indicating that 24 h after TCDD or coal tar treatment, the response is highly similar. **b)** Genome browser screenshots of *CYP1A1* and *CYP1B1* on RNA-seq tracks. **c)** RT-qPCR validation of *CYP1A1* and *CYP1B1*. Data shown as mean ±SEM, N=5 technical replicates, two-way ANOVA, ns p value > 0.05, * p value <0.05, ** p value <0.01, *** p value <0.001. **d)** Hierarchical clustering of differentially expressed genes (p value <0.05). Z-score was calculated based on log10 (FPKM+0.01) of each gene. e GO annotation of ERGs, accompanied by a pie chart showing the number and percentage of TFs within the f GO annotation of LRGs, accompanied by a pie chart showing the number and percentage of TFs within the cluster.

AHR activation promotes dynamic alterations of the enhancer landscape

To identify AHR target genes, including TFs, we set out to first map enhancers bound by AHR. Being a receptor of environmental cues, AHR was expected to bind to chromatin in a swift and transient manner, and therefore we first performed AHR targeted chromatin immunoprecipitation followed by gPCR (ChIP-gPCR) to determine the binding time frame. At 30 min of ligand treatment, AHR binding signals were detected at the loci of the known AHR target gene CYP1A2 (Fig. 2a).

Such fast binding of AHR was consistent with the translocation of AHR from the cytoplasm to the nucleus as shown by immunofluorescent staining after 30 min of ligand treatment (Fig. 2b). Notably, the AHR binding signals decreased after 90 min of ligand treatment (Fig. 2a), confirming the transient character of AHR interaction to its target loci. The dynamic binding on the genome by AHR in primary keratinocytes is consistent with our observations on gene expression changes upon AHR activation (Fig. 1d).

Since we consistently observed similar gene expression and AHR binding following both TCDD and CT treatments, we continued our experiments with only TCDD stimulation to model AHR activation. To identify AHR-responsive enhancers that are involved in gene activation, we performed H3K27ac ChIP-sequencing after TCDD treatment for 30 and 90 min. Clustering of enhancer regions based on H3K27ac signals gave rise to four clusters consisting of 4,604 enhancers (Fig. 2c and Supplementary Data 2). Subsequently, motif analysis was performed to predict TFs that potentially bind to these enhancers (Fig. 2e, Supplementary Data 2). Among the four clusters, only cluster 1 (shown as C1) containing a small number (186) of enhancer regions showed decreased activity upon AHR activation by TCDD at 30 min (Fig. 2c), and motif analysis did not yield statistically enriched TF motifs (Supplementary Data 2). Cluster 2 (C2) represents 945 enhancer regions that showed a reasonable level of H3K27ac signals in the control (0 min) and increased signals at 30 min of TCDD treatment. The H3K27ac signals remained high after 90 min. Genes nearby these enhancers are mainly involved in 'omega-hydroxylase P450 pathway' shown by the GO analysis (Fig. 2d), and contain many known AHR targets, such as CYP1A1 and CYP1A2. TF motif analysis showed that the AHR motif was the only highly enriched motif in C2, indicating that this cluster of enhancers are likely directly bound by AHR (Fig. 2e, Supplementary Data 2). Cluster 3 (C3) contains 2470 enhancer regions maintaining high signals at 0 and 30 min, which decreased after 90 min of TCDD treatment. Genes nearby these enhancers are mainly involved in 'regulation of Notch signaling pathway', e.g., BMP7, HES1, JAG1, and 'immune system development', e.g., BCL6 and CD28 (Fig. 2d). CHOP, ATF4, AARE and CEBP binding motifs from the AP-1 motif family were enriched in C3 enhancers (Fig. 2e, Supplementary Data 2). The last cluster, cluster 4 (C4), consisted of 1003 enhancers showing higher activity only after 90 min of TCDD treatment, with nearby genes being predominantly involved in 'keratinocyte differentiation', e.g., FLG and HRNR. This cluster did not contain significantly enriched TF binding motifs (Supplementary Data 2).

To confirm the motif analysis of C2 in which the AHR motif was enriched, we performed AHR ChIP-sequencing with TCDD treatment and obtained 57 AHR binding sites (adjusted p value = 1e-4, Supplementary Data 3). When examining H3K27ac signals at AHR binding sites, we observed persistent H3K27ac signals at both 30 min and 90 min of treatments (Fig. 2f), fully consistent with C2 cluster enhancer signals (Fig. 2c), confirming this cluster of enhancers being direct targets of AHR. Of note, the apparent H3K27ac signals at most of the C2 cluster enhancers in the control without ligands indicate that AHR binds to open chromatin regions. At the same time, AHR binding signals peaked at 30 min and went down after 90 min of treatment (Fig. 2g), in line with the transient AHR binding observed from ChIP-qPCR analysis of the CYP1A2 locus (Fig. 2a).

In summary, these data demonstrate a transient nature of AHR-enhancer binding, leading to early activation of enhancer targets (C2) and the late activation of enhancers near epidermal differentiation genes (C4). This distinct activation scheme is consistent with the temporal divided expression pattern of ERGs and LRGs (Fig. 1).

Transcription factor AP-2 Alpha (TFAP2A) is direct target of AHR

To confirm our hypothesis that AHR-controlled TFs among ERGs regulate keratinocyte differentiation program as the secondary response to AHR activation, and to identify such candidate TFs, we integrated the RNA-sequencing, AHR ChIP-sequencing and H3K27ac ChIP-sequencing data. We set the criteria of such intermediate TFs to: exhibiting up-regulated gene expression upon AHR activation by ligands (cluster 4 in Fig. 1d) and denoted by a nearby AHR-bound active enhancer as indicated by AHR and H3k27ac ChIP-sequencing signals. Based on these criteria, we identified several transcription factors, including Transcription Factor AP-2 Alpha (TFAP2A), HES2 and FOSL1 (Suppl. Fig. 1).

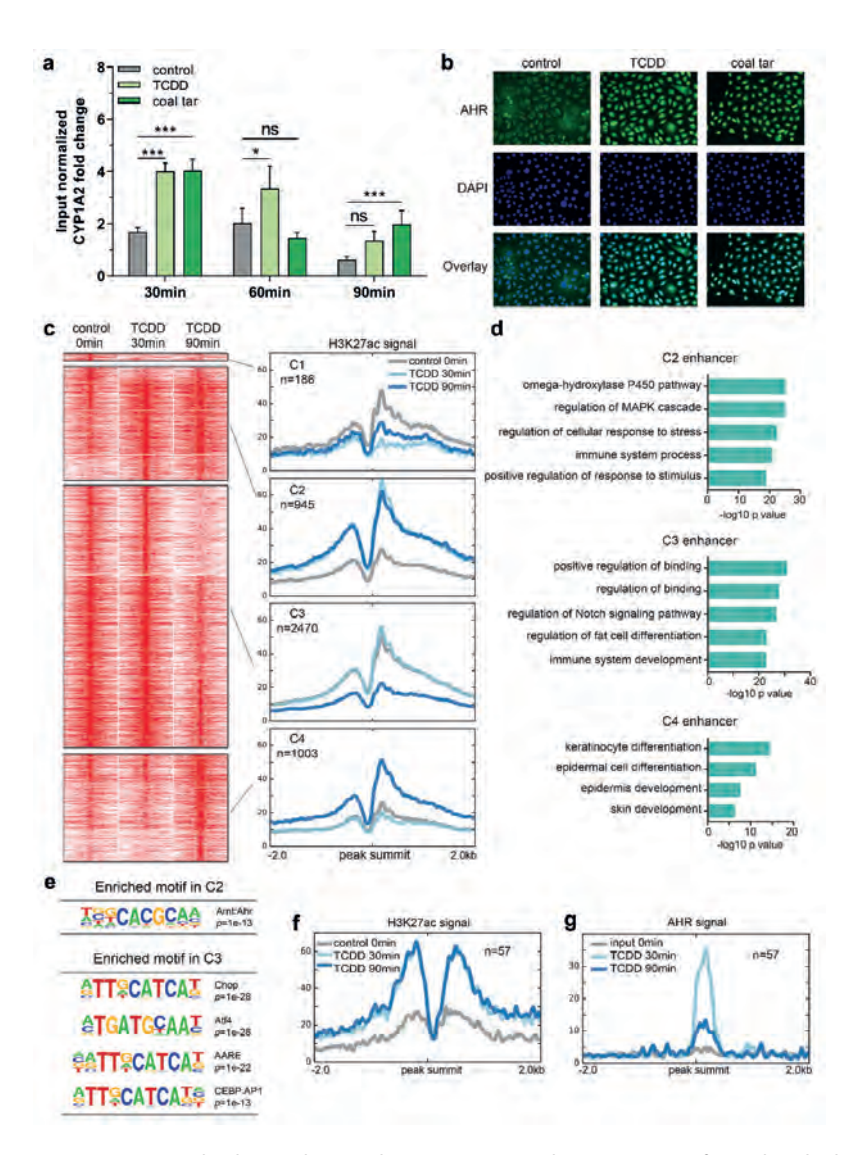


Figure 2. AHR activation leads to enhancer dynamics. a) AHR ChIP-RT-qPCR performed at the loci of CYP1A2 (as a positive control) at different time point after ligand treatment. Input normalized fold change is relative to both input DNA and negative control loci (chr11). Data shown as mean ±SEM, N=6 technical replicates, two-way ANOVA, ns p value > 0.05, * p value <0.05, *** p value <0.001. b) AHR translocation from the cytoplasm to the nucleus after 30min of ligand treatment. c) Clustering of the dynamic enhancers upon AHR activation. Heat maps and band plots are shown in a 4-kb window with summits of enhancers in the middle. Color intensity in heat maps represents normalized read counts. In the band plots, the median enrichment was shown. d) GO annotation of enhancers in C2, C3 and C4. e) Significantly enriched motifs found in C2 and C3 of dynamic enhancers shown in c. f) Band plot showing the quantification H3K27ac ChIP-seg signals at AHR binding sites upon ligand treatment. g Band plot showing the quantification AHR ChIP-seg signals at AHR binding sites upon ligand treatment.

As TFAP2A is known to play a role in keratinocyte differentiation [316, 317], we decided to focus on dissecting TFAP2A's interaction with AHR. TFAP2A is among ERGs and has an intronic AHR-bound enhancer with a high H3K27 signal (Fig. 3a). AHR binding at this locus was validated by ChIP-qPCR (Fig. 3b), establishing TFAP2A as a likely direct AHR target.

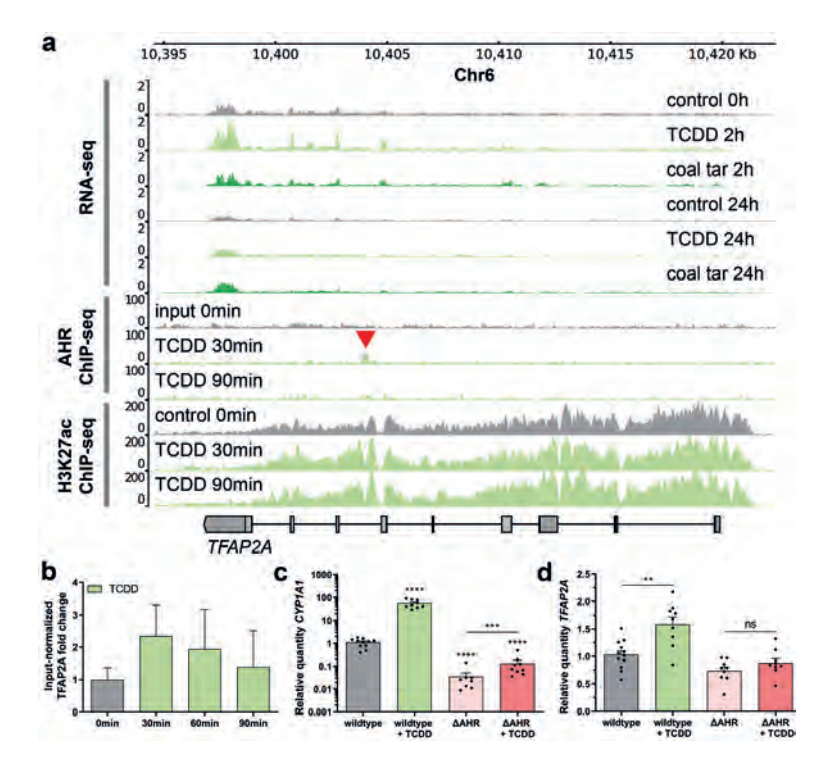


Figure 3. AHR targets TFAP2A in the early response to AHR ligands. **a)** Genome browser screenshots of the *TFAP2A* coding region show RNA-seq, AHR ChIP-seq, and H3K27ac ChIP-seq tracks upon treatment with coal tar and TCDD. Red arrow indicates AHR binding site within the *TFAP2A* locus. **b)** AHR ChIP-RT-qPCR validation at the loci of *TFAP2A* at different time point after ligand treatment. Input normalized fold change is relative to both input DNA and negative control loci (chr11). Data are shown as mean \pm SEM, N=2 technical replicates. **c, d)** Knockout of AHR (Δ AHR) is accompanied by the loss of CYP1A1 (as classical AHR target) and *TFAP2A* expression. Data shown as mean \pm SEM, N> 5 technical replicates, one-way ANOVA. ns p value > 0.05, ** p value <0.01, *** p value <0.001, *** p value <0.0001.

To functionally validate whether TFAP2A is a primary AHR target, clonal homozygous AHR knockout (Δ AHR) keratinocytes were generated using CRISPR/Cas9 in the immortalized N/TERT-2G keratinocyte cell line [262]. After clonal expansion of the knockout pool, a full Δ AHR clonal keratinocyte cell line was identified using PCR and subsequent Sanger sequencing. On both alleles one nucleotide was deleted

resulting in a frameshift after 76 amino acids, and an early stop codon that translates to a loss-of-function truncated AHR protein. As expected, the expression of a known AHR target gene CYP1A1 was significantly lower in ΔAHR keratinocytes than that in wildtype cells, and CYP1A1 expression in ΔAHR keratinocytes was only marginally enhanced by TCDD treatment, in contrast to wildtype cells (Fig. 3c). Importantly, ΔAHR keratinocytes showed a loss of target gene expression and TCDD treatment of \triangle AHR keratinocytes did not increase the *TFAP2A* expression level, in contrast to the enhanced expression of AHR wildtype keratinocytes (Fig. 3d), which is in line with our notion that TFAP2A is indeed an AHR direct target gene.

AHR-TFAP2A axis controls the epidermal differentiation program

Next, we investigated the contribution of TFAP2A activation in AHR-mediated keratinocyte differentiation. We knocked down TFAP2A in monolayer primary keratinocyte cultures using siRNAs (52% knockdown compared to siControl; Fig. 4a, b), treated TFAP2A knockdown keratinocytes with TCDD for 24h to activate AHR signaling, performed RNA-sequencing analysis, and detected 435 genes that were differentially expressed between TCDD-treated siCtrl and siTFAP2A (Supplementary Data 4). To identify TFAP2A-mediated AHR signaling, we examined the effect of TFAP2A knockdown on TCDD-induced gene expression and compared them to the earlier identified panel of AHR-responsive genes (from Fig. 1d, all clusters, 3084 DEGs in total, 1976 genes up- and 1108 genes downregulated). Among the 435 differentially expressed genes upon TFAP2A knockout, 214 are overlapping with the identified 3084 AHR-responsive genes. The overlapping genes were clustered according to their expression patterns (Fig. 4c, Supplementary Data 4). Clusters 1 and 2 (18 and 40 genes, respectively) contain genes that are downregulated by TCDD and remain downregulated (cluster 1) or become upregulated (cluster 2) upon TCDD treatment in TFAP2A knockdown condition. Cluster 3 and 4 (57 and 99 genes, respectively) contain genes that are upregulated by TCDD treatment and remain upregulated in both conditions (cluster 3) or become downregulated upon TCDD treatment in TFAP2A knockdown condition (cluster 4). Because cluster 4 genes were induced by TCDD and the induction was abolished by TFAP2A knockdown, these genes were marked as a TFAP2A-mediated AHR response genes. Cluster 4 was found to be enriched for LRGs (mean fold enrichment 20.8, hypergeometric p-value 7.11e-47), including IVL, several S100 genes, and SPRR genes that are involved in terminal differentiation of epidermal keratinocytes. In line with this, functional annotation of the genes in cluster 4 resulted in 57 significantly enriched GO terms, such as 'epidermis development' and 'keratinocyte differentiation' (Fig. 4d).

To investigate whether TFAP2A directly regulates these genes, we sought for the TFAP2A binding motif near promoter and enhancers of genes in cluster 4. We found that 64 out of 99 genes have a TFAP2A binding motif at their promoter regions while all 99 genes have TFAP2A motif at their enhancer regions (Supplementary Data 5). These results indicate that TFAP2A likely regulate these cluster 4 genes directly, and support the notion that AHR controls keratinocyte differentiation through activation of TFAP2A.

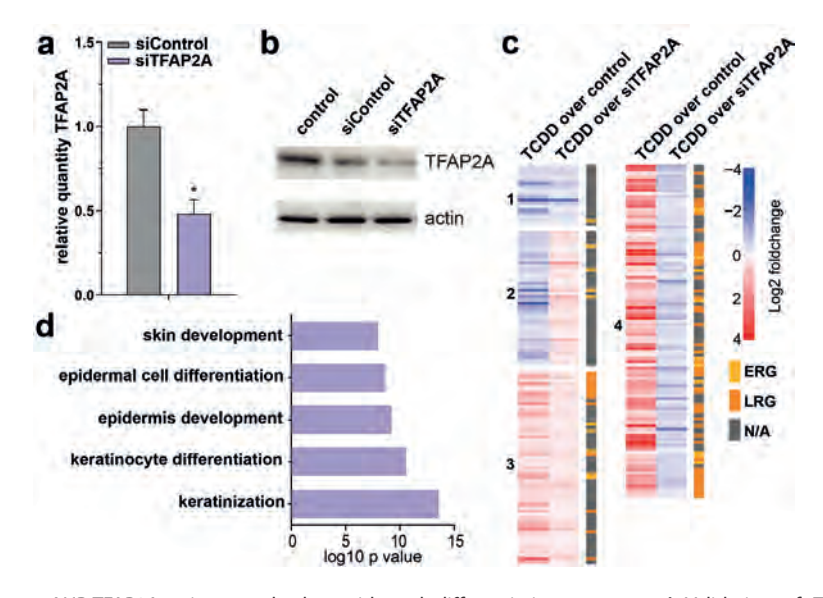
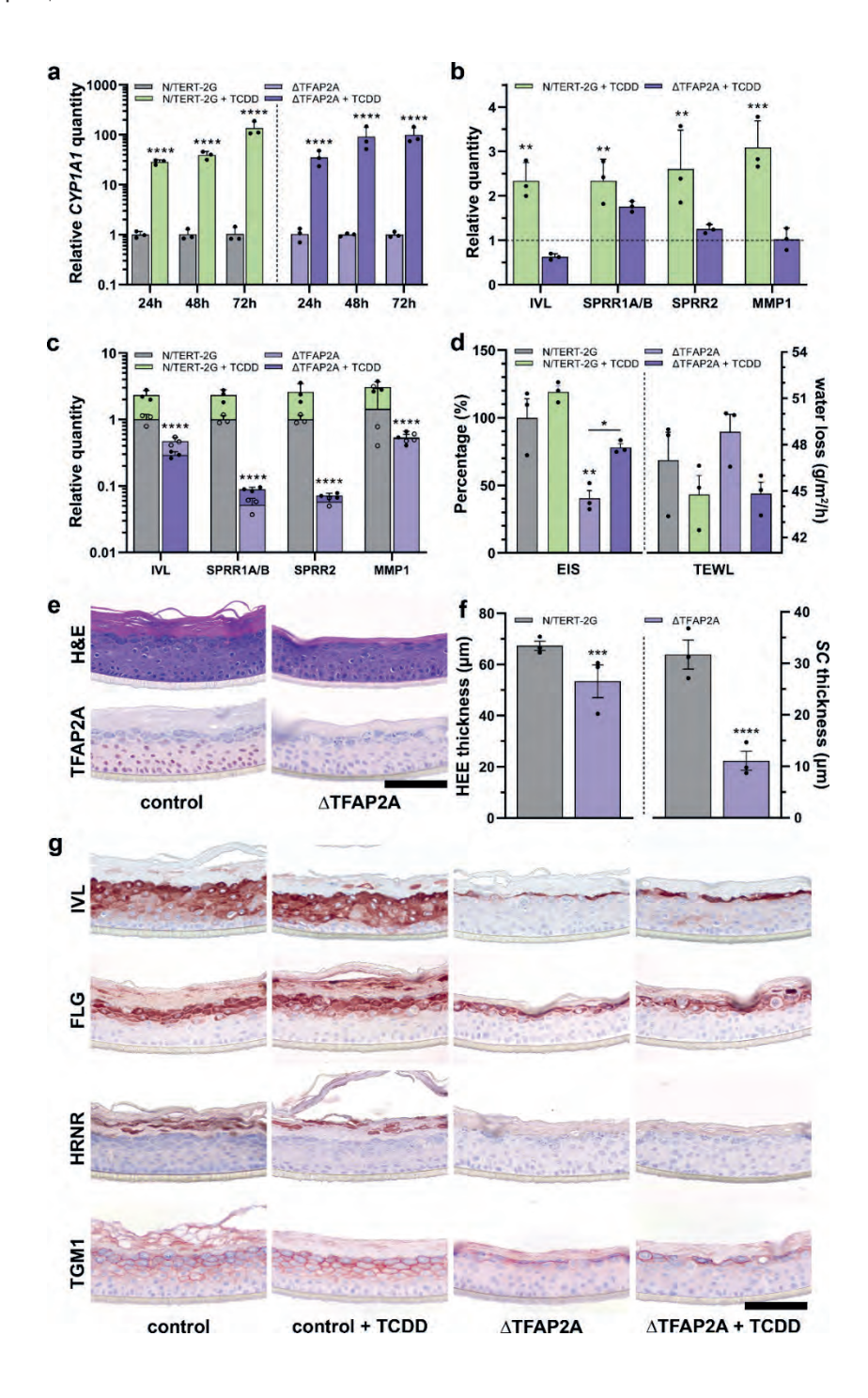


Figure 4. AHR-TFAP2A axis controls the epidermal differentiation program **a)** Validation of *TFAP2A* knockdown by RT-qPCR, normalized to reference gene *hARP*. Data shown as mean ±SEM, N=3 technical replicates, unpaired T-test, *p value <0.05. **b)** Western blot validation of TFAP2A knockdown. Actin was used as a loading control for the quantification of TFAP2A protein levels. **c)** Heatmap of differentially expressed genes (p value <0.05), accompanied by ERG (yellow) or LRG (orange) nomination. Z-score was calculated based on log10 (FPKM+0.01) of each gene. d GO annotation of genes in cluster 4 of the heatmap.

Finally, the importance of the identified AHR-TFAP2A axis in keratinocyte differentiation was investigated by knocking out TFAP2A using CRISPR/Cas9 on immortalized N/TERT-2G keratinocytes. Clonal homozygous TFAP2A knockout (Δ TFAP2A) N/TERT-2G keratinocytes were generated, grown in monolayer cultures, and treated with TCDD for up to 72 h, similar to the conditions of the previously described AHR-activated siRNA experiment. The upregulation of the AHR target gene *CYP1A1* by TCDD was not altered in Δ TFAP2A keratinocytes, indicating that *CYP1A1* is not regulated through TFAP2A (Fig. 5a). However, differentiation-related AHR-responsive genes, e.g., *IVL*, *SPRR1A/B*, *SPRR2*, and *MMP1*, of which expression

could be induced by TCDD in wildtype keratinocytes, were not upregulated in ΔTFAP2A keratinocytes (Fig. 5b). The expression patterns of these genes upon TCDD treatment with TFAP2A depletion are consistent with those observed from the siTFAP2A experiment (cluster 4)(Fig. 5b, compared to untreated condition, only 72 h timepoint shown). Consistently, the lack of mRNA upregulation induced by TCDD in ΔTFAP2A keratinocytes was observed for many other epidermal differentiation genes detected by RT-gPCR, e.g., PRR9, DSG1, DSC1, S100A8, TRPV3, and TGM3 (Suppl. Fig. 2a). Importantly, already at baseline, ΔTFAP2A keratinocytes showed significantly less expression of these genes as compared to wildtype N/ TERT-2G keratinocytes (Fig. 5c), indicating that loss of TFAP2A is not adequately compensated. Interesting to note, expression of AHR was not hampered in ΔTFAP2A keratinocytes (Suppl. Fig. 2b), implying that TFAP2A is not part of a selfregulating AHR signaling feedback loop. In summary, these data demonstrate that TFAP2A is an indispensable regulator in the molecular cascade of AHR-mediated keratinocyte differentiation. although it is unlikely that TFAP2A is involved in other AHR-mediated biological processes, such as xenobiotic metabolism where CYP1A1 is a target.

ΔTFAP2A organotypic human epidermal equivalents (ΔTFAP2A-HEEs) were generated to examine whether TFAP2A knockout and accompanied loss of keratinocyte differentiation gene expression gives rise to morphological changes and epidermal barrier defects. Quantitative epidermal barrier properties were analyzed by electrical impedance spectroscopy (EIS) and transepidermal water loss (TEWL) (Fig. 5d, complete EIS spectrum in Suppl. Fig. 2c). ΔTFAP2A-HEEs showed reduced electrical impedance, indicating functional skin barrier defects of ΔTFAP2A-HEEs, which agrees with the altered keratinocyte differentiation gene expression. Of note, we observed statistically significant improvement in the EIS values upon AHR activation by TCDD in ΔTFAP2A-HEEs, which was corroborated by a non-significant trend of reduction in TEWL. The loss of TFAP2A expression was confirmed by immunochemistry staining (Fig. 5e), which coincided with altered epidermal morphology, e.g., a significantly thinner viable epidermis and stratum corneum (Fig. 5f), and stratum granulosum appearing to consist of less layers. As expected based on the epidermal morphology of the ΔTFAP2A-HEEs, aberrant protein expression of a panel of important terminal differentiation proteins was detected, including IVL, FLG, HRNR, and TGM1 (Fig. 5g). Treatment of ΔTFAP2A-HEEs with TCDD did alleviate some of the diminished protein expression, suggesting that loss of TFAP2A can partially be alleviated by AHR activation, presumably via other AHR-induced ERGs (e.g., OVOL-1 [136], fold change 2.29 (Supplementary Data 1)) that cooperate in the terminal differentiation program.



< Figure 5. AHR-TFAP2A axis in keratinocyte differentiation and function. a) Monolayer N/TERT-2G and ΔΤFAP2A were treated with TCDD for up to 72 h and AHR activation was validated by CYP1A1 RT-qPCR. Data are shown as mean ±SEM, N=3 technical replicates, two-way ANOVA. b) RT-qPCR analysis of several genes from cluster 4 (Fig. 4c) displays AHR-dependent induction in the N/TERT-2G keratinocytes but not in ΔTFAP2A keratinocytes. Data are compared to their respective untreated condition and shown as mean ±SEM, N=3 technical replicates, two-way ANOVA. c) In addition, RT-qPCR analysis shows significant reduction of basal gene expression in ΔTFAP2A keratinocytes regardless of AHR activation. TCDD treatment data (closed circles) shown superimposed on untreated data (open circles). Data depicted as mean ±SEM, N=3 technical replicates. d) Functional skin barrier analyses EIS and TEWL on HEEs and ΔTFAP2A-HEEs displays reduced electrical impedance and increased transepidermal water loss, indicating a reduced barrier functionality. Barrier functionality is improved by TCDD treatment, as EIS increases and TEWL reduces. Data shown as mean ±SEM, N=3 technical replicates, one-way ANOVA.TEWL differences are not significant due to variation in the untreated HEEs. Full EIS spectrum in Supplementary Fig. 2c. e) H&E staining shows the diminished HEE thickness, stratum corneum thickness, and reduced stratum granulosum. Immunohistochemistry confirms the complete loss of TFAP2A expression. f) HEE and stratum corneum thickness measurements quantified and shown as mean ±SEM, N=3 technical replicates, two-way ANOVA. q) Immunohistochemistry further indicates the reduction of IVL, FLG, HRNR, and TGM1 expression, while TCDD treatment marginally upregulates the expression of IVL and FLG. Scale bar = 100 μm. * p value <0.05, ** p value <0.01, *** p value <0.001, **** p value <0.0001.

Discussion

In this study, we aimed to elucidate the signaling cascades by which the AHR exerts transcriptional regulation of terminal differentiation and skin barrier formation. We combined transcriptomic and epigenomic analyses to characterize the temporal gene regulatory events following AHR activation using keratinocytes as a model system for barrier epithelia. We identified that in a temporal distinct early response, AHR directly regulates the expression of several TFs known to be important for skin development and keratinocyte differentiation, e.g., TFAP2A [317-319]. Studies on human and animal models indicated that TFAP2A, together with interferon regulatory factor (IRF)6, grainyhead like transcription factor (GRHL)3, and tumor protein (TP)63, forms a core gene regulatory network as loss of any of these genes results in similar craniofacial, epidermal, and limb development defects [320]. We found that TFAP2A directly enhances epidermal differentiation as a secondary response to AHR activation and thereby contributes to skin barrier integrity. Low-level activation of AHR by endogenous, circulating, weak AHR agonists might drive the TFAP2Amediated keratinocyte differentiation in vivo. As such, these findings further elucidate the molecular mechanisms of action by which AHR induces its target effects.

Among the many biological roles that AHR has been associated with in the skin, our study specifically unravels the molecular mechanism behind AHR-mediated keratinocyte differentiation. We identified distinct early and late responses upon

AHR activation where TFs activated during the early response such as TFAP2A regulate keratinocyte differentiation genes in the late response. In addition, we demonstrate that AHR activation leads to enhancer dynamics that distinguish direct targets from secondary effects. The AHR: ARNT binding motif was significantly enriched in enhancers which were pre-established open chromatin regions with visible H3K27ac signals already before the treatment started. Thus, instead of establishing de novo enhancers, like pioneer transcription factors (e.g., TP63) that orchestrate the cell-type-specific enhancer landscape [321, 322], AHR seems to exploit a pre-specified landscape of targets. This enables a swift response towards external threats through regulation of canonical pathways like the cytochrome P450 pathway and mitogen-activated protein kinase (MAPK)[323]. Enhancers that showed dynamic H3K27ac signals at later time points were located near genes involved in 'keratinocyte differentiation', of which activation represents secondary effects of AHR activation. Interestingly, many of these genes are considered AMPs, consistent with our and others' recent findings that AHR activation in keratinocytes induces AMP expression[77, 212]. It is important to note that AHR direct targets that have AHR:ARNT motif-containing enhancers nearby, e.g., CYP1A1, are not all regulated by TFs such as TFAP2A, indicating the specificity of AHR action in different biological processes. In addition, immune system related functions appear to be associated with both pre-established and dynamic chromatin regions, suggesting that different immune genes are either induced or repressed at different time points upon AHR activation (Supplementary Data 2). This intriguing complexity and in the temporal cooperation between different immune pathways in response to environmental threats are subject to future research and may shed further light on the Janus-faced role of AHR [122].

Unlike AHR binding profiles in cancer cell lines that contain thousands of AHR binding sites (including TFAP2A) [324], our AHR ChIP-seq in keratinocytes yielded 'only' 57 AHR binding site, probably due to the transient binding nature of AHR upon ligand activation in normal cells. The validation of several sites by ChIP-RT-qPCR strengthens our confidence that these are genuine AHR-bound regions having biological relevance. The use of cancer cell lines (e.g., HaCaT keratinocytes) in this field of research may thus overestimate the number of target genes that are actually bound by AHR under physiological conditions.

The similarity observed between TCDD and CT treatment *in vitro* is striking, when considering that these are on the opposite sides of the health spectrum: TCDD being highly toxic while CT is used as a dermatological therapy for psoriasis and atopic dermatitis [75, 77, 325-327]. Previous studies reported decreased TFAP2A

expression in lesional psoriasis skin and identified TFAP2A as a core transcription factor to regulate the psoriasis transcriptome [328, 329]. Restoration of TFAP2A expression in both conditions may therefore be part of the therapeutic effect of CT. TCDD and CT both activated AHR similarly, provoking an adjective transcriptional response in keratinocytes. However, it is important to realize that the short-term effects of AHR activation in an experimental in vitro system do not take into account the ligand metabolism, degradation and elimination that would normally occur in vivo. TCDD's extreme long half-life (not being a substrate for xenobiotic metabolism) and systemic exposure has devastating chronic effects through sustained AHR activation [330]. In contrast, CT is a highly complex mixture of many different chemicals that could counter-act or compensate for the agonistic effects and is given only localized and periodically to psoriasis and atopic dermatitis patients. This raises an interesting question on the proposed AHR ligand promiscuity at the molecular level [157]. The dosage and half-life of AHR ligands and thus strength and duration of AHR activation may determine the biological effect. Whether AHR ligands are stable, rapidly metabolized, or whether secondary metabolites are involved in activities independent of AHR signaling pathways requires further investigation [81]. Herein, timing seems to be of utmost importance and timecourse global gene expression profiling in vivo is an essential next step to evaluate AHR activation and to dissect this regulatory cascade to greater detail.

Over the years, evidence has grown that serum levels of dietary-derived or microbiota-derived components can activate the AHR in several barrier organs in vivo. For example, indole-3-carbinole (I3C) can robustly activate the AHR in the intestine [331] whereas tryptophan metabolites can regulate AHR activation in the skin (e.g., FICZ [332], kynurenine [333], and kynurenic acid [162]). This implies that dietary intervention can be helpful in controlling AHR activation and thus support TFAP2A-mediated skin barrier integrity.

To conclude, our findings indicate that activation of AHR triggers a regulatory cascade mediating keratinocyte differentiation and this cascade relies on TFs such as TFAP2A that play an intermediate but indispensable role. Our identification of the AHR-TFAP2A axis exemplifies how environmental factors can dictate the terminal differentiation process, and unveil alternative routes and targets that may be hijacked to foster barrier formation and repair in the skin (and presumably other barrier organs) without the need for AHR activation per se.

Material and methods

Cell culture and drug treatment

Human abdominal or breast skin was obtained from plastic surgery procedures after informed consent and in line with the principles and guidelines of the Declaration of Helsinki. Skin biopsies were taken and human primary keratinocytes were isolated as previously described [334] and stored in liquid nitrogen until further use. Human primary keratinocytes were cultured in Keratinocyte Basal Medium (KBM, Lonza #CC-4131) supplemented with 0.4% (vol/vol) bovine pituitary extract, 0.5 µg/ mL hydrocortisone, 5 μg/mL insulin and 10 ng/mL epidermal growth factor (Lonza #CC-4131). Medium was refreshed every other day until near confluency before treatment commencement. Dimethylsulfoxide (DMSO) was purchased from Merck (Darmstadt, Germany), 2,3,7,8-Tetrachlorodibenzo-p-dioxin (TCDD) was purchased from Accustandard (New Haven, CT, USA), and coal tar (CT) was purchased from Fagron BV (Capelle aan den IJssel, The Netherlands). Cells were treated with either DMSO (0.1% vol/vol), CT (4 µg/mL), or TCDD (10 nM). Total RNA was collected for RNA-seg and gPCR-based validation purposes. Chromatin was harvested for ChIPseq experiments. Lysates containing proteins were harvested for western blotting purposes. No mycoplasma contaminations were found during cell culture.

N/TERT-2G culture and human epidermal equivalent (HEE) generation

Human N/TERT keratinocyte cell line N/TERT-2G, purchased from J. Rheinwald laboratory (Harvard Medical School, Boston, MA, USA), was cultured in Epilife medium (MEPI500CA, ThermoFisher Scientific, Waltham, MA, USA), complemented with human keratinocyte growth supplement (S0015, ThermoFisher Scientific) and 1% penicillin/streptomycin (P4333, Sigma-Aldrich, Saint-Louis, MO, USA). Human epidermal equivalents (HEEs) were generated as previously described [263], with minor adjustments. Briefly, inert Nunc cell culture inserts (141002, ThermoFisher Scientific) were coated with rat tail collagen (100 µg/mL, BD Biosciences, Bedford, USA) at 4°C for 1 hour. 1.5x10⁵ N/TERT-2G keratinocytes (either wildtype, ΔAHR, or ΔTFAP2A keratinocytes) were seeded on the transwells in 150 μL Epilife medium (ThermoFisher Scientific) supplemented with 1% penicillin/streptomycin (Sigma-Aldrich) in a 24 wells format. After 48 h, cultures were switched to a mixture of CnT-PR-3D medium (CELLnTEC, Bern, Switzerland) and DMEM medium (60:40 (v/v)) without penicillin/streptomycin for 24 h and then cultured at the airliquid interface for an additional ten days. Culture medium was refreshed every other day until harvesting at day ten of the air-exposed phase.

Western blotting and Immunofluorescence

Cell lysates of human primary keratinocytes were collected after treatment using RIPA lysis buffer. Afterwards, the lysates were sonicated (10x 5s on/off) and the samples were loaded onto SDS PAGE gel and transferred to PVDF membranes using the NuPAGE system (Life technologies) and visualized using SuperSignal West Femto Maximum Sensitivity Substrate (ThermoFisher, #34095). For analysis of AHR translocation to the nucleus, direct immunofluorescence (IF) labeling was performed as described [75]. Antibodies for western blotting and IF are listed in Table 5.

Transcriptional analysis by quantitative real-time PCR

Total RNA was isolated using the Favorprep total tissue RNA kit (Favorgen Biotech, Taiwan), according to the manufacturer's protocol, cDNA was generated after DNase treatment and used for quantitative real-time PCR (RT-qPCR) by use of the MyiQ Single-Colour Real-Time Detection System (Bio-Rad laboratories, Hercules, CA, USA) for quantification with Sybr Green and melting curve analysis. Primers (Table 2) were obtained from Biolegio (Nijmegen, The Netherlands) or Merck. Target gene expression levels were normalized to the expression of human acidic ribosomal phosphoprotein P0 (RPLP0). The relative expression levels of all genes of interest were measured using the 2- $\Delta\Delta$ CT method [246].

Table 2. PCR, RT-qPCR and ChIP qPCR primers

Gene	Usage	Forward (5' – 3')	Reverse (5' – 3')
TFAP2A	PCR	ATGGCGTGAGGTAAGGAGTG	GCTGGGCACTGTAGGTCAAT
AHR	PCR	TTCCACCAAACAATGGCTAA	AGAAGCTCTTGGCTCTCAGG
CYP1A1	RT-qPCR	CTGGAGACCTTCCGACACTCTT	GTAAAAGCCTTTCAAACTTGTGTCTCT
CYP1B1	RT-qPCR	TGGCTGCTCCTCTTCAC	CCACGACCTGATCCAATTCTG
TFAP2A	RT-qPCR	TCTCCGCCATCCCTATTAAC	TGTACTTCGAGGTGGAGCTG
KRT2	RT-qPCR	CGCCACCTACCGCAAACT	GAAATGGTGCTGCTTGTCACA
TGM3	RT-qPCR	GGAAGGACTCTGCCACAATGTC	TGTCTGACTTCAGGTACTTCTCATACTG
hARP	RT-qPCR	CACCATTGAAATCCTGAGTGATGT	TGACCAGCCCAAAGGAGAAG
CYP1A2	ChIP qPCR	TCTCCAGGTGTCAGTTCAGG	GAGGGCACAGGAGATAGAGG
TFAP2A	ChIP qPCR	TCCGGGTAAGTTCAACACAA	AAGGGTCAGCAAGGTAAAGC
CHR11	ChIP qPCR	TTGCATATAAAGGAAACTGAAATGCT	TTACTGCCATGGGTCCGTATC
HES2	ChIP qPCR	ACCTCGGGTAACAAGACACC	AGTTTCACCTGGGGTTTTCA
FOSL1	ChIP qPCR	CATGACTCAGCCACTTCCAC	GTCTCACCGAATCGGAATTT

RNA sequencing and analysis pipeline

RNA sequencing was performed as described previously [321] with the starting material of 500 ng total RNA, to obtain double-strand cDNA (ds-cDNA). After purification with the MinElute Reaction Cleanup Kit (Qiagen #28206), 3 ng ds-cDNA was processed for library construction using KAPA Hyper Prep Kit (Kapa Biosystems #KK8504) according to the standard protocol except that a 15-min USER enzyme (BioLab # M5505L) incubation step was added before library amplification. The prepared libraries were quantified with the KAPA Library Quantification Kit (Kapa Biosystems #KK4844), and then sequenced in a paired-ended manner using the NextSeg 500 (Illumina) according to standard Illumina protocols.

Sequencing reads were aligned to human genome assembly hg19 (NCBI version 37) using STAR 2.5.0 [200] with default options. Briefly, STAR has the option to generate inhouse reference genome from the genome fastq file. In this study, hq19 genome was used to generate the in-house reference genome with the following command: STAR --runThreadN8--runModegenomeGenerate--genomeDirdirectory/--genomeFastaFiles hg19.fa --sidbGTFfile Homo sapiens.GRCh37.75.qtf --sidbOverhang 100. Then STAR was run and it automatically generated read-counts directly. For data visualization, wigToBigWig from the UCSC genome browser tools was used to generate bigwig files and uploaded to UCSC genome browser. Genes with the mean of DESeg2normalized counts ("baseMean")> 10 were considered to be expressed. Differential gene expression (adjusted P value <0.05) and principal-component analysis were performed with the R package DESeg2 using read counts per gene [201]. Hierarchical clustering was performed based on log10 (FPKM+0.01). Functional annotation of genes was performed with DAVID[335]. For the experiments containing siRNAs, read counts were generated as described above. Differential expression analysis was performed using R community-created R packages stringr [336] and dplyr [337], and the DESeg2 package with normalization on siRNA treatment (DESeg design = siRNA). Read counts from control and TCDD treated samples at the 24 h stimulation time point were re-analyzed in a separate DESeq2 differential expression analysis (DESeq design = treatment). Significant differentially expressed genes overlapping between both experiments (Benjamini & Hochberg adjusted p-value < 0.05)[338] were visualized in a heatmap using the ComplexHeatmap package [202]. Gene Ontology analysis of interesting groups was performed using clusterProfiler [203]. Identification of TFs was performed as described before [339].

ChIP sequencing and analysis pipeline

Chromatin for ChIP was prepared as previously described [322, 340]. ChIP assays were performed following a standard protocol [341] with minor modifications. On

average, 0.5M keratinocytes were used in each ChIP. For histone mark H3K27ac, 2x ChIP reactions were pooled to prepare 1x ChIP-seq sample; for AHR, 4x ChIP reactions are pooled to prepare 1 ChIP-seq sample. Antibodies against H3K27ac (Diagenode C15410174) and AHR (Santa Cruz Biotechnology Inc. Santa Cruz, CA, USA, sc-5579) were used in each ChIP assay. Resulted DNA fragments from four independent ChIP assays were purified and subjected to a ChIP-qPCR quality check, Afterwards 5ng DNA fragments were pooled and proceeded on with library construction using KAPA Hyper Prep Kit (Kapa Biosystems #KK8504) according to the standard protocol. The prepared libraries were then sequenced using the NextSeg 500 (Illumina) according to standard Illumina protocols.

Sequencing reads were aligned to human genome assembly hg19 (NCBI version 37) using BWA [342]. Mapped reads were filtered for quality, and duplicates were removed for further analysis. In addition. The bamCoverage script was used to generate and normalize bigwig files with the RPKM formula. The peak calling was performed with the MACS2 [343] against a reference input sample from the same cell line with standard settings and a q value of 0.05. Only peaks with a p value < 10e-5 were used for differential analysis with MAnorm [344]. Association of peaks to genes and associated GO annotation were performed with GREAT[345], with the 'single nearest gene within 1 Mb' association rule. P values were computed with a hypergeometric distribution with FDR correction. k-means clustering and heat map and band plot generation were carried out with a Python package fluff [346]. HOMER (http://homer.salk.edu/homer/motif/) was used for motif scan against corresponding background sequences. One thing needs to be mentioned is that we overlapped dynamic enhancers with published DNAse I hypersensitivity sites to narrow down regions for motif scan.

ATAC-seq and motif analysis

ATAC-seg dataset (GSE123711) was downloaded and used for motif enrichment analysis as described before [347]. Briefly, ATAC-seg peaks within TSS-1Kb to TSS+0.5Kb were defined as promoter regions, whereas ATAC-seg peaks TSS-1Mb to TSS+1Mb were defined as enhancer regions. Differential motif analysis and TFAP2A motif scan within promoter regions and enhancer regions were separately performed using HOMER tool using default parameters (http://homer.salk.edu/homer/motif/).

siRNA knockdown

Human primary keratinocytes were grown to 10-15% confluency before 500 nM of Accell human SMARTpool gene targeting or non-targeting siRNA (Dharmacon, Lafayette, CO, USA) was added for 48 h. Culture medium was subsequently

Single guide RNA design, single strand donor oligonucleotide and synthetic Cas9

Synthetic sgRNAs to knockout *AHR* and *TFAP2A* gene, and purified Edit-R Cas9 nuclease protein (NLS, #CAS11200) were bought from Invitrogen (Waltham, MA, USA) and IDT Technologies (Coralville, IA, USA), respectively. See Table 3 for details on the sgRNAs used.

Table 3. Sequences of the sgRNAs

Target gene	Name	sgRNA sequence (5' – 3')	PAM site	Manufacturer
AHR	CRISPR980378_SGM	AAGTCGGTCTCTATGCCGCT	TGG	Invitrogen TrueGuide Synthetic gRNA
TFAP2A	CRISPR887200_SGM	GGAGTAAGGATCTTGCGACT	GGG	Invitrogen TrueGuide Synthetic gRNA
TFAP2A	CRISPR887208_SGM	TGTAGTCCCTGCGAGGATCC	AGG	Invitrogen TrueGuide Synthetic gRNA

Electroporation of ribonucleoprotein (RNP) complexes and analysis of editing efficiency

N/TERT-2G keratinocytes were electroporated using the NEON transfection system 10µL kit (ThermoFisher Scientific). N/TERT-2G keratinocytes were detached from culture plastic and washed twice with dPBS (without Ca²⁺ and Mg²⁺) as described above. Meanwhile, per electroporation condition, synthetic sqRNA (300ng) and Cas9 (1.5 µg) were incubated with 5 µL resuspension buffer R for 20 min before adding 1x10⁵ N/TERT-2G keratinocytes. After mixing the cell suspension, the cells were electroporated using 1 pulse of 1700V for a duration of 20ms before immediate seeding in a pre-warmed 6 well plate. DNA was isolated using the QIAamp DNA blood mini kit (51106, Qiagen, Hilden, Germany) according to manufacturer's protocol after a couple of days and CRISPR/Cas9 induced editing efficiency was analyzed by PCR and separation of amplicon on 2% agarose gel containing 1:10.000 GelRed nucleic acid gel stain (41003, Biotium Inc., Fremont, CA, USA). Amplicons were purified by MinElute Gel extraction kit (28606, Qiagen) using the manufacturers protocol and sanger sequenced to assess editing efficiency. Sanger sequencing reads were analyzed using the Inference of CRISPR edits (ICE) webtool (ice.synthego.com, v3, Synthego Corporation, Menlo Park, CA, USA). See Table 4 for details on the PCR primers used.

Generation of clonal ΔAHR and ΔTFAP2A N/TERT keratinocytes

N/TERT-2G keratinocyte cell pools carrying AHR or TFAP2A knockouts were diluted to seed one cell per well (~600 cells per 60 mL of Epilife medium, 100µL per well) into 6x96 well plates and allowed to grow for one week before refreshing the medium. After another week of culture, cells were passaged, as described above, into 24 well plates, 6 wells plates, T25 flasks, and T75 flasks subsequently before freezing them. Cell clonality was assessed by sanger sequencing and analyzing genomic DNA at the targeted locus with help of the ICE webtool (ice.synthego.com, v3, Synthego Corporation).

In silico search for potential off-target effects

CRISPOR (version 4.99)[265] was used to search for potential off-target effects dependent on the streptococcus pyogenes derived Cas9 (SpCas9) PAM site (5'-NGG-3'), target genome (homo sapiens GRCh38/hg38) and our specific guide RNA selection. Using genomic DNA of the N/TERT-2G keratinocyte knockout clones, the top-5 off-target sites for all guide RNAs were amplified by PCR and analyzed by sanger sequencing to assure no off-target mutations occurred. See Supplementary Data 6 for off-target analysis results and Table 4 for details on the PCR primers used for off-target analysis.

Epidermal barrier measurements TEWL and EIS

Epidermal barrier capabilities of epidermal equivalent cultures were studied by use of transepidermal water loss (TEWL) measurements and electrical impedance spectroscopy (EIS). After habituation of the cultures to room temperature, TEWL was measured using the Aguaflux AF200 (Biox, UK) on day 10 of the air-exposed phase of the HEE culture. TEWL was measured in triplicate in wildtype N/TERT-2G keratinocyte and ΔTFAP2A keratinocyte HEEs. Significance was assessed using one-way ANOVA with multiple comparisons correction (Tukey). EIS was measured using the real-time impedance detector Locsense Artemis (Locsense, Enschede, The Netherlands) with the SmartSense lid for monitoring cells in conventional transwell plates with inserts. Impedance (Ω) measurements were performed on day 10 of the air-exposed phase of the HEE culture after habituation of the HEE cultures to room temperature. EIS was measured in triplo on wildtype N/TERT-2G keratinocytes and Δ TFAP2A keratinocyte HEEs. After calibration, continuous impedance (Ω) was measured using standard settings e.g., sweeping frequency from 10Hz to 100.000Hz. Afterwards, measured impedance was corrected with blank impedance measurements per electrode and corrected for the size of the culture insert $(0,47\text{cm}^2)$, resulting in impedance per cm² values (Ω/cm^2) . Significance was assessed using one-way ANOVA with multiple comparisons correction (Tukey).

 Table 4. Regular PCR primers for predicted off-target site analysis

)				
gRNA	Target	CFD*	Forward (5' – 3')	Reverse (5′ – 3′)
CRISPR887200_SGM (TFAP2A)	intergenic:CCDC141-SESTD1	0.53	GTACTGGGTCCTTCCCTTCA	AAGAGTGGGGCAGACTTTGT
	intergenic:RP11-20A20.2-AL157830.1	0.35	AAGTTAGCCTGGGCTTGTGT	GAAGCATCAAGGTCAGTTGTG
	exon:LTN1	0.32	ATCCATGTTCCCAGAGCTTC	GCCCACGCTGATTAAAAGAT
	intergenic:CHP2-PRKCB	0.31	AAAAACAGGGCTGAGAATGG	TCATAGCTCACCGCTCAAAC
	intergenic:AC092017.1-RCOR3	0.31	CACATCCCCAAAGACATGAG	GCTGACATTTCTTGGCTTGA
CRISPR887208_SGM (TFAP2A)	intergenic:ATP6V1G1P7-RPL7P45	0.75	TTCATCTACCTTTGCAGGTTGT	TCCATAGCAGAGGGAGACT
	intron:METAP1D	0.38	GGTTAGGGCGTTGCCTATAA	GACAGCCATACTGCTTGTTGA
	intron:FAM160A1	0.31	TTTCCGTTTGTAGCAGTTGG	GCATCCTCTCAGCACTCA
	intergenic:RP11-91K8.2-SNORA33	0.29	TTCCACCTGCACACATTTTT	TTTCATTTGACAGGCAGAGC
	intergenic:GPRIN3-RP11-115D19.1	0.27	CTTCACCCAGTTTCCCCTAA	ACGCAAACCAAGAATGATGA
CRISPR980378_SGM (AHR)	intergenic:CTC-419K13.1-ENC1	0.29	GAGGCCACAAAACCATACAA	GGACTTGGAGAAAGCCAGAG
	intergenic:ACA64-SNX29	0.27	TGAAGGAAATGAACCAGTGC	GCCACAGCCATTTGCTTAT
	exon:AHRR/PDCD6	0.24	CACCTGACCCAGACCATCT	CAGGACAGAAAGCTTGTCCA
	intron:HECW2	0.21	GGGGGATGAAAAGCATTAAA	TTCTCTGAGTGGTGCTCAGG
	intron:AOX1	0.17	TACACCTGCCGACCAAATAA	TCAATTCTCTGCCCATCAGA

*Cutting frequency determination (CFD) indicates likeliness of off-target cleavage at this particular site, based on Doench et. al. 2016 [296]

Morphological and immunohistochemical analysis of HEEs

HEEs were fixed in 4% formalin solution for 4 h and subsequently embedded in paraffin. 6 µm sections were stained with hematoxylin and eosin (H&E, Sigma-Aldrich) or processed for immunohistochemical analysis. Sections were blocked for 15 min with 5% normal goat or horse serum in phosphate-buffered saline (PBS) and subsequently incubated with the specific antibodies for 1 h at room temperature. Next, a 30 min incubation step with biotinylated horse anti-mouse, or goat anti-rabbit (Vector Laboratories, Burlingame, USA) was performed, followed by a 30 min incubation with avidin-biotin complex (Vector Laboratories). The peroxidase activity of 3-Amino-9ethylcarbazole (AEC) was used to visualize the protein expression and the sections were mounted using glycerol gelatin (Sigma-Aldrich). See Table 5 for details on the antibodies used for immunofluorescence, western blot, and immunohistochemistry. HEE and stratum corneum thickness were measured using Zen 3.2 (Blue Edition).

Table 5. Antibodies used in immunohistochemistry and western blot

Purpose*	Antibody	Manufacturer and catalog number	Dilution
IF	Rabbit anti-AHR	Santa Cruz Biotechnology, SC-5579	1:200
IHC	Mouse anti-CYP1A1	Santa Cruz Biotechnology, SC-25304	1:25
WB / IHC	Mouse anti-TFAP2A	Invitrogen, MA1-872	WB 1:300 IHC 1:50
WB	Mouse anti-β-Actin, AC-15	Merck, Darmstadt, Germany	1:100.000
IHC	Mouse anti-FLG	Leica Biosystems, Newcastle, UK	1:100
IHC	Rabbit anti-HRNR	Sigma-Aldrich, HPA031469	1:500
IHC	Mouse anti-IVL, Mon150	Van Duijnhoven et al[204]	1:20
IHC	Rabbit anti-Ki67	Abcam, Cambridge, UK, ab16667	1:50
IHC	Horse anti-mouse, biotinylated	Vector Laboratories, BA-200-1.5	1:200
IHC	Goat anti-rabbit, biotinylated	Vector Laboratories, BA-5000-1.5	1:200

^{*}IF = immunofluorescence: WB = western blot: IHC = immunohistochemistry

Statistics and reproducibility

Data set statistics were analyzed using the GraphPad Prism software. Differences under p value < 0.05 were considered statistically significant, ns p value > 0.05, * p value <0.05, ** p value <0.01, *** p value <0.001, **** p value <0.0001. Gene expression analysis by RT-qPCR was performed in biological duplicates (at least n=3); data are shown as mean ± standard error of the mean unless otherwise specified. Statistics was performed on dCT values using one-way ANOVA with multiple comparison correction (Tukey). Other statistical methods used are specified in the methods sections.

Acknowledgements

This research has been a long endeavor with many collaborative efforts on the various aspects of the experimental work and data analysis. We are grateful for all funders throughout the years: Radboud Institute for Molecular Life Science (RIMLS; JSc and EB), National Institutes of Health (ES028244); Dutch Research Council VENIgrant 91616054 (EB), Chinese Scholarship Council grant 201406330059 (JQ), and LEO Foundation grant LF18068 (PZ and EB). We thank all members from the Departments of Dermatology, Molecular Developmental Biology, and Molecular Biology for discussion and suggestions on the project. We especially thank Chet Loh for discussion and useful input. We thank Eva Janssen-Megens, Siebe van Genesen and Rita Bylsma for operating the Illumina analyzer. We thank the ENCODE Consortium for sharing their data and Gary H. Perdew for the critical reading of our manuscript.

Author contributions

JSm, JQ, HZ, and EB conceived and designed the study and experiments and supervised the data analysis. JSm, JQ, NB, DRO, and IVW performed the wet-lab experiments. The AHR knockout line was generated by NB, the TFAP2A knockout line by JSm. JSm, JQ, FP, NB, SH, HZ, and EB analyzed the data. For the omics-analysis in particular, FP performed the siRNA transcriptome data analysis, JQ, SH and HZ were responsible for the data integration. JSm, JQ, FP, NB, JSc, PZ, HZ, and EB wrote and/or revised the manuscript.

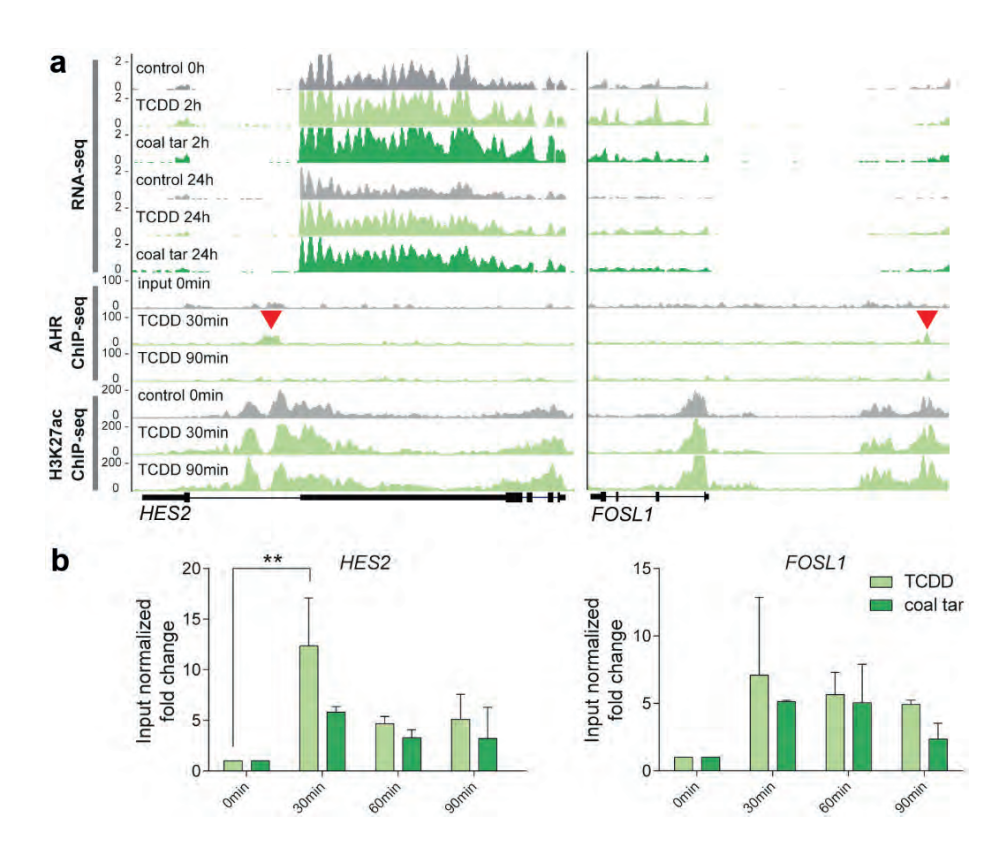
Declaration of interests

The authors declare no competing interests.

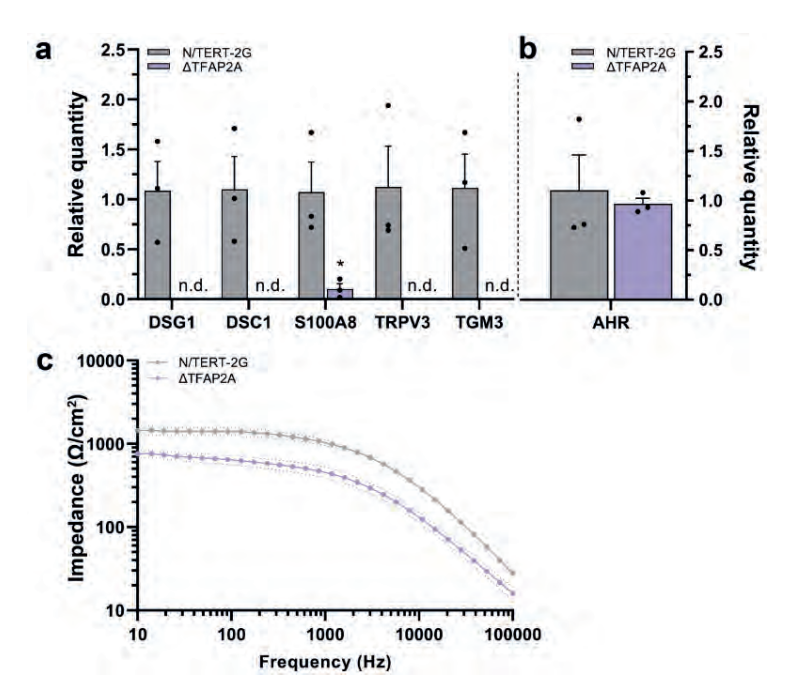
Data availability

All raw sequencing files including RNA-seq and ChIP-seq analyses generated in this study have been deposited in the GEO database with the accession number GSE226047.

Supplementary material



Supplementary Figure 1. a) Genome browser screenshots of the HES2 (left) and FOSL1 (right) coding region show RNA-seq, AHR ChIP-seq, and H3K27ac ChIP-seq tracks upon treatment with coal tar and TCDD. Red arrow indicates AHR binding site within the HES2 and FOSL1 loci. b) AHR ChIP-RT-qPCR validation at the loci of HES2 (left) and FOSL1 (right) at different time point after ligand treatment. Input normalized fold change is relative to both input DNA and negative control loci (chr11). Data are shown as mean ±SEM, N=2 technical replicates. ** p value <0.01.



Supplementary Figure 2. a) RT-qPCR analysis of monolayer untreated N/TERT-2G and ΔTFAP2A keratinocytes indicates that loss of TFAP2A results in severe downregulation of several epidermal differentiation genes (n.d. = nondetectable). Data are compared to N/TERT-2G keratinocytes and shown as mean ±SEM, N=3 technical replicates, one-way ANOVA. b) AHR expression is not changed in monolayer ΔTFAP2A keratinocytes as shown per RT-qPCR analysis. Data shown as mean ±SEM, N=3 technical replicates, one-way ANOVA. c) Full EIS spectrum of HEEs and ΔTFAP2A-HEEs (from Fig. 5d) showing reduced electrical impedance of ΔTFAP2A-HEEs. Data shown as mean ±SEM, N=3 technical replicates, * p value < 0.05.



Chapter 6

Electrical impedance spectroscopy quantifies skin barrier function in organotypic *in vitro* epidermis models

Noa J.M van den Brink^{1,†}, Felicitas Pardow^{1,2,†}, Luca D. Meesters^{1,2}, Ivonne van Vlijmen-Willems¹, Diana Rodijk-Olthuis¹, Hanna Niehues¹, Patrick A.M. Jansen¹, Susan H. Roelofs³, Matthew G. Brewer⁴, Ellen H. van den Bogaard^{1,#} and Jos P.H. Smits^{1,5,#}

¹Department of Dermatology, Radboudumc, Nijmegen, The Netherlands;

²Department of Molecular Developmental Biology, Faculty of Science, Radboud University, Nijmegen, The Netherlands;

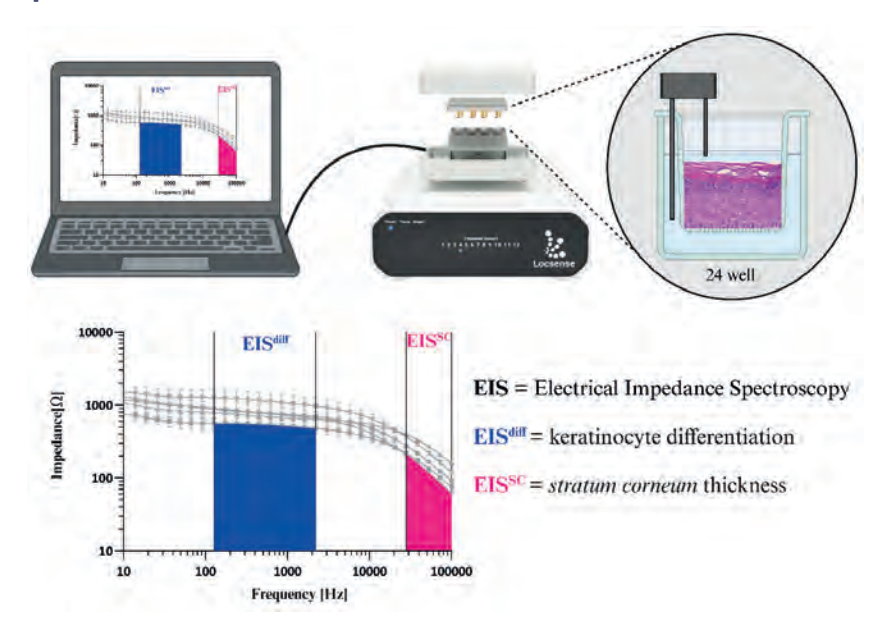
³Locsense B.V., Enschede, The Netherlands;

⁴Department of Dermatology, University of Rochester Medical Center, Rochester, New York, USA;

⁵Department of Dermatology, Heinrich Heine University, University Hospital Düsseldorf, Düsseldorf, Germany;

[†] contributed equally (arranged in alphabetical order), #shared senior authorship (arranged in alphabetical order).

Graphical abstract



Abstract

Three-dimensional human epidermal equivalents (HEEs) are a state-of-the-art organotypic culture model in preclinical investigative dermatology and regulatory toxicology. In this study, we investigated the utility of electrical impedance spectroscopy (EIS) for noninvasive measurement of HEE epidermal barrier function. Our setup comprised a custom-made lid fit with 12 electrode pairs aligned on the standard 24-transwell cell culture system. Serial EIS measurements for 7 consecutive days did not impact epidermal morphology and readouts showed comparable trends with HEEs measured only once. We determined two frequency ranges in the resulting impedance spectra: a lower frequency range termed EISdiff correlated with keratinocyte terminal differentiation independent of epidermal thickness and a higher frequency range termed EIS^{sc} correlated with *stratum corneum* thickness. HEEs generated from CRISPR/Cas9-engineered keratinocytes that lack key differentiation genes FLG, TFAP2A, AHR or CLDN1 confirmed that keratinocyte terminal differentiation is the major parameter defining EISdiff. Exposure to proinflammatory psoriasis- or atopic dermatitisassociated cytokine cocktails lowered the expression of keratinocyte differentiation markers and reduced EISdiff. This cytokine–associated decrease in EISdiff was normalized after stimulation with therapeutic molecules. In conclusion, EIS provides a noninvasive system to consecutively and quantitatively assess HEE barrier function and to sensitively and objectively measure barrier development, defects and repair.

Introduction

Intact physical barriers are of highest importance for our body to define a biophysically enclosed environment. The skin, our largest barrier organ, serves a dual role: it forms an outside-in barrier, protecting the insides of our body from mechanical damage and environmental triggers, and it protects the epidermis and subjacent tissues from dehydration as an inside-out barrier. Barrier functionality is achieved most prominently by a highly organized physical barrier, constituted of tight junctions in the stratum aranulosum and corneodesmosomes in the stratum corneum [348]. Stratum corneum corneocytes also are coated with a heavily crosslinked cornified envelope [349] and the intercellular space between is filled with lipids, generating a hydrophobic environment [350]. Next to this physical barrier, the additional chemical, microbial and immunological barriers completes the multifaceted barrier function of mammalian skin [19, 351].

The importance of the skin barrier is apparent from its malfunction in common skin diseases, such as psoriasis and atopic dermatitis. The disease-associated pro-inflammatory milieu also negatively affects keratinocyte differentiation and impairs tight junction and corneodesmosome function [32, 352, 353]. Next to these multifactorial diseases, monogenic diseases caused by sequence variation in skin barrier-related genes illustrate the devastating effects of impaired skin barrier function on our health and wellbeing [354, 355]. Aside from these intrinsic factors, environmental factors including exhaust fumes or detergents influence the skin barrier function of healthy individuals and patients [356]. Determining the functional consequences of such genetic and environmental risk factors on the skin barrier will aid in our understanding of disease pathogenesis and may help in the possible future prevention of disease onset or exacerbation.

To investigate skin barrier function, in vitro organotypic skin and human epidermal equivalents (HEEs) have become a mainstay approach. By mimicking epidermal barrier morphology and function, HEEs offer advantages over in vitro monolayer cultures that lack epidermal stratification and stratum corneum formation. In addition, HEEs are considered relevant alternatives to in vivo animal models that prompt ethical questions and require depilation to measure biophysical barrier function. HEEs are used from fundamental research to preclinical drug testing to regulatory toxicology in a broad range of applications [19, 357].

To assess skin barrier function in HEEs, various technologies can be used ranging from mathematical penetration modelling [358, 359] and computational simulation of lipid organization [360] to ultrastructural imaging [361] and measuring gene and/or protein expression. In a recent consensus paper, we and others have discussed the requirements and methodologies for barrier studies in organotypic skin models [362]. In summary, functional barrier assessment using Franz cell diffusion and permeation flux studies provide most accurate estimates of the outside–in barrier [363-365]. On the other hand, water evaporation (e.g. transepidermal water loss (TEWL)) is considered most relevant to describe inside–out barrier function [362, 366]. Unfortunately, these methods are often labor intensive and rely on highly specific expertise and equipment (Franz cell diffusion assay), are poorly standardized (transepithelial electrical resistance (TEER), TEWL) or require destructive endpoint measurements (permeation studies) (Table S1). Furthermore, the mechanistic correlation of such measurements to skin barrier function often remains unclear [353].

Electrical impedance spectroscopy (EIS) has been developed and implemented for the assessment of skin barrier function *in vivo* and appears to correlate well with disease severity of atopic dermatitis lesions [367]. For assessment of *in vitro* barrier function, EIS has been implemented for gut, airway and neuroepithelial *in vitro* cultures [368, 369] and *ex vivo* pig ear skin models [370]. Explorative studies have applied EIS in *in vitro* epidermis models [371, 372] and link EIS to viable epidermis and *stratum corneum* barrier properties [372]. Yet, a comprehensive study which extensively assesses EIS applicability and its relationship to skin barrier properties in a broad range of experimental models and disease conditions is missing. In this study, we demonstrate and validate the use of EIS as a reproducible, noninvasive and quantitative high–throughput system for HEE barrier assessment and assess its correlation to epidermal barrier physiology.

Results

Development of an EIS device for in vitro HEE application

For quantitative and reproducible *in vitro* skin barrier analysis we sought to develop and validate an EIS devise for use in HEEs. The system comprises a smart lid with fixed gold-plated electrodes that are customized to fit the individual wells of a Nunc carrier plate with cell culture inserts. The setup enables standardized and automated measurements with a run time of 2 minutes per well for a maximum of 12 wells (within a 24 well-plate format). To perform the measurements, the smart lid with fixed electrodes is placed onto the HEE-carrying culture plate and the connected measurement device (Figure 1a). The electrodes apply a very low

alternating voltage V in a frequency range from 10 Hz to 100 kHz through the culture while measuring the amplitude and phase shift of the resulting alternating current I. The EIS device returns the impedance, which reflects the opposition to an alternating current over time:

Impedance
$$Z = \frac{V(t)}{I(t)}$$

Impedance and phase spectra are reported in the form of a Bode plot (Figure 1b, c).

For quantitative analysis of EIS spectra, an electrical equivalent circuit model of the examined culture system is required. In conventional 2-dimensional monolayer cultures, there are two main routes of the current: a paracellular, which is determined by the ionic conductance of cell junctions serving as a paracellular resistance (R_a), and a transcellular, which consists of the resistance and capacitance of apical and basolateral membrane (R_a, R_g) and $C_a, C_g)$ next to the resistance of the cytoplasm R_{Cyt} [139, 373] (Figure 1d). In a simplified model, both membranes can be reduced to R_{Cell} and C_{Cell} respectively. In 2-dimensional monolayers, the high cellular resistance R_{Coll} and the low cytoplasmatic resistance R_{Coll} results in paracellular flux being determined by the cellular capacitance C_{Cell} [373]. In 3-dimensioanIHEEs, multiple individual cell layers result in a parallel series of n resistor-capacitor electrical circuits [371]. While we speculate $R_{p'}$ $R_{Cvt'}$ R_{Cell} and C_{Cell} to be changing depending on cell-cell contacts, differentiation status and the cell shape in the corresponding layer, we assume the dominance of C_{Cell} over R_{Cell} and R_{Cvt} to be persistent in 3-dimensional (Figure 1e). Lastly, the resistance of the culture medium R_{Medium} and the electrodes, acting as pure capacitors with a capacitance C_{EV} conclude the electrical circuit.

These electrical circuit elements also determine the generated impedance spectrum (Figure 1f) $^{[373]}$. Both, R_{Medium} and C_{FI} are fixed parameters whose characteristics are determined by the chosen setup and device. The variable parameters paracellular resistance R_p and cellular capacitance C_{cell} are determined by the measured cells and the chosen culture system (monolayer vs 3-dimensional organoid). They influence the height and frequency span of a midrange plateau and the onset of its decline [374] (Figure 1g, h). To link EIS to epidermal barrier properties, we determined two frequency ranges in the HEE impedance spectrum approximately indicating R_p and C_{coll} contribution, EISdiff (127–2212 Hz) and EISSC (28072-100000 Hz) respectively, which we analyzed by calculating their area under the curve [373] (Figure 1i).

To determine whether EIS can be used to monitor the development of HEEs noninvasively, serial measurements were performed over consecutive days of immortalized N/TERT-2G keratinocyte air-liquid interface culture. When comparing serial with end point measurements performed directly before harvesting, EIS spectra showed similar trends (Figure 2a, b) and differences in EISdiff and EISSC were not significant (Figure 2c, d). Morphological analysis by hematoxylin and eosin (H&E) staining did not indicate destructive effects of EIS in endpoint or in serial measurements (Figure 2e, top panel). In addition, neither keratinocytes proliferation capacity (Ki67 staining), expression of differentiation proteins (involucrin (IVL) and filaggrin (FLG)), nor the expression of stress-related markers (keratin 16 (KRT16) and skin-derived antileukoproteinase (SKALP)) were changed by EIS measurements (Figure 2e). Of note, expression levels of SKALP and the proliferation marker KRT16 are known to be higher in neonatal-derived immortal N/TERT-2G than in primary adult keratinocytes [263, 334]. To further evaluate EIS' reliability, HEEs were subjected to EIS measurements six times within one hour (Figure 2f), clearly indicating a very high repeatability. When checking for potentially delayed cytotoxic effects, HEEs harvested 24 hours after repeated EIS measurements showed no morphological signs of cytotoxicity and continuing maturation, as seen by the formation of additional epidermal layers (Figure 2g).

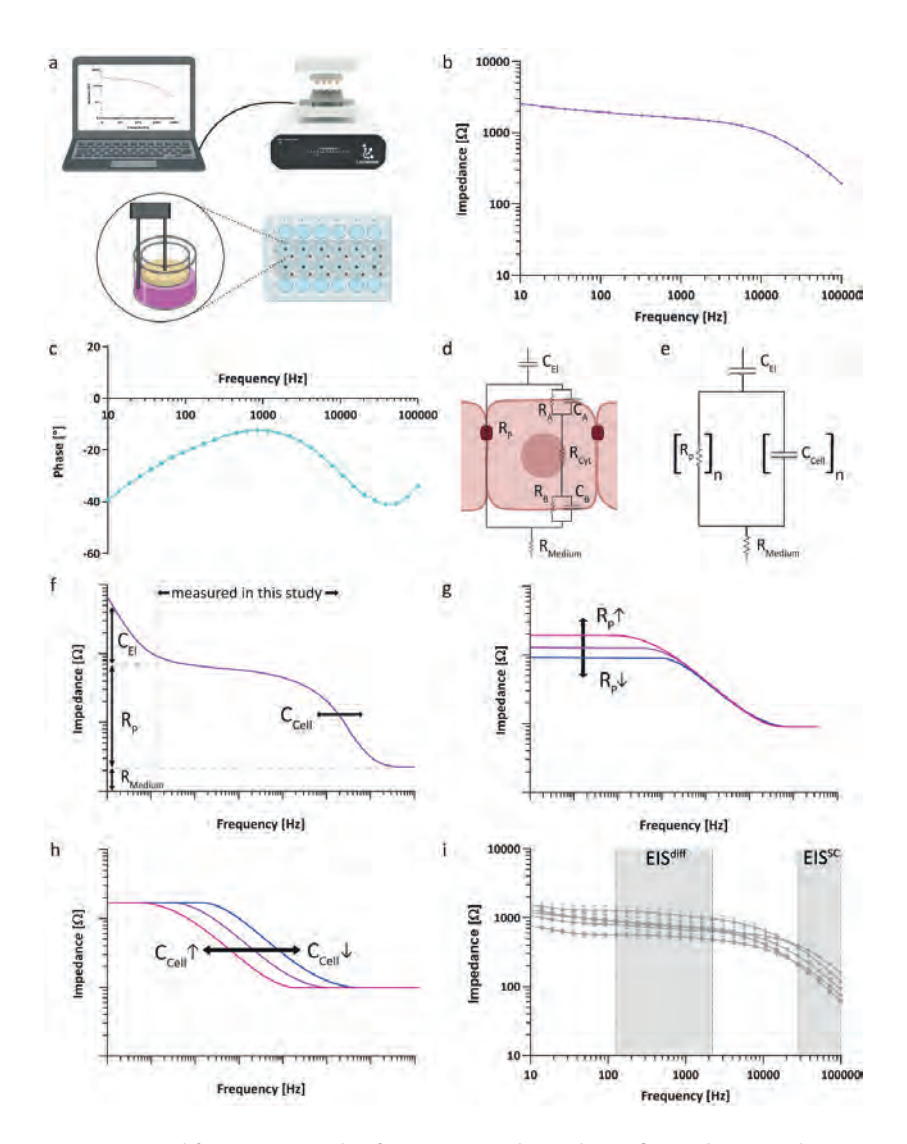


Figure 1. Design and function principle of a custom-made EIS device fitting the HEE culture system. (a) Schematic overview of the EIS setup on HEE cultures. (b) Impedance and (c) phase spectrum of a fully-developed NHEK HEE culture after 8 days of air exposure. (d) Extended electrical equivalent circuit of an epidermal monolayer culture made up of the capacitance of the electrodes C_{EV} paracellular $resistance \ R_{pr} \ transcellular \ resistance \ of \ cytoplasm \ R_{Cyt'} \ apical \ and \ basolateral \ membrane \ R_{A'} \ R_{B} \ as \ well$ as their capacitance $C_{A'}$ C_{B} and the resistance of the medium R_{Medium} (adapted from [374]). **(e)** Simplified electrical equivalent circuit of an HEE with the capacitance of both membranes taken together as C_{cell} which together with R_p extends to a series of n parallel circuits in multilayered 3-dimensionalculture systems (adapted from [139] and [371]). (f) Schematic overview indicating the contribution of individual electrical circuit parameters to the impedance spectrum (adapted from [373]). $(\mathbf{g},\,\mathbf{h})$ Simulated impedance spectra illustrating the influence of changes in (\mathbf{g}) paracellular flux $(R_{\scriptscriptstyle D})$ and (h) transcellular flux (C_{Cell}) (adapted from [374]). (i) EIS impedance spectrum displaying EIS^{diff} (127-2212 Hz) and EISSC (28072-100000 Hz).

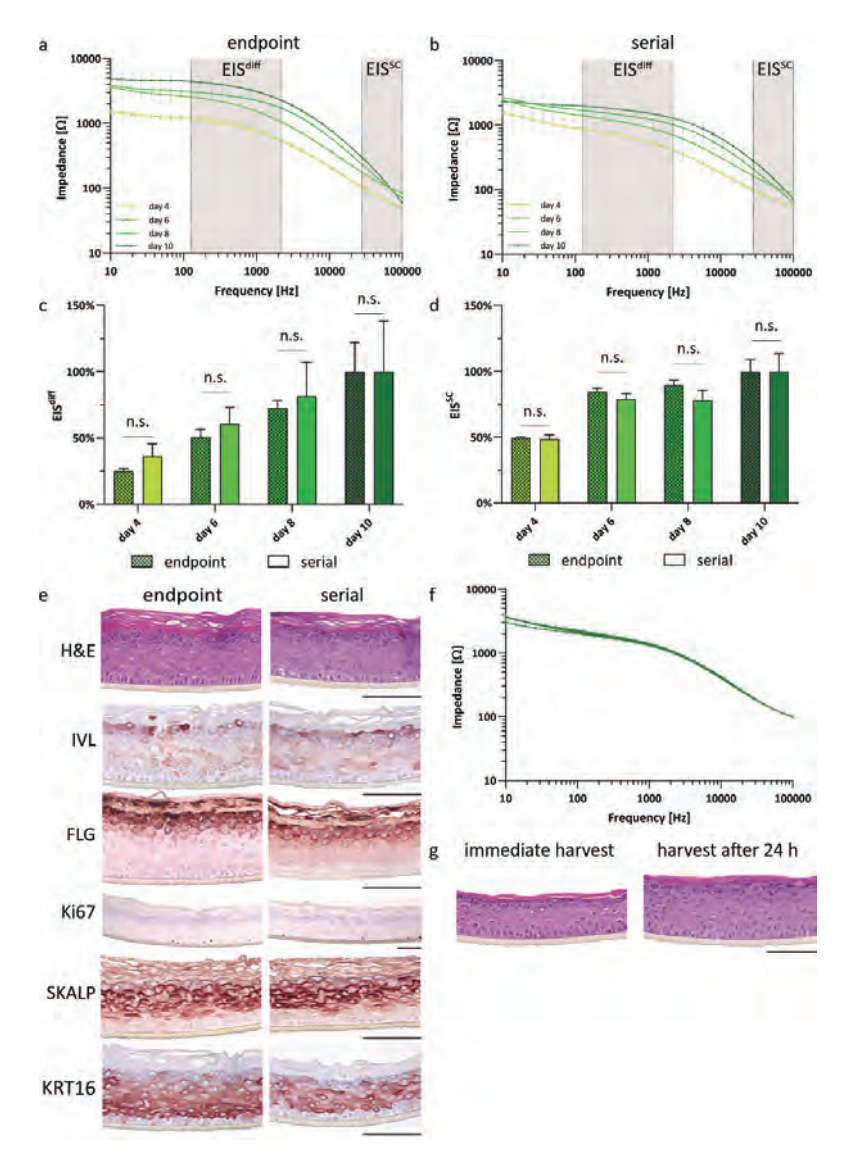


Figure 2. Relative EIS measurements are reproducible and do not impair HEE development. (**a, b**) EIS impedance spectra during HEE development with constructs being harvested (**a**) directly after measurements (endpoint measurements) and (**b**) at day 10 of air exposure (serial measurements). Each timepoint averages three biological replicates. (**c**) Comparison of EISdiff and (**d**) EIS SC between endpoint and serial measurements. (**e**) Histological comparison of HEEs undergoing endpoint or serial EIS measurements based on general morphology (H&E staining), differentiation status (FLG, IVL expression), proliferation (Ki67) and stress response (SKALP, KRT16). Pictures represent three biological replicates at day 10 of air exposure and taken at either 20x (Ki67) or 40x magnification. Size bars indicate 100 μm. (**f**) Impedance spectrum of HEEs (n = 3) measured 6 times within 1 hour at day 6 of air exposure. (**g**) Histological comparison of HEEs measured 6 times in 1 hour, either harvested directly or 24 hours after EIS measurements. Pictures represent three biological replicates and were taken at 40x magnification. Size bar indicates 100 μm.

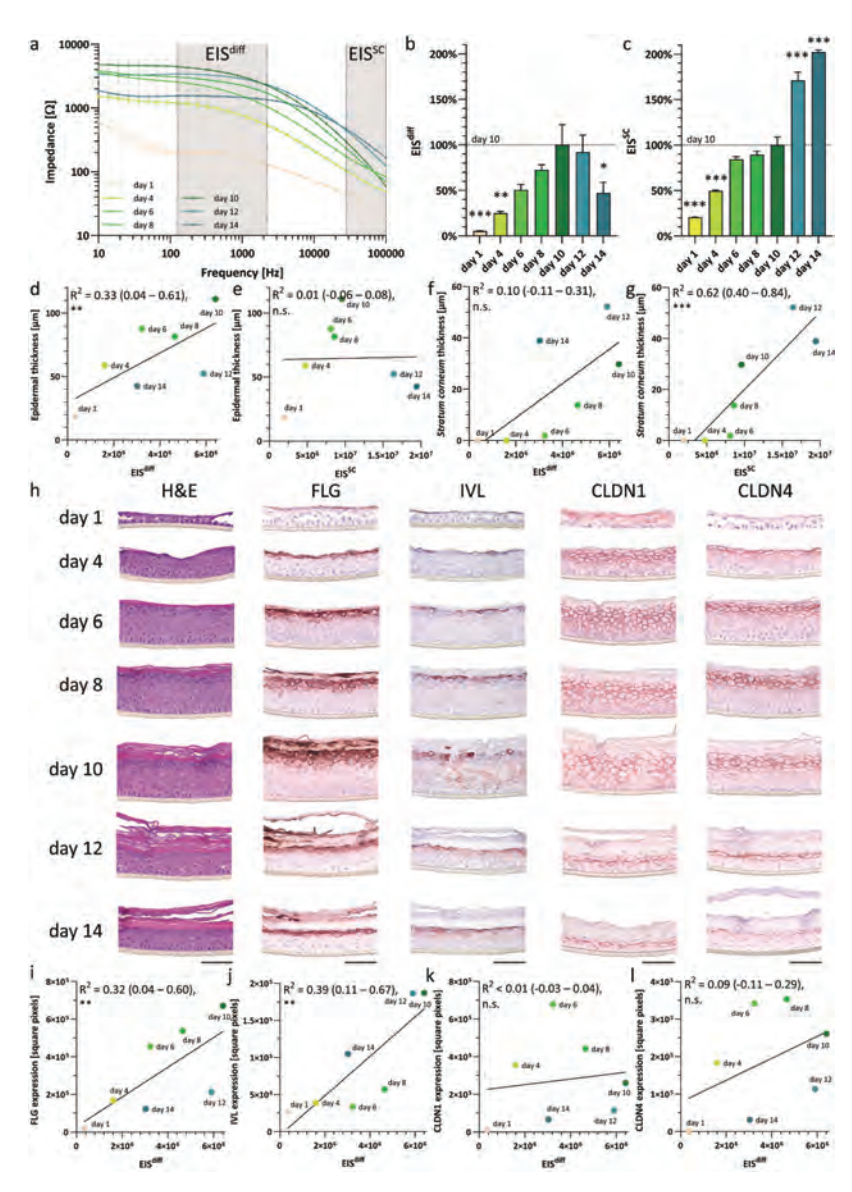


Figure 3. During HEE development, EISdiff correlates with keratinocyte differentiation and epidermal thickness while EIS^{SC} correlates with stratum corneum thickness. (a) Endpoint-measured impedance spectra, (b) EISdiff and (c) EISSC during HEE development. Each timepoint represents three biological replicates and ElS^{diff} and ElS^{SC} were compared to 10 day air-exposed cultures. (d - g) Correlation of epidermal thickness with (d) EIS^{diff} and (e) EIS^{SC} and stratum corneum thickness with (f) EIS^{diff} and (g) EIS^{SC}. Each timepoint averages three biological replicates, R² values and significances indicate the correlation of individual replicates. (h) Staining of general morphology (H&E), keratinocyte differentiation (FLG, IVL) and cell-cell adhesions (CLDN1, CLDN4) during HEE development. Pictures represent three biological replicates and were taken at 40x magnification. Size bars indicate 100 μm. (i - I) Correlation of (i) FLG, (j) IVL, (k) CLDN1 and (l) CLDN4 protein expression with EISdiff. Each timepoint averages three biological replicates, R² values and significances indicate the correlation of individual replicates.

Different electrical impedance spectra can be linked to keratinocyte differentiation and stratum corneum thickness

The EIS device measures impedance over a broad range of frequencies, which we sought to correlate with epidermal barrier properties. For this, we determined EISdiff and EISSC of HEEs during barrier development (Figure 3a-c) and performed correlation analysis with principle epidermal barrier compartments (Figure 3d-q). We observed the thickness of viable epidermal layers to be increasing from day 1–10 before decreasing at day 12 and 14 (Figure S1a, b), which correlated with EISdiff but not with EISSC (Figure 3d, e). At the same time stratum corneum thickness did not correlate with EISdiff but strongly correlated with EISSC explaining 62 % of its variance (Figure 3f-q). Since keratinocyte terminal differentiation plays a major role in the formation of the skin barrier, we also investigated the protein expression of essential terminal differentiation proteins in relation to EISdiff (Figure 3jh-l). EISdiff correlated with the quantified expression of keratinocyte differentiation markers FLG and IVL which increased in early days of HEE development before decreasing after maturation at day 14 (Figure 3 h-j). Expression of the tight junction proteins, claudin 1 (CLDN1) and claudin 4 (CLDN4) could not be linked to EISdiff (Figure 3h, k-l). When investigating the contributions of FLG, IVL, CLDN1 and CLDN4 altogether, CLDN1 and CLDN4 were not observed contributing to EISdiff during HEE development and did not add additional explanatory value to the correlation model (Figure S1c, d). The expression of FLG, IVL and their collaborative interaction on the other hand together could explain 76 % of EISdiff (Figure S1e, f).

Cytokine stimulation proves that EISdiff is independent of epidermal thickness

After examining EIS in epidermal homeostasis we aimed to study the relevance of EIS in the context of disturbed homeostasis and to deepen our investigation into the correlation between EIS^{diff}, epidermal thickness and terminal differentiation. Therefore, HEEs from normal human epidermal keratinocytes (NHEKs) were stimulated with single cytokines (interleukin–(IL–) 17A or IL–22) or cytokine mixes (IL–17A + IL–22 and IL–4 + IL–13) to mimic a proinflammatory milieu that is known to affect keratinocyte proliferation (IL–4, IL–13, IL–17A), the cell volume (IL–22), and terminal differentiation (all cytokines) [55] (Figure 4a). We hypothesized that if EIS^{diff} would merely quantify epidermal thickness, cytokines known to increase epidermal thickness would increase EIS^{diff}. Nevertheless, while IL–4 + IL–13 stimulation of HEEs significantly increased epidermal thickness, a reduction of EIS^{diff} was observed (Figure 4b, d). Stimulation with IL–17A did not change epidermal thickness but resulted in increased EIS^{diff} and EIS^{SC} (Figure 4b–d). In contrast, IL–22 did not induce any changes in EIS^{diff}, while significantly increasing the epidermal thickness

(Figure 4b-d). Correlation analysis furthermore showed no correlation between epidermal thickness and EISdiff (Figure 4e). To reassess the relationship between EISdiff and terminal differentiation, we analyzed the expression levels of key terminal differentiation proteins FLG and IVL which are known to be reduced in human skin related to barrier defects, and known to be affected upon stimulation with IL-4 + IL-13 cytokines in vitro [375]. Indeed, decreased expression levels of FLG and IVL as well as unchanged levels of CLDN4 in HEEs treated with IL-4 + IL-13 cytokines (Figure 4g) corresponded to reduced EISdiff (Figure 4b). On the other hand, IL-17A treatment, which is known to strengthen tight junction function [376], significantly increased EISdiff, while epidermal thickness and FLG and IVL expression appeared unchanged (Figure 4b, d, g). This again indicates EISdiff to quantify the complex dynamics of terminal differentiation and skin barrier formation rather than mirroring epidermal thickness. Quantifying FLG and IVL protein expression was not sufficient to model EISdiff behavior (data not shown), indicating that the complex effect of cytokines on epidermal barrier function cannot be explained by the expression of FLG and IVL alone. EIS^{SC}, however, was also found here to significantly correlate with stratum corneum thickness (Figure 4f).

Knockout out of epidermal differentiation and cell-cell adhesion genes links EISdiff to HEE differentiation

To further test our hypothesis that keratinocyte terminal differentiation significantly defines EISdiff, we knocked out key epidermal differentiation proteins by clustered regularly interspaced short palindromic repeats (CRISPR)/CRISPR-associated protein 9 (Cas9)-mediated genome editing through nonhomologous end-joining. We created keratinocyte cell lines lacking terminal differentiation protein FLG [377], tight junction protein CLDN1 [378] or transcription factors known to coordinate terminal differentiation namely aryl hydrocarbon receptor (AHR) [379] and transcription factor activating enhancer binding protein 2 alpha (TFAP2A) [379]. All knockout lines showed a reduction in EISdiff and EISSC (Figure 5a-c). Notably, CLDN1 knockout caused reduced EISdiff but showed only mildly reduced EIS^{SC} in concordance with observed parakeratosis and increased *stratum corneum* compaction (Figure 5d). FLG expression was clearly decreased in AHR, TFAP2A and CLDN1 knockout lines and completely absent in the FLG knockout line (Figure 5d). Expression of IVL was decreased in all knockout cell lines, except the FLG knockout.

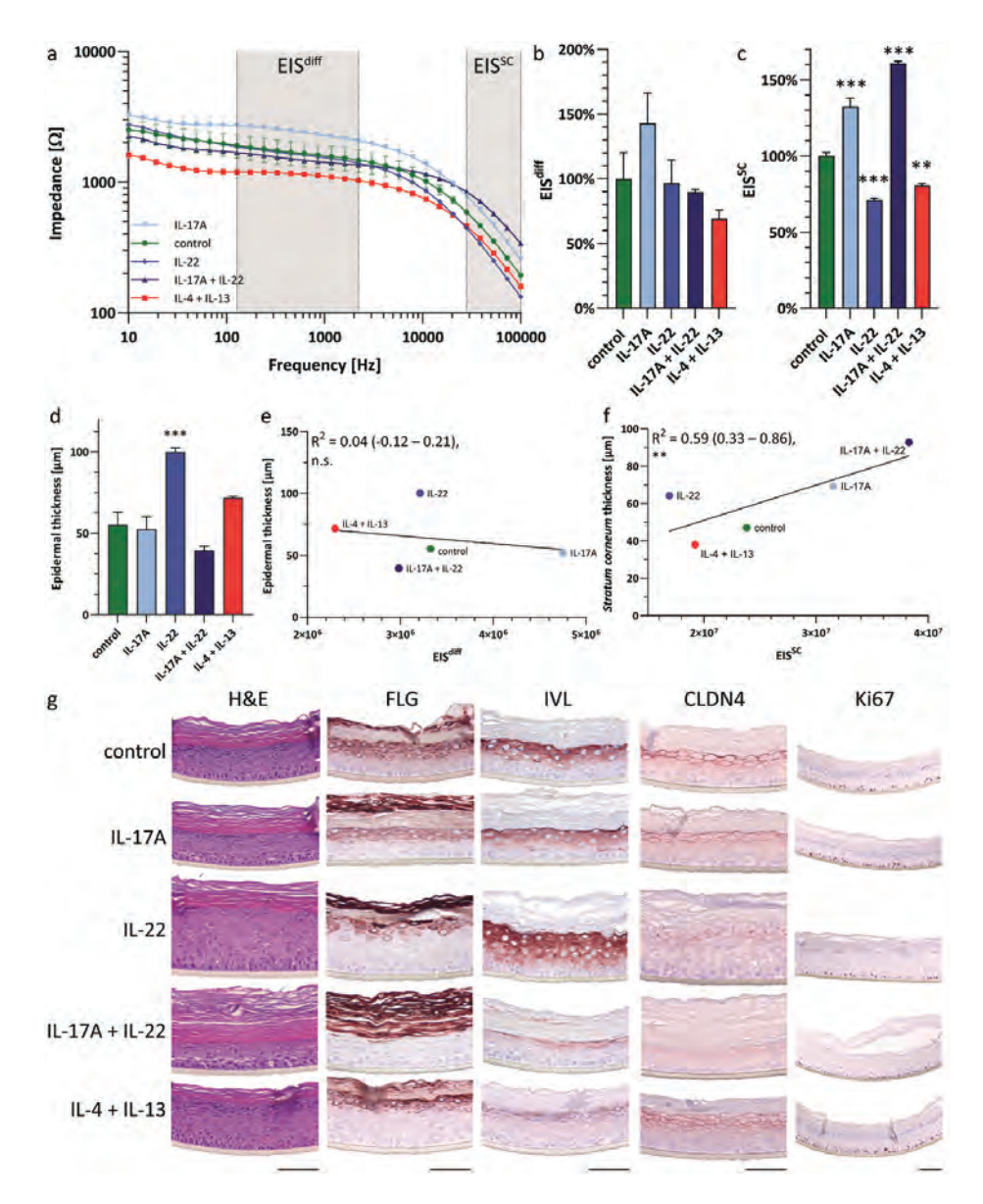


Figure 4. Stimulation with cytokines proves ElSdiff—determined barrier function to be independent of epidermal thickness. (a) Endpoint—measured impedance spectra, (b) ElSdiff and (c) ElSSC of cytokine—stimulated HEEs at day 8 of air exposure. Each condition represents three biological replicates and ElSdiff and ElSSC were compared to control. (d) Epidermal thickness of cytokine—stimulated HEEs as compared to control. Correlation of (e) epidermal thickness to ElSdiff and (f) stratum corneum thickness to ElSSC. Each condition averages three biological replicates, R² values and significances indicate the correlation of individual replicates. (g) HEEs stained for differentiation (FLG, IVL) and cell—cell adhesion (CLDN4) and proliferation (Ki67) proteins. Pictures represent three biological replicates and were taken at 20x (Ki67) or 40x magnification. Size bars indicate 100 μm.

CLDN1 (only fully absent in CLDN1 knockout) and CLDN4 expression appeared unchanged related to the epidermal cell layers which were affected by all genotypes as compared to control (Figure 5d). Hence, we conclude that EISdiff is strongly determined by the degree of epidermal terminal differentiation.

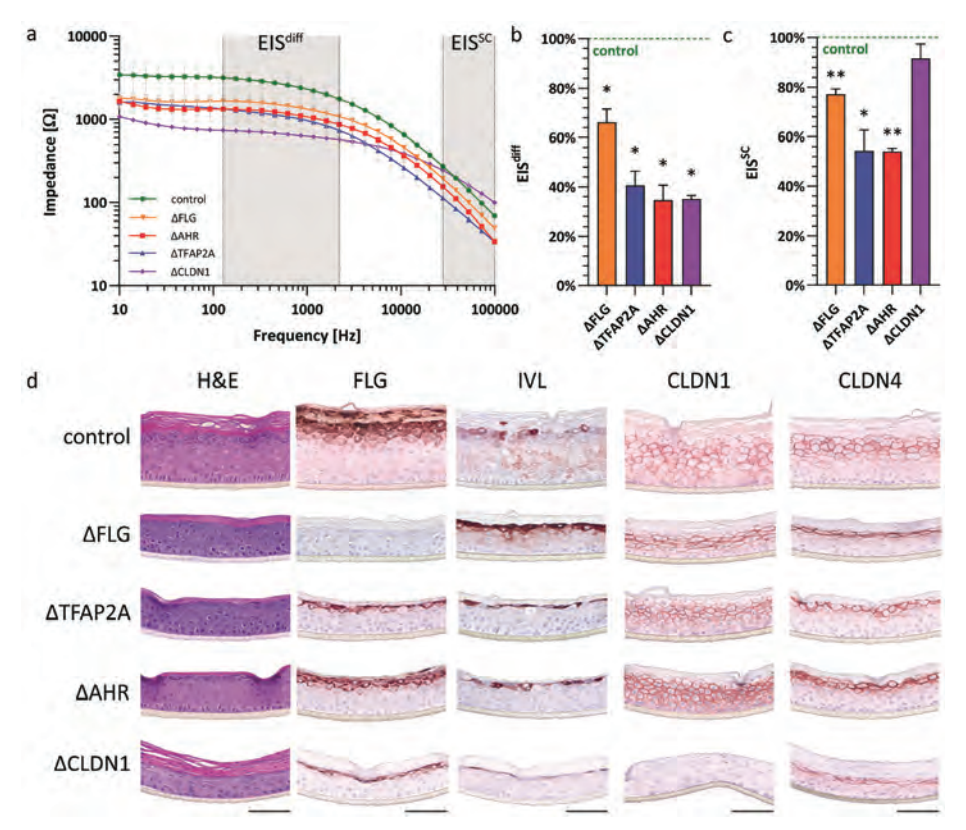


Figure 5. Knockout of genes involved in keratinocyte differentiation and cell-cell adhesion decreases EIS^{diff}. (a) Endpoint-measured impedance spectrum, (b) EIS^{diff} and (c) EIS^{sc} of HEEs with knockout of target gene at day 10 of air exposure. Each condition represents three biological replicates and EISdiff and EISsc are compared to control. Each (d) HEEs stained for differentiation (FLG, IVL) and cell-cell adhesion (CLDN1, CLDN4) proteins. Pictures represent three biological replicates and were taken at 40x magnification. Size bars indicate 100 μm.

EIS detects therapeutic response in proinflammatory IL-4 + IL-13 epidermis model

Besides detecting or monitoring epidermal defects, reversing these defects is a key component in the treatment of inflammatory skin diseases and an important parameter in the development of potential novel therapeutics. Therefore, we investigated if EIS can measure the reversal of barrier defects for future implementation in pre–clinical drug screening. For this we chose pharmacological molecules known to activate AHR, a key regulator of epidermal differentiation (Figure 5d) and novel target for topical anti–inflammatory treatment [75, 241]. Hereto, IL–4 and IL–13 stimulated HEEs were additionally treated with an array of AHR–activating ligands (L1–5) known to have a therapeutic effect, next to structurally–related nonactivating compounds (M1–2) (Table S2). AHR–activating compounds resulted in restored IL–4 + IL–13–impaired EIS^{diff} and EIS^{SC} impedance spectra, indicating capability of EIS to measure the AHR–dependent repair of skin barrier defects (Figure 6a–c). Compounds that do not activate AHR signaling (M1–2) did not restore the cytokine–mediated reduction in EIS (Figure 6a–c). In fact, these compounds known to block endogenous AHR signaling and further decreased EIS^{SC} significantly with similar trends in EIS^{diff}.

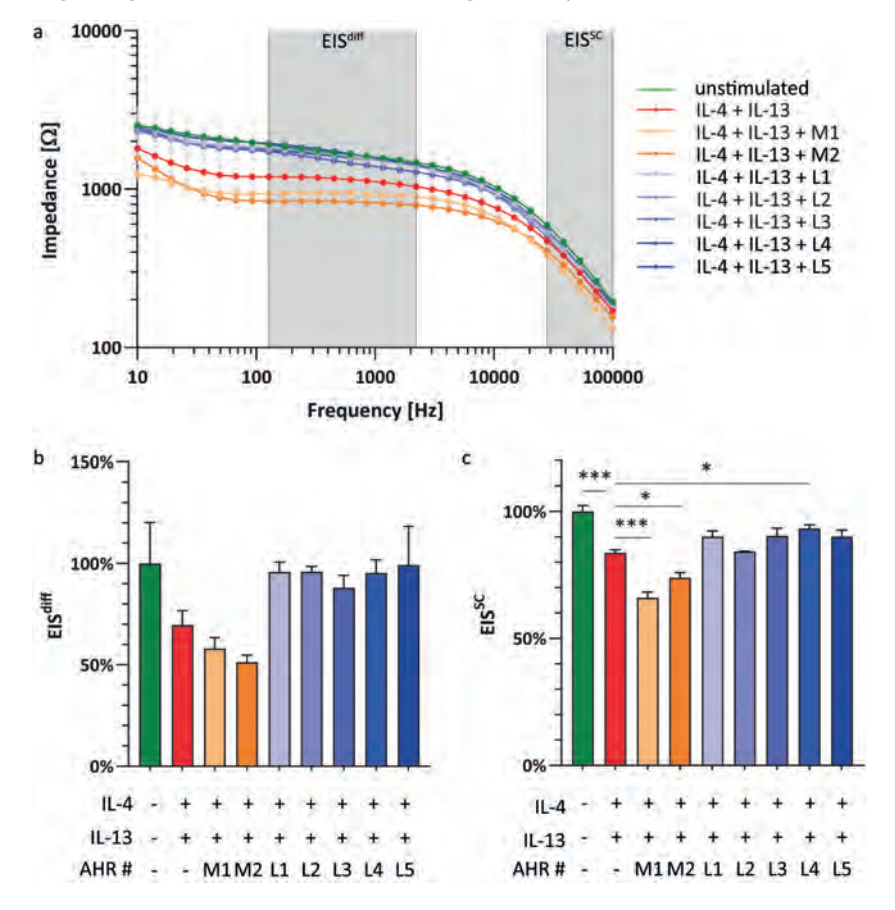


Figure 6. EIS detects therapeutic AHR response in a proinflammatory epidermis model. **(a)** Endpoint-measured impedance spectrum, **(b)** EIS^{diff} and **(c)** EIS^{SC} of HEEs stimulated with IL–4 and IL–13 cytokines alone and in combination with AHR activating therapeutic compounds at day 8 of air exposure. Each condition represents three biological replicates and EIS^{diff} and EIS^{SC} of control conditions and AHR-binding compounds are compared to IL–4 + IL–13 stimulation.

Since we now confidently determined that EISdiff measurements correlate with keratinocyte differentiation, we assumed that expression levels of differentiation proteins FLG and IVL would also correlate with the rescue in EISdiff by AHR ligands. This we could demonstrate clearly for IVL, as AHR agonists were partially able to restore the dampened IVL expression by IL-4 and IL-13. AHR-binding but nonactivating compounds (M1-2) did not restore IVL expression (Figure S2a). FLG protein levels followed a similar expression pattern as IVL albeit differences were less pronounced. Again, the expression of tight junction protein CLDN4 remained unchanged throughout treatments (Supplemental Figure 2) confirming earlier results.

Discussion

In this study, we investigated the applicability of EIS to assess skin barrier function in 3-dimensional HEE in vitro organotypic epidermis models. EIS proved an easy to handle and noninvasive system to obtain real-time quantitative readouts correlating to functional barrier properties.

While fit here to the Nunc carrier plate system, the device can be customized to various transwell cell culture platforms. Running costs are low and the measurements are performed in a semiautomated fashion. The fixed electrode setup additionally standardizes the measurements and produced results are highly repeatable when taking into account that electrical impedance readouts dependent on cell passage number, culture medium and temperature [139]. Reported readout trends are reproducible while absolute values have been observed to differ between replicated experiments. Sample readouts therefore need to be correlated with controls within the same experiment (see technical recommendations). While endpoint measurements cater to less variance, measurements can be performed and repeated in high quantities at virtually any time during HEE culture without harming tissue integrity. With current functional barrier assessments structurally relying on invasive endpoint measurements (permeation studies, Franz cell diffusion assay) and / or being laborious and sensitive to handling (Franz cell diffusion assay, TEWL, TEER), EIS provides a noninvasive, semiautomated and reproducible alternative.

EIS measures a broad range of frequencies in contrast to single frequency TEER measurements [139, 380] therefore being able to capture different functional skin barrier parameters. For quantitative analysis, experimentally obtained impedance spectra are usually fit to the corresponding electrical circuit model to isolate individual electrical parameters [381]. To aid biologic interpretation, we here chose to correlate the obtained impedance spectra with known biological barrier properties. Theoretical considerations in combination with our own data highlighted two frequency ranges which we described through calculating their area under the curve.

Frequencies on a plateau around 100–2000 Hz were termed EISdiff as they quantified differentiation in viable keratinocytes as assessed by the expression of differentiation markers FLG and IVL, which together predicted 76 % of EIS^{diff} during HEE development. While EISdiff exhibits clear independence of viable epidermis and stratum corneum thickness, a correlation with tight junction function remains uncertain. On the one hand, EIS^{diff} was observed to be independent from CLDN1 and CLDN4 protein expression during HEE development and cytokine stimulations. ΔCLDN1 HEEs exhibit a strongly reduced EIS^{diff}, but this can be explained by a concomitant reduced expression of keratinocyte differentiation markers as CLDN1 knockout is known to alter pro-FLG processing [382]. On the other hand, EISdiff frequencies overlap with R_a impedance contribution, with R_a being the electrical circuit model element to describe the resistance of tight junctions [139]. Furthermore, during IL-17A cytokine stimulation EISdiff increased independent of differentiation protein expression, which could be a result of an IL-17A strengthening effect on tight junction function [376]. In conclusion, EISdiff uniquely quantifies keratinocyte differentiation independent of CLDN1 and CLDN4 protein expression, however a contribution of tight junction function cannot be ruled out since sole protein expression does not entirely mirror tight junction functionality [383, 384].

Frequencies of a higher frequency range between 20,000 Hz and 100,000 Hz were termed EIS^{SC} and overlap with $C_{Cell'}$ a parameter describing ability of a cell to store an electrical charge. EIS^{SC} conclusively quantifies *stratum corneum* rather than complete HEE thickness. However, further experiments should investigate the relationship between EIS^{SC} , lipid organization and *stratum corneum* composition.

This study used EIS to assess HEE skin barrier function during formation, to study the effects of single genes and to assess skin barrier function under inflammatory conditions and treatment. EIS was able to measure the defects induced by knockout of cardinal differentiation–driving transcription factors (AHR and TFAP2A) and differentiation effector genes (FLG). The observed defects were congruent with other barrier function assessments reporting an elevated TEWL in ΔTFAP2A and ΔFLG HEEs and in human FLG loss–of–function variants [31, 377, 379, 385]. Cytokine–induced proinflammatory conditions resulted in keratinocyte differentiation deficiencies and changes in *stratum corneum* thickness, which

could be captured and quantified by EIS. The IL-4 + IL-13 induced decrease in EISdiff and EISSC in vitro also replicates the in vivo situation where the IL-4 and IL-13 driven skin disease atopic dermatitis is accompanied by elevated TEWL and decreased EIS values measured on in vivo patient skin [254, 367, 386, 387]. In vivo, EIS can also detect therapeutic improvements of atopic dermatitis associated with improvements in clinical scoring and reduced expression of inflammatory biomarkers [367, 388] similar to the detected therapeutic improvements in our in vitro atopic dermatitis model.

To conclude, we propose EIS to be a valuable tool to noninvasively study epidermal barrier function in organotypic skin models. The dual viable epidermis/stratum corneum barrier assessment and the quantification of keratinocyte differentiation are, to our knowledge, singular across all barrier evaluation techniques. The proposed semiguantitative EIS analysis is easy to replicate and uniquely correlates impedance readouts with biological barrier properties. We suggest EIS to be especially suited for longitudinal studies of barrier development, keratinocyte differentiation and barrier-disrupting skin diseases including preclinical therapeutic studies. In addition, EIS can be used in multi-cell type models to investigate the interplay between epidermis, extrinsic and intrinsic factors, potentially in combination with patient-derived cells, immune cells and/or bacteria. The possibility to correlate in vitro and in vivo EIS measurements facilitates a unique translational approach from bedside to bench and back.

Technical recommendations

To ensure optimal, reproducible EIS measurements without compromising culture integrity, we propose several guidelines for implementing EIS in the laboratory:

- Measurements depend on temperature and ion content of the surrounding fluid. To ensure maximum comparability between conditions, use an isotonic buffer solution (e.g. phosphate-buffered saline (PBS)) and allow samples to adjust to room temperature for at least 30 minutes before measurements.
- To minimize variation when performing serial measurements at various days of the cell culture, the time of topical exposure to PBS should be kept minimal and PBS should be carefully removed after measurements to maintain the air-liquid interface as much as possible for proper barrier formation and function.
- Before commencing measurements, blank measurements on PBS only or empty filters should be performed, as this provides information on intrinsic capacitance of the electrodes and the resistance of PBS and filters. When analyzing the results, blanks should be subtracted from measured sample values.

- Previous publications have normalized EIS based on the surface area of the used cell culture system using various methods [389-391]. Considering the lack of consensus, we report uncorrected EIS values and the surface area of HEEs (0.47 cm²) to aid comparisons.
- · Control conditions should be taken along for each individual experiment and measurement time point to interpret relative changes in preference to absolute values.
- EISdiff (127-2212 Hz) and EISSC (28,072-100,000 Hz) are determined through calculating the area under the curve at respective frequencies.

Materials & Methods

Cell culture

Human primary keratinocytes were isolated from surplus human skin obtained through plastic surgery according to the principles and guidelines of the principles of Helsinki. From the skin, biopsies were taken and keratinocytes were isolated as described previously [334]. N/TERT-2G keratinocytes were a kind gift of James Rheinwald, Brigham's Woman hospital [262] and were cultured as monolayers in CnT-prime (CELLnTEC, Bern, Switzerland, CnT-PR) until confluent before use in HEE cultures [263]. Knockout N/TERT-2G cell lines were generated through CRISPR/Cas9 and validated previously (FLG [377], CLDN1 [378], TFAP2A [379], AHR [379]).

Generation of HEEs

HEE cultures were performed as previously described [377]. In short, cell culture inserts in a 24-wells carrier plate (Nunc, Thermo Fisher Scientific, 141002) were coated using 100 µg/mL rat tail collagen (Sigma-Aldrich, C3867) for 1 hour at 4 °C. After phosphate-buffered saline (PBS) washing the filters, 150,000 cells were seeded and submerged in CnT-prime medium (CELLnTEC, CnT-PR) at the lowest insert stand. After 48 hours, the medium was switched to differentiation medium (40 % Dulbecco's modified Eagle's Medium (Sigma-Aldrich, D6546) and 60 % 3 D barrier medium (CELLnTEC, CnT-PR-3D)) and 24 hours afterwards the HEEs were lifted to the highest stand and air-exposed, and medium was refreshed every other day. For stimulation experiments, IL-4, IL-13, IL-17A or IL-22 (50 ng/mL per cytokine, Peprotech, Rocky Hill, NJ, USA, 200-04/200-13/200-17/200-22) supplemented with 0.05 % bovine serum albumin (Sigma-Aldrich, A2153) were added to the medium of HEEs of primary keratinocytes from day 5 of air exposure until day 8. AHR ligands (Table S2) were supplemented in the culture medium as previously described [310].

EIS measurements

For the EIS measurements the Locsense Artemis (Locsense, Enschede, the Netherlands) device was used and equipped with a custom-made incubator compatible smart lid. The Artemis consists of a detector element that is connected to the smart lid with electrodes aligning to the two middle rows of a 24-well plate. A laptop equipped with the Locsense Artemis monitoring software (version 2.0) displays the readouts. During the measurements each well contains two electrodes: one disc-shaped 4.2 mm diameter electrode situated in the center of the transwell insert and a rod-shaped 1.9 mm diameter electrode passing sideways of the transwell insert. Before measurements, HEEs were acclimated to room temperature and cultures were lowered to the middle position in the transwell plate while 1600 uL PBS at room temperature was added below and 500 uL PBS on top of the filter. Thereafter, the smart lid was placed on the wells ensuring both electrodes being submerged. Following device self-calibration, impedance was measured over a frequency range from 10 Hz to 100,000 Hz in 30 logarithmic intervals. Measurement output contains impedance as well as phase values. Phase values can be interpreted as raw values, while a PBS only blank measurement was subtracted from the corresponding electrode of the impedance output. For further specific considerations during measurements, see technical recommendations. For EISdiff (127–2212 Hz) and EISSC (28,072–100,000 Hz) the area under the curve was calculated using the respective frequency ranges.

Immunohistochemistry

For histological processing, 4 mm biopsies were fixated in 4 % formalin solution for 4 hours and embedded in paraffin. Afterwards, 6 µm sections were deparaffinized and either stained with hematoxylin (Klinipath, 4085.9005) and eosin (Klinipath, 4082.9002) or by antibodies listed in Supplemental Table S3 followed by avidinbiotin complex (Vectastain, AK-5000). Epidermal thickness specifies the average of three measurements on H&E stained sample pictures while stratum corneum thickness was determined by subtracting epidermal from total construct thickness. Protein expression was quantified with ImageJ following sections C-E of [392] by freehand selecting the viable epidermis and measuring the "area" i.e. number of staining-positive square pixels.

Statistics

Datasets were analyzed using the GraphPad Prism 10 software version 10.1.1. All barplots are shown as mean ± standard error of the mean and significance testing was performed using one-way analysis of variance (ANOVA) in combination with Dunnett correction for multiple testing and unpaired t-testing (exclusively

Correlation analysis of EIS to protein expression and HEE morphology

Correlation analysis was conducted using simple (epidermis thickness and *stratum corneum* thickness) and multiple linear regression modelling (protein expression) in Graphpad Prism and the R programming language (version 4.2.3) with the psychometric package. All correlation analysis were conducted with individual replicates, figures depict replicate averages for readability.

Data availability statement

The impedance data related to this article can be found at https://doi.org/1 0.34973/yfca-cr43, hosted at the Radboud University Data Repository. Pictures of immunohistochemistry staining are available from the corresponding author upon request.

Conflict of interest

SR is CEO and founder of Locsense B.V., which contributed in–kind to this work. The results presented in the study are not influenced nor determined by the views or wishes of Locsense, nor did Locsense provide any financial support for this study that may conflicted with the results interpretation or presentation of data. The contribution of Locsense was limited to the development of the smart lid to fit the cell culture system and to providing technical support. Discussions with Locsense on the data representation and electrical circuit interpretation aided in correlating the data output to biological interpretations. The remaining authors declare no conflicts of interest.

Acknowledgements

We thank Joachim Wegener (University of Regensburg, Germany) for the critical reading of our manuscript and all members of the Van den Bogaard group for the lively discussions and suggestions. We thank Ewald Bronkhorst for advice on the correlation analysis. This collaborative work was supported by NIH R35 grant ES028244, PAST4FUTURE grant LSHM20043-HSGF and European Innovation Council (EIC) under grant agreement No. 101098826 (SKINDEV) and the Radboud university medical center (EB). The FLG knockout cells were generated under a LEO Foundation grant LF-OC-22-001056 (JS and EB).

Author contributions

Conceptualization: NB, FP, LM, JS, and EB; Data Curation: NB, FP, and LM; Formal Analysis: NB and FP; Funding Acquisition: JS, EB; Investigation: NB, FP, LM, HN, IVW, MB, DRO, PJ JS; Methodology: NB, FP, LM, JS; Project Administration: EB; Software: SR; Supervision: JS and EB; Validation: NB and FP; Visualization: NB and FP; Writing - Original Draft Preparation: NB and FP; Writing - Review and Editing: all authors.

Supplementary material

Supplemental Table S1. Overview of methodologies used for measurement of in vitro epidermal barrier function

Technique	Principle of analysis	Assessed barrier component	Advantages	Disadvantages	References
Permeation studies	Paracellular diffusion of dyes/tracers of various molecular weights	tight junction pore size, corneodesmosome integrity, lipid barrier	relatively cheap easy to implement	 destructive end-point parameter conventionally non-quantitative and not high-throughput 	[362,363]
Franz cell diffusion assay	Assessment of drug permeation from donor chamber through HEE into acceptor chamber	outside—in barrier function including s <i>tratum corneum</i> and tight junction barrier function	gold standard for assessing outside–in barrier quantitative	 destructive end-point parameter high level of expertise required model system must stay intact during sampling period after harvest highly influenced by temperature, sampling frequency and stirring conditions 	[364, 393]
Transepidermal water loss (TEWL)	Measurement of changes in air humidity on top of HEE	lipid barrier function in relation to <i>stratum corneum</i> thickness	non-destructive quantitative	 highly influenced by probe type and angle, contact pressure, temperature and atmospheric pressure high variability between different instruments high background readings labor intensive 	[366, 394]
Transepithelial electrical resistance (TEER)	2 electrodes apply low alternating current over the HEE at a single frequency	tight junction ionic conductance ("tight junction tightness")	non–destructive quantitative easy to implement	 highly influenced by electrode positioning, temperature and medium composition not designed for complex tissues labor intensive 	[139]

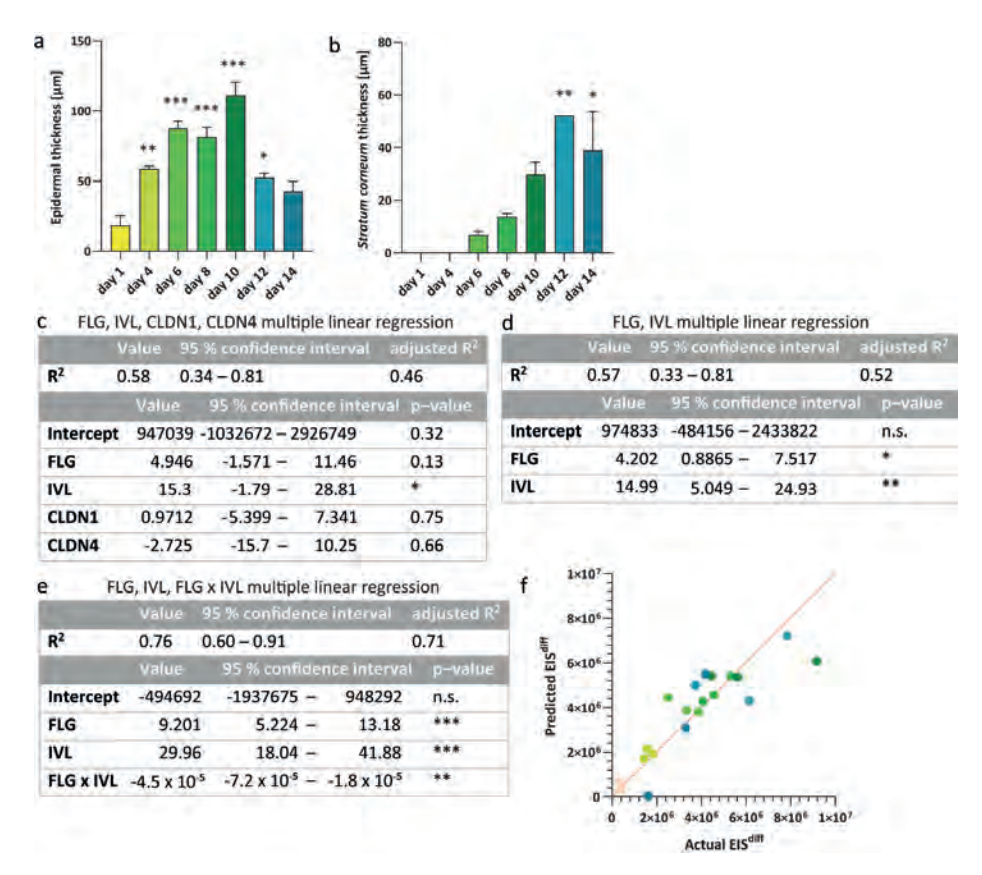
HEE: human epidermal equivalent; TEER: transepithelial electrical resistance; TEWL: transepidermal water loss

Supplemental Table S2. AHR-binding compounds

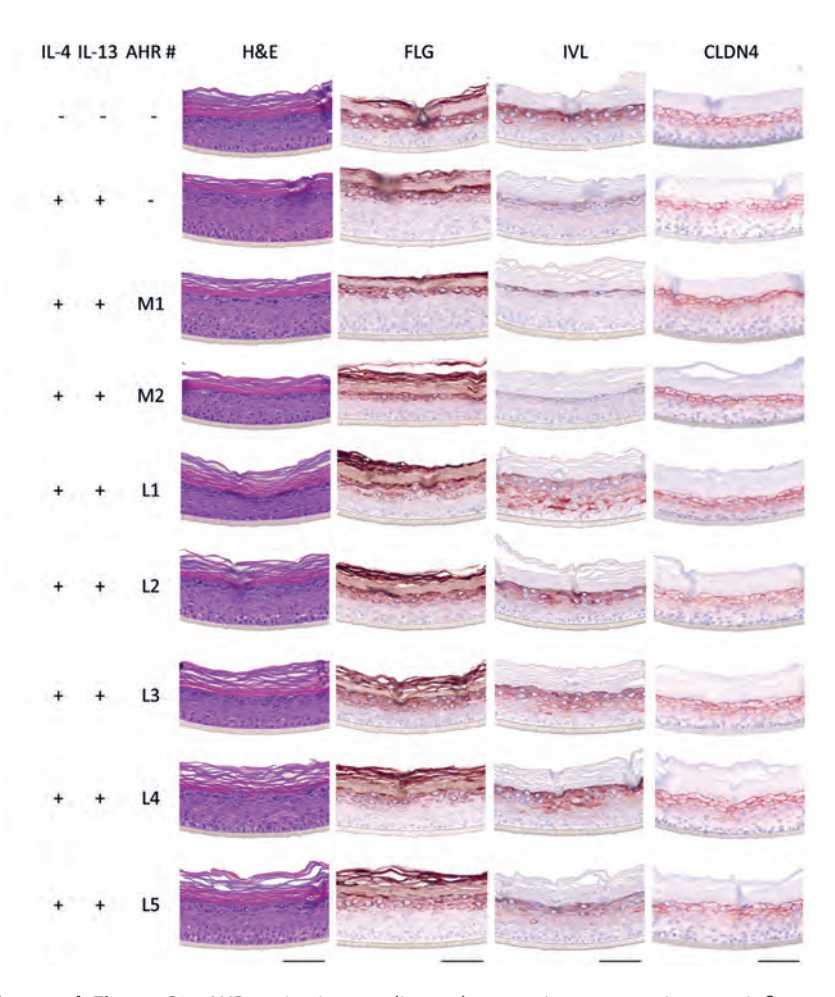
Abbreviation	Compound	Concentration	Reference
M1	SGA360	10 nM	[310]
M2	Teriflunomide	10 μΜ	[395]
L1	coal tar	2 μg/mL	[75]
L2	SGA388	10 nM	[310]
L3	Leflunomide	10 μΜ	[395]
L4	IMA-7101	1 nM	[177]
L5	TCDD	10 nM	[396, 397]

Supplemental Table S3. Antibodies used for immunohistochemical analysis

			-
Antigen	Species	Dilution	Company
FLG	Mouse	1:100	Thermo Fisher
IVL	Mouse	1:20	Mon 150 (own antibody)
CLDN1	Rabbit	1:200	Invitrogen
CLDN4	Mouse	1:200	Invitrogen
Ki67	Rabbit	1:200	Abcam
SKALP	Rabbit	1:4000	Own antibody
KRT16	Mouse	1:200	Santa-Cruz
Goat anti-rabbit	Goat	1:200	Vector laboratories
Horse anti-mouse	Mouse	1:200	Vector laboratories



Supplemental Figure S1. FLG, IVL and FLG x IVL interaction significantly influence EIS^{diff} during HEE development. **(a-b) (a)** Epidermal thickness and **(b)** *stratum corneum* thickness of during HEE development compared to day 1. Each condition represents three biological replicates. **(c-e)** Multiple linear regression using **(c)** FLG, IVL, CLDN1 and CLDN4, **(d)** FLG and IVL and **(e)** FLG, IVL and FLG x IVL expression to predict EIS^{diff}. Analysis is based on all timepoints and replicates from figure 3. **(f)** Correlation of actual and FLG, IVL, FLG x IVL regressed EIS^{diff}.



Supplemental Figure S2. AHR activation mediates therapeutic response in a proinflammatory epidermis model. HEEs stained for differentiation (FLG, IVL) and cell-cell adhesion (CLDN4) proteins. Pictures represent three biological replicates of HEEs at day 8 of air exposure and were taken with 40x magnification. Size bars indicate $100 \ \mu m$.



Chapter 7

Coal tar attenuates acute experimentally-induced dermatitis: insights into AHR-targeting therapies for inflammatory skin diseases

Noa J.M. van den Brink¹, Jade G.M. Logger¹, Tessa A. Kouwenhoven¹, Ivonne M.J.J. van Vlijmen-Willems¹, Ivone Jakasa², Piet E. van Erp¹, Jos P.H. Smits^{1,3}, Ellen H. van den Bogaard^{1*}

¹Department of Dermatology, Research Institute for Medical Innovation, Radboud University Medical Center, Nijmegen, The Netherlands.

²Department of Public and Occupational Health, Amsterdam UMC, University of Amsterdam, Amsterdam, The Netherlands.

³Department of Dermatology, Heinrich Heine University, University Clinic Düsseldorf, Düsseldorf, Germany.

^{*}Corresponding author: Ellen.vandenBogaard@radboudumc.nl, Department of Dermatology, Research Institute for Medical Innovation,
Radboud University Medical Center, Geert Grooteplein 10A, 6525GA, Nijmegen, The Netherlands.

Abstract

Atopic dermatitis and psoriasis lesions are characterized by specific immune cell infiltrates, keratinocyte hyperproliferation, and disturbed terminal differentiation leading to skin barrier impairment. Targeting of the aryl hydrocarbon receptor (AHR) in skin by topical therapeutics including coal tar and tapinarof are proven effective and safe in counteracting the abovementioned disease hallmarks. To complement our previous experimental studies on the therapeutic modes of action by coal tar and effects of structurally diverse AHR ligands on skin, we know aimed to gain knowledge on the cellular processes contributing to skin barrier repair and dampening inflammation by AHR activation in vivo. Hereto, coal tar (5% pix lithanthracis in vehicle cream was applied for four days on skin of healthy volunteers before or after superficial skin damage by stratum corneum tape stripping. Coal tar application on intact skin significantly increased numbers of proliferating keratinocytes which correlated to the induction of AHR-target protein expression, CYP1A1, in the basal layer of the epidermis. Elevated erythema was observed and a concomitant increase in transepidermal water loss indicated a compromised barrier function as compared to untreated or vehicle treated skin. Upon stratum corneum damage by tape stripping, vehicle cream under occlusion induced unexpected acute dermatitis. Dermatitis-hallmarks were abrogated by coal tar demonstrated by reduced keratinocyte hyperproliferation and epidermal acanthosis. Lower levels of human beta defensin-2, a skin inflammation marker, was observed in the epidermis and stratum corneum of coal tar-treated skin as compared to vehicle. Coal tar also counteracted or prevented the migration of Langerhans cells from the epidermis to the dermis, and a lower number of dermal MPO+ cells and CD45+T-cells was observed in coal tar-treated skin. Skin barrier parameters (TEWL, hydration and natural moisturizing factors) were not improved after four days of coal tar treatment post tape stripping. Our study highlights the Janus-faced effects of AHR activation in skin being detrimental under normal conditions, yet therapeutic for combatting inflammatory processes. Understanding the sequence of events and key target cells and pathways underlying harmful vs. therapeutic effectiveness of AHR modulating ligands under normal and inflammatory conditions in skin requires further investigation.

Introduction

The skin forms an important defensive layer for the human body, preventing excessive water loss and protecting against potential harmful external substances. Chronic inflammatory skin diseases, such as psoriasis and atopic dermatitis (AD), are characterized by immunological or genetics-associated defects in the skin barrier, leading to increased water loss through the skin [31, 398], and in the case of AD, recurrent skin infections. These barrier defects are linked to aberrant epidermal differentiation, cornification and desquamation accompanied by keratinocyte hyperproliferation resulting in epidermal acanthosis. Patients suffer from itchy, scaly patches of skin accompanied by skin dehydration marked by increased epidermal water loss [399]. AD is mostly treated with topical emollients and corticosteroids possibly combined with systemic immunosuppressants (e.g., cyclosporine, dupilumab or JAK inhibitors) in moderate to severe disease [400, 401]. Aside from major developments in the precision targeting of the immunological component of the disease, non-steroidal topical therapeutics and targeted medicine to restore skin barrier formation and function are still warranted for the mainly pediatric population or those affected by mild symptoms and not eligible for systemic drugs or biologicals [39].

Our research into the molecular mechanisms of topical coal tar treatment [402], directed the dermatology field and pharmaceutical industry towards the therapeutic targeting of the aryl hydrocarbon receptor (AHR) in skin. Coal tar is one of the oldest treatments for inflammatory skin diseases and is comprised of a complex chemical mixture including a wide spectrum of polycyclic aromatic hydrocarbons. Even though polycyclic aromatic hydrocarbons have been described to be mutagenic, for example in air pollution [104] or in the past chimney sweepers [403], coal tar has been shown to be safe, even after long term exposure for dermatological use [78]. Coal tar's exact treatment mechanism remained elusive for a long time. We discovered that coal tar alleviates AD by activation of the AHR in skin cells, with our research focused on keratinocytes [75]. Upon ligand activation, the AHR translocates towards the nucleus, binds its nucleic partner ARNT, and regulates several transcriptional processes including xenobiotic metabolism [404], keratinocyte differentiation (including upregulation of antimicrobial peptides [76, 125, 405]) and proliferation. Coal tar restores these mechanisms altered in inflammatory skin diseases [76, 125, 405], effectively ameliorating inflammation. Notwithstanding these health benefits, AHR signaling when uncontrolled can also be detrimental for human health, inducing cellular toxicity, mutagenesis and cancer by hazardous environmental toxins [122].

Recently, a novel AHR-targeting molecule, Tapinarof, has been approved for treatment of psoriasis and AD [406, 407], also for pediatric AD patients of 2 years and older. Although AHR-activating compounds such as coal tar and Tapinarof have proven anti-inflammatory effects, the cellular mechanisms appear diverse and most of these effects have been studied in *in vitro* models of human skin or in animal models [148, 153]. Additionally, whether the anti-inflammatory effects of AHR-activation are constrained to specific inflammatory pathways or whether it is a general effect remains to be investigated. Finally, the sequence of events that are related to the treatment response, e.g., whether ligand-activated AHR first results in barrier repair followed by dampening of inflammation, or vice versa, is still unclear.

In this study, we investigated the prophylactic and therapeutic effects of coal tar treatment after complete removal of the *stratum corneum* in human volunteers by repeated application and removal of cellotape, called tape stripping. Skin barrier parameters (trans-epidermal water loss (TEWL), water content, natural moisturizing factors (NMF)), *stratum corneum* protein profiles and skin morphology were determined to increase our understanding of the role of AHR-activation in barrier repair and dampening of specific immune responses.

Results

Demographics

For this study, 17 healthy volunteers were included (see Table 1 for participant details). Volunteers were divided into two groups: in group 1 prophylactic effects of AHR activation by coal tar prior to tape-stripping was investigated; in group 2 the therapeutic effects of coal tar barrier impairment of the skin was assessed. For both groups, majority of volunteers were females aged between 20 and 26.

Pre-treatment with coal tar is not beneficial for skin barrier recovery

We hypothesized that prophylactic effects of AHR activation, by treatment with coal tar prior to tape stripping, could prime the skin for faster repair of the *stratum corneum*. Hereto, skin areas of 2cm² each located on the lower back were left untreated, were treated with coal tar (5% pix lithanthracis) or vehicle emollient cream (vaseline lanette) (all conditions under occlusion) (Figure 1A). After four days of pre-treatment, skin areas were completely tape stripped until skin was glistening, marking complete *stratum corneum* removal. Before and after tape stripping, biophysical measurements were taken to study erythema, trans-epidermal water loss (TEWL) and water content of the skin. Treatment of skin with coal tar cream

prior to tape stripping for four days caused an increased TEWL (Figure 1B) and increased erythema (Figure 1C) as compared to no cream or vehicle-treated skin. No changes were observed for *stratum corneum* water content (Figure 1D).

Table 1. Demographics

	Group 1	Group 2
Subjects, N	8	9
Sex, N - Male - Female	3 6	1 8
Age*, median (range)	22.7 (20.8-26.4)	21.8 (20.0-26.4)
Skin type, N - II - III	6 3	8 1
Skin disease, yes, N	0	0
Skin disease in family, yes, N Sensitive skin, yes, N	0	4 (parents: N=4) 1

^{*}Non-normal distribution due to small group size

During the course of the study, several adverse events were noted: Treatment setting: itch (N=3), burning sensation (N=2), erythema (N=1), mild folliculitis (N=1) at day 2/4. Prophylactic setting: itch (N=6), erythema (N=3), mild folliculitis (N=2) at day 0. All adverse events were localized to the location of application and temporary.

To investigate the potential mechanism behind the changes in TEWL and erythema by coal tar application, we analyzed skin biopsies for morphology and protein expression changes (Figure 1E). All skin sites under occlusion for four days demonstrated increased epidermal thickness as compared to untreated control biopsies. Only for coal tar, this mild acanthosis was accompanied by a markedly increased number of Ki67 positive cells, indicative of keratinocyte hyperproliferation. Levels of involucrin and late cornified envelope (LCE) 3, epidermal differentiation proteins induced in hyperproliferative conditions, were also increased by coal tar, as compared to no cream or vehicle cream treatment. These protein expression changes correlated with the induced expression of cytochrome P450 1A1 (CYP1A1), marking AHR activation in the epidermis. After stratum corneum removal by tape stripping regardless of treatment, TEWL (p<0.0001), erythema (p=0.171), and water content (p<0.0001) decreased over time (Figure 1F). No significant differences between treatments were found. These results indicate that coal tar application onto healthy intact skin activates AHR signaling in the epidermis resulting in a hyperproliferative epidermis with signs of altered epidermal differentiation and increased epidermal water loss. No beneficial effects of the prophylactic use of coal tar on skin barrier regeneration were observed.

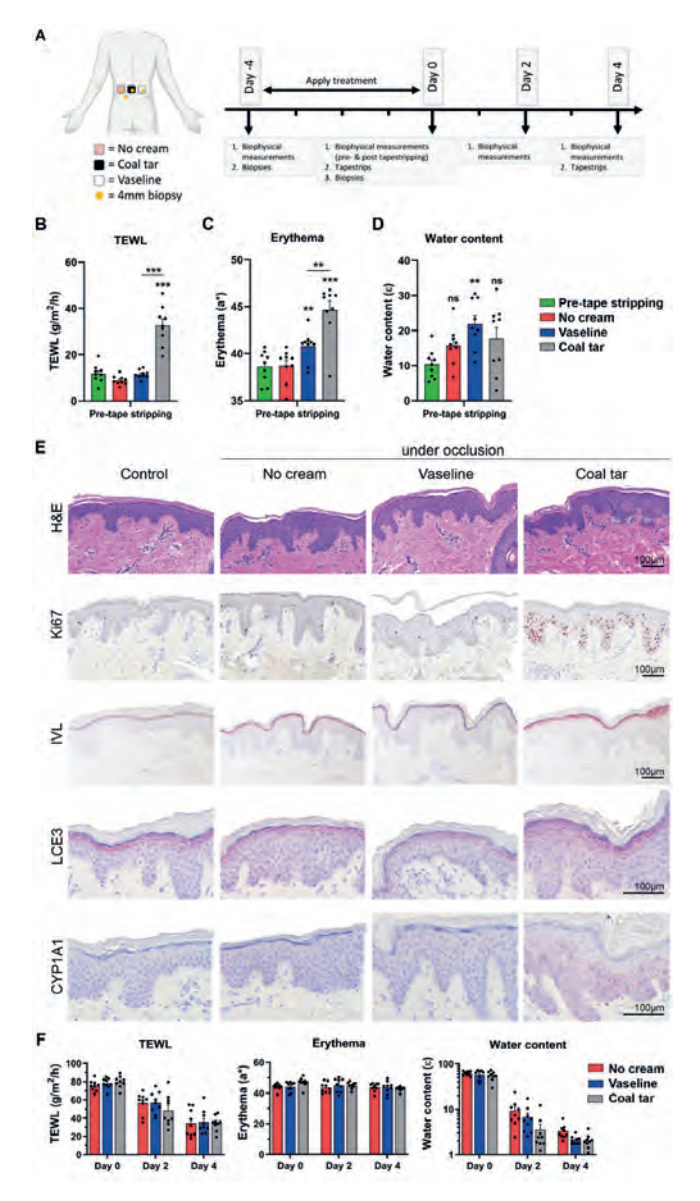


Figure 1. Prophylactic coal tar treatment is not beneficial for skin barrier recovery. **A)** Schematic treatment schedule indicating when and where biophysical measurements were performed, skin was tape stripped, biopsies were taken, and creams were applied. Volunteers in the prophylactic group were treated in a prophylactic setting, treating sites on the lower back with no cream, vaseline, or coal tar cream – under occlusion – before tape stripping. After tape stripping, the skin was allowed to heal without treatment nor occlusion. **B-D)** Biophysical measurements: trans-epidermal water loss (TEWL), erythema, and water content measured at day 0 pre-tape stripping, marking the initial values before start of the treatment phase. **E)** Morphological (H&E staining) and immunohistochemical analysis of Ki67, IVL (20x magnification), LCE3, and CYP1A1 (40x magnification). **F)** Biophysical measurements: trans-epidermal water loss (TEWL), erythema, and water content measured during the treatment phase at day 0, 2 and 4.

Coal tar and vaseline increase TEWL and erythema in damaged skin

To study the effects of coal tar during skin barrier repair, healthy skin was first tape stripped followed by vaseline or coal tar cream application, or left untreated (all under occlusion for four days, Figure 2A). Skin sites were analyzed for TEWL, water content and erythema. All parameters were increased as expected directly after the tape stripping procedure indicating the successful removal of the stratum corneum and disruption of skin barrier function (Figure 2B-D). For both coal tar and vaseline treated skin, significantly less recovery of TEWL levels was observed as compared to skin devoid of cream after four days. Recovery also appeared slower than in skin having no cream applied to (Figure 2B). Only in skin with no cream, erythema returned to baseline within four days.

Remarkably, both vehicle and coal tar treated skin showed an opposite erythema response, being significantly induced after 2 days of treatment, and erythema measurements remained elevated at day four of treatment (Figure 2C). During the recovery period, stratum corneum water content levels returned to baseline levels with no significant difference between treatments (Figure 2D).

Based on these parameters, we suspected that vehicle and/or coal tar cream had induced local dermatitis which we further investigated microscopically (Figure 2E). Skin biopsies revealed distinct epidermal acanthosis and a substantial dermal and epidermal immune cell infiltrate of vehicle treated skin, as compared to the mild acanthosis of skin left without cream. Remarkably, the epidermis of coal tar treated skin appeared less thickened (Figure 2F) with minor immune cell infiltration as compared to the vehicle treated skin (Figure 2E). Although not reflected by improved skin barrier parameters, stratum corneum regeneration after tape stripping was most apparent by microscopy in sites treated with coal tar. Expression of CYP1A1 (Figure 2E) was only detected in the coal tar treated skin, confirming correct cream application and successful induction of AHR activation.

Coal tar reduces dermatitis-associated epidermal hallmarks following tape stripping

To determine if the differences in epidermal thickness and stratum corneum regeneration were accompanied by altered keratinocyte proliferation rates or expression of epidermal differentiation proteins, immunohistochemical analysis of the skin biopsies was performed. Keratinocyte hyperproliferation, as indicated by increased Ki67 positive cell numbers, was apparent in both coal tar and vehicle treated skin as compared to no cream, with higher numbers in vehicle than coal tar (Figure 3A, Figure 3C). Expression of terminal keratinocyte differentiation markers filaggrin (FLG), involucrin (IVL), and late cornified envelope 3 (LCE3) were increased by both creams as compared to control or tape stripped skin with no cream (Figure 3B). Keratin 2, which is normally expressed in upper spinous and granular layers, was detected almost down to the basal layer (Figure 3B).

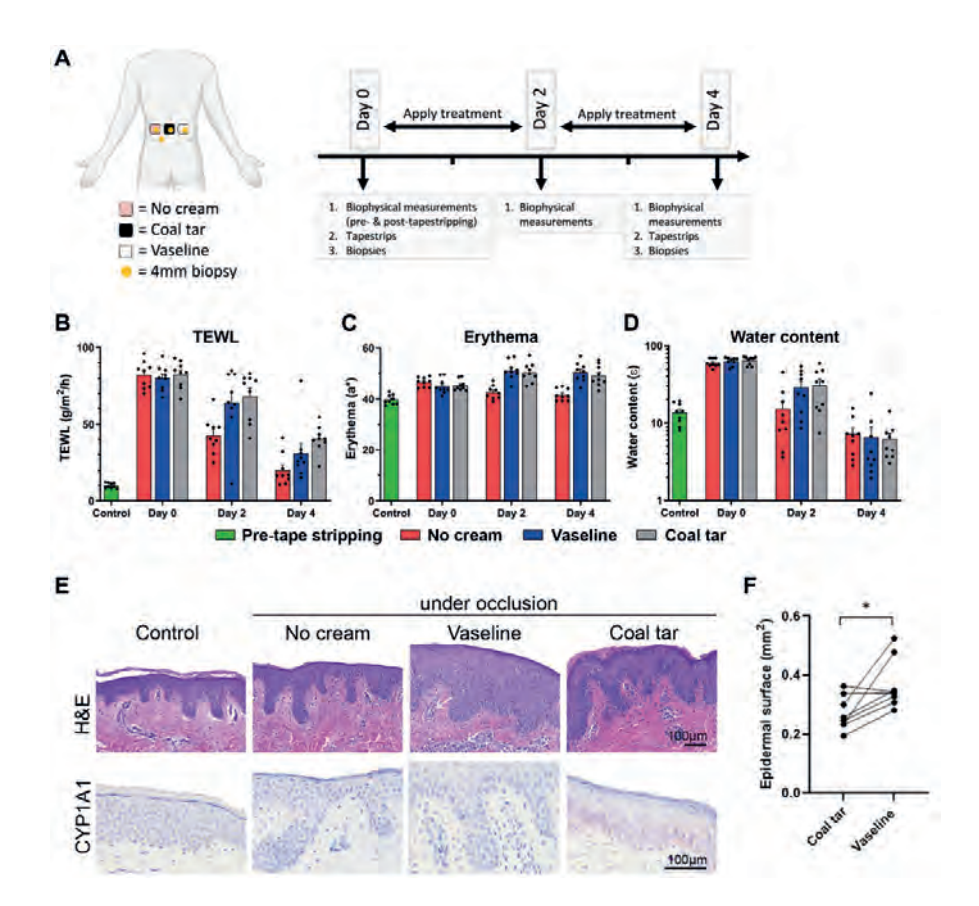


Figure 2. Coal tar and vaseline increase TEWL and erythema in damaged skin. **A)** Treatment schedule indicating when and where biophysical measurements were performed, skin was tape stripped, biopsies were taken, and creams were applied. Volunteers in the treatment group were first tape stripped followed by treatment with no cream, vaseline or coal tar cream during four consecutive days. **B-D)** Trans-epidermal water loss (TEWL), erythema, and water content were measured during several days with the following statistically significant changes observed: no cream (p<0.0001), vaseline (p<0.0001), and coal tar (p<0.0001) reduced TEWL over time, no cream treatment was more effective than coal tar treatment (p<0.01). Erythema was increased after tape stripping, and further upon vaseline (p<0.01) and coal tar treatment (p<0.01). No cream treatment reduced erythema (p<0.01). Water content increased upon tape stripping and diminished over time in all treatment groups (no cream p<0.0001, vaseline p<0.0001, coal tar p<0.0001), but is not significantly different between treatment groups. **E)** Morphological (H&E staining) and immunohistochemical analysis of CYP1A1. **F)** Quantification of epidermal thickness from microscopic images. The average thickness is taken from all donors (N=8) and shown per treatment condition.

The observed increase in FLG protein expression led us to analyze its breakdown products, histidine (Figure 3D) and trans-urocanic acid that are considered natural moisturizing factors (NMF) important for skin barrier function. These NMF were strongly decreased in the regenerated stratum corneum after tape stripping as compared to normal skin with no significant differences between treatment conditions found at day four of the recovery period (Figure 3E).

Both coal tar and vaseline are reported to upregulate epidermal antimicrobial proteins (AMPs) [77, 408], as also indicated by the induction of LCE3 (Figure 3B). We further explored expression of other inducible AMPs, skin-derived antileukoproteinase (SKALP/elafin) and human beta defensin (hBD)2, being also associated to skin inflammation (Figure 3F) [60, 409]. SKALP/elafin was increased by vaseline and coal tar, and its expression was absent in normal skin and tape stripped skin without cream exposure. Interestingly, hBD2 was only expressed in vaseline treated skin, whilst protein expression could not be detected in coal tar treated skin. nor in control skin and tape stripped skin without cream exposure. The differential expression in hBD2 between vaseline and coal tar was confirmed at mRNA level in the biopsies (DEFB4A, Figure 3G) and stratum corneum protein concentrations in collected tape strips (Figure 3H). These results indicate that prolonged exposure of vaseline lanette cream on damaged skin induces acute local dermatitis and delayed skin barrier recovery, which in part was counteracted by coal tar having antiinflammatory effects demonstrated by dampening of epidermal hyperproliferation and hBD2 expression.

AHR activation by coal tar impedes immune cell trafficking in skin

To better characterize the inflammation process and potential anti-inflammatory mechanisms of coal tar, biopsies were stained for CD45 and myeloperoxidase (MPO) expression to identify involvement of innate and adaptive immune cells, respectively. CD45+ and MPO+ cell numbers were significantly increased in the dermis after treatment with vehicle but remained similar to skin with no cream upon coal tar treatment (Figure 4A, B, D). Epidermal CD45 mRNA expression followed the same pattern, indicating epidermal immune cell infiltration due to vehicle application, but not coal tar (Figure 4C). Given our prior studies on IL-17 induced hBD2 expression in keratinocytes and identification of IL-17A as a keratinocyte mitogen in vitro [55, 410], we analyzed the presence of IL-17+ cells in the dermis. The number of IL-17+ cells varied between volunteers but actually appeared reduced upon inflammation and lowest in vaseline treated skin (Figure 4E-F), indicating involvement of other cell types in the inflammatory process.

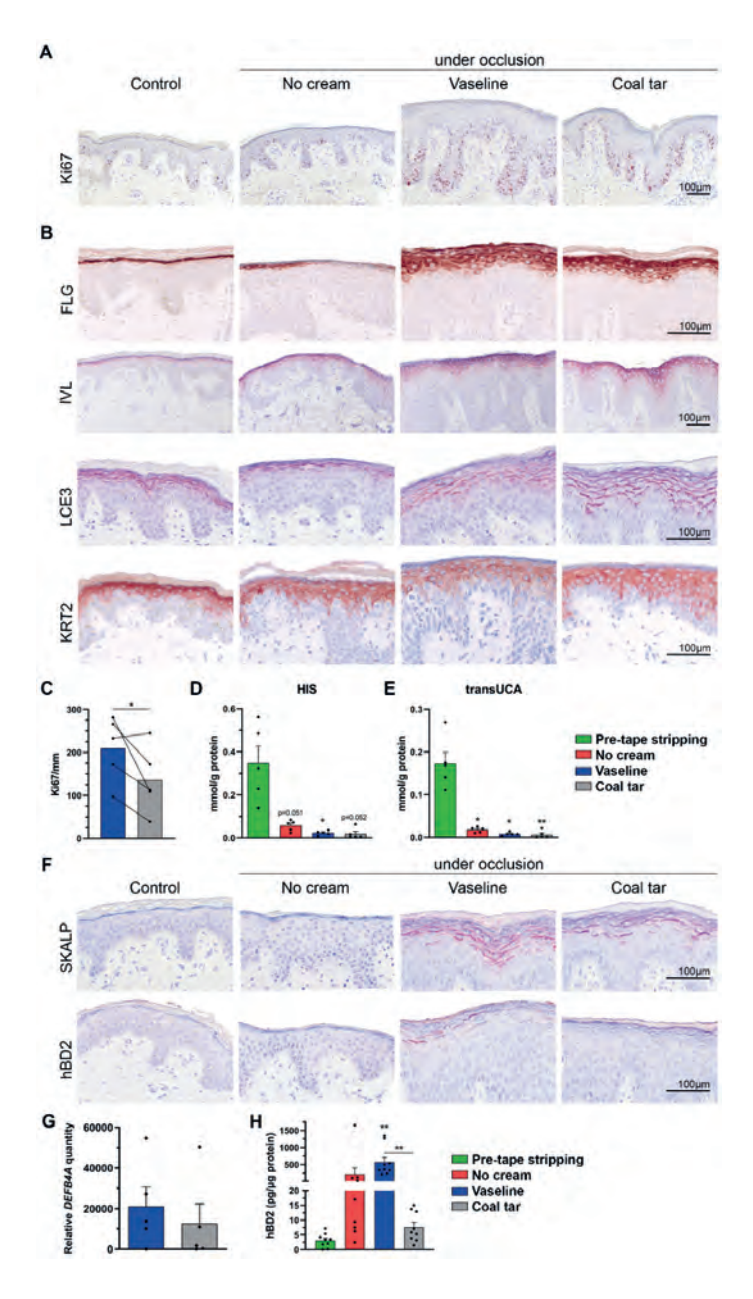


Figure 3. Coal tar and vaseline induce keratinocyte proliferation and differentiation following tape stripping. **A)** Ki67 immunostaining, and **B)** FLG, IVL, and LCE3 immunostaining of biopsies from volunteers treated after tape stripping. **C)** Quantification of Ki67 positive nuclei. Lines indicate paired measurements within the same volunteer. **D-E)** NMF (histidine (HIS) and trans-UCA) measurements in tapes after 4 days of treatment. NMF values are normalized for total protein concentration per sample. **F)** SKALP and hBD2 immunostaining. **G-H)** *DEFB4* (hBD2) mRNA expression and protein quantity analyzed by qPCR and ELISA, respectively.

Given the dermal infiltration of innate and adaptive immune cells, a process likely initiated by antigen presentation of tissue-resident antigen presenting cells (APCs) such as Langerhans cells could be involved. Normally, Langerhans cells (marked by CD1a expression) are constrained to the epidermis (Figure 4E, control). In vehicletreated inflamed skin, Langerhans cells mostly localized in the dermis, indicative of their activation and migration (Figure 4E, vehicle). Interestingly, the localization and number of Langerhans cells in coal tar treated skin was similar to control skin and tape-stripped skin without inflammation (Figure 4E, coal tar). Hence, the anti-inflammatory effects of coal tar may be orchestrated by inhibition of antigen presentation and T-cell recruitment in the early events that initiate skin inflammation.

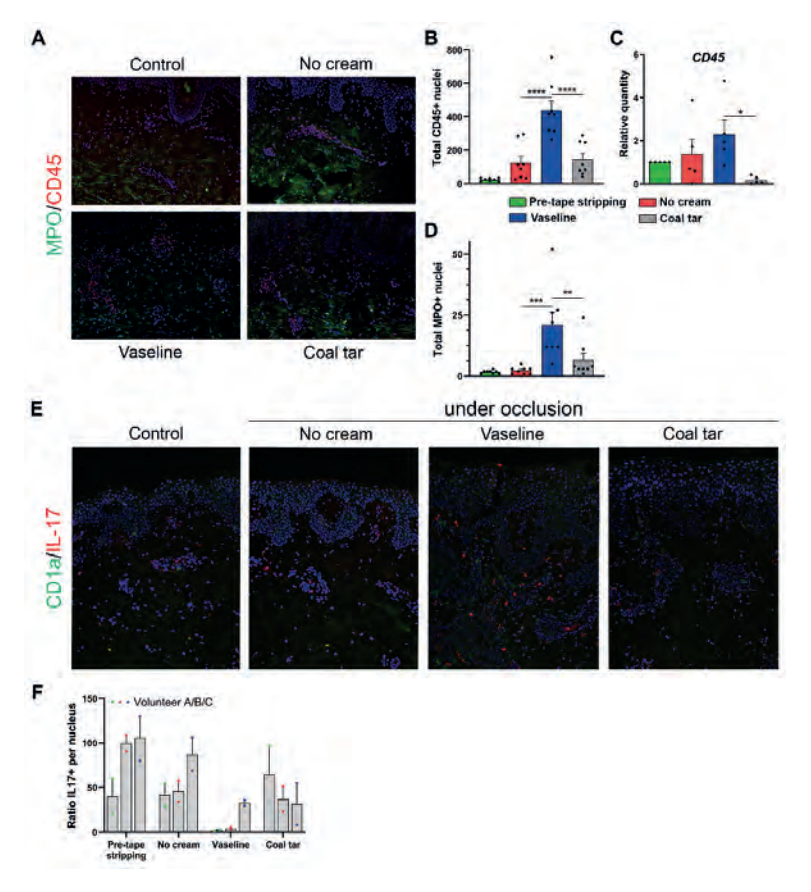


Figure 4. Coal tar hampers immune cell trafficking in skin. A) Characterization of immune cell infiltrate by immunofluorescence staining for MPO and CD45 on skin biopsies from volunteers treated after tape stripping. B) Quantification of CD45 immunofluorescent staining C). Relative CD45 mRNA expression in epidermis. D) Quantification of MPO immunofluorescent staining. Quantifications are an average of representative donors (N=3) E) Immunofluorescent staining of CD1a and IL-17 expression. F) Ratio of IL-17 positive cells.

Discussion

In this study, we investigated the ability of coal tar to prime skin for faster barrier function recovery after superficial skin wounding. However, no beneficial prophylactic effects were seen from coal tar treatment when treating healthy skin before the skin barrier is damaged. On the contrary, rather detrimental effects on epidermal biology were observed. We also explored the use of coal tar during the first days of skin barrier repair upon superficial injury of healthy skin. Whilst no beneficial effects on skin barrier parameters were observed, neither by coal tar nor vehicle cream, our study permitted investigations into the anti-inflammatory effects by coal tar due to the unexpected acute dermatitis caused by the combination of tape stripping followed by repeated application of vaseline lanette cream (vehicle) under occlusion.

Vaseline lanette is often described as an inert cream, however the recipe of the cream used in this study comprised sodium lauryl sulfate (SLS) and polyethylene glycol (PEG). SLS is a known irritant, whilst PEG is classified as a skin sensitizer [411]. Both have likely contributed to the acute (allergic or irritant) contact dermatitis that we observed in tape stripped skin. We postulate that the removal of the *stratum corneum* by the tape stripping procedure resulted in direct exposure of keratinocytes to SLS and PEG, and the prolonged exposure period (four days) under occlusion presumably have led to the observed inflammation. This inflammation was not observed in the prophylactic setting where creams were applied on intact skin, whilst being occluded and repetitively exposed. Hence, the presence of the intact *stratum corneum* and sufficient barrier function prevented the elicitation of inflammation by vaseline lanette cream.

In contrast, the AHR activating molecules in coal tar were able to penetrate the intact *stratum corneum* of healthy skin, activating keratinocytes in the basal layers and increasing their proliferation rates. This keratinocyte hyperproliferation was accompanied by elevation in other epidermal protein markers often seen elevated in hyperproliferative conditions, like psoriasis [295, 412]. Persistent activation of the AHR in healthy human skin, for example by the potent AHR activator 2,3,7,8-tetrachlorodibenzo-p-dioxin (TCDD), is known to cause persisting chloracne, which is amongst others characterized by keratinocyte hyperproliferation and follicular plugging [330]. Similarly, AHR activation by air pollution is linked to dermatitis-like skin conditions [150]. Also *in vitro*, AHR signaling appears required for keratinocyte proliferation [124]. Although coal tar is more readily metabolized as compared to TCDD, these transient effects of keratinocyte hyperproliferation can be causally linked to AHR signaling and as we now observe also to skin barrier defects [76]. Hence, under

physiological conditions, AHR ligands can finetune the balance between epidermal proliferation and differentiation and thereby steer epidermal regeneration and maintenance. Disturbances in AHR ligand availability and signaling activation, being too much or too little have been earlier described as the Janus-faced roles of AHR activation in skin and may interfere with epidermal homeostasis [122]. Hence, both the hero and villain aspects of AHR activation require further investigation when considering the AHR as a therapeutic target for the treatment of skin diseases.

Next to our focus on AHR activation in keratinocytes, we broadened our scope to tissue resident and infiltrating immune cells. Skin-resident immune cells, such as Langerhans cells, play an important role in the presentation of antigens to the immune system [413]. We found increasing numbers of Langerhans cells in the dermis of vehicle treated inflamed skin sites indicating the Langerhans cell migration typically seen in irritant and allergic contact dermatitis. Interestingly, this dermal migration was not observed in no cream or coal tar treated sites. This could be due to activation of AHR in Langerhans cells, considering that Langerhans cell specific ablation of AHR results in an elevated Th-2 and regulatory T-cell response [199]. In addition, tryptophan metabolites which activate the AHR in Langerhans cells negatively regulate their activation and in turn dampen the inflammatory response in the skin [414, 415]. Alternatively, activating cues from keratinocytes to Langerhans cells may be suppressed by activated AHR signaling in keratinocytes [179]. Considering the study design, we were unable to pinpoint the key events and target cells as only biopsies were taken after four days and the inflammation had already flared.

We and others previously reported the induction of epidermal barrier genes such as filaggrin by coal tar [75]. In this study we again observed an increased expression of barrier genes such as filaggrin in sites treated with coal tar. However, this was not accompanied by an improved barrier function as measured by TEWL, water content, erythema or NMF levels. Of note, skin sites only under occlusion also did not recover to baseline levels within the four-day period. Indeed, multiple studies have shown barrier defects due to occlusion from the skin, for example increased TEWL after wearing fire fighters' clothes or after occlusion with emollients [416, 417]. As seen per biopsy morphology, stratum corneum was not fully developed four days post- tape stripping likely preventing the skin barrier function to return to baseline levels. Hence, longer follow-up periods should be considered in future studies to evaluate skin barrier recovery interventions.

In conclusion, we demonstrate differential effects of coal tar when either applied to an intact or disrupted stratum corneum indicating that AHR targeted intervention in dermatology should be carefully balanced and monitored to not tip the balance towards aggravating epidermal defects. Our study also highlights the effects of AHR activation on inhibition of Langerhans cell migration that coincided with lower immune cell infiltration which may hint towards effectiveness of AHR targeting therapeutics in other forms of dermatitis next to the currently indicated AD and psoriasis.

Methods

Inclusion of volunteers

Both male and female healthy human volunteers between age 20-26 were included for this study. Healthy is defined as not having visible inflammatory skin disease or a history of psoriasis or AD. Volunteers were excluded if having known hypersensitivity to coal tar cream or using any other emollients or corticosteroids. Volunteers were provided with oral and written information before the start of the research and individual informed consent was obtained. This study was approved by the local medical ethical committee (Commissie Mensgebonden Onderzoek Arnhem-Nijmegen). The study was performed according to the Declaration of Helsinki principles.

Treatment schedule

The lower back of participants was first measured for erythema, TEWL and water content (see biophysical measurements). Three skin areas were completely tape stripped until the skin was glistening. The first ten tape strips were stored for NMF and protein analysis. Before or after tape stripping, participants were asked to apply coal tar cream (5% pix lithanthracis in vaseline lanette) and vehicle cream vaseline lanette to different designated areas twice daily and leave one area untreated. Each area was occluded with a Tegaderm plaster. At set time points, biophysical measurements (TEWL, erythema and water content), biopsies and tape strips were taken (see Figure 1A, 2A for a schematic representation) prior and after treatment.

Biophysical measurements

Measurements of the three noninvasive parameters (erythema, TEWL, water content) were performed using previously published protocols [418]. The skin was acclimatized to the ambient air for at least 15 minutes prior to measurements. Room temperature and air humidity were kept as constant as possible (17.6-25.0°C and 31.2-56.9% respectively). Volunteers were laid down in supine position during acclimatization period and measurements to prevent possible orthostatic interactions. First, erythema was measured with a portable spectrophotometer (CM-2600d/2500d, Konica Minolta, USA). Before each measuring session, calibration to

a standard white plate provided with the meter was performed. After pressing the calibration button, three calibration measurements were automatically taken. Then, three measurements per measurement location were taken; the device was lifted and gently reapplied between each recording. The average of the three consecutive erythema measurements was automatically calculated by the device. Next, TEWL was measured with the Aquaflux (AF200, Biox, UK). After calibration, three measurements per location were performed with standard settings and a maximum measurement time of 200s. The average of the three measurements per location was calculated. Thirdly, water content was determined by performing one measurement per location with the Epsilon (E100, Biox, UK). The Burst mode option was used with a 5s measurement delay after first skin contact to rule out initial variation in skin occlusion. A frame interval of 1s and a total measurement window of 30s was selected.

Histology and immunohistochemistry

Half a 4 mm biopsy was processed for histology and fixed in 4% formalin for 4 hours and paraffin embedded according to routine histology procedure. Sections of 6 µm were deparaffinized and stained using hematoxylin and eosin (Sigma-Aldrich). Immunohistochemical analysis was performed using indirect immunoperoxidase technique and avidin-biotin complex. Used antibodies are listed in Supplemental Table S1.

Immunofluorescent staining and quantification

Immunofluorescent staining was performed using Alexa Fluor 594-Fab and 488-Fab secondary antibodies targeting primary antibodies of interest and mounted using Fluoromount-G. Used antibodies are listed in Supplemental Table S1. High resolution images were acquired using a ZEISS Axio Imager equipped with a ZEISS Axiocam 105 color Digital Camera and a 40x objective. Quantification of number of positive cells was performed using Cell Profiler (analysis pipelines available upon request) and data was visualized as total number of positive cells using Graphpad Prism 10.0.

RNA extraction and qPCR

Half a 4mm biopsy was processed for RNA extraction and gPCR. To only obtain the epidermis, biopsies were pre-treated with dispase for 4 hours, after which the epidermis was placed in RNA lysis buffer. RNA was isolated using the Omega Biotek RNA extraction kit following manufacturer's protocol. RNA was first treated with DNAsel (Invitrogen) according to manufacturer's protocol. cDNA synthesis was performed using Ultrascript 2.0 (PCRBiosystems). RT-gPCR was performed using SYBR Green (Bio-Rad). Relative expression levels were next calculated using the ddCt method [246]and normalized using human acidic ribosomal phosphoprotein P0 (RPLP0). Primers sequences are listed below.

Gene symbol	Forward primer	Reverse primer
DEFB4A	gatgcctcttccaggtgttttt	ggatgacatatggctccactctt
CD45	gggaacaagcatcacaagagtaca	tgtttccgcactttctaagagattt
RPLP0	caccattgaaatcctgagtgatgt	tgaccagcccaaaggagaag

hBD2 ELISA

Protein samples were obtained from tape strips by needle sonication. To do so, tape strips were placed in a tube containing cold PBS/0.005% Tween with the adhesive side facing inwards. Tape strips were sonicated six times for ten seconds. After sonication, tape strips were removed from the tubes and protein concentration in the supernatant was determined using a micro BCA assay kit (Thermofisher Scientific), following manufacturer's protocol.

For the hBD2 ELISA, 96-wells plates were coated overnight at 4°C with goat-antihuman hBD2 (ABCAM) 1:500 in PBS. After, plates were washed twice with PBS and blocked with 1%BSA/1% normal goat serum (Vector laboratories) in PBS for 1 hour at 37°C. Afterwards plates were washed 4 times with PBS/0.05% Tween20. Next, samples and standard dilutions were incubated on the plate for 1 hour at 37°C. Plate was washed again for 4 times with PBS/0.05% Tween20. Plates were incubated with rabbit-anti hBD2 M47 (1:1000) for 1 hour at 37°C and afterwards washed 4 times with PBS/0.05% Tween20. Goat anti-rabbit biotinylated antibody (1:500, Vector laboratories) was added and incubated for 30 minutes at 37°C and afterwards washed with PBS/0.05% Tween20 4 times. Avidine-biotine complex was added (1:250, Vector laboratories), incubated for 30 minutes at 37°C and washed 4 times with PBS/0.05% Tween20. Next, TMB substrate (Thermo Scientific) was added and reaction was stopped using H2SO4. hBD2 concentration was determined using a plate reader (Biorad) at 450nm. Antibody details are provided in Supplemental Table S1.

Supplemental Table

NMF analysis

NMFs were extracted from tape strips by placing the strips in a cryo-vial with the adhesive side facing inwards. Ultrapure water was added so that the entire strip was in contact with water and vortexed for 15 minutes. Water with NMF is then transferred to a new tube and the procedure is repeated one more time. NMF content was measured as previously described [421] and NMF abundance was corrected for by total protein content. Visualization of data was performed using GraphPad prism 10.0.

Supplemental Table S1. Antibodies used in this study

Antigen	Species	Dilution	Company	Catalog number
FLG	Mouse	1:100	Thermo Fisher	MA5-13440
IVL	Mouse	1:20	Mon 150	Own antibody [204]
CYP1A1	Mouse	1:25	Santa Cruz	Sc-25304
LCE3	Mouse	1:5000	Abmart	Own antibody [419]
Ki67	Rabbit	1:200	Abcam	Ab16667
SKALP	Rabbit	1:4000	Own antibody	Own antibody [420]
KRT2	Mouse	1:200	Progen	65191
hBD2	Goat	1:200	Abcam	Ab9871
MPO	Rabbit	1:400	Dako	MAB3174
CD45	Mouse	1:50	Dako	M0701
CD1a	Mouse	1:50	Dako	M3571
IL-17	Goat	1:50	R&D	AF 317 NA
Goat anti-rabbit	Goat	1:200	Vector laboratories	BA-1000
Horse anti-mouse	Horse	1:200	Vector laboratories	BA-2000
Donkey anti-goat Fab594	Donkey	1:200	Invitrogen	A11058
Donkey anti-mouse Fab488	Donkey	1:200	Abcam	Ab150105

Statistics

Statistical analysis was performed using GraphPad Prism 10.0 on N=8 or N=3 volunteers. To determine whether changes in gene expression or cell number were significant, paired one-way analysis of variance (ANOVA) was performed followed by post hoc testing using Tukey's multiple comparison.



Chapter 8

English summary

In the introduction of this thesis (Chapter 1), the skin and its important role as a barrier organ were introduced. In brief, the skin barrier is made up of four components, namely the physical, chemical, immunological, and microbiological barrier. In inflammatory skin diseases, such as atopic dermatitis (AD) and psoriasis (PS), the skin barrier is affected by aberrant keratinocyte differentiation, an inflammatory response and a disbalanced microbiome of the skin. Treatment of inflammatory skin diseases ranges from applying topical emollients and corticosteroids on the skin to systemic treatment with general and targeted antiinflammatory drugs. One of the oldest treatments of inflammatory skin diseases is coal tar, which was found to have its therapeutic effect through activation of the aryl hydrocarbon receptor (AHR). Although the AHR was first discovered as an environmental sensor of xenobiotics, the AHR is able to bind a wide variety of both exogenous and endogenous ligands and functions as a gene regulatory transcription factor. The AHR acts through several pathways, described as either the canonical signaling pathway with its binding partner aryl hydrocarbon nuclear translocator (ARNT), and the non-canonical signaling pathway with other binding partners. The AHR was found to influence many processes in the skin, having an effect on keratinocyte proliferation and differentiation as well as influencing the skin barrier function. Additionally, the AHR controls the inflammatory response of the skin, making it a suitable target in the treatment of inflammatory skin diseases. In this thesis, the physiological effects of the AHR in skin barrier formation and maintenance were investigated as well as the potential of novel AHR-targeting therapeutics for alleviating inflammatory skin diseases.

In Chapter 2 and 3 we investigated two novel groups of AHR-binding compounds for their potential in the treatment of AD. In Chapter 2, a group of selective modulators of AHR activation called 'SGA derivatives' were investigated. A wide variety of SGA derivates were first screened for their potential to activate the AHR. This led to the identification of several derivatives with varying potential to activate the AHR. The strongest AHR activators were first tested in mouse and human primary keratinocyte cell lines. In both species, the selected derivatives were able to activate the AHR, whilst being non-toxic to the cells. In monolayer cell cultures, expression of keratinocyte differentiation genes such as hornerin and filaggrin was induced in an AHR-dependent manner. In 3D human epidermal equivalents, similar effects were seen in terms of inducing keratinocyte differentiation. To investigate the therapeutic potential of these derivatives to treat AD, AD-like 3D human epidermal equivalents were treated with these SGA derivatives. RNA sequencing was performed to provide an overview of the biological effects that were induced by these compounds. Here, clusters of genes were found that showed the potential

of SGA derivatives to induce keratinocyte differentiation and reduce keratinocyte proliferation together with dampening of the inflammatory response. These effects were verified on protein level in 3D human epidermal equivalents. Lastly, the antiinflammatory effects were investigated in an in vivo mouse model. SGA derivatives were able to prevent acute dermatitis-related epidermal thickness, erythema, and neutrophilic infiltration. Taken together, these results show a promising potential for SGA derivatives for topical treatment of inflammatory skin diseases.

In Chapter 3 another group of compounds, carboxamide derivatives, were investigated for their potential to activate the AHR and to treat AD-like features in in vitro models. Similarly to the SGA compounds, carboxamide derivatives were first screened for their potential to activate the AHR, leading to the selection of several carboxamides with high activating potential, whilst not influencing the cell viability. In 3D human epidermal equivalents, addition of carboxamides induced keratinocyte differentiation, both on a gene and protein level. In AD-like human epidermal equivalents, the carboxamides showed the potential to restore epidermal differentiation. This indicates that a variety of AHR activating compounds can be developed as novel therapeutics in the treatment of inflammatory skin diseases.

As highlighted in the introduction, the AHR can bind a wide variety of ligands and signals through different pathways. To understand the physiological role of AHR in our skin and rule out other activated pathways by ligands, suitable models are essential. Therefore, we aimed to develop a keratinocyte cell line without functional AHR by CRISPR/Cas9 genome editing. While keratinocytes are notoriously difficult to genetically modify, we demonstrated the proof of principle of CRISPR/Cas9-based editing in the immortalized N/TERT-2G keratinocyte cell line (Chapter 4). Here, filaggrin (FLG), a key component of the skin barrier and risk gene for developing AD, was knocked out using CRISPR/Cas9 methodology. Guide RNAs targeting exon 3 were developed and transfected into N/TERT-2G cells. Clonal cell lines were investigated for their loss of FLG on a genetic level. From selected clonal knock out cell lines, 3D human epidermal equivalents were generated, showing the loss of the granular layer associated with FLG mutations, as well as loss of FLG protein. Moreover, skin barrier function was affected, resulting in increased permeability of the FLG deficient human epidermal equivalents. To show that these effects were dependent on the introduced FLG mutation, FLG expression was restored in the knockout cell lines by reverting the mutation, using CRISPR/Cas9-mediated homology directed repair. This repaired defects on keratinocyte differentiation and the skin barrier. Using similar techniques, we generated an AHR knockout cell line to study specific effects of AHR deficiency in keratinocyte biology in further chapters.

To understand the mechanisms of AHR binding to the genome and its downstream functions, RNA- and ChIP-sequencing experiments were performed in Chapter 5. Keratinocytes stimulated with dioxin (TCDD) or coal tar showed similar changes in RNA expression, with distinct early and late response gene clusters being identified. Early response genes included processes of epithelium development and protein phosphorylation, whilst late response genes were involved in keratinocyte differentiation and epidermis development. To determine where AHR binds the enhancer landscape, ChIP-sequencing using AHR and H3K27ac antibodies was performed. This vielded genomic regions bound by AHR immediately after AHR activation and a distinct subset of active enhancer regions related to early AHR binding, while different regions related to secondary effects of AHR activation. This led us to hypothesize that AHR binds enhancer elements regulating other transcription factors which in turn regulate the expression of epidermal differentiation genes as a secondary event. Integrating both seguencing datasets led to the identification of Transcription Factor AP-2 alpha (TFAP2A), being bound by AHR and known for its role in epidermal differentiation. To validate that TFAP2A is indeed regulated by AHR, AHR knockout cell lines were generated as described in Chapter 4. Addition of TCDD to AHR knockout cell lines did not increase TFAP2A expression, in contrast to AHR wildtype cell lines. This indicated that TFAP2A is indeed regulated by AHR. Additionally, TFAP2A knockout cell lines were generated to demonstrate the involvement of the AHR-TFAP2A axis in epidermal differentiation. AHR responsive genes involved in epidermal differentiation were not upregulated to the same extent in TFAP2A knockout cell lines as compared to TFAP2A wildtype cell lines. TFAP2A knockout epidermal equivalents appeared underdeveloped showing aberrant epidermal differentiation. Where TCDD treatment in wildtype epidermal equivalents induces epidermal differentiation, treatment of TFAP2A knockout models showed only a minor increase in epidermal differentiation, again indicating that the AHR-TFAP2A axis is important for epidermal development and stratification.

In my thesis, I also aimed to understand the functional consequences of AHR signaling for the formation of the skin barrier. This called for quantitative measurement techniques to longitudinally follow development of the skin barrier without harming the organotypic epidermal models. In **Chapter 6**, we examined such a novel method, namely electrical impedance spectroscopy (EIS). Electrical impedance was measured non-invasive using a frequency sweep to follow barrier development in time, without harming cells and epidermal morphology. Our EIS measurements, combined with morphological and histological analyses, led to the identification of different parts of the impedance plots, where impedance at lower frequencies was associated with epidermal development and impedance at

higher frequencies was associated with stratum corneum thickness. We validated these findings using CRISPR-Cas9 modification of epidermal differentiation genes or regulators, like TFAP2A and AHR. We also investigated the potential of EIS to measure therapeutic effects of AHR agonists in combination with our IL-4-induced AD-like epidermal equivalent model. These models, mimicking AD pathology and demonstrated barrier defects, were treated with different AHR agonists, including the SGA derivatives and carboxamide compounds. While IL-4 reduced the skin barrier function and lowered the electrical impedance, all used AHR agonists were able to rescue this impairment. Altogether, these data show both the potential of AHR activating therapeutics as well as the ability of impedance measurements to monitor these effects in pre-clinical disease models.

The pre-clinical studies in my thesis demonstrated that AHR activation has therapeutic potential in reversing barrier defects in inflammatory skin diseases. These experiments included in vitro models or in vivo murine models. In Chapter 7, we aimed to translate our research to in vivo human skin and investigated the effects of coal tar application on skin barrier function in healthy human volunteers. To induce skin barrier defects, skin was tape stripped before or after application of coal tar or its vehicle cream. We were unable to demonstrate barrier function improvement in coal tar treated skin, potentially due to the short nature of treatment. In addition, the chosen vehicle cream inadvertently induced acute skin inflammation upon superficial wounding by the tape stripping procedure. However, this allowed us to demonstrate the anti-inflammatory effects of coal tar. The increased epidermal thickness and dermal infiltrate was significantly less pronounced in coal tar exposed skin. Both innate and adaptive immune cells were significantly less abundant in coal tar treated skin compared to vehicle treated skin and Langerhans cell migration was impaired by coal tar exposure, demonstrating the inhibitory effects of coal tar on these important immune cell-driven cascades in AD and psoriasis.

Finally, in Chapter 8, I integrate the findings of my empirical studies to final conclusions and provide a general discussion with future perspectives. I focus on the prospects for therapeutic developments of AHR ligands highlighting the diversity of ligands and their affinities, the cell specificity of AHR expression and the role for the tissue and cell microenvironment that influences the outcome of AHR signaling. To conclude, the research in my thesis sheds light onto the function of AHR in the human skin. I demonstrated that AHR signaling is important for keratinocyte proliferation, differentiation, skin barrier function and inflammatory processes and cell migration highlighting the therapeutic nature of AHR activation in chronic inflammatory skin diseases.



Chapter 9

Discussion and future perspectives

The many faces of AHR signaling: prospects for therapeutic developments

In my thesis I demonstrate the prospects of the AHR as a therapeutic target in the treatment of inflammatory skin diseases (chapters 2 and 3). The AHR was long regarded as a target to avoid in drug development pipelines due to being associated with carcinogenic effects. This was shown in several studies where activation of the AHR resulted the development of cancer, while blocking the AHR was shown therapeutic [87, 422, 423]. On the contrary, AHR activating ligands used in this thesis show promising therapeutic effects for the treatment of inflammatory skin diseases as AHR activation dampens the pro-inflammatory JAK/STAT-driven response to The cytokines and induces the expression of epidermal barrier proteins [75, 309]. Additionally, AHR-activating coal tar has long been used to treat inflammatory skin diseases, without increased risk of any cancer type development [78]. This indicates the contradiction in downstream effects of AHR activation and the need to thoroughly investigate the cell- and tissue-specific effects of AHR activation by diverse ligands in order to unleash their therapeutic potential. Herein, the ligand binding affinity, cell specificity and the local milieu in which binding occurs should be taken into consideration.

One explanation for the variety in effects could be found in the **diversity of ligands** that have affinity for binding the AHR. Ligands originating from environmental pollution, such as TCDD and PAHs, are associated with negative effects after activating the AHR. TCDD was shown to be the causative agent in the development of chloracne, whilst PAHs from air pollution have been associated with the development of several types of cancer [330, 424]. TCDD is not metabolized and thus having a long half-life plus being a high affinity AHR ligand. This results in prolonged, unregulated constitutive activation of the AHR [425]. PAHs are metabolized upon AHR activation by phase I cytochrome p450 metabolism. Several of the formed metabolites are mutagenic and associated with the development of cancer [426]. On the other hand, therapeutic molecules induce a transient activation of the receptor, followed by a negative feedback loop due to induction of repressor proteins which may account for the positive effects in the treatment of several diseases [427]. Transient activation is more similar to physiological conditions in which AHR activation by endogenous ligands is fast and tightly regulated by its own negative feedback loop [428]. For the development of potential new therapeutics, it is therefore important to understand the ligand's affinity for the AHR. The differences in affinity are caused by structure of the ligands and the structure of the binding pocket in the AHR. Recently, the crystal structure of human AHR was uncovered and provided insights in the ligand

binding [117], allowing future investigation into the differences in binding between therapeutic compounds, such as the SAhRMs and carboxamides (chapters 2 and 3), and carcinogenic compounds such as TCDD and PAHs as a possible explanation in their differential effects

Additionally, effects of AHR might be **cell specific**. In my thesis, this is investigated using in vitro cell culture models or in vivo studies using mice or human volunteers. In vivo, the skin harbors multiple cell types, including but not limited to keratinocytes, fibroblasts, endothelial cells and a wide variety of immune cells. Understanding how the activation of AHR affects each cell type will provide valuable insight in addition to the overall effects of AHR activation in the tissue. While we choose for formalin fixation and paraffin embedding of biopsies, next to bulk RNA isolation, the effects on different cell types may be better dissected using single-cell analysis techniques, such as single cell RNA- or ATAC- sequencing, single cell spatial transcriptomics or mass spectrometry. Alternatively, single cell mass cytometry (e.g, Cytof) could still be explored on the samples we harvested. Thereby, hypothetically, the cellspecific effects can be correlated to physiological state of that cell, including ligand metabolite levels and AHR expression, downstream gene expression (i.e., CYP1A1), or expression of its negative feedback mechanism (through AHRR). While our in vitro model consists of keratinocytes only, these cells are actually in different stages of differentiation and their gene expression profile changes as they progress through different layers of the epidermis. We studied the effect on different layers of the epidermis through immunohistochemical staining of protein expression. This visualizes tissue morphology, protein localization, and protein quantity in the skin in order to determine the effect of AHR activation. However, this only shows the final result of changes in AHR activation status. Underlying mechanisms, driven by gene expression, could not be studied in this way. Recently, novel techniques that employ fluorescent probes to target RNA molecules on skin tissue sections were developed [429]. This single cell transcriptomics methodology could be employed on our epidermal models, to investigate changes in gene expression levels related to the spatial position of the cells in the epidermis. Additionally, novel computational models are continuously developed to predict gene interactions and signaling pathways. Inferring gene expression data, for example from cells stimulated with AHR agonists, can predict binding partners and downstream effects based on preexisting knowledge of the signaling pathways [430]. In my thesis, all investigations into the effects of AHR activation on gene expression were performed in bulk, where effects on separate cells, cell types and their specific milieu are less well distinguished. Novel techniques such as single-cell transcriptions, metabolomics and proteomics are developing at a rapid pace and are already used to investigate expression profiles for single cells and cell types in the skin [431-433]. For future *in vivo* and *in vivo* studies, single-cell analyses will provide insight into differential effects of AHR activation in cells, depending on their cellular context and which cell types are affected most by AHR targeting. The differences in expression level of AHR in the *strata* or cell types of the skin may already provide us with clues. In the *stratum spinosum* and *stratum granulosum* the AHR expression is higher than in the *stratum basale* or *stratum corneum*. Additionally, expression of AHR is higher in keratinocytes and melanocytes, but virtually absent in fibroblasts (based on data from the Human Protein Atlas) [121]. This indicates that the addition of AHR agonists may have a cell-specific effect based on their expression of AHR.

Lastly, effects of AHR are dependent on the microenvironment in which cells reside when activated. This was also shown in our in vivo study (chapter 7), where treatment of healthy skin using topical coal tar application led to an induction of proliferation. This contrasts with effects of agonists in skin affected by an inflammatory cue, as AHR activation reduces keratinocyte hyperproliferation in that context (as shown in chapter 2). This has important implications for treatment of patients, as only local, topical application of affected skin is necessary to achieve therapeutic effects, and application to healthy skin could enhance inflammation. Additionally, systemic effects need to be studied further even if creams are applied locally. Compounds can permeate through the skin and have additional effects elsewhere in the body. Considering that the AHR is expressed in a large number of organs and cells from the immune system, activating compounds could have effects elsewhere in the body that require monitoring. While the use of the AHR agonist coal tar has no negative side effects after long term use [78], this does not rule out adverse effects by other AHR agonists. The complex nature of coal tar, including potentially receptor antagonists, may yield a different response to creams with only pure AHR agonists. Besides the potential of the AHR to be employed as a therapeutic target, I also aimed to further understand the physiological role of the AHR in our skin, specifically in the formation and maintenance of the skin barrier. In my thesis, I developed and applied a technique to measure epidermal barrier function in in vitro epidermal models by electrical impedance spectroscopy (EIS). This system was implemented to investigate the effects of AHR deficiency on the skin barrier, as well as the effect of AHR activation. The importance of AHR in skin development was demonstrated in chapter 6. Knockout of the AHR in the immortalized human keratinocyte cell line N/TERT-2G showed impaired barrier function in our in vitro models. This can be explained through impaired expression of differentiation genes and therefore a defect in keratinocyte differentiation and consequent formation of the skin barrier. Possibly, lack of endogenous AHR signaling leads to changes in lipid composition and formation of the stratum corneum. These in vitro experiments with AHR knockout cells prove the importance of AHR in formation of the epidermal skin barrier, as previously demonstrated by AHR antagonists which hamper epidermal development [76]. While Ahr knockout mice do not show a severe skin phenotype, the barrier function appears affected as seen from the elevated transepidermal water loss due to impaired keratinocyte intercellular connectivity and changed expression of barrier-associated genes [141]. This is in accordance with our results seen in human AHR knockout cell lines. The benefits of using knockout cell lines over treatment with receptor antagonists, is the potential non-selective nature of antagonists affecting other pathways. Also, our knockout epidermal models allow for investigation of the absence of AHR on the development of the skin barrier in early stages, whereas addition of antagonists in these early stages is often harmful or even lethal to the developing epidermis. The knockout model is therefore more similar to in vivo mice models, where Ahr knockout mice are able to form an epidermis, albeit with hampered skin barrier.

Additionally, we showed that the addition of AHR ligands can reverse barrier defects that are induced by inflammatory cues. In atopic dermatitis-mimicking models, the skin barrier was shown to be impaired. Addition of a variety of AHR ligands, including coal tar, SAhRMs and carboxamides used in this thesis, were able to enhance the skin barrier through increasing expression of keratinocyte differentiation genes and perhaps lipid composition [434], although the latter was not studied in this thesis. The anti-inflammatory effects and enhancement of keratinocyte differentiation were shown in previous studies using partial AHR agonists [435, 436]. We have come to learn that activation of the AHR can have a positive effect on restoring deregulated epidermal differentiation, proliferation and inflammation. The mechanism behind these effects is starting to be unraveled, as more binding partners (such as stimulator of interferon response cGAMP interactor 1 (STING1) [437], the estrogen receptor (ER) [438] and circadian clock proteins [439]) and the target genes that are bound by the AHR (e.g., TFAP2A in chapter 5) are discovered. Future studies on patients treated with AHR agonists will shed further light on the intricate signaling cascades in which the AHR is involved.

The recent FDA approved topical AHR agonist cream Tapinarof (VTAMA) will play a key role in these discoveries. Tapinarof is now approved for the treatment of psoriasis and atopic dermatitis for adults and children over 2 years [440], sparking major interest by dermatologists and the pharmaceutical industry. Follow up clinical studies investigating the effects of Tapinarof treatment will now emerge soon with phase 3 trials being finalized [441-443]. Since AHR activating therapeutics have such a strong barrier restoring effect, this could imply that patients with severe barrier effects could benefit significantly from treatment with AHR agonists. Since skin barrier function can easily be measured in a non-invasive way, by measuring transepidermal water loss or water content of the skin, this provides possibilities to study the differential effects of AHR agonist treatment in different disease severity stages and degrees of skin barrier defects. Patients most likely to benefit from this treatment could easily be pre-selected using aforementioned non-invasive methods in daily clinical practice.

Experimental models to investigate AHR function in skin

For future research into the mechanism underlying therapeutic effects of AHR activation and its physiological role in the skin barrier, faithful models are essential. Whilst animal models (mice) provide a physiological complete model, their skin is different from human skin and ethical issues with animal use are becoming more prominent nowadays. On the other hand, research using human volunteers is time consuming, also limited by ethical considerations, and the number of tissue samples that can be obtained. We also experienced these culprits in our in vivo study (chapter 7), where only a few biopsies per volunteer could be taken which limited our analyses, and predicting the optimal time point for biological sampling proved difficult and suboptimal. In vitro human skin models that faithfully mimic disease states could overcome these limitations. In most of our studies, we used an organotypic human in vitro epidermis model based on the culture of solely keratinocytes on a plastic filter. Exposure of these keratinocytes to air in combination with specific media supplements, leads to differentiation of these cells into a mature epidermis, containing all layers of the epidermis including a stratum corneum. While only modeling the upper layer of skin, it has the advantage that keratinocyte-specific effects can be studied separately from other cell types. These models are relatively simple to culture in a short amount of time (<2 weeks), making them useful for manipulation by for example addition of cytokine mixtures or therapeutics, or utilizing genome editing techniques for gene function analysis.

In chapter 5 and 6 of this thesis we aimed to develop a model to dissect AHRdependent cellular functions. This research was enabled by previous work of our department on the characterization of the immortalized N/TERT cell line and creating methodologies for knocking out genes by CRISPR/Cas9, as shown in chapter 4. Although all protocols appeared operational, such genome editing studies are difficult to perform in keratinocytes and creating a viable clonal cell line knockout for AHR was tedious, possibly due to the role of AHR in keratinocyte proliferation. This made clonal expansion challenging, as AHR proficient cells quickly overgrew AHR-KO cells. Eventually "only" one validated keratinocyte knock out line could be generated. For these cells it is important to realize that compensatory mechanisms may have occurred to compensate for the loss in AHRdriven proliferation. This may possibly affect other processes in these cells and therefore complementary studies with AHR antagonists, or developing rescue experiments to convert the knockout cells back to wildtype (using homology directed repair (like in **chapter 4**) are necessary to uncover effects that are solely based on lack of AHR

As discussed in my introduction, the AHR affects gene expression both through canonical signaling with ARNT and non-canonical signaling with other binding partners. CRISPR/Cas9-mediated knockout of ARNT would provide a model for differentiating between canonical signaling and non-canonical signaling. Investigating solely non-canonical signaling would help distinguish the different effects of AHR signaling and provide a basis for research into the mechanism behind therapeutic AHR signaling. Although our current epidermal models provide an important gateway into research of human skin, several elements are still lacking that are found in *in vivo* human skin. These elements include a physiological stratum corneum with shedding ability, an immune cell compartment and microbiota.

Modelling physiological stratum corneum cornification and desquamation

One lacking factor in our in vitro models is a shedding stratum corneum, a process called desquamation. The stratum corneum is the most outer layer of our skin and has an essential role in the skin barrier. It consists of dead corneocytes that are shed regularly in vivo. Research into stratum corneum formation is important. as the AHR was shown to have a role in the development of the stratum corneum and its composition [76]. In this thesis, knockout of the AHR was already shown to impact the skin barrier function by reduced epidermal differentiation and electrical impedance values (Chapter 6). Recently, a role for the AHR in ceramide synthesis has been discovered. Ceramides are lipids present between cells in the stratum corneum and have an important role in the skin barrier and water retention in the skin. Activation of the AHR induced expression of the ceramide metabolizing enzyme uridine diphosphate glucose ceramide glucosyltransferase (UGCG) and increased levels of ceramides in the skin [434]. Since AHR has a regulatory role in stratum corneum formation and maintenance, models with physiological stratum corneum that can be studied separately are vital. Herein, cell culture conditions are important to consider. 3D skin models are cultured in incubators, at which cells are kept at 37°C with high relative humidity. However, stratum corneum naturally resides in a colder (32°C) and dryer environment. Higher temperatures and humidity might have an effect on processes in the cell that are involved in the formation of the epidermis and specifically the outermost layer, the stratum corneum. Although, higher humidity and temperature do not appear to affect the lipid composition of the stratum corneum, epidermal thickness and differentiation rate of the models [444, 445] which may influence the study outcome.

Another difference with the in vivo situation is that in vitro stratum corneum is not regularly shed since no mechanical abrasion occurs in the cell culture. Shedding can potentially be modeled by tape stripping, removing several layers of stratum corneum by cellotape. This could also provide a model for investigating breaches and repairing mechanisms of the skin barrier in model systems. However, tape stripping in vitro is difficult due to the delicate nature of the models. We attempted creating a tape stripping model using our 3D human epidermal model, both for modelling of our in vivo coal tar study findings as well as study the role of the stratum corneum in electrical resistance in our EIS study (chapter 7 and 6, respectively). Nevertheless, we found that tape stripping creates mechanical friction, causing stress on the cells in the viable epidermis or even complete rupture of the tissue. The lower strength of the basement membrane that holds the epidermis in place, aberrant crosslinking or enzyme activity involved in the desquamation process may be causal factors. Further refinement of the tape stripping method or epidermal modeling itself is therefore needed. Also more subtle removal of the stratum corneum (e.g. by chemical peeling) could prevent the mechanical stress and cytotoxicity of the epidermal cells. Alternatively, ex vivo models of surplus skin from plastic surgery may be used having a native stratum corneum that can be removed using conventional tape stripping methods allowing investigations into the repair mechanisms ex vivo [446] and studies on the therapeutic nature of in our case AHR agonists.

Addition of an immune cell compartment

In vivo human skin is a complex tissue and often multiple factors play a role in the development and maintenance of skin diseases. In inflammatory skin diseases, immune cells are important disease drivers and are target cells for treatment, i.e. through biologics. The models used throughout my thesis lack immune cells that

are important to skin homeostasis, such as cells from the innate immune system as well as tissue resident immune cells such as Langerhans cells or tissue resident T-cells. In these immune cells, the AHR plays a key role in their development, maturation and plasticity [447, 448]. The importance for immunocompetent models is illustrated by our in vivo study on the anti-inflammatory role of the AHR (chapter 7). We were able to demonstrate the anti-inflammatory regulation by coal tar-mediated AHR activation, however the pilot nature of the study setup and limited biopsy material hampered important additional analyses. Also herein, ex vivo skin models may be good alternatives. Techniques such as tape stripping and topical application of creams are possible on ex vivo skin, yet the availability of donor material is rather limited and highly dependent on optimal logistics with nearby plastic surgery clinics. Also, for more extended experiments, large pieces of skin have to be available. Additionally, while providing presence of certain immune cells, such as Langerhans cells in the epidermis and dermal immune cells at time of biopsy, influx of immune cells from the circulation cannot be studied herein. Solving these issues, research is ongoing to develop the much-needed immunocompetent in vitro skin models allowing the migration of T-cells, or dendritic cells [410, 449, 450] and bioprinting techniques that enable precise spatial reconstruction are developing at a fast pace [391, 451]. These future immunocompetent models could provide a foundation to investigate the treatment of inflammatory skin diseases and incorporating specific patient characteristics, allowing for research into the effects of AHR activation on the skin and immune component simultaneously in a biologically relevant setting.

A role for the microbiome through AHR signaling

Microbes play an important role in our skin barrier, such as preventing colonization of pathogenic microbes. Microbial metabolites from commensals in our gut were already shown to activate AHR signaling in gut epithelial cells and resident immune cells. These metabolites were identified as tryptophan metabolites [452]. Recently, skin commensals were shown to produce similar tryptophan metabolites that interact with the AHR and through AHR signaling affect the skin barrier [30]. Similarly, in germ-free mice the skin barrier is impaired but rescued by addition of AHR activating agonists, which upregulated genes involved in keratinocyte differentiation and enhanced skin barrier function [212]. Skin barrier function could also be restored by addition of human skin microbes that influence AHR signaling [212]. This underscores the importance of microbiome interaction with host AHR to establish the skin barrier, with microbial metabolites also being key to upregulate keratinocyte proteins

associated to antimicrobial host defense. Such auto-regulatory loop by microorganisms through host AHR signaling may be disturbed in many skin diseases [213]. Several inflammatory skin diseases, such as AD, are associated with dysbiosis in the skin microbiome but the causal relationship between the microbial dysbiosis, the diminished physiological AHR activation, impaired skin barrier and more severe disease phenotype has yet to be established. Recently, our group developed new models that allow culturing of microbes on the 3D human epidermal equivalents that I used in my thesis [453]. Merging these research efforts will fuel future research into the interaction mechanisms of our microbiota with host AHR, with possible dissecting of canonical (AHR/ARNT driven) and non-canonical signaling pathways (AHR/other). This could have an impact beyond the dermatology field, as not only in the skin our microbiome influences barrier function through AHR signaling. Gut homeostasis is regulated similarly where tryptophan metabolites produced by microbes are shown to have barrier promoting and anti-inflammatory effects. In intestinal bowel disease, tryptophan metabolite levels as well as AHR activity is known to be lowered in patient fecal samples [454]. This highlights that the anti-inflammatory effects of AHR activation are conserved in different organ systems and underscores the potential for AHR-activating therapeutics to treat a variety of inflammatory diseases. Effects of AHR activation in the gut also have the ability to influence processes in other sites of the body, such as the liver and the lung [454]. Dietary AHR ligands (e.g., broccoliderived indole-3-carbinol) where additionally shown to influence inflammatory processes in the skin [455], directing towards the potential for lifestyle interventions in clinical practice.

Concluding remarks

Taken together, the research in my thesis provides further insight into the function of AHR in the human skin. I demonstrated that AHR signaling is important for keratinocyte proliferation, differentiation, skin barrier function and inflammatory processes in the skin. My research highlights that AHR is an important therapeutic target in the treatment of inflammatory skin diseases and should not be feared for its association with toxicity and cancer development considering ligand- and microenvironment dependent outcomes. Future research to scrutinize AHR's ligand-dependent signaling and interplay with different signaling partners in different cell types will be aided by technological developments such as single-cell omics and genetic engineering approaches, combined with the important quantitative assessment of epidermal function and further refinement and complexification of in vitro skin models.



Chapter 10

References

- Fuchs, E., Epidermal differentiation: the bare essentials. J Cell Biol, 1990. 111(6 Pt 2): p. 2807-14.
- 2. Fuchs, E., Keratins and the skin. Annu Rev Cell Dev Biol, 1995. 11: p. 123-53.
- Freeman, S.C. and S. Sonthalia, Histology, Keratohyalin Granules, in StatPearls. 2022: Treasure 3. Island (FL).
- 4. Rogerson, C., D. Bergamaschi, and R.F.L. O'Shaughnessy, Uncovering mechanisms of nuclear degradation in keratinocytes: A paradigm for nuclear degradation in other tissues. Nucleus, 2018. 9(1): p. 56-64.
- 5. Matsui, T. and M. Amagai, Dissecting the formation, structure and barrier function of the stratum corneum. Int Immunol, 2015. 27(6): p. 269-80.
- Candi, E., R. Schmidt, and G. Melino, The cornified envelope: a model of cell death in the skin. Nat Rev Mol Cell Biol, 2005. 6(4): p. 328-40.
- Hoste, E., et al., Caspase-14 is required for filaggrin degradation to natural moisturizing factors in the skin. J Invest Dermatol, 2011. 131(11): p. 2233-41.
- Rawlings, A.V. and C.R. Harding, Moisturization and skin barrier function. Dermatol Ther, 2004. 17 Suppl 1: p. 43-8.
- Eckert, R.L., et al., AP1 transcription factors in epidermal differentiation and skin cancer. J Skin Cancer, 2013. 2013: p. 537028.
- 10. Deng, Z., et al., Grainyhead-like transcription factors: quardians of the skin barrier. Vet Dermatol, 2021. **32**(6): p. 553-e152.
- 11. Segre, J.A., C. Bauer, and E. Fuchs, Klf4 is a transcription factor required for establishing the barrier function of the skin. Nat Genet, 1999. 22(4): p. 356-60.
- 12. Furue, M., A. Hashimoto-Hachiya, and G. Tsuji, Aryl Hydrocarbon Receptor in Atopic Dermatitis and Psoriasis. Int J Mol Sci, 2019. 20(21).
- 13. Brandner, J.M., Importance of Tight Junctions in Relation to Skin Barrier Function. Curr Probl Dermatol, 2016. 49: p. 27-37.
- 14. Schmitt, T. and R.H.H. Neubert, State of the art in Stratum Corneum research: The biophysical properties of ceramides. Chem Phys Lipids, 2018. 216: p. 91-103.
- 15. Schroder, J.M. and J. Harder, Antimicrobial skin peptides and proteins. Cell Mol Life Sci, 2006. 63(4): p. 469-86.
- 16. Schauber, J. and R.L. Gallo, Antimicrobial peptides and the skin immune defense system. J Allergy Clin Immunol, 2008. 122(2): p. 261-6.
- 17. Herb, M., et al., Mitochondrial reactive oxygen species enable proinflammatory signaling through disulfide linkage of NEMO. Sci Signal, 2019. 12(568).
- 18. Naik, E. and V.M. Dixit, Mitochondrial reactive oxygen species drive proinflammatory cytokine production. J Exp Med, 2011. 208(3): p. 417-20.
- 19. Niehues, H., et al., 3D skin models for 3R research: The potential of 3D reconstructed skin models to study skin barrier function. Exp Dermatol, 2018. 27(5): p. 501-511.
- 20. Ma, Q., Role of nrf2 in oxidative stress and toxicity. Annu Rev Pharmacol Toxicol, 2013. 53: p. 401-26.
- 21. Al-Gubory, K.H., Environmental pollutants and lifestyle factors induce oxidative stress and poor prenatal development. Reprod Biomed Online, 2014. 29(1): p. 17-31.
- 22. Miao, Q., et al., Cigarette smoke induces ROS mediated autophagy impairment in human corneal epithelial cells. Environ Pollut, 2019. 245: p. 389-397.
- 23. Jiang, Y., et al., Cytokinocytes: the diverse contribution of keratinocytes to immune responses in skin. JCI Insight, 2020. 5(20).

1.0

- 24. Piipponen, M., D. Li, and N.X. Landen, *The Immune Functions of Keratinocytes in Skin Wound Healing*. Int J Mol Sci, 2020. **21**(22).
- 25. Kashem, S.W., M. Haniffa, and D.H. Kaplan, *Antigen-Presenting Cells in the Skin*. Annu Rev Immunol, 2017. **35**: p. 469-499.
- 26. Saravia, J., N.M. Chapman, and H. Chi, *Helper T cell differentiation*. Cell Mol Immunol, 2019. **16**(7): p. 634-643.
- 27. Byrd, A.L., Y. Belkaid, and J.A. Segre, *The human skin microbiome*. Nat Rev Microbiol, 2018. **16**(3): p. 143-155.
- 28. Zeeuwen, P.L., et al., *Microbiome and skin diseases*. Curr Opin Allergy Clin Immunol, 2013. **13**(5): p. 514-20.
- Zeeuwen, P.L., et al., Microbiome dynamics of human epidermis following skin barrier disruption. Genome Biol, 2012. 13(11): p. R101.
- 30. van der Krieken, D.A., et al., *Gram-positive anaerobic cocci guard skin homeostasis by regulating host-defense mechanisms*. iScience, 2023. **26**(4): p. 106483.
- 31. Yang, G., et al., *Skin Barrier Abnormalities and Immune Dysfunction in Atopic Dermatitis.* Int J Mol Sci, 2020. **21**(8).
- 32. Orsmond, A., et al., Skin Barrier Dysregulation in Psoriasis. Int J Mol Sci, 2021. 22(19).
- 33. Chu, S., et al., Burden of skin disease and associated socioeconomic status in Europe: An ecologic study from the Global Burden of Disease Study 2017. JAAD Int, 2020. 1(2): p. 95-103.
- 34. Langan, S.M., A.D. Irvine, and S. Weidinger, Atopic dermatitis. Lancet, 2020. 396(10247): p. 345-360.
- 35. Rendon, A. and K. Schakel, Psoriasis Pathogenesis and Treatment. Int J Mol Sci, 2019. 20(6).
- 36. Paller, A.S., et al., *The atopic march and atopic multimorbidity: Many trajectories, many pathways.* J Allergy Clin Immunol, 2019. **143**(1): p. 46-55.
- 37. Nutten, S., Atopic dermatitis: global epidemiology and risk factors. Ann Nutr Metab, 2015. **66 Suppl** 1: p. 8-16.
- 38. Moosbrugger-Martinz, V., et al., *Revisiting the Roles of Filaggrin in Atopic Dermatitis*. Int J Mol Sci, 2022. **23**(10).
- 39. van den Bogaard, E.H., et al., *Targeting Skin Barrier Function in Atopic Dermatitis*. J Allergy Clin Immunol Pract, 2023. **11**(5): p. 1335-1346.
- 40. Thyssen, J.P., et al., Filaggrin Expression and Processing Deficiencies Impair Corneocyte Surface Texture and Stiffness in Mice. J Invest Dermatol, 2020. **140**(3): p. 615-623 e5.
- 41. Niehues, H., et al., *Epidermal equivalents of filaggrin null keratinocytes do not show impaired skin barrier function.* J Allergy Clin Immunol, 2017. **139**(6): p. 1979-1981 e13.
- 42. Brown, S.J., et al., Intragenic copy number variation within filaggrin contributes to the risk of atopic dermatitis with a dose-dependent effect. J Invest Dermatol, 2012. **132**(1): p. 98-104.
- 43. Ferreira, M.A., et al., Shared genetic origin of asthma, hay fever and eczema elucidates allergic disease biology. Nat Genet, 2017. **49**(12): p. 1752-1757.
- 44. Paternoster, L., et al., Multi-ancestry genome-wide association study of 21,000 cases and 95,000 controls identifies new risk loci for atopic dermatitis. Nat Genet, 2015. **47**(12): p. 1449-1456.
- 45. Mucha, S., et al., *Protein-coding variants contribute to the risk of atopic dermatitis and skin-specific gene expression*. J Allergy Clin Immunol, 2020. **145**(4): p. 1208-1218.
- 46. He, H., et al., Single-cell transcriptome analysis of human skin identifies novel fibroblast subpopulation and enrichment of immune subsets in atopic dermatitis. J Allergy Clin Immunol, 2020. **145**(6): p. 1615-1628.

- 48. Hasegawa, T., T. Oka, and S. Demehri, *Alarmin Cytokines as Central Regulators of Cutaneous Immunity*. Front Immunol, 2022. **13**: p. 876515.
- 49. Andrews, A.L., et al., *IL-4 receptor alpha is an important modulator of IL-4 and IL-13 receptor binding: implications for the development of therapeutic targets.* J Immunol, 2006. **176**(12): p. 7456-61.
- 50. Huang, I.H., et al., *JAK-STAT signaling pathway in the pathogenesis of atopic dermatitis: An updated review.* Front Immunol, 2022. **13**: p. 1068260.
- 51. Shiratori-Hayashi, M., et al., *STAT3-dependent reactive astrogliosis in the spinal dorsal horn underlies chronic itch*. Nat Med, 2015. **21**(8): p. 927-31.
- 52. Montero-Vilchez, T., et al., Skin Barrier Function in Psoriasis and Atopic Dermatitis: Transepidermal Water Loss and Temperature as Useful Tools to Assess Disease Severity. J Clin Med, 2021. 10(2).
- 53. Luger, T., et al., *Atopic dermatitis: Role of the skin barrier, environment, microbiome, and therapeutic agents.* J Dermatol Sci, 2021. **102**(3): p. 142-157.
- 54. Mobus, L., et al., *Atopic dermatitis displays stable and dynamic skin transcriptome signatures.*J Allergy Clin Immunol, 2021. **147**(1): p. 213-223.
- 55. Niehues, H., et al., *Identification of Keratinocyte Mitogens: Implications for Hyperproliferation in Psoriasis and Atopic Dermatitis*. JID Innov, 2022. **2**(1): p. 100066.
- 56. Dand, N., et al., Psoriasis and Genetics. Acta Derm Venereol, 2020. 100(3): p. adv00030.
- 57. Coto, E., et al., New psoriasis susceptibility genes: momentum for skin-barrier disruption. J Invest Dermatol, 2011. **131**(5): p. 1003-5.
- 58. de Cid, R., et al., *Deletion of the late cornified envelope LCE3B and LCE3C genes as a susceptibility factor for psoriasis.* Nat Genet, 2009. **41**(2): p. 211-5.
- 59. Hollox, E.J., et al., *Psoriasis is associated with increased beta-defensin genomic copy number.* Nat Genet, 2008. **40**(1): p. 23-5.
- 60. Harder, J., et al., A peptide antibiotic from human skin. Nature, 1997. 387(6636): p. 861.
- 61. Lowes, M.A., M. Suarez-Farinas, and J.G. Krueger, *Immunology of psoriasis*. Annu Rev Immunol, 2014. **32**: p. 227-55.
- 62. Lee, E.B., et al., *Psoriasis risk factors and triggers*. Cutis, 2018. **102**(5S): p. 18-20.
- 63. Li, B., et al., The role of Th17 cells in psoriasis. Immunol Res, 2020. **68**(5): p. 296-309.
- 64. Diani, M., G. Altomare, and E. Reali, *T Helper Cell Subsets in Clinical Manifestations of Psoriasis*. J Immunol Res, 2016. **2016**: p. 7692024.
- 65. Kagami, S., et al., Circulating Th17, Th22, and Th1 cells are increased in psoriasis. J Invest Dermatol, 2010. 130(5): p. 1373-83.
- 66. Hawkes, J.E., et al., *Discovery of the IL-23/IL-17 Signaling Pathway and the Treatment of Psoriasis.*J Immunol, 2018. **201**(6): p. 1605-1613.
- 67. Araviiskaia, E., et al., *The Role of a Novel Generation of Emollients, 'Emollients Plus', in Atopic Dermatitis*. Clin Cosmet Investig Dermatol, 2022. **15**: p. 2705-2719.
- 68. Stacey, S.K. and M. McEleney, *Topical Corticosteroids: Choice and Application*. Am Fam Physician, 2021. **103**(6): p. 337-343.
- 69. Fishbein, A.B., et al., *Update on Atopic Dermatitis: Diagnosis, Severity Assessment, and Treatment Selection.* J Allergy Clin Immunol Pract, 2020. **8**(1): p. 91-101.
- 70. Reid, C. and C.E.M. Griffiths, *Psoriasis and Treatment: Past, Present and Future Aspects.* Acta Derm Venereol, 2020. **100**(3): p. adv00032.

- 71. Neagu, N., et al., Dupilumab ocular side effects in patients with atopic dermatitis: a systematic review. J Eur Acad Dermatol Venereol, 2022. 36(6): p. 820-835.
- 72. Narla, S., J.I. Silverberg, and E.L. Simpson, Management of inadequate response and adverse effects to dupilumab in atopic dermatitis. J Am Acad Dermatol, 2022. 86(3): p. 628-636.
- 73. Bruin-Weller, M., et al., Disease burden and treatment history among adults with atopic dermatitis receiving systemic therapy: baseline characteristics of participants on the EUROSTAD prospective observational study. J Dermatolog Treat, 2021. 32(2): p. 164-173.
- 74. in CADTH Canadian Drug Expert Committee Recommendation: Dupilumab (Dupixent Sanofi-Aventis Canada Inc.): Indication: Atopic dermatitis. 2020: Ottawa (ON).
- 75. van den Bogaard, E.H., et al., Coal tar induces AHR-dependent skin barrier repair in atopic dermatitis. J Clin Invest, 2013. 123(2): p. 917-27.
- 76. van den Bogaard, E.H., et al., Genetic and Pharmacological Analysis Identifies a Physiological Role for the AHR in Epidermal Differentiation. Journal of Investigative Dermatology, 2015. 135(5): p. 1320-1328.
- 77. Smits, J.P.H., et al., Targeting the Cutaneous Microbiota in Atopic Dermatitis by Coal Tar via AHR-Dependent Induction of Antimicrobial Peptides. J Invest Dermatol, 2020. 140(2): p. 415-424 e10.
- 78. Roelofzen, J.H., et al., No increased risk of cancer after coal tar treatment in patients with psoriasis or eczema. J Invest Dermatol, 2010. 130(4): p. 953-61.
- 79. Conney, A.H., E.C. Miller, and J.A. Miller, Substrate-induced synthesis and other properties of benzpyrene hydroxylase in rat liver. J Biol Chem, 1957. 228(2): p. 753-66.
- 80. Wei, Y.D., et al., Rapid and transient induction of CYP1A1 gene expression in human cells by the tryptophan photoproduct 6-formylindolo[3,2-b]carbazole. Chem Biol Interact, 1998. 110(1-2): p. 39-55.
- 81. Heath-Pagliuso, S., et al., Activation of the Ah receptor by tryptophan and tryptophan metabolites. Biochemistry, 1998. 37(33): p. 11508-15.
- 82. Hubbard, T.D., et al., Dietary Broccoli Impacts Microbial Community Structure and Attenuates Chemically Induced Colitis in Mice in an Ah receptor dependent manner. J Funct Foods, 2017. 37: p. 685-698.
- 83. Omiecinski, C.J., et al., Xenobiotic Metabolism, Disposition, and Regulation by Receptors: From Biochemical Phenomenon to Predictors of Major Toxicities. Toxicological Sciences, 2011. 120: p. S49-S75.
- 84. Lusska, A., E. Shen, and J.P. Whitlock, Protein-DNA Interactions at a Dioxin-Responsive Enhancer - Analysis of 6 Bona-Fide DNA-Binding Sites for the Liganded Ah Receptor. Journal of Biological Chemistry, 1993. 268(9): p. 6575-6580.
- 85. Sun, M., et al., Tryptophan (Trp) modulates gut homeostasis via aryl hydrocarbon receptor (AhR). Crit Rev Food Sci Nutr, 2020. 60(10): p. 1760-1768.
- 86. Neavin, D.R., et al., The Role of the Aryl Hydrocarbon Receptor (AHR) in Immune and Inflammatory Diseases. Int J Mol Sci, 2018. 19(12).
- 87. Murray, I.A., A.D. Patterson, and G.H. Perdew, Aryl hydrocarbon receptor ligands in cancer: friend and foe. Nat Rev Cancer, 2014. 14(12): p. 801-14.
- 88. Rowlands, J.C. and J.A. Gustafsson, Aryl hydrocarbon receptor-mediated signal transduction. Crit Rev Toxicol, 1997. 27(2): p. 109-34.
- 89. Schecter, A., et al., *Dioxins: an overview*. Environ Res, 2006. **101**(3): p. 419-28.
- 90. Gonzalez, F.J. and P. Fernandez-Salguero, The aryl hydrocarbon receptor Studies using the AHR-null mice. Drug Metabolism and Disposition, 1998. 26(12): p. 1194-1198.
- 91. Boysen, G. and S.S. Hecht, Analysis of DNA and protein adducts of benzo[a]pyrene in human tissues using structure-specific methods. Mutation Research/Reviews in Mutation Research, 2003. 543(1): p. 17-30.

- 92. Guengerich, F.P., Cytochrome P450 and chemical toxicology, Chemical Research in Toxicology, 2008. **21**(1): p. 70-83.
- 93. Uno, S., et al., Oral benzo[a]pyrene in Cyp1 knockout mouse lines: CYP1A1 important in detoxication, CYP1B1 metabolism required for immune damage independent of total-body burden and clearance rate. Molecular Pharmacology, 2006. 69(4): p. 1103-1114.
- 94. Fernandez-Salguero, P.M., et al., Aryl-hydrocarbon receptor-deficient mice are resistant to 2,3,7,8-tetrachlorodibenzo-p-dioxin-induced toxicity. Toxicol Appl Pharmacol, 1996. 140(1): p. 173-9.
- 95. Lebwohl, M.G., et al., Phase 3 Trials of Tapinarof Cream for Plaque Psoriasis. N Engl J Med, 2021. **385**(24): p. 2219-2229.
- 96. Hahn, M.E., et al., Unexpected diversity of aryl hydrocarbon receptors in non-mammalian vertebrates: insights from comparative genomics. Journal of Experimental Zoology Part a-Ecological Genetics and Physiology, 2006. 305a(9): p. 693-706.
- 97. Fritsche, E., et al., Lightening up the UV response by identification of the arylhydrocarbon receptor as a cytoplasmatic target for ultraviolet B radiation. Proceedings of the National Academy of Sciences of the United States of America, 2007. 104(21): p. 8851-8856.
- 98. Jin, U.H., et al., Microbiome-Derived Tryptophan Metabolites and Their Aryl Hydrocarbon Receptor-Dependent Agonist and Antagonist Activities. Molecular Pharmacology, 2014. 85(5): p. 777-788.
- 99. Tan, Y.Q., et al., The citrus flavonone hesperetin attenuates the nuclear translocation of aryl hydrocarbon receptor. Comparative Biochemistry and Physiology C-Toxicology & Pharmacology, 2018. **210**: p. 57-64.
- 100. Huff, J.E., et al., Long-term carcinogenesis studies on 2,3,7,8-tetrachlorodibenzo-p-dioxin and hexachlorodibenzo-p-dioxins. Cell Biol Toxicol, 1991. **7**(1): p. 67-94.
- 101. Panteleyev, A.A., et al., 2,3,7,8-tetrachlorodibenzo-p-dioxin (TCCD) affects keratin 1 and keratin 17 gene expression and differentially induces keratinization in hairless mouse skin. J Invest Dermatol, 1997. 108(3): p. 330-5.
- 102. Reggiani, G., Acute human exposure to TCDD in Seveso, Italy. J Toxicol Environ Health, 1980. 6(1): p. 27-43.
- 103. Ito, T., et al., TCDD exposure exacerbates atopic dermatitis-related inflammation in NC/Nga mice. Toxicol Lett, 2008. 177(1): p. 31-7.
- 104. Stading, R., et al., Molecular mechanisms of pulmonary carcinogenesis by polycyclic aromatic hydrocarbons (PAHs): Implications for human lung cancer. Semin Cancer Biol, 2021. 76: p. 3-16.
- 105. Sousa, G., et al., Exposure to PAHs during Firefighting Activities: A Review on Skin Levels, In Vitro/In Vivo Bioavailability, and Health Risks. Int J Environ Res Public Health, 2022. 19(19).
- 106. Furue, M., et al., Implications of tryptophan photoproduct FICZ in oxidative stress and terminal differentiation of keratinocytes. G Ital Dermatol Venereol, 2019. 154(1): p. 37-41.
- 107. Syed, D.N. and H. Mukhtar, FICZ: A Messenger of Light in Human Skin. J Invest Dermatol, 2015. 135(6): p. 1478-1481.
- 108. Yu, J., et al., A tryptophan metabolite of the skin microbiota attenuates inflammation in patients with atopic dermatitis through the aryl hydrocarbon receptor. J Allergy Clin Immunol, 2019. 143(6): p. 2108-2119 e12.
- 109. Aoki, R., et al., Protective effect of indole-3-pyruvate against ultraviolet b-induced damage to cultured HaCaT keratinocytes and the skin of hairless mice. PLoS One, 2014. 9(5): p. e96804.
- 110. Murray, I.A. and G.H. Perdew, Ligand activation of the Ah receptor contributes to gastrointestinal homeostasis. Curr Opin Toxicol, 2017. 2: p. 15-23.
- 111. Szelest, M., K. Walczak, and T. Plech, A New Insight into the Potential Role of Tryptophan-Derived AhR Ligands in Skin Physiological and Pathological Processes. Int J Mol Sci, 2021. 22(3).

- 112. Lee, J.S., et al., AHR drives the development of gut ILC22 cells and postnatal lymphoid tissues via pathways dependent on and independent of Notch. Nat Immunol, 2011. 13(2): p. 144-51.
- 113. Esakky, P., et al., Cigarette smoke-induced cell cycle arrest in spermatocytes [GC-2spd(ts)] is mediated through crosstalk between Ahr-Nrf2 pathway and MAPK signaling. J Mol Cell Biol, 2015. **7**(1): p. 73-87.
- 114. Yin, J.H., et al., Role of AhR in positive regulation of cell proliferation and survival. Cell Proliferation, 2016. **49**(5): p. 554-560.
- 115. Hanieh, H., et al., Novel Aryl Hydrocarbon Receptor Agonist Suppresses Migration and Invasion of Breast Cancer Cells. Plos One, 2016. 11(12).
- 116. Zhou, B., et al., Mitochondrial activity and oxidative stress functions are influenced by the activation of AhR-induced CYP1A1 overexpression in cardiomyocytes. Molecular Medicine Reports, 2017. **16**(1): p. 174-180.
- 117. Gruszczyk, J., et al., Cryo-EM structure of the agonist-bound Hsp90-XAP2-AHR cytosolic complex. Nat Commun, 2022. 13(1): p. 7010.
- 118. Kimura, E., et al., Excessive activation of AhR signaling disrupts neuronal migration in the hippocampal CA1 region in the developing mouse. Journal of Toxicological Sciences, 2017. 42(1): p. 25-30.
- 119. Gialitakis, M., et al., Activation of the Aryl Hydrocarbon Receptor Interferes with Early Embryonic Development. Stem Cell Reports, 2017. 9(5): p. 1377-1386.
- 120. Zhang, N., The role of endogenous aryl hydrocarbon receptor signaling in cardiovascular physiology. J Cardiovasc Dis Res, 2011. 2(2): p. 91-5.
- 121. Uhlen, M., et al., Proteomics. Tissue-based map of the human proteome. Science, 2015. 347(6220): p. 1260419.
- 122. Haarmann-Stemmann, T., C. Esser, and J. Krutmann, The Janus-Faced Role of Aryl Hydrocarbon Receptor Signaling in the Skin: Consequences for Prevention and Treatment of Skin Disorders. J Invest Dermatol, 2015. 135(11): p. 2572-2576.
- 123. Gao, Z., et al., TCDD promoted EMT of hFPECs via AhR, which involved the activation of EGFR/ERK signaling. Toxicol Appl Pharmacol, 2016. 298: p. 48-55.
- 124. Kalmes, M., et al., Impact of aryl hydrocarbon receptor (AhR) knockdown on cell cycle progression in human HaCaT keratinocytes. Biol Chem, 2011. 392(7): p. 643-51.
- 125. Cai, Z., et al., Benvitimod inhibits MCM6-meditated proliferation of keratinocytes by regulating the JAK/STAT3 pathway. J Dermatol Sci, 2023. 109(2): p. 71-79.
- 126. Zhu, X., et al., The opposite effect of tapinarof between IMQ and IL-23 induced psoriasis mouse models. Exp Dermatol, 2023.
- 127. Bernd, A., et al., [Antiproliferative activity of a highly purified coal tar preparation in comparison with clobetasol-17-propionate]. Arzneimittelforschung, 1990. 40(7): p. 782-7.
- 128. Wanner R., et al., The Differentiation-Related Upregulation of Aryl Hydrocarbon Receptor Transcript Levels Is Suppressed by Retinoic Acid. Biochemical and Biophysical Research Communications, 1995. 209(2): p. 706-711.
- 129. Loertscher, J.A., et al., In utero exposure to 2,3,7,8-tetrachlorodibenzo-p-dioxin causes accelerated terminal differentiation in fetal mouse skin. Toxicol Sci, 2002. 68(2): p. 465-72.
- 130. Wright, C.W., et al., Comparative chemical and biological analysis of coal tar-based therapeutic agents to other coal-derived materials. J Appl Toxicol, 1985. 5(2): p. 80-8.
- 131. Proper, S.P., et al., Aryl hydrocarbon receptor and IL-13 signaling crosstalk in human keratinocytes and atopic dermatitis. Front Allergy, 2024. 5: p. 1323405.
- 132. Tsuji, G., et al., Aryl hydrocarbon receptor activation restores filaggrin expression via OVOL1 in atopic dermatitis. Cell Death & Disease, 2017. 8.

- 133. Sutter, C.H., H.M. Rainwater, and T.R. Sutter, Contributions of Nitric Oxide to AHR-Ligand-Mediated Keratinocyte Differentiation. Int J Mol Sci, 2020. 21(16).
- 134. Sutter, C.H., et al., The AHR regulates metabolic reprogramming to promote SIRT1-dependent keratinocyte differentiation. J Invest Dermatol, 2018.
- 135. Ito, T., et al., Activation of the OVOL1-OVOL2 Axis in the Hair Bulb and in Pilomatricoma, Am J Pathol, 2016. **186**(4): p. 1036-43.
- 136. Nair, M., et al., Ovol1 regulates the growth arrest of embryonic epidermal progenitor cells and represses c-myc transcription. J Cell Biol, 2006. 173(2): p. 253-64.
- 137. Edamitsu, T., et al., AHR and NRF2 in Skin Homeostasis and Atopic Dermatitis. Antioxidants (Basel), 2022. 11(2).
- 138. Mansbridge, J.N. and A.M. Knapp, Penetration of lucifer yellow into human skin: a lateral diffusion channel in the stratum corneum. J Histochem Cytochem, 1993. 41(6): p. 909-14.
- 139. Srinivasan, B., et al., TEER measurement techniques for in vitro barrier model systems. J Lab Autom, 2015. 20(2): p. 107-26.
- 140. Farahmand, S., et al., Measuring transepidermal water loss: a comparative in vivo study of condenserchamber, unventilated-chamber and open-chamber systems. Skin Res Technol, 2009. 15(4): p. 392-8.
- 141. Haas, K., et al., Aryl Hydrocarbon Receptor in Keratinocytes Is Essential for Murine Skin Barrier Integrity. Journal of Investigative Dermatology, 2016. 136(11): p. 2260-2269.
- 142. Kiyomatsu-Oda, M., et al., Protective role of 6-formylindolo[3,2-b]carbazole (FICZ), an endogenous ligand for arylhydrocarbon receptor, in chronic mite-induced dermatitis. Journal of Dermatological Science, 2018. 90(3): p. 284-294.
- 143. Quintana, F.J., et al., Control of T(reg) and T(H)17 cell differentiation by the aryl hydrocarbon receptor. Nature, 2008. 453(7191): p. 65-71.
- 144. Rothhammer, V. and F.J. Quintana, The aryl hydrocarbon receptor: an environmental sensor integrating immune responses in health and disease. Nat Rev Immunol, 2019. 19(3): p. 184-197.
- 145. Gutierrez-Vazquez, C. and F.J. Quintana, Regulation of the Immune Response by the Aryl Hydrocarbon Receptor. Immunity, 2018. 48(1): p. 19-33.
- 146. van der Fits, L., et al., Imiquimod-Induced Psoriasis-Like Skin Inflammation in Mice Is Mediated via the IL-23/IL-17 Axis. Journal of Immunology, 2009. 182(9): p. 5836-5845.
- 147. Lee, E., et al., Increased expression of interleukin 23 p19 and p40 in lesional skin of patients with psoriasis vulgaris. Journal of Experimental Medicine, 2004. 199(1): p. 125-130.
- 148. Di Meglio, P., et al., Activation of the Aryl Hydrocarbon Receptor Dampens the Severity of Inflammatory Skin Conditions. Immunity, 2014. 40(6): p. 989-1001.
- 149. Tauchi, M., et al., Constitutive expression of aryl hydrocarbon receptor in keratinocytes causes inflammatory skin lesions. Molecular and Cellular Biology, 2005. 25(21): p. 9360-9368.
- 150. Hidaka T., et al., The aryl hydrocarbon receptor AhR links atopic dermatitis and air pollution via induction of the neurotrophic factor artemin. Nature Immunology, 2017(18): p. 64-73.
- 151. Bissonnette, R., et al., Efficacy and safety of topical WBI-1001 in patients with mild to moderate psoriasis: results from a randomized double-blind placebo-controlled, phase II trial. J Eur Acad Dermatol Venereol, 2012. 26(12): p. 1516-21.
- 152. Bissonnette, R., et al., Efficacy and Safety of Topical WBI-1001 in the Treatment of Atopic Dermatitis: Results From a Phase 2A, Randomized, Placebo-Controlled Clinical Trial. Archives of Dermatology, 2010. **146**(4): p. 446-449.
- 153. Smith, S.H., et al., Tapinarof Is a Natural AhR Agonist that Resolves Skin Inflammation in Mice and Humans. Journal of Investigative Dermatology, 2017. 137(10): p. 2110-2119.

- 154. Gu, Y.Z., J.B. Hogenesch, and C.A. Bradfield, The PAS superfamily: sensors of environmental and developmental signals. Annu Rev Pharmacol Toxicol, 2000. 40: p. 519-61.
- 155. Beischlag, T.V., et al., The aryl hydrocarbon receptor complex and the control of gene expression. Crit Rev Eukaryot Gene Expr, 2008. 18(3): p. 207-50.
- 156. Esser, C. and A. Rannug, The aryl hydrocarbon receptor in barrier organ physiology, immunology, and toxicology. Pharmacol Rev, 2015. 67(2): p. 259-79.
- 157. Denison, M.S., et al., Exactly the same but different: promiscuity and diversity in the molecular mechanisms of action of the aryl hydrocarbon (dioxin) receptor. Toxicol Sci, 2011. 124(1): p. 1-22.
- 158. Hubbard, T.D., I.A. Murray, and G.H. Perdew, Indole and Tryptophan Metabolism: Endogenous and Dietary Routes to Ah Receptor Activation. Drug Metab Dispos, 2015. 43(10): p. 1522-35.
- 159. Murray, I.A., et al., Development of a selective modulator of aryl hydrocarbon (Ah) receptor activity that exhibits anti-inflammatory properties. Chem Res Toxicol, 2010. 23(5): p. 955-66.
- 160. Fritz, W.A., et al., The selective aryl hydrocarbon receptor modulator 6-methyl-1,3,8trichlorodibenzofuran inhibits prostate tumor metastasis in TRAMP mice. Biochem Pharmacol, 2009. **77**(7): p. 1151-60.
- 161. Gasiewicz, T.A., et al., Distribution, excretion, and metabolism of 2,3,7,8-tetrachlorodibenzo-p-dioxin in C57BL/6J, DBA/2J, and B6D2F1/J mice. Drug Metab Dispos, 1983. 11(5): p. 397-403.
- 162. Dinatale, B.C., et al., Kynurenic Acid is a Potent Endogenous Ah Receptor Ligand that Synergistically Induces Interleukin 6 in the Presence of Inflammatory Signaling. Toxicol Sci, 2010. 115: p. 89-97.
- 163. Mezrich, J.D., et al., An interaction between kynurenine and the aryl hydrocarbon receptor can generate regulatory T cells. J Immunol, 2010. 185(6): p. 3190-8.
- 164. Smirnova, A., et al., Evidence for New Light-Independent Pathways for Generation of the Endogenous Aryl Hydrocarbon Receptor Agonist FICZ. Chem Res Toxicol, 2016. 29(1): p. 75-86.
- 165. Hubbard, T.D., et al., Adaptation of the human aryl hydrocarbon receptor to sense microbiotaderived indoles. Sci Rep, 2015. 5: p. 12689.
- 166. Mexia, N., et al., Pityriazepin and other potent AhR ligands isolated from Malassezia furfur yeast. Arch Biochem Biophys, 2015. 571: p. 16-20.
- 167. Esser, C., et al., Functions of the aryl hydrocarbon receptor in the skin. Semin Immunopathol, 2013. **35**(6): p. 677-91.
- 168. Sadek, C.M. and B.L. Allen-Hoffmann, Cytochrome P450IA1 is rapidly induced in normal human keratinocytes in the absence of xenobiotics. J Biol Chem, 1994. 269(23): p. 16067-74.
- 169. Furue, M., et al., Gene regulation of filaggrin and other skin barrier proteins via aryl hydrocarbon receptor. J Dermatol Sci. 2015. 80(2): p. 83-8.
- 170. Lozza, L., et al., The Henna pigment Lawsone activates the Aryl Hydrocarbon Receptor and impacts skin homeostasis. Sci Rep, 2019. 9(1): p. 10878.
- 171. Sutter, C.H., et al., 2,3,7,8-Tetrachlorodibenzo-p-dioxin increases the expression of genes in the human epidermal differentiation complex and accelerates epidermal barrier formation. Toxicol Sci, 2011. **124**(1): p. 128-37.
- 172. Doi, K., et al., Antioxidant Houttuynia cordata extract upregulates filaggrin expression in an aryl hydrocarbon-dependent manner. Fukuoka Igaku Zasshi, 2014. 105(11): p. 205-13.
- 173. Nakahara, T., et al., Antioxidant Opuntia ficus-indica Extract Activates AHR-NRF2 Signaling and Upregulates Filaggrin and Loricrin Expression in Human Keratinocytes. J Med Food, 2015. 18(10): p. 1143-9.
- 174. Takei, K., et al., Antioxidant soybean tar Glyteer rescues T-helper-mediated downregulation of filaggrin expression via aryl hydrocarbon receptor. J Dermatol, 2015. 42(2): p. 171-80.

- 176. Denison, M.S. and S.C. Faber, *And Now for Something Completely Different: Diversity in Ligand-Dependent Activation of Ah Receptor Responses*. Curr Opin Toxicol, 2017. **2**: p. 124-131.
- 177. Rikken, G., et al., Carboxamide Derivatives Are Potential Therapeutic AHR Ligands for Restoring IL-4 Mediated Repression of Epidermal Differentiation Proteins. Int J Mol Sci, 2022. **23**(3).
- 178. Kawajiri, K. and Y. Fujii-Kuriyama, *The aryl hydrocarbon receptor: a multifunctional chemical sensor for host defense and homeostatic maintenance.* Experimental animals, 2017. **66**(2): p. 75-89.
- 179. Jux, B., S. Kadow, and C. Esser, *Langerhans cell maturation and contact hypersensitivity are impaired in aryl hydrocarbon receptor-null mice*. The Journal of Immunology, 2009. **182**(11): p. 6709-6717.
- 180. Platzer, B., et al., Aryl hydrocarbon receptor activation inhibits in vitro differentiation of human monocytes and Langerhans dendritic cells. The Journal of Immunology, 2009. **183**(1): p. 66-74.
- 181. Brandstätter, O., et al., Balancing intestinal and systemic inflammation through cell type-specific expression of the aryl hydrocarbon receptor repressor. 2016. **6**: p. 26091.
- 182. Steffan, R.J., et al., Synthesis and activity of substituted 4-(indazol-3-yl)phenols as pathway-selective estrogen receptor ligands useful in the treatment of rheumatoid arthritis. J Med Chem, 2004. **47**(26): p. 6435-8.
- 183. Bruning, J.B., et al., Coupling of receptor conformation and ligand orientation determine graded activity. Nat Chem Biol, 2010. **6**(11): p. 837-43.
- 184. Chadwick, C.C., et al., *Identification of pathway-selective estrogen receptor ligands that inhibit NF-kappaB transcriptional activity.* Proc Natl Acad Sci U S A, 2005. **102**(7): p. 2543-8.
- 185. Keith, J.C., Jr., et al., The utility of pathway selective estrogen receptor ligands that inhibit nuclear factor-kappa B transcriptional activity in models of rheumatoid arthritis. Arthritis Res Ther, 2005. **7**(3): p. R427-38.
- 186. Opal, S.M., et al., The activity of pathway-selective estrogen receptor ligands in experimental septic shock. Shock, 2005. **24**(6): p. 535-40.
- 187. Murray, I.A., et al., Evidence for ligand-mediated selective modulation of aryl hydrocarbon receptor activity. Mol Pharmacol, 2010. **77**(2): p. 247-54.
- 188. Safe, S., C. Qin, and A. McDougal, *Development of selective aryl hydrocarbon receptor modulators* for treatment of breast cancer. Expert Opin Investig Drugs, 1999. **8**(9): p. 1385-96.
- 189. Muku, G.E., et al., Ligand-mediated cytoplasmic retention of the Ah receptor inhibits macrophage-mediated acute inflammatory responses. Lab Invest, 2017. **97**(12): p. 1471-1487.
- 190. Narayanan, G.A., et al., Selective aryl hydrocarbon receptor modulator-mediated repression of CD55 expression induced by cytokine exposure. J Pharmacol Exp Ther, 2012. **342**(2): p. 345-55.
- 191. Long, W.P., et al., Protein kinase C activity is required for aryl hydrocarbon receptor pathway-mediated signal transduction. Mol Pharmacol, 1998. **53**(4): p. 691-700.
- 192. Baglole, C.J., et al., The aryl hydrocarbon receptor attenuates tobacco smoke-induced cyclooxygenase-2 and prostaglandin production in lung fibroblasts through regulation of the NF-kappaB family member RelB. J Biol Chem, 2008. **283**(43): p. 28944-57.
- 193. Kao, J.S., et al., Short-term glucocorticoid treatment compromises both permeability barrier homeostasis and stratum corneum integrity: inhibition of epidermal lipid synthesis accounts for functional abnormalities. J Invest Dermatol, 2003. **120**(3): p. 456-64.
- 194. Yang, K., et al., AhRE2F1KGFR signaling is involved in KGFinduced intestinal epithelial cell proliferation. Mol Med Rep, 2017. **15**(5): p. 3019-3026.

- 195. Pollet, M., et al., The AHR represses nucleotide excision repair and apoptosis and contributes to UVinduced skin carcinogenesis. Cell Death Differ, 2018. 25(10): p. 1823-1836.
- 196. Poland, A., et al., Photoaffinity labeling of the Ah receptor. J Biol Chem, 1986. 261(14): p. 6352-65.
- 197. Garrison, P.M., et al., Species-specific recombinant cell lines as bioassay systems for the detection of 2.3.7.8-tetrachlorodibenzo-p-dioxin-like chemicals. Fundam Appl Toxicol, 1996. 30(2): p. 194-203.
- 198. Dlugosz, A.A., et al., Isolation and utilization of epidermal keratinocytes for oncogene research. Methods Enzymol, 1995. 254: p. 3-20.
- 199. de Jongh, G.J., et al., High expression levels of keratinocyte antimicrobial proteins in psoriasis compared with atopic dermatitis. J Invest Dermatol, 2005. 125(6): p. 1163-73.
- 200. Dobin, A., et al., STAR: ultrafast universal RNA-seq aligner. Bioinformatics, 2013. 29(1): p. 15-21.
- 201. Love, M.L. W. Huber, and S. Anders, Moderated estimation of fold change and dispersion for RNA-sea data with DESeq2. Genome Biol, 2014. 15(12): p. 550.
- 202. Gu, Z., R. Eils, and M. Schlesner, Complex heatmaps reveal patterns and correlations in multidimensional genomic data. Bioinformatics, 2016. 32(18): p. 2847-9.
- 203. Yu, G., et al., clusterProfiler: an R package for comparing biological themes among gene clusters. OMICS, 2012. **16**(5): p. 284-7.
- 204. van Duijnhoven, J.L., et al., MON-150, a versatile monoclonal antibody against involucrin: characterization and applications. Arch Dermatol Res, 1992. 284(3): p. 167-72.
- 205. McQuin, C., et al., CellProfiler 3.0: Next-generation image processing for biology. PLoS Biol, 2018. **16**(7): p. e2005970.
- 206. Palmer, C.N., et al., Common loss-of-function variants of the epidermal barrier protein filaggrin are a major predisposing factor for atopic dermatitis. Nat Genet, 2006. 38(4): p. 441-6.
- 207. Sandilands, A., et al., Comprehensive analysis of the gene encoding filaggrin uncovers prevalent and rare mutations in ichthyosis vulgaris and atopic eczema. Nat Genet, 2007. 39(5): p. 650-4.
- 208. Knuppel, S., et al., Multi-locus stepwise regression: a haplotype-based algorithm for finding genetic associations applied to atopic dermatitis. BMC Med Genet, 2012. 13: p. 8.
- 209. Trzeciak, M., et al., Association of a Single Nucleotide Polymorphism in a Late Cornified Envelope-like Proline-rich 1 Gene (LELP1) with Atopic Dermatitis. Acta Derm Venereol, 2016. 96(4): p. 459-63.
- 210. Marenholz, I., et al., Association screening in the Epidermal Differentiation Complex (EDC) identifies an SPRR3 repeat number variant as a risk factor for eczema. J Invest Dermatol, 2011. 131(8): p. 1644-9.
- 211. Loertscher, J., C. Sattler, and B. Allen-Hoffmann, 2, 3, 7, 8-Tetrachlorodibenzo-p-dioxin alters the differentiation pattern of human keratinocytes in organotypic culture. Toxicology and applied pharmacology, 2001. 175(2): p. 121-129.
- 212. Uberoi, A., et al., Commensal microbiota regulates skin barrier function and repair via signaling through the aryl hydrocarbon receptor. Cell Host Microbe, 2021. 29(8): p. 1235-1248 e8.
- 213. van den Bogaard, E.H., C. Esser, and G.H. Perdew, The aryl hydrocarbon receptor at the forefront of host-microbe interactions in the skin: A perspective on current knowledge gaps and directions for future research and therapeutic applications. Exp Dermatol, 2021. 30(10): p. 1477-1483.
- 214. Roman, A.C., et al., Dioxin receptor deficiency impairs angiogenesis by a mechanism involving VEGF-A depletion in the endothelium and transforming growth factor-beta overexpression in the stroma. J Biol Chem, 2009. 284(37): p. 25135-48.
- 215. Furue, M., et al., Role of AhR/ARNT system in skin homeostasis. Arch Dermatol Res, 2014. 306(9): p. 769-79.
- 216. Quintana, F.J. and D.H. Sherr, Aryl hydrocarbon receptor control of adaptive immunity. Pharmacol Rev, 2013. 65(4): p. 1148-61.

- 218. Boros, F. and L. Vecsei, *Progress in the development of kynurenine and quinoline-3-carboxamide-derived drugs*. Expert Opin Investig Drugs, 2020. **29**(11): p. 1223-1247.
- 219. Kaye, J., et al., Laquinimod arrests experimental autoimmune encephalomyelitis by activating the aryl hydrocarbon receptor. Proc Natl Acad Sci U S A, 2016. **113**(41): p. E6145-E6152.
- 220. Bruck, W. and C. Wegner, *Insight into the mechanism of laquinimod action*. J Neurol Sci, 2011. **306**(1-2): p. 173-9.
- 221. Wegner, C., et al., Laquinimod interferes with migratory capacity of T cells and reduces IL-17 levels, inflammatory demyelination and acute axonal damage in mice with experimental autoimmune encephalomyelitis. J Neuroimmunol, 2010. 227(1-2): p. 133-43.
- 222. Nilsson, B., New use of quinoline-3-carboxamide compounds, P. AB, Editor. 1995: Sweden. p. 17.
- 223. Pettersson, L., 1,2-dihydro-4-hydroxy-2-oxo-quinoline-3-carboxanilides as AHR activators. 2012.
- 224. Mahiout, S., et al., *In vitro toxicity and in silico docking analysis of two novel selective AH-receptor modulators*. Toxicol In Vitro, 2018. **52**: p. 178-188.
- 225. Mahiout, S., et al., Toxicological characterisation of two novel selective aryl hydrocarbon receptor modulators in Sprague-Dawley rats. Toxicol Appl Pharmacol, 2017. **326**: p. 54-65.
- 226. Kennedy, L.H., et al., *2,3,7,8-Tetrachlorodibenzo-p-dioxin-mediated production of reactive oxygen species is an essential step in the mechanism of action to accelerate human keratinocyte differentiation*. Toxicol Sci, 2013. **132**(1): p. 235-49.
- 227. Vu, Y.H., et al., *IL-24 Negatively Regulates Keratinocyte Differentiation Induced by Tapinarof, an Aryl Hydrocarbon Receptor Modulator: Implication in the Treatment of Atopic Dermatitis.* Int J Mol Sci, 2020. **21**(24).
- 228. de Wit, R., et al., EORTC phase II study of daily oral linomide in metastatic renal cell carcinoma patients with good prognostic factors. Eur J Cancer, 1997. **33**(3): p. 493-5.
- 229. Mackean, M.J., et al., *A feasibility study of roquinimex (Linomide) and alpha interferon in patients with advanced malignant melanoma or renal carcinoma*. Br J Cancer, 1998. **78**(12): p. 1620-3.
- 230. Noseworthy, J.H., et al., *Linomide in relapsing and secondary progressive MS: part I: trial design and clinical results. North American Linomide Investigators.* Neurology, 2000. **54**(9): p. 1726-33.
- 231. Isaacs, J.T., et al., Identification of ABR-215050 as lead second generation quinoline-3-carboxamide anti-angiogenic agent for the treatment of prostate cancer. Prostate, 2006. **66**(16): p. 1768-78.
- 232. Jonsson, S., et al., Synthesis and biological evaluation of new 1,2-dihydro-4-hydroxy-2-oxo-3-quinolinecarboxamides for treatment of autoimmune disorders: structure-activity relationship. J Med Chem, 2004. **47**(8): p. 2075-88.
- 233. Haggiag, S., S. Ruggieri, and C. Gasperini, *Efficacy and safety of laquinimod in multiple sclerosis:* current status. Ther Adv Neurol Disord, 2013. **6**(6): p. 343-52.
- 234. Polman, C., et al., *Treatment with laquinimod reduces development of active MRI lesions in relapsing MS*. Neurology, 2005. **64**(6): p. 987-91.
- 235. Rouhi, F., et al., The effects and side effects of laquinimod for the treatment of multiple sclerosis patients: a systematic review and meta-analysis of clinical trials. Eur J Clin Pharmacol, 2020. **76**(5): p. 611-622.
- 236. Gong, P., et al., *Efficacy of tasquinimod in men with metastatic castration-resistant prostate cancer:* A meta-analysis of randomized controlled trials. Medicine (Baltimore), 2018. **97**(46): p. e13204.
- 237. Williamson, S.C., A.E. Hartley, and R. Heer, *A review of tasquinimod in the treatment of advanced prostate cancer.* Drug Des Devel Ther, 2013. **7**: p. 167-74.

- 238. Bock, K.W., From TCDD-mediated toxicity to searches of physiologic AHR functions. Biochem Pharmacol, 2018. 155: p. 419-424.
- 239. Androutsopoulos, V.P., A.M. Tsatsakis, and D.A. Spandidos, Cytochrome P450 CYP1A1: wider roles in cancer progression and prevention. BMC Cancer, 2009. 9: p. 187.
- 240. van den Bogaard, E.H. and G.H. Perdew, The Enjama of AHR Activation in the Skin: Interplay amona Ligands, Metabolism, and Bioavailability. J Invest Dermatol, 2021. 141(6): p. 1385-1388.
- 241. Bissonnette, R., et al., Tapinarof in the treatment of psoriasis: A review of the unique mechanism of action of a novel therapeutic aryl hydrocarbon receptor-modulating agent. J Am Acad Dermatol, 2021. **84**(4): p. 1059-1067.
- 242. Konstantinou, M.P., et al., Tapinarof-induced folliculitis: The paradigm of activation of the aryl hydrocarbon signaling pathway. J Am Acad Dermatol, 2021. 85(1): p. e37-e38.
- 243. Rikken, G., H. Niehues, and E.H. van den Bogaard, Organotypic 3D Skin Models: Human Epidermal Equivalent Cultures from Primary Keratinocytes and Immortalized Keratinocyte Cell Lines. Methods Mol Biol, 2020. 2154: p. 45-61.
- 244. Nygaard, U.H., et al., Antibiotics in cell culture: friend or foe? Suppression of keratinocyte growth and differentiation in monolayer cultures and 3D skin models. Exp Dermatol, 2015. 24(12): p. 964-5.
- 245. Kamsteeg, M., et al., Type 2 helper T-cell cytokines induce morphologic and molecular characteristics of atopic dermatitis in human skin equivalent. Am J Pathol, 2011. 178(5): p. 2091-9.
- 246. Livak, K.J. and T.D. Schmittgen, Analysis of relative gene expression data using real-time quantitative PCR and the 2(-Delta Delta C(T)) Method. Methods, 2001. 25(4): p. 402-8.
- 247. Smith, F.J., et al., Loss-of-function mutations in the gene encoding filaggrin cause ichthyosis vulgaris. Nat Genet, 2006. 38(3): p. 337-42.
- 248. Scott, I.R. and C.R. Harding, Filaggrin breakdown to water binding compounds during development of the rat stratum corneum is controlled by the water activity of the environment. Dev Biol, 1986. 115(1): p. 84-92.
- 249. Horii, I., et al., Stratum corneum hydration and amino acid content in xerotic skin. Br J Dermatol, 1989. **121**(5): p. 587-92.
- 250. Kezic, S., et al., Loss-of-function mutations in the filaggrin gene lead to reduced level of natural moisturizing factor in the stratum corneum. J Invest Dermatol, 2008. 128(8): p. 2117-9.
- 251. Riethmuller, C., et al., Filaggrin breakdown products determine corneocyte conformation in patients with atopic dermatitis. J Allergy Clin Immunol, 2015. 136(6): p. 1573-1580 e2.
- 252. Kawasaki, H., et al., Altered stratum corneum barrier and enhanced percutaneous immune responses in filaggrin-null mice. J Allergy Clin Immunol, 2012. 129(6): p. 1538-46 e6.
- 253. Jakasa, I., et al., Skin barrier function in healthy subjects and patients with atopic dermatitis in relation to filaggrin loss-of-function mutations. J Invest Dermatol, 2011. 131(2): p. 540-2.
- 254. Flohr, C., et al., Filaggrin loss-of-function mutations are associated with early-onset eczema, eczema severity and transepidermal water loss at 3 months of age. Br J Dermatol, 2010. **163**(6): p. 1333-6.
- 255. Winge, M.C., et al., Filaggrin genotype determines functional and molecular alterations in skin of patients with atopic dermatitis and ichthyosis vulgaris. PLoS One, 2011. 6(12): p. e28254.
- 256. Jinek, M., et al., A programmable dual-RNA-quided DNA endonuclease in adaptive bacterial immunity. Science, 2012. 337(6096): p. 816-21.
- 257. Gasiunas, G., et al., Cas9-crRNA ribonucleoprotein complex mediates specific DNA cleavage for adaptive immunity in bacteria. Proc Natl Acad Sci U S A, 2012. 109(39): p. E2579-86.
- 258. Cong, L., et al., Multiplex genome engineering using CRISPR/Cas systems. Science, 2013. 339(6121): p. 819-23.

- 259. Mali, P., et al., RNA-guided human genome engineering via Cas9. Science, 2013. 339(6121): p. 823-6.
- 260. Shi, H., et al., Research Techniques Made Simple: Delivery of the CRISPR/Cas9 Components into Epidermal Cells. J Invest Dermatol, 2021. 141(6): p. 1375-1381 e1.
- 261. Smits, J.P.H., et al., CRISPR-Cas9Based Genomic Engineering in Keratinocytes: From Technology to Application, JID Innov, 2022, 2(2); p. 100082.
- 262. Dickson, M.A., et al., Human keratinocytes that express hTERT and also bypass a p16(INK4a)-enforced mechanism that limits life span become immortal yet retain normal growth and differentiation characteristics. Mol Cell Biol, 2000. 20(4): p. 1436-47.
- 263. Smits, J.P.H., et al., Immortalized N/TERT keratinocytes as an alternative cell source in 3D human epidermal models. Sci Rep, 2017. 7(1): p. 11838.
- 264. Evrard, C., et al., Deletion of TNFAIP6 Gene in Human Keratinocytes Demonstrates a Role for TSG-6 to Retain Hyaluronan Inside Epidermis. JID Innov, 2021. 1(4): p. 100054.
- 265. Concordet, J.P. and M. Haeussler, CRISPOR: intuitive guide selection for CRISPR/Cas9 genome editing experiments and screens. Nucleic Acids Res, 2018. 46(W1): p. W242-W245.
- 266. Chen, Y., et al., COOH terminus of occludin is required for tight junction barrier function in early Xenopus embryos. J Cell Biol, 1997. 138(4): p. 891-9.
- 267. Furuse, M., et al., Claudin-based tight junctions are crucial for the mammalian epidermal barrier: a lesson from claudin-1-deficient mice. J Cell Biol, 2002. 156(6): p. 1099-111.
- 268. Gallagher, D.N. and J.E. Haber, Repair of a Site-Specific DNA Cleavage: Old-School Lessons for Cas9-Mediated Gene Editing. ACS Chem Biol, 2018. 13(2): p. 397-405.
- 269. Barker, J.N., et al., Null mutations in the filaggrin gene (FLG) determine major susceptibility to earlyonset atopic dermatitis that persists into adulthood. J Invest Dermatol, 2007. 127(3): p. 564-7.
- 270. de Veer, S.J., et al., Proteases: common culprits in human skin disorders. Trends Mol Med, 2014. **20**(3): p. 166-78.
- 271. Ovaere, P., et al., The emerging roles of serine protease cascades in the epidermis. Trends Biochem Sci, 2009. 34(9): p. 453-63.
- 272. Matsui, T., et al., SASPase regulates stratum corneum hydration through profilaggrin-to-filaggrin processing. EMBO Mol Med, 2011. 3(6): p. 320-33.
- 273. Sakabe, J., et al., Kallikrein-related peptidase 5 functions in proteolytic processing of profilaggrin in cultured human keratinocytes. J Biol Chem, 2013. 288(24): p. 17179-89.
- 274. List, K., et al., Loss of proteolytically processed filaggrin caused by epidermal deletion of Matriptase/ MT-SP1. J Cell Biol, 2003. 163(4): p. 901-10.
- 275. Pearton, D.J., et al., Proprotein convertase expression and localization in epidermis: evidence for multiple roles and substrates. Exp Dermatol, 2001. 10(3): p. 193-203.
- 276. Kamata, Y., et al., Neutral cysteine protease bleomycin hydrolase is essential for the breakdown of deiminated filaggrin into amino acids. J Biol Chem, 2009. 284(19): p. 12829-36.
- 277. Presland, R.B., et al., Evidence for specific proteolytic cleavage of the N-terminal domain of human profilaggrin during epidermal differentiation. J Invest Dermatol, 1997. 108(2): p. 170-8.
- 278. Ishida-Yamamoto, A., et al., Translocation of profilaggrin N-terminal domain into keratinocyte nuclei with fragmented DNA in normal human skin and loricrin keratoderma. Lab Invest, 1998. 78(10): p. 1245-53.
- 279. Zhang, D., et al., Characterization of mouse profilaggrin: evidence for nuclear engulfment and translocation of the profilaggrin B-domain during epidermal differentiation. J Invest Dermatol, 2002. **119**(4): p. 905-12.

- 280. Aho, S., et al., Regulatory role for the profilaggrin N-terminal domain in epidermal homeostasis. J Invest Dermatol, 2012. 132(10): p. 2376-2385.
- 281. Pearton, D.J., B.A. Dale, and R.B. Presland, Functional analysis of the profilaggrin N-terminal peptide: identification of domains that regulate nuclear and cytoplasmic distribution. J Invest Dermatol, 2002. **119**(3): p. 661-9.
- 282. Mildner, M., et al., Knockdown of filaggrin impairs diffusion barrier function and increases UV sensitivity in a human skin model. J Invest Dermatol, 2010. 130(9): p. 2286-94.
- 283. van Leersum, F.S., et al., Improving the diagnostic yield for filaggrin: Concealed mutations in the Dutch population. J Allergy Clin Immunol, 2020. 145(6): p. 1704-1706 e2.
- 284. Oji, V., et al., Ichthyosis vulgaris: novel FLG mutations in the German population and high presence of CD1a+ cells in the epidermis of the atopic subgroup. Br J Dermatol, 2009. 160(4): p. 771-81.
- 285. Pendaries, V., et al., Knockdown of filaggrin in a three-dimensional reconstructed human epidermis impairs keratinocyte differentiation. J Invest Dermatol, 2014. 134(12): p. 2938-2946.
- 286. Wu, Z., et al., Highly complex peptide aggregates of the \$100 fused-type protein hornerin are present in human skin. J Invest Dermatol, 2009. 129(6): p. 1446-58.
- 287. Kim, B.E., et al., Loricrin and involucrin expression is down-regulated by Th2 cytokines through STAT-6. Clin Immunol, 2008. 126(3): p. 332-7.
- 288. Pellerin, L., et al., Defects of filaggrin-like proteins in both lesional and nonlesional atopic skin. J Allergy Clin Immunol, 2013. **131**(4): p. 1094-102.
- 289. Steijlen, P.M., et al., Genetic linkage of the keratin type II gene cluster with ichthyosis bullosa of Siemens and with autosomal dominant ichthyosis exfoliativa. J Invest Dermatol, 1994. 103(3): p. 282-5.
- 290. Kremer, H., et al., Ichthyosis bullosa of Siemens is caused by mutations in the keratin 2e gene. J Invest Dermatol, 1994. 103(3): p. 286-9.
- 291. Traupe, H., et al., Ichthyosis bullosa of Siemens: a unique type of epidermolytic hyperkeratosis. J Am Acad Dermatol, 1986. 14(6): p. 1000-5.
- 292. Voorberg, A.N., et al., Vesicular hand eczema transcriptome analysis provides insights into its pathophysiology. Exp Dermatol, 2021. 30(12): p. 1775-1786.
- 293. Eckhart, L., et al., Cell death by cornification. Biochim Biophys Acta, 2013. 1833(12): p. 3471-3480.
- 294. Gutowska-Owsiak, D., et al., Orchestrated control of filaggrin-actin scaffolds underpins cornification. Cell Death Dis, 2018. 9(4): p. 412.
- 295. Bergboer, J.G., et al., Psoriasis risk genes of the late cornified envelope-3 group are distinctly expressed compared with genes of other LCE groups. Am J Pathol, 2011. 178(4): p. 1470-7.
- 296. Doench, J.G., et al., Optimized sgRNA design to maximize activity and minimize off-target effects of CRISPR-Cas9. Nat Biotechnol, 2016. 34(2): p. 184-191.
- 297. Rice, P., I. Longden, and A. Bleasby, EMBOSS: the European Molecular Biology Open Software Suite. Trends Genet, 2000. **16**(6): p. 276-7.
- 298. Freinkel, R.K. and D.T. Woodley, The biology of the skin. 2001: CRC Press.
- 299. Nestle, F.O., et al., Skin immune sentinels in health and disease. Nature Reviews Immunology, 2009.
- 300. Angelova-Fischer, I., et al., Distinct barrier integrity phenotypes in filaggrin-related atopic eczema following sequential tape stripping and lipid profiling. Experimental dermatology, 2011. 20(4):
- 301. Nomura, I., et al., Distinct patterns of gene expression in the skin lesions of atopic dermatitis and psoriasis: a gene microarray analysis. Journal of Allergy and Clinical Immunology, 2003. 112(6): p. 1195-1202.

- 302. Candi, E., et al., p63 in epithelial development. Cell Mol Life Sci, 2008. 65(20): p. 3126-33.
- 303. Denison, M.S. and S.R. Nagy, Activation of the aryl hydrocarbon receptor by structurally diverse exogenous and endogenous chemicals. Annual review of pharmacology and toxicology, 2003. 43(1): p. 309-334.
- 304. Yao, E.F. and M.S. Denison, DNA sequence determinants for binding of transformed Ah receptor to a dioxin-responsive enhancer. Biochemistry, 1992. 31(21): p. 5060-5067.
- 305. Ray, S.S. and H.I. Swanson, Dioxin-induced immortalization of normal human keratinocytes and silencing of p53 and p16INK4a. Journal of Biological Chemistry, 2004. 279(26): p. 27187-27193.
- 306. Pirkle, J.L., et al., Estimates of the half-life of 2,3,7,8-tetrachlorodibenzo-p-dioxin in Vietnam Veterans of Operation Ranch Hand. J Toxicol Environ Health, 1989. 27(2): p. 165-71.
- 307. Rannuq, A., et al., Certain photooxidized derivatives of tryptophan bind with very high affinity to the Ah receptor and are likely to be endogenous signal substances. J Biol Chem, 1987. 262(32): p. 15422-7.
- 308. Rannug, U., et al., Structure elucidation of two tryptophan-derived, high affinity Ah receptor ligands. Chem Biol, 1995. 2(12): p. 841-5.
- 309. McLean, W.I. and A.D. Irvine, Old King Coal-molecular mechanisms underlying an ancient treatment for atopic eczema. The Journal of clinical investigation, 2013. 123(2).
- 310. Rikken, G., et al., Lead optimization of aryl hydrocarbon receptor ligands for treatment of inflammatory skin disorders. Biochem Pharmacol, 2023. 208: p. 115400.
- 311. Ramadoss, P. and G.H. Perdew, The transactivation domain of the Ah receptor is a key determinant of cellular localization and ligand-independent nucleocytoplasmic shuttling properties. Biochemistry, 2005. 44(33): p. 11148-11159.
- 312. Vogel, C.F., et al., Transgenic overexpression of aryl hydrocarbon receptor repressor (AhRR) and AhRmediated induction of CYP1A1, cytokines, and acute toxicity. Environmental health perspectives, 2016. **124**(7): p. 1071.
- 313. Hollingshead, B.D., et al., Inflammatory signaling and aryl hydrocarbon receptor mediate synergistic induction of interleukin 6 in MCF-7 cells. Cancer Res, 2008. 68(10): p. 3609-17.
- 314. Smith, K.J., et al., Editor's Highlight: Ah Receptor Activation Potentiates Neutrophil Chemoattractant (C-X-C Motif) Ligand 5 Expression in Keratinocytes and Skin. Toxicol Sci, 2017. 160(1): p. 83-94.
- 315. Wang, Z., et al., How the AHR Became Important in Cancer: The Role of Chronically Active AHR in Cancer Aggression. Int J Mol Sci, 2020. 22(1).
- 316. Schorle, H., et al., Transcription factor AP-2 essential for cranial closure and craniofacial development. Nature, 1996. 381(6579): p. 235.
- 317. Maytin, E.V., et al., Keratin 10 gene expression during differentiation of mouse epidermis requires transcription factors C/EBP and AP-2. Developmental biology, 1999. 216(1): p. 164-181.
- 318. Mazina, O.M., et al., Redistribution of transcription factor AP-2alpha in differentiating cultured human epidermal cells. J Invest Dermatol, 2001. 117(4): p. 864-70.
- 319. McDade, S.S., et al., Genome-wide analysis of p63 binding sites identifies AP-2 factors as co-regulators of epidermal differentiation. Nucleic Acids Res, 2012. 40(15): p. 7190-206.
- 320. Kousa, Y.A. and B.C. Schutte, Toward an orofacial gene regulatory network. Dev Dyn, 2016. 245(3): p. 220-32.
- 321. Kouwenhoven, E.N., et al., Transcription factor p63 bookmarks and regulates dynamic enhancers during epidermal differentiation. EMBO Rep, 2015. 16(7): p. 863-78.
- 322. Qu, J., et al., Mutant p63 affects epidermal cell identity through rewiring the enhancer landscape. 2018.
- 323. Whitlock Jr, J.P., Induction of cytochrome P4501A1. Annual review of pharmacology and toxicology, 1999. **39**(1): p. 103-125.

- 324. Lo, R. and J. Matthews, *High-resolution genome-wide mapping of AHR and ARNT binding sites by ChIP-Sea*. Toxicological sciences, 2012. **130**(2): p. 349-361.
- 325. Forrester, A.R., et al., Induction of a chloracne phenotype in an epidermal equivalent model by 2, 3, 7, 8-tetrachlorodibenzo-p-dioxin (TCDD) is dependent on aryl hydrocarbon receptor activation and is not reproduced by aryl hydrocarbon receptor knock down. Journal of dermatological science, 2014. 73(1): p. 10-22.
- 326. Sorg, O., AhR signalling and dioxin toxicity. Toxicology letters, 2014. 230(2): p. 225-233.
- 327. Tang, N.-J., et al., Expression of AhR, CYP1A1, GSTA1, c-fos and TGF-α in skin lesions from dioxinexposed humans with chloracne. Toxicology letters, 2008. **177**(3): p. 182-187.
- 328. Racz, E., et al., GATA3 expression is decreased in psoriasis and during epidermal regeneration; induction by narrow-band UVB and IL-4. PLoS One, 2011. 6(5): p. e19806.
- 329. Zolotarenko, A., et al., Integrated computational approach to the analysis of RNA-seq data reveals new transcriptional regulators of psoriasis. Exp Mol Med, 2016. **48**(11): p. e268.
- 330. Panteleyev, A.A. and D.R. Bickers, *Dioxin-induced chloracne--reconstructing the cellular and molecular mechanisms of a classic environmental disease.* Exp Dermatol, 2006. **15**(9): p. 705-30.
- 331. Hammerschmidt-Kamper, C., et al., *Indole-3-carbinol, a plant nutrient and AhR-Ligand precursor, supports oral tolerance against OVA and improves peanut allergy symptoms in mice.* PLoS One, 2017. **12**(6): p. e0180321.
- 332. Wincent, E., et al., *The suggested physiologic aryl hydrocarbon receptor activator and cytochrome P4501 substrate 6-formylindolo[3,2-b]carbazole is present in humans.* J Biol Chem, 2009. **284**(5): p. 2690-2696.
- 333. Opitz, C.A., et al., An endogenous tumour-promoting ligand of the human aryl hydrocarbon receptor. Nature, 2011. **478**(7368): p. 197-203.
- 334. Tjabringa, G., et al., *Development and validation of human psoriatic skin equivalents*. Am J Pathol, 2008. **173**(3): p. 815-23.
- 335. Huang da, W., B.T. Sherman, and R.A. Lempicki, *Systematic and integrative analysis of large gene lists using DAVID bioinformatics resources*. Nat Protoc, 2009. **4**(1): p. 44-57.
- 336. Wickham, H., stringr: Simple, Consistent Wrappers for Common String Operations. 2019.
- 337. Wickham, H., dplyr: A Grammar of Data Manipulation. 2020.
- 338. Benjamini, Y. and Y. Hochberg, Controlling the False Discovery Rate a Practical and Powerful Approach to Multiple Testing. Journal of the Royal Statistical Society Series B-Statistical Methodology, 1995. **57**(1): p. 289-300.
- 339. Saeed, S., et al., Epigenetic programming of monocyte-to-macrophage differentiation and trained innate immunity. Science, 2014. **345**(6204): p. 1251086.
- 340. Kouwenhoven, E.N., et al., Genome-Wide Profiling of p63 DNA-Binding Sites Identifies an Element that Regulates Gene Expression during Limb Development in the 7q21 SHFM1 Locus. PLoS Genet, 2010. **6**(8).
- 341. Novakovic, B., et al., *β-Glucan Reverses the Epigenetic State of LPS-Induced Immunological Tolerance*. Cell, 2016. **167**(5): p. 1354-1368. e14.
- 342. Li, H. and R. Durbin, Fast and accurate short read alignment with Burrows-Wheeler transform. Bioinformatics, 2009. **25**(14): p. 1754-60.
- 343. Zhang, Y., et al., Model-based Analysis of ChIP-Seq (MACS). Genome Biol, 2008. 9(9): p. R137.
- 344. Shao, Z., et al., MAnorm: a robust model for quantitative comparison of ChIP-Seq data sets. Genome Biol, 2012. **13**(3): p. R16.

- 345. McLean, C.Y., et al., GREAT improves functional interpretation of cis-regulatory regions. Nat Biotechnol, 2010. 28(5): p. 495-501.
- 346. Georgiou, G. and S.J. van Heeringen, fluff: exploratory analysis and visualization of high-throughput sequencing data. PeerJ, 2016. 4: p. e2209.
- 347. Qu, J., G. Yi, and H. Zhou, p63 cooperates with CTCF to modulate chromatin architecture in skin keratinocytes. Epigenetics Chromatin, 2019. 12(1): p. 31.
- 348. Natsuga, K., Epidermal barriers. Cold Spring Harb Perspect Med, 2014. 4(4): p. a018218.
- 349. Evora, A.S., et al., Corneocytes: Relationship between Structural and Biomechanical Properties. Skin Pharmacol Physiol, 2021. 34(3): p. 146-161.
- 350. van Smeden, J., et al., The important role of stratum corneum lipids for the cutaneous barrier function. Biochim Biophys Acta, 2014. 1841(3): p. 295-313.
- 351. Everich, S., et al., Cutaneous Barriers and Skin Immunity: Differentiating A Connected Network. Trends Immunol, 2018. 39(4): p. 315-327.
- 352. Al Kindi, A., et al., Staphylococcus aureus second immunoglobulin-binding protein drives atopic dermatitis via IL-33. J Allergy Clin Immunol, 2021. 147(4): p. 1354-1368 e3.
- 353. Yoshida, T., L.A. Beck, and A. De Benedetto, Skin barrier defects in atopic dermatitis: From old idea to new opportunity. Allergol Int, 2022. 71(1): p. 3-13.
- 354. Hadj-Rabia, S., et al., Claudin-1 gene mutations in neonatal sclerosing cholangitis associated with ichthyosis: a tight junction disease. Gastroenterology, 2004. 127(5): p. 1386-90.
- 355. van den Bogaard, E.H.J., et al., Deficiency of the human cysteine protease inhibitor cystatin M/E causes hypotrichosis and dry skin. Genet Med, 2019. 21(7): p. 1559-1567.
- 356. Celebi Sozener, Z., et al., Environmental factors in epithelial barrier dysfunction. J Allergy Clin Immunol, 2020. 145(6): p. 1517-1528.
- 357. El Ghalbzouri, A., et al., Leiden reconstructed human epidermal model as a tool for the evaluation of the skin corrosion and irritation potential according to the ECVAM guidelines. Toxicol In Vitro, 2008. 22(5): p. 1311-20.
- 358. Pecoraro, B., et al., Predicting Skin Permeability by Means of Computational Approaches: Reliability and Caveats in Pharmaceutical Studies. J Chem Inf Model, 2019. 59(5): p. 1759-1771.
- 359. Roberts, M.S., et al., Topical drug delivery: History, percutaneous absorption, and product development. Adv Drug Deliv Rev, 2021. 177: p. 113929.
- 360. Shamaprasad, P., et al., Using molecular simulation to understand the skin barrier. Prog Lipid Res, 2022. **88**: p. 101184.
- 361. Riethmuller, C., Assessing the skin barrier via corneocyte morphometry. Exp Dermatol, 2018. 27(8): p. 923-930.
- 362. van den Bogaard, E., et al., Perspective and Consensus Opinion: Good Practices for Using Organotypic Skin and Epidermal Equivalents in Experimental Dermatology Research. J Invest Dermatol, 2021. 141(1): p. 203-205.
- 363. Arik, Y.B., et al., Barriers-on-chips: Measurement of barrier function of tissues in organs-on-chips. Biomicrofluidics, 2018. 12(4): p. 042218.
- 364. Neupane, R., et al., Alternatives to Biological Skin in Permeation Studies: Current Trends and Possibilities. Pharmaceutics, 2020. 12(2).
- 365. Tarnoki-Zach, J., et al., Development and Evaluation of a Human Skin Equivalent in a Semiautomatic Microfluidic Diffusion Chamber. Pharmaceutics, 2021. 13(6).
- 366. Alexander, H., et al., Research Techniques Made Simple: Transepidermal Water Loss Measurement as a Research Tool. J Invest Dermatol, 2018. 138(11): p. 2295-2300 e1.

- 367. Rinaldi, A.O., et al., Electrical impedance spectroscopy for the characterization of skin barrier in atopic dermatitis. Allergy, 2021. 76(10): p. 3066-3079.
- 368. Fernandes, J., et al., Real-time monitoring of epithelial barrier function by impedance spectroscopy in a microfluidic platform. Lab Chip, 2022. 22(10): p. 2041-2054.
- 369. Wegener, J., A. Hakvoort, and H.J. Galla, Barrier function of porcine choroid plexus epithelial cells is modulated by cAMP-dependent pathways in vitro. Brain Res, 2000. 853(1): p. 115-24.
- 370. Morin, M., et al., Skin hydration dynamics investigated by electrical impedance techniques in vivo and in vitro. Sci Rep, 2020. 10(1): p. 17218.
- 371. Groeber, F., et al., Impedance spectroscopy for the non-destructive evaluation of in vitro epidermal models. Pharm Res, 2015. 32(5): p. 1845-54.
- 372. Mannweiler, R., et al., Direct assessment of individual skin barrier components by electrical impedance spectroscopy. Allergy, 2021. **76**(10): p. 3094-3106.
- 373. Benson, K., S. Cramer, and H.J. Galla, Impedance-based cell monitoring: barrier properties and beyond. Fluids Barriers CNS, 2013. 10(1): p. 5.
- 374. Yeste, J., et al., Engineering and monitoring cellular barrier models. J Biol Eng, 2018. 12: p. 18.
- 375. Furue, M., Regulation of Filaggrin, Loricrin, and Involucrin by IL-4, IL-13, IL-17A, IL-22, AHR, and NRF2: Pathogenic Implications in Atopic Dermatitis. Int J Mol Sci, 2020. 21(15).
- 376. Brewer, M.G., et al., Antagonistic Effects of IL-4 on IL-17A-Mediated Enhancement of Epidermal Tight Junction Function. Int J Mol Sci, 2019. 20(17).
- 377. Smits, J.P.H., et al., Investigations into the FLG Null Phenotype: Showcasing the Methodology for CRISPR/Cas9 Editing of Human Keratinocytes. J Invest Dermatol, 2023. 143(8): p. 1520-1528 e5.
- 378. Arnold, K.A., et al., CLDN1 knock out keratinocytes as a model to investigate multiple skin disorders. Exp Dermatol, 2024. 33(5): p. e15084.
- 379. Smits, J.P.H., et al., The Aryl Hydrocarbon Receptor Regulates Epidermal Differentiation through Transient Activation of TFAP2A. J Invest Dermatol, 2024. 144(9): p. 2013-2028 e2.
- 380. Faway, E., et al., Towards a Standardized Procedure for the Production of Infective Spores to Study the Pathogenesis of Dermatophytosis. J Fungi (Basel), 2021. 7(12).
- 381. Magar, H.S., R.Y.A. Hassan, and A. Mulchandani, Electrochemical Impedance Spectroscopy (EIS): Principles, Construction, and Biosensing Applications. Sensors (Basel), 2021. 21(19).
- 382. Sugawara, T., et al., Tight junction dysfunction in the stratum granulosum leads to aberrant stratum corneum barrier function in claudin-1-deficient mice. J Dermatol Sci, 2013. 70(1): p. 12-8.
- 383. Basler, K., et al., The role of tight junctions in skin barrier function and dermal absorption. J Control Release, 2016. 242: p. 105-118.
- 384. Kirschner, N., et al., Tight junctions and differentiation--a chicken or the egg question? Exp Dermatol, 2012. **21**(3): p. 171-5.
- 385. Nemoto-Hasebe, I., et al., Clinical severity correlates with impaired barrier in filaggrin-related eczema. J Invest Dermatol, 2009. 129(3): p. 682-9.
- 386. Chamlin, S.L., et al., Ceramide-dominant barrier repair lipids alleviate childhood atopic dermatitis: changes in barrier function provide a sensitive indicator of disease activity. J Am Acad Dermatol, 2002. **47**(2): p. 198-208.
- 387. Sugarman, J.L., et al., The objective severity assessment of atopic dermatitis score: an objective measure using permeability barrier function and stratum corneum hydration with computer-assisted estimates for extent of disease. Arch Dermatol, 2003. 139(11): p. 1417-22.

- 388. Breternitz, M., et al., Placebo-controlled, double-blind, randomized, prospective study of a glycerolbased emollient on eczematous skin in atopic dermatitis: biophysical and clinical evaluation. Skin Pharmacol Physiol, 2008. 21(1): p. 39-45.
- 389. Chen, S., R. Einspanier, and J. Schoen, Transepithelial electrical resistance (TEER): a functional parameter to monitor the quality of oviduct epithelial cells cultured on filter supports. Histochem Cell Biol, 2015. **144**(5): p. 509-15.
- 390. Haorah, J., et al., Activation of protein tyrosine kinases and matrix metalloproteinases causes bloodbrain barrier injury: Novel mechanism for neurodegeneration associated with alcohol abuse. Glia, 2008. **56**(1): p. 78-88.
- 391. Liu, X., et al., A biofabricated vascularized skin model of atopic dermatitis for preclinical studies. Biofabrication, 2020. 12(3): p. 035002.
- 392. Crowe, A.R. and W. Yue, Semi-quantitative Determination of Protein Expression using Immunohistochemistry Staining and Analysis: An Integrated Protocol. Bio Protoc, 2019. 9(24).
- 393. Luengo, J., et al., Human Skin Permeation Enhancement Using PLGA Nanoparticles Is Mediated by Local pH Changes. Pharmaceutics, 2021. 13(10).
- 394. Klotz, T., et al., Devices measuring transepidermal water loss: A systematic review of measurement properties. Skin Res Technol, 2022. 28(4): p. 497-539.
- 395. O'Donnell, E.F., et al., The anti-inflammatory drug leflunomide is an agonist of the aryl hydrocarbon receptor. PLoS One, 2010. 5(10).
- 396. Poland, A., E. Glover, and A.S. Kende, Stereospecific, high affinity binding of 2,3,7,8-tetrachlorodibenzo-p-dioxin by hepatic cytosol. Evidence that the binding species is receptor for induction of aryl hydrocarbon hydroxylase. J Biol Chem, 1976. 251(16): p. 4936-46.
- 397. Safe, S.H., Comparative toxicology and mechanism of action of polychlorinated dibenzo-p-dioxins and dibenzofurans. Annu Rev Pharmacol Toxicol, 1986. 26: p. 371-99.
- 398. Szczepanik, M.P., et al., Correlation between transepidermal water loss (TEWL) and severity of clinical symptoms in cats with atopic dermatitis. Can J Vet Res, 2018. 82(4): p. 306-311.
- 399. Egeberg, A., et al., Clinical characteristics, symptoms and burden of psoriasis and atopic dermatitis in adults. Br J Dermatol, 2020. 183(1): p. 128-138.
- 400. Armstrong, A.W. and C. Read, Pathophysiology, Clinical Presentation, and Treatment of Psoriasis: A Review. JAMA, 2020. 323(19): p. 1945-1960.
- 401. Mandlik, D.S. and S.K. Mandlik, Atopic dermatitis: new insight into the etiology, pathogenesis, diagnosis and novel treatment strategies. Immunopharmacol Immunotoxicol, 2021. 43(2): p. 105-125.
- 402. Roelofzen, J.H., et al., Coal tar in dermatology. J Dermatolog Treat, 2007. 18(6): p. 329-34.
- 403. Alhamdow, A., et al., Cancer-related proteins in serum are altered in workers occupationally exposed to polycyclic aromatic hydrocarbons: a cross-sectional study. Carcinogenesis, 2019. 40(6): p. 771-781.
- 404. Larigot, L., et al., AhR signaling pathways and regulatory functions. Biochim Open, 2018. 7: p. 1-9.
- 405. Fernandez-Gallego, N., F. Sanchez-Madrid, and D. Cibrian, Role of AHR Ligands in Skin Homeostasis and Cutaneous Inflammation. Cells, 2021. 10(11).
- 406. Noqueira, S., et al., Tapinarof for the treatment of psoriasis. Dermatol Ther, 2022: p. e15931.
- 407. Tlacuilo-Parra, J.A., et al., Leflunomide in the treatment of psoriasis: results of a phase II open trial. Br J Dermatol, 2004. **150**(5): p. 970-6.
- 408. Czarnowicki, T., et al., Petrolatum: Barrier repair and antimicrobial responses underlying this "inert" moisturizer. J Allergy Clin Immunol, 2016. 137(4): p. 1091-1102 e7.
- 409. Schalkwijk, J., et al., Skin-derived antileucoproteases (SKALPs): characterization of two new elastase inhibitors from psoriatic epidermis. Br J Dermatol, 1990. 122(5): p. 631-41.

- 410. van den Bogaard, E.H., et al., Crosstalk between keratinocytes and T cells in a 3D microenvironment: a model to study inflammatory skin diseases. J Invest Dermatol, 2014. 134(3): p. 719-727.
- 411. Wenande, E. and L.H. Garvey, Immediate-type hypersensitivity to polyethylene glycols: a review. Clin Exp Allergy, 2016. 46(7): p. 907-22.
- 412. Miyaqaki, T. and M. Suqaya, Recent advances in atopic dermatitis and psoriasis: genetic background, barrier function, and therapeutic targets. J Dermatol Sci, 2015. 78(2): p. 89-94.
- 413. Harder, J., et al., Differential gene induction of human beta-defensins (hBD-1, -2, -3, and -4) in keratinocytes is inhibited by retinoic acid. J Invest Dermatol, 2004. 123(3): p. 522-9.
- 414. Liang, S.C., et al., Interleukin (IL)-22 and IL-17 are coexpressed by Th17 cells and cooperatively enhance expression of antimicrobial peptides. J Exp Med, 2006. 203(10): p. 2271-9.
- 415. Lowes, M.A., A.M. Bowcock, and J.G. Krueger, Pathogenesis and therapy of psoriasis. Nature, 2007. **445**(7130): p. 866-73.
- 416. van den Eijnde, W., et al., Skin Barrier Impairment due to the Occlusive Effect of Firefighter Clothing. Ann Work Expo Health, 2020. 64(3): p. 331-337.
- 417. Nedorost, S., A sticky mess-Are moisturizers overused in dermatitis care? J Am Acad Dermatol, 2024.
- 418. Logger, J.G.M., et al., Noninvasive Skin Barrier Assessment: Multiparametric Approach and Pilot Study. Cosmetics, 2019. 6(1): p. 20.
- 419. Niehues, H., et al., Late cornified envelope (LCE) proteins: distinct expression patterns of LCE2 and LCE3 members suggest nonredundant roles in human epidermis and other epithelia. Br J Dermatol, 2016. **174**(4): p. 795-802.
- 420. Schalkwijk, J., et al., Immunohistochemical localization of SKALP/elafin in psoriatic epidermis. J Invest Dermatol, 1993. 100(4): p. 390-3.
- 421. Kezic, S., et al., Natural moisturizing factor components in the stratum corneum as biomarkers of filaggrin genotype: evaluation of minimally invasive methods. Br J Dermatol, 2009. 161(5): p. 1098-104.
- 422. Leclerc, D., et al., Detrimental activation of AhR pathway in cancer: an overview of therapeutic strategies. Curr Opin Immunol, 2021. 70: p. 15-26.
- 423. Paris, A., et al., AhR and Cancer: From Gene Profiling to Targeted Therapy. Int J Mol Sci, 2021. 22(2).
- 424. Holme, J.A., et al., Lung cancer associated with combustion particles and fine particulate matter (PM(2.5)) - The roles of polycyclic aromatic hydrocarbons (PAHs) and the aryl hydrocarbon receptor (AhR). Biochem Pharmacol, 2023. 216: p. 115801.
- 425. Farmahin, R., et al., Time-dependent transcriptomic and biochemical responses of 6-formylindolo[3,2-b]carbazole (FICZ) and 2,3,7,8-tetrachlorodibenzo-p-dioxin (TCDD) are explained by AHR activation time. Biochem Pharmacol, 2016. 115: p. 134-43.
- 426. Moorthy, B., C. Chu, and D.J. Carlin, Polycyclic aromatic hydrocarbons: from metabolism to lung cancer. Toxicol Sci, 2015. 145(1): p. 5-15.
- 427. Mitchell, K.A. and C.J. Elferink, Timing is everything: consequences of transient and sustained AhR activity. Biochem Pharmacol, 2009. 77(6): p. 947-56.
- 428. Hahn, M.E., L.L. Allan, and D.H. Sherr, Regulation of constitutive and inducible AHR signaling: complex interactions involving the AHR repressor. Biochem Pharmacol, 2009. 77(4): p. 485-97.
- 429. Schabitz, A., et al., Spatial transcriptomics landscape of lesions from non-communicable inflammatory skin diseases. Nat Commun, 2022. 13(1): p. 7729.
- 430. Sato, N., et al., CBNplot: Bayesian network plots for enrichment analysis. Bioinformatics, 2022. 38(10): p. 2959-2960.
- 431. Schepps, S., et al., Skin in the game: a review of single-cell and spatial transcriptomics in dermatological research. Clin Chem Lab Med, 2024. 62(10): p. 1880-1891.

- 432. Houser, A.E., et al., The Use of Single-Cell RNA-Sequencing and Spatial Transcriptomics in Understanding the Pathogenesis and Treatment of Skin Diseases. JID Innov, 2023. 3(4): p. 100198.
- 433. Mitamura, Y., et al., Spatial transcriptomics combined with single-cell RNA-sequencing unravels the complex inflammatory cell network in atopic dermatitis. Allergy, 2023. 78(8): p. 2215-2231.
- 434. Sutter, C.H., et al., Ligand Activation of the Aryl Hydrocarbon Receptor Upregulates Epidermal Uridine Diphosphate Glucose Ceramide Glucosyltransferase and Glucosylceramides. J Invest Dermatol, 2023. **143**(10): p. 1964-1972 e4.
- 435. Sorgdrager, F.J.H., et al., Tryptophan Metabolism in Inflammaging: From Biomarker to Therapeutic Target. Front Immunol, 2019. 10: p. 2565.
- 436. Gargaro, M., et al., Tryptophan Metabolites at the Crossroad of Immune-Cell Interaction via the Aryl Hydrocarbon Receptor: Implications for Tumor Immunotherapy. Int J Mol Sci, 2021. 22(9).
- 437. Zhang, R., et al., Nuclear localization of STING1 competes with canonical signaling to activate AHR for commensal and intestinal homeostasis. Immunity, 2023. 56(12): p. 2736-2754 e8.
- 438. Matthews, J. and J.A. Gustafsson, Estrogen receptor and aryl hydrocarbon receptor signaling pathways. Nucl Recept Signal, 2006. 4: p. e016.
- 439. Tischkau, S.A., Mechanisms of circadian clock interactions with aryl hydrocarbon receptor signalling. Eur J Neurosci, 2020. 51(1): p. 379-395.
- 440. Elder, A.J., P. Patel, and S. Daveluy, Tapinarof, in StatPearls. 2024: Treasure Island (FL).
- 441. Silverberg, J.I., et al., Tapinarof cream 1% once daily: Significant efficacy in the treatment of moderate to severe atopic dermatitis in adults and children down to 2 years of age in the pivotal phase 3 ADORING trials. J Am Acad Dermatol, 2024.
- 442. Kircik, L., et al., Rapid Improvements in Itch with Tapinarof Cream 1% Once Daily in Two Phase 3 Trials in Adults with Mild to Severe Plaque Psoriasis. Dermatol Ther (Heidelb), 2024. 14(1): p. 201-211.
- 443. Bagel, J., et al., Tapinarof cream 1% once daily for the treatment of plaque psoriasis: Patient-reported outcomes from the PSOARING 3 trial. J Am Acad Dermatol, 2023. 89(5): p. 936-944.
- 444. Mieremet, A., et al., Characterization of human skin equivalents developed at body's core and surface temperatures. J Tissue Eng Regen Med, 2019. 13(7): p. 1122-1133.
- 445. Mieremet, A., et al., Unravelling effects of relative humidity on lipid barrier formation in human skin equivalents. Arch Dermatol Res, 2019. 311(9): p. 679-689.
- 446. Berkers, T., et al., Compromising human skin in vivo and ex vivo to study skin barrier repair. Biochim Biophys Acta Mol Cell Biol Lipids, 2019. 1864(8): p. 1103-1108.
- 447. Helm, E.Y. and L. Zhou, Transcriptional regulation of innate lymphoid cells and T cells by aryl hydrocarbon receptor. Front Immunol, 2023. 14: p. 1056267.
- 448. Hong, C.H., et al., Selective AhR knockout in langerin-expressing cells abates Langerhans cells and polarizes Th2/Tr1 in epicutaneous protein sensitization. Proc Natl Acad Sci U S A, 2020. 117(23): p. 12980-12990.
- 449. Michielon, E., et al., Micro-environmental cross-talk in an organotypic human melanoma-in-skin model directs M2-like monocyte differentiation via IL-10. Cancer Immunol Immunother, 2020. 69(11): p. 2319-2331.
- 450. Mulder, P.P.G., et al., Monocytes and T cells incorporated in full skin equivalents to study innate or adaptive immune reactions after burn injury. Front Immunol, 2023. 14: p. 1264716.
- 451. Kim, B.S., et al., 3D Cell Printing of Perfusable Vascularized Human Skin Equivalent Composed of Epidermis, Dermis, and Hypodermis for Better Structural Recapitulation of Native Skin. Adv Healthc Mater, 2019. 8(7): p. e1801019.

- 452. Muku, G.E., I.A. Murray, and G.H. Perdew, Activation of the Ah Receptor Modulates Gastrointestinal Homeostasis and the Intestinal Microbiome. Current Pharmacology Reports, 2019. 5(5): p. 319-331.
- 453. Rikken, G., et al., Novel methodologies for host-microbe interactions and microbiome-targeted therapeutics in 3D organotypic skin models. Microbiome, 2023. 11(1): p. 227.
- 454. Dong, F. and G.H. Perdew, The aryl hydrocarbon receptor as a mediator of host-microbiota interplay. Gut Microbes, 2020. 12(1): p. 1859812.
- 455. Cros, A., et al., Homeostatic activation of aryl hydrocarbon receptor by dietary ligands dampens cutaneous allergic responses by controlling Langerhans cells migration. Elife, 2023. 12.



Addendum

Nederlandse samenvatting

Research data stewardship and accessibility

List of abbreviations

Acknowledgements (dankwoord)

Curriculum vitae

PhD portfolio

List of publications

Nederlandse samenvatting

In de introductie van mijn proefschrift (**Hoofdstuk 1**) is de huid en zijn belangrijke functie als barrièreorgaan beschreven. Samengevat bestaat de huidbarrière uit vier componenten: de fysische, chemische, immunologische en microbiologische barrière. Bij inflammatoire huidziekten, zoals atopisch eczeem (AD) en psoriasis, is de huidbarrière aangedaan door een afwijkende differentiatie van keratinocyten, een inflammatoire respons en een disbalans in het huidmicrobioom. De behandeling van inflammatoire huidziekten bestaat uit het smeren van hydraterende en vettende crèmes, het smeren van corticosteroïden, maar ook systemische behandelingen met ontstekingsremmende medicijnen. Eén van de oudste behandelingen van inflammatoire huidziekten is koolteer, waarvan ontdekt werd dat het zijn therapeutische effect uitoefent via activatie van de aryl koolwaterstof receptor (AHR). Hoewel de AHR oorspronkelijk ontdekt is als een omgevingssensor voor xenobiotica, kan de AHR een grote variëteit aan zowel endogene als exogene liganden binden en functioneert het zo als een transcriptiefactor die de genexpressie reguleert. De AHR werkt via verschillende intracellulaire signaleringsroutes, die gekenmerkt worden door specifieke interacties met andere eiwitten zoals de arylkoolwaterstof nucleaire translocator (ARNT). Hierdoor heeft de AHR invloed op vele diverse processen in de huid, waaronder de celdeling en differentiatie van keratinocyten en de vorming van de huidbarrière. Ook reguleert de AHR de inflammatoire respons in de huid, waardoor het een geschikt doelwit is in de behandeling van inflammatoire huidziekten. In dit proefschrift zijn de fysiologische effecten van AHR signalering op de vorming en het behoud van de huidbarrière onderzocht, evenals de mogelijkheden voor nieuwe AHR-gerichte therapieën in de behandeling van AD.

In **Hoofdstuk 2** en **3** zijn twee nieuwe groepen van AHR-bindende stoffen (liganden) bestudeerd. In **Hoofdstuk 2** is een groep selectieve liganden, genaamd SGA verbindingen, onderzocht. Een groot aantal SGAs is eerst onderzocht op hun potentie tot AHR activatie. Dit leidde tot identificatie van enkele liganden met een wisselende potentie. De sterkste AHR liganden zijn eerst getest in muis- en humane keratinocyt cellijnen. In beiden activeerden zij de AHR, zonder schadelijke bijwerkingen. In monolaag celkweken was de expressie van genen die geassocieerd zijn met keratinocytdifferentiatie, zoals hornerine en filaggrine, verhoogd op een AHR-afhankelijke manier. In 3D humane epidermis equivalenten werd eenzelfde effect gezien ten aanzien van de differentiatie status van keratinocyten. Vervolgens is de effectiviteit van geselecteerde SGAs in het verminderen van AD-gerelateerde kenmerken in de epidermis equivalenten. Middels RNA-sequencing werden clusters

van AD-gerelateerde genen gevonden die onder invloed van de SGAs veranderen. Herstel vond met name plaats in processen betrokken bij de keratinocyt differentiatie en hyperproliferatie de inflammatoire respons. Deze effecten konden gevalideerd worden op eiwit-niveau. Tenslotte werden de ontstekingsremmende effecten onderzocht in een in vivo muismodel voor acute huidontsteking. Ook in dit model was topicale toediening van SGAs effectief in het reduceren van roodheid, verdikking en de infiltratie van neutrofiele granulocyten in de huid. Samengevat tonen deze resultaten aan dat SGAs veelbelovend zijn in de ontwikkeling van een lokale behandeling voor inflammatoire huidziekten.

In Hoofdstuk 3 is een andere groep verbindingen, carboxamides, onderzocht op hun vermogen om de AHR te activeren en AD-kenmerken in in vitro modellen te verminderen. Zoals in de eerdere studie met de SGAs, zijn de carboxamides en hun concentratie eerst geselecteerd op basis van AHR activatie en cellulaire vitaliteit. In 3D humane epidermis equivalenten leidde het toevoegen van carboxamides tot een verhoogde keratinocyt differentiatie, zowel op gen- als eiwit-niveau. In humane epidermis equivalenten met AD kenmerken, waren ook de carboxamides effectief in het reduceren ervan. Dit toont aan dat een verscheidenheid aan AHR activerende liganden bruikbaar zijn als mogelijke medicatie voor inflammatoire huidziekten, zoals AD.

Zoals besproken in de introductie, kan de AHR een grote verscheidenheid aan liganden binden en zo zijn effect uitoefenen via verschillende cellulaire signaalroutes. Om de fysiologische rol van de AHR in de huid te begrijpen en andere geactiveerde signaalroutes door de AHR liganden uit te sluiten, zijn geschikte in vitro modellen essentieel. Daarom is een keratinocyt cellijn ontwikkeld middels de CRISPR/Cas9 techniek waarin de AHR niet aanwezig is (knock out). Deze CRISPR-Cas9 techniek moest eerst geoptimaliseerd worden voor het gebruik in keratinocyten, hetgeen beschreven is in Hoofdstuk 4. In deze "proof-of-concept" studie is een onsterfelijke keratinocyt cellijn (N/TERT-2G) zodanig aangepast met CRISPR-Cas9 zodat filaggrine (FLG), een belangrijke component van de huidbarrière en risico-gen voor het ontwikkelen van AD, uitgeschakeld is. Zogeheten "guide-RNAs" gericht tegen exon 3 werden ontwikkeld en vervolgens getransfecteerd in N/TERT-2G cellen, tezamen met synthetisch Cas9 eiwit. Uit geselecteerde klonale cellijnen met variaties in het FLG gen waardoor geen functioneel filaggrine eiwit tot expressie komt, zijn 3D humane epidermis equivalenten gemaakt. Deze equivalenten lieten verlies zien van de granulaire laag in de epidermis, wat geassocieerd is met FLG mutaties, en verlies van filaggrine eiwitexpressie. Daarbij was ook de huidbarrière aangedaan, dat resulteerde in barrière defecten van

filaggrine-deficiënte equivalenten. Om te laten zien dat deze effecten het gevolg waren van de geïntroduceerde *FLG* mutatie, werd het *FLG* gen succesvol hersteld in de filaggrine-deficiënte lijnen met behulp van CRISPR/Cas9 "homology directed repair". Met een vergelijkbaar protocol genereerden we AHR deficiënte cellen om het specifieke effect van AHR op de biologie van keratinocyten te onderzoeken, als onderdeel van **Hoofdstuk 5.**

In Hoofdstuk 5 werden RNA- en ChIP-sequencing experimenten uitgevoerd om het moleculaire mechanisme volgend op AHR activatie in de cel beter te begrijpen. Keratinocyten, gestimuleerd met dioxine (TCDD) of koolteer, lieten tijdsafhankelijke vergelijkbare veranderingen zien in RNA-expressie. Door de identificatie van vroege en late responsgenen suggereren wij dat een deel van de AHR respons in keratinocyten in feite een secundair effect van AHR activatie is. Vroege responsgenen waren betrokken bij processen zoals epitheelontwikkeling en eiwitfosforylering, terwijl late responsgenen een rol speelden in keratinocyt differentiatie en epidermisontwikkeling. Door ChIP-sequencing uitgevoerd met AHR- en H3K27ac-antilichamen hebben wij genomische regio's geïdentificeerd die direct na AHR-activering door AHR worden gebonden, evenals een specifieke subset van actieve enhancerregio's geassocieerd met deze AHR-binding. Daarnaast werden verschillende regio's geïdentificeerd die verband hielden met secundaire (late) effecten van AHR-activatie. De AHR kan dus enhancer-elementen in het genoom binden waardoor het de werking van andere transcriptiefactoren kan reguleren. Wij veronderstelden dat deze transcriptiefactoren op hun beurt de expressie van epidermale differentiatiegenen aansturen als secundair proces. Om deze hypothese te toetsen, zijn beide datasets geïntegreerd resulterend in de identificatie van transcriptie factor AP-2 alpha (TFAP2A). De expressie van deze transcriptiefactor wordt direct gereguleerd door de AHR, en is bekend een rol te spelen in ontwikkeling van de epidermis. De door ons gemaakte AHR-deficiënte cellijnen gestimuleerd met TCDD lieten inderdaad geen verhoging zien van TFAP2A expressie, in tegenstelling tot AHR wildtype lijnen. Daarnaast werden ook TFAP2A-deficiënte cellijnen gegenereerd middels CRISPR-Cas9, waarmee wij de rol van de AHR-TFAP2A signaalroute in epidermale differentiatie aantoonden. Epidermale equivalenten gemaakt van TFAP2A-deficiënte keratinocyten waren onderontwikkeld, met een afwijkende keratinocyt differentiatie. Activatie van de AHR in deze TFAP2A-deficiënte modellen liet slechts een minimale verhoging zien in epidermale differentiatie, waarschijnlijk veroorzaakt door andere familieleden uit de AP1/AP2 familie van transcriptiefactoren. Deze studie levert bewijs voor de aanwezigheid van een AHR-TFAP2A signaalroute die nodig is voor een goede ontwikkeling van de epidermis en barrièrefunctie van de huid.

In mijn proefschrift heb ik tevens getracht de fysiologische rol van de AHR in de vorming van de huidbarrière beter te begrijpen door de ontwikkeling van kwantitatieve meettechnieken. In Hoofdstuk 6 onderzochten we een nieuwe methode waarbij met elektrische impedantie spectroscopie (EIS) de epidermale barrièrefunctie gemeten kan worden, zonder daarbij de huid equivalenten te schaden. Middels EIS, gemeten over een frequentierange, konden wij de ontwikkeling van de huidbarrière volgen in de tijd, zonder daarvoor de huid equivalenten te oogsten. Onze EIS-metingen, gecombineerd met morfologische en histologische analyses, leidden tot de correlatie van verschillende delen van de impedantiegrafieken aan diverse processen betrokken bij de ontwikkeling van de huidbarrière. Impedantie op lage frequenties bleek geassocieerd met epidermisontwikkeling en hoge frequenties werden geassocieerd met de dikte van het stratum corneum. Ook konden we door toepassing van EIS het therapeutische effect van AHR liganden bepalen in vitro. In AD-epidermale modellen die de pathologie van AD nabootsen door toevoeging van ziekte-gerelateerde ontstekingsmediatoren, herstelden alle AHR liganden (waaronder de SGAs en carboxamides) de barrière defecten.

De preklinische studies in mijn proefschrift tonen aan dat AHR een therapeutisch target is voor het herstellen van barrièredefecten in inflammatoire huidzieken. In deze experimentele studies gebruikten we in vitro humane modellen of in vivo muismodellen. Hoofdstuk 7 omvat een translatie van deze laboratorium modellen naar de mens waarbij wij het effect van koolteer op de huidbarrière onderzocht hebben in gezonde humane vrijwilligers. Hiervoor werd de hoornlaag van de huid verwijderd met plakband (tape strippen) om huiddefecten, zoals in AD, na te bootsen. Voor of na het tape strippen werd de huid blootgesteld aan koolteercrème of de basiscrème. Onverwacht veroorzaakte de basiscrème een acute ontsteking van de huid nadat deze getapestript was. Dit gaf ons de mogelijkheid om de ontstekingsremmende effecten van koolteer te onderzoeken. De verdikking van de epidermis en het aantal afweercellen in de huid, die verhoogd was door de basiscrème, was significant minder in de met koolteer behandelde huid. Ook bleek de migratie van specifieke antigeen presenterende cellen (Langerhans cellen) van de epidermis naar de dermis verminderd na koolteerbehandeling in vergelijking met de basiscrème. Koolteer remt dus de acute infiltratie van immuuncellen in de huid die ook belangrijk zijn in chronische ontstekingsziekten, zoals AD.

Ten slotte integreer ik in hoofdstuk 8 de bevindingen van mijn experimentele studies met een algemene discussie en toekomstperspectieven. Ik richt me in mijn discussie op de vooruitzichten voor therapeutische ontwikkeling van AHR-liganden. Daarbij leg ik de nadruk op de diversiteit van liganden en hun receptoraffiniteit, de celspecificiteit van AHR expressie, en de rol voor het weefselen de celmicro-omgeving in het beïnvloeden van de effecten van AHR signalering. Concluderend heeft mijn onderzoek meer kennis geleverd over de functie van AHR signalering in de huid. Ik heb aangetoond dat AHR signalering belangrijk is voor keratinocytproliferatie, differentiatie en huidbarrièrefunctie, evenals de regulatie van ontstekingsprocessen en afweercellen in de huid. Met deze kennis kunnen we de therapeutische waarde van AHR-activerende moleculen, en hun bijwerkingen, in de behandeling van chronische inflammatoire huidziekten beter in kaart brengen.

Research data stewardship and accessibility (FAIR)

Open access publications

The following chapters in this thesis have been published under open access and are accessible through their mentioned DOIs. Datasets can be requested through contacting the last author:

Chapter 2 Lead optimization of aryl hydrocarbon receptor ligands for treatment of inflammatory skin disorders.

Biochemical Pharmacology. February 2023.

DOI: 10.1016/j.bcp.2022.115400

Chapter 3 Carboxamide derivatives are potential therapeutic AHR ligands for restoring IL-4 mediated repression of epidermal differentiation proteins.

International Journal of Molecular Sciences. February 2022.

DOI: 10.3390/ijms23031773

Chapter 4 Investigations into the FLG null phenotype: showcasing the methodology for CRISPR/Cas9 editing of human keratinocytes.

Journal of Investigative Dermatology. August 2023.

DOI: 10.1016/j.jid.2023.02.021

Chapter 5 The aryl hydrocarbon receptor regulates epidermal differentiation through transient activation of TFAP2A.

Journal of Investigative Dermatology. September 2024.

DOI: 10.1016/j.jid.2024.01.030

Chapter 6 Electrical impedance spectroscopy quantifies skin barrier function in organotypic in vitro epidermis models.

Journal of Investigative Dermatology. November 2024.

DOI: 10.1016/j.jid.2024.03.038

Data availability

Data from all chapters was stored and processed on local department servers, which are supported and backed up regularly by the ICT department of Radboudumc. Execution of experiments was documented either in the electronic labjournal labguru, which is accessible for all members of the department, or in paper labjournals which are stored at the department at Radboudumc. These secure storage options safeguard the availability, integrity and confidentiality of the data.

In addition, data and metadata are stored in the Radboud Data Repository under the same title as this thesis and available upon request Lastly, several large datasets are accessible through the Gene Expression omnibus (see below).

Chapter 2 Large RNA sequencing datasets of chapter 2 (Lead optimization of aryl hydrocarbon ligands for treatment of inflammatory skin disorders, *Biochemical Pharmacology*, February 2023) were made available at the Gene Expression Omnibus (GEO) database under accession number GSE212539 (https://www.ncbi.nlm.nih.gov/geo/guery/acc.cgiacc=GSE212539).

Chapter 5 Large RNA sequencing and H3K27ac data sets from chapter 5 (The aryl hydrocarbon receptor regulates epidermal differentiation through transient activation of TFAP2A, *Journal of Investigative Dermatology*, September 2024) were made available at the Gene Expression Omnibus (GEO) database under accession number GSE226047

(https://www.ncbi.nlm.nih.gov/geo/query/acc.cgi?acc=GSE226047).

Ethics and privacy

Chapter 7 The data in chapter 7 is based on the results of research involving human participants, which were conducted in accordance with relevant national and international legislation and regulations, guidelines, codes of conduct and Radboudumc policy. Ethical approval for these studies was granted by medical ethical committee (Commissie Mensgebonden Onderzoek) Arnhem-Nijmegen under file number 2017-3177 and NL-number NL60891.091.17. Informed consent was obtained from all participants before participation. The privacy of participants in this study was warranted by the use of fully anonymized data.

List of abbreviations

3D	three dimensional	GPAC	gram-positive anaerobic cocci
AD	atopic dermatitis	GRHL	grainyhead like transcription factor
AHR	aryl hydrocarbon receptor	H3K27ac	histone 3 lysin 27 acetylation
AMP	antimicrobial peptides	hBD	human beta defensin
ANOVA	analysis of variance	HDR	homology directed repair
APC	antigen presenting cell	HE	hematoxylin and eosin
ARNT	aryl hydrocarbon	HEE	human epidermal equivalent
	nuclear translocator	HRNR	hornerin
bHLH/PAS	basic-helix-loop-helix/per-arnt-sim	Hsp90	heat shock protein 90
BLMH	bleomycin hydrolase	I3C	indole-3-carbinole
$C_{A'}$	cellular membrane capacitance	IF	immunofluorescence
Cas-9	CRISPR associated protein 9	IL	interleukin
CASP14	caspase 14	IMA	immunahr
C_{Cell}	cellular capacitance	IRF	interferon regulatory factor
C _{FI}	electrode capacitance	IV	ichthyosis vulgaris
CFD	cutting frequency determination	IVL	involucrin
ChIP	chromatin immunoprecipitation	IMQ	imiquimod
CLDN	claudin	JAK	Janus kinase
CRISPR	clustered regularly interspaced	KLF4	Krüppel-like factor 4
	short palindromic repeats	KLK	kallikrein-related peptidase
c-SRC	cellular SRC kinase	KRT	keratin
CYP	cytochrome P450	LAQ	laquinimod
CT	coal tar	LCE	late cornified envelope
DEG	differentially expressed gene	LOR	loricrin
DMSO	dimethylsulfoxide	LRG	late responsive gene
DRE	dioxin responsice element	LY	lucifer yellow
EDC	epidermal differentiation complex	MAPK	mitogen-activated protein kinase
EGFR	epidermal growth factor receptor	MCM6	mini-chromosome maintenance
EIS	electrical impedance spectroscopy		protein 6
EISdiff	keratinocyte differentiation-	MPO	myeloperoxidase
	attributable electrical impedance	MT-SP1	matriptase
EIS ^{SC}	stratum corneum-attributable	NHEJ	non-homologous end joining
	electrical impedance	NHEK	normal human
ERG	early responsive gene		epidermal keratinocytes
FICZ	6-formylindolo(3,2-b)carbazole	NMF	natural moisturizing factor
FLG	filaggrin	NOS	nitric oxide syntathase
GO	gene ontology	NRF2	NF-E2 p45-related factor 2

TFAP2A

OVOL1	ovo like transcriptional repressor 1
PAH	polycyclic aromatic hydrocarbon
PAM	protospacer adjacent motif
PBS	phosphate-buffered saline
PCA	2-pyrrolidone-5-carboxylic acid
PCA	principal component analysis
PEG	polyethylene glycol
PI	peptidase inhibitor
qPCR	quantitative PCR
Pso	psoriasis
$R_{A'}R_{B}$	cellular membrane resistance
R_Cell	cellular resistance
R_{Cyt}	cytoplasmic resistance
R_{Medium}	culture medium resistance
RNP	ribonucleoprotein complex
RNS	reactive nitrogen species
ROQ	roquinimex
ROS	reactive oxygen species
R_p	paracellular resistance
SAhRM	selective AH receptor modulator
SASPase	skin-specific retroviral
	aspartic protease
SC	stratum corneum
SG	stratum granulosum
sgRNA	single guide RNA
SKALP	skin-derived antileukoproteinase
SLS	sodium lauryl sulfate
SNP	single nucleotide polymorphism
SPRR3	small proline rich protein 3
ssODN	single strand donor oligonucleotide
STAT	signal transducer and activator
	of transcription
TASQ	tasquinimod
TCDD	2,3,7,8-tetrachlorodibenzo- <i>p</i> -dioxin
TEER	transepithelial electrical resistance
TERT	telomerase reverse transcriptase
TEWL	transepidermal water loss
TF	transcription factor

transcription factor AP-2α

TGM1 transglutaminase 1 TNF tumor necrosis factor TP tumor protein 12-O-tetradecanoylphorbol-TPA 13-acetate Treg T-regulatory TSLP thymic stromal lymphopoietin UCA urocanic acid XAP2 X-associated protein 2 XME xenobiotic metabolizing enzyme xenobiotic response element XRE

Dankwoord

'T is moëi gewaes. Een einde aan dit hoofdstuk. Maar wat ben ik dankbaar dat ik mijn PhD heb mogen doen bij de warme mensen die de afdeling Dermatologie van het Radboudumc maken. Vanuit mijn stage kon ik bij jullie aan de slag als PhD. Jullie hebben me enorm veel geleerd over het doen van onderzoek, maar daarnaast ook over mezelf en over wat ik verder wil. Ik denk dat de meeste van jullie me kennen als rustig persoon en vooral als iemand van niet te veel woorden. Mijn dankwoord zal dan misschien niet een heel epistel worden, maar weet dat alles wat ik zeg gemeend is. En dat ik boven alles vooral erg dankbaar ben voor de mogelijkheid om me bij jullie te hebben kunnen ontwikkelen tot waar ik nu sta.

Om te beginnen mijn promotieteam. Bedankt voor alle spar sessies en creatieve ideeën die ervoor gezorgd hebben dat dit boekje tot stand heeft kunnen komen. Dat het met tijden met ups en downs ging weten we allemaal, maar bedankt dat jullie me daarin gepusht hebben en de kans gegeven hebben om mezelf te ontwikkelen. We mogen samen trots zijn op dit resultaat! Beste (**Prof. Dr.**) Ellen. Je hebt de rol als mijn promotor gedurende miin PhD overgenomen van Joost. En wat heb ie dat goed gedaan, Je creatieve ideeën en manieren om het bruikbare in alle resultaten te zien (ook al vond ik het experiment mislukt) zijn bewonderenswaardig. Je hebt me laten zien dat het onderzoek niet altijd zwart en wit is, maar vooral ook heel veel grijs. Naast dat je mij hebt laten groeien in de persoon die ik nu ben, heb ik jou ook mogen zien groeien tijdens mijn PhD. Je mag trots zijn op de manier waarop jij verschillende onderzoeksvelden bij elkaar kan brengen, soms wat gewaagde ideeën voor onderzoek hebt, maar vooral ook de warme groep mensen waar je leiding aan geeft. Ik ben benieuwd naar wat de toekomst jullie mag brengen aan resultaten en kijk uit naar toekomstige publicaties.

Beste (Dr.) Jos, begonnen als jouw stagiair op het CRISPR/Cas9 onderzoek tijdens mijn master. Jouw enthousiasme over het onderzoek en de mogelijkheden in de dermatologie werkten aanstekelijk, dus toen de kans zich voordeed om vanuit mijn stage verder te gaan als PhD bij jullie groep nam ik die kans met beide handen aan. Daarna als kamergenootjes tijdens het afronden van je eigen PhD. Eerst op de achterste kamer, waar de nodige 'diepzinnige' gesprekken hebben plaatsgevonden. Later een stukje naar voren in de gang als mijn copromotor. Bedankt voor alle inspiratie en het praktisch meedenken tijdens mijn eigen onderzoek. Het was enorm fijn om een copromotor te hebben die zo dicht op de werkvloer staat en daarom ook zeker over de praktische zaken mee kon denken. Ook met persoonlijke vragen of met de 'hoe werkt dit nu weer' vragen, kon ik altijd bij je terecht. Je hebt me begeleid tijdens mijn hele traject tot onderzoeker, enorm bedankt daarvoor!

(**Dr.**) **Patrick,** ik wist altijd precies wat ik aan je had. Lekker direct, duidelijk en met oog voor detail. Maar daarnaast ook een schat aan kennis over het onderzoek doen. Mocht er ergens troubleshooting nodig zijn, had jij daar altijd wel ideeën over. Daarvoor heb ik ook wel eens oude labjournalen van jou gebruikt en ik denk dat er maar weinig mensen zijn die zo precies en duidelijk kunnen documenteren wat er gedaan is. Ook de liefde voor oude rockers deelden we, ondanks dat de muzieksmaak op het lab op zijn minst divers te noemen was. Bedankt voor de begeleiding tijdens het schrijven van dit boekje. Jij kon precies de vinger leggen

op waar nog verduidelijking nodig was. Dat er heel wat minder dubbele spaties en

dubbele referenties in dit onderzoek staan, heb jij zeker aan meegeholpen.

(**Prof. Dr.**) **Joost Schalkwijk**, je hebt me begeleid tijdens het eerste jaar van mijn PhD. Bedankt dat je mij deze kans bood om in deze mooie groep mijn onderzoek voort te zetten. Ik heb je leren kennen als rustige persoonlijkheid, maar met enorm veel kennis van het vakgebied. Je hebt de fundering gelegd voor een groep warme mensen die nog steeds enorm mooi en vooruitstrevend onderzoek leveren, daar mag je trots op zijn! Hopelijk geniet je nu heerlijk van je pensioen met veel tijd voor je familie en hobby's.

Lieve collega's van het lab dermatologie. Wat zijn jullie een leuke gezellige groep mensen die altijd voor elkaar klaar staan, daar mogen jullie trots op zijn! Hoewel de groep 'multicultureel' was (zeker met mij als Limburger) was iedereen altijd welkom voor een praatje over het onderzoek of persoonlijke leven, een grap of gewoon een goed feestje tijdens congres.

Ivonne en **Diana**, de praktische krachten die altijd een helpende hand wilden bieden tijdens het uitvoeren van mijn onderzoek. Bedankt voor de bergen werk die jullie voor mij verzet hebben, ook al kon ik soms iets chaotisch zijn in het overbrengen van mijn ideeën en plannen. Jullie gingen altijd weer met hetzelfde enthousiasme aan de slag. Maar ook voor een persoonlijk gesprek kon ik altijd bij jullie terecht. Ik ga de vele gesprekken over het werk, de (klein)kinderen maar zeker ook de voor- en nabespreking van het Songfestival missen.

Patrick (PJ), altijd in voor een grapje en vooral veel lol hebben als mensen hapten (ja, ook ik). Het was altijd te horen als jij als eerste op het lab de muziek had aangezet en ik heb dan ook van jou een heel nieuw muziekgenre leren kennen (zo af en toe draai ik stiekem nog wat Gunther). Maar ik heb ook gebruik kunnen maken van jouw kennis tijdens mijn PhD, maar ook al tijdens mijn stage. Niet alleen over het moleculaire werk, maar ook bij de AIVD kerstpuzzels die elk jaar tijdens de pauzes

gemaakt moesten worden. Bedankt voor het meedenken over mijn onderzoek, maar ook voor de lach tijdens de werkdag als ik de grap niet altijd meteen doorhad.

Hanna, je bood altijd een rustig luisterend oor en opperde nieuwe, inspirerende ideeën voor mijn onderzoek tijdens onze labmeetings. Maar ook voor een feestje bij de borrels of tijdens congressen was je zeker te porren. Tijdens mijn PhD heb ik je je eigen onderzoekslijn zien opbouwen, maar daarnaast ook een eigen gezin. Hoe je daar de balans in bewaard is iets waar je trots op mag zijn. Ik wens je hier dan ook veel geluk mee in de toekomst.

Felicitas, mijn roomie tijdens mijn PhD. We zaten ongeveer in dezelfde periode van onze PhD en konden dan ook naast het onderzoek goed praten over de praktische zaken van het schrijven van een thesis (met de nodige klaag momentjes). We hadden een gedeelde onderzoekslijn en hebben ook een aantal papers samen geschreven. Jouw precisie en handigheid met computerprogramma's heb ik daarin zeker kunnen waarderen. We zijn samen op congres geweest in Amerika en onze road trip door New York heb ik als erg bijzonder ervaren. Wat hebben we moeten rennen om de voorstelling van Wicked te halen, maar het is ons gelukt! En nu rennen we allebei naar de eindstreep van onze PhD. Ik wens je heel veel succes met het afronden van je eigen traject, maar dat gaat ook zeker lukken!

Luca, op dezelfde dag kregen we te horen dat onze theses geaccepteerd waren, daar kunnen we trots op zijn! We kunnen nu dan ook samen sparren over het drukwerk en de laatste voorbereidingen. Ik heb je leren kennen als een goed georganiseerd persoon die elke uitdaging aangaat. Naast de soms lange dagen samen op het lab voor het EIS paper, hebben we ook genoeg gelachen samen. Van het organiseren van labuitjes, gezamenlijke verjaardags traktaties en het vieren van het afscheid van ons lab met airfryers en dansen op de lege tafels. Ik wens je veel succes met je eigen verdediging binnenkort en ook heel veel geluk samen met Brandon gewenst op jullie bruiloft.

Gijs, op het moment dat ik dit schrijf heb je net je eigen verdediging gehad. En wat heb je het goed gedaan! Samen hebben we een aantal papers afgemaakt en mede daardoor kon ik een vliegende start maken aan mijn eigen onderzoek. Je wist altijd alle ballen in de lucht te houden: je eigen onderzoek, het verbouwen van een huis en het uitbreiden van je eigen gezin. En altijd met een lach en de woorden 'komt goed'. En goed is het ook zeker gekomen! Veel geluk en plezier gewenst bij je verdere loopbaan!

Danique, even hebben we nog bij elkaar gezeten op de achterste kamer en dat was altijd erg gezellig. De nodige sterke verhalen hebben de revue gepasseerd. Een tijd geleden alweer heb je je eigen PhD verdedigd. Ik vind het knap hoe je dit afgerond hebt terwijl je al een nieuwe baan had en ook nog je eigen gezin hebt uitgebreid. Veel geluk gewenst met je verdere toekomst en wie weet spreken we elkaar op mijn verdediging!

Dan alle PhDs die 'na mijn tijd' zijn gekomen: Noor, je bent begonnen als mijn stagiair en hier liet je al zien wat voor creatief persoon je was. Naast het goed uitvoeren van experimenten waar je aan een half woord van mij genoeg had, kon ie ook nog eens heerlijk bakken. Je enthousjasme was blijkbaar groot genoeg om een eigen PhD traject bij derma te beginnen. Heel veel succes met het afronden van je eigen project! **Aranka**, ik ken je nog vooral van je stage bij ons waar je goed georganiseerd kon werken. Succes bij ie nieuwe baan in Utrecht! Rens, ik heb alleen je sollicitatie mee mogen maken, maar daar liet je al zien dat je een enthousiast en gedreven persoon was die zich goed had ingelezen in ons vakgebied. Heel veel succes met je eigen project!

Piet, de oud gediende tussen ons jonge broekies, maar wel de handigste met techniek. Als er een programma geschreven moest worden voor het tellen van cellen of er was (weer eens) iets met de software van de microscoop konden we altijd bij jou aankloppen. Maar die interesse voor techniek leidde ook wel eens tot mislukte experimenten met niet helemaal werkende nieuwe apparaten om huideigenschappen te meten. Gelukkig liet jij je niet uit het veld slaan en was je overal even enthousiast over. Geniet van je pensioen en de tijd met je gezin!

Lieve medewerkers van het secretariaat, zonder jullie zou de afdeling een heel stuk minder soepel draaien. Op de oude afdeling stond de deur altijd open en konden we altijd binnen lopen voor het maken van een praatje of het bespreken van het weekend. Ook als er weer eens een stagiair aangemeld moest worden of er iets anders praktisch geregeld moest worden, waren we bij jullie altijd aan het juiste adres.

De afdeling dermatologie is natuurlijk niet compleet zonder de mensen van de kliniek. Mensen van de klinische staf, waaronder (prof. dr.) Elke de Jong en (dr.) Juul van den Reek, bedankt voor jullie opmerkingen en ideeën over het onderzoek en het perspectief van de patiënt wat jullie hierin konden uitlichten. Jullie herinnerden ons eraan waar we het onderzoek voor doen en ik moet eerlijk zeggen dat jullie verhalen ook mijn eigen interesse voor het helpen van patiënten heeft aangewakkerd. Dan alle arts-onderzoekers, er zijn er vele geweest tijdens mijn onderzoek, dus ik hoop dat jullie me vergeven als ik niet iedereen bij naam noem. Het luisteren naar jullie onderzoek tijdens de journal clubs was altijd erg

interessant. Ik wens jullie heel veel succes met het afronden van jullie onderzoek en verdere opleiding! In het bijzonder een dankjewel voor Jade Logger en Tessa Kouwenhoven. Bedankt voor het organiseren en verzorgen van de klinische onderzoeken voor het koolteer paper. Ja het is nog steeds niet gepubliceerd... Maar deze resultaten zullen vast en zeker een mooie plaats krijgen. Ook een dankjewel aan Mirjam Schaap. Fijn dat ik jou kon helpen bij het experimenteel werk voor je onderzoek naar detectie van huideiwitten in psoriasis. Het is een mooi paper geworden, daar mag je trots op zijn!

Dear **Gary Perdew**, a combined grant with your research group allowed me to perform my own PhD trajectory in the interesting world of the aryl hydrocarbon receptor. We got to meet during the AHR meeting at Penn State University. Here I learned about all the different fields in which the AHR plays an important role. Thank you for the opportunity to talk and gain new ideas about the AHR for my own research. A thanks also goes out to the members of your group with which we collaborated to show the potential of the SGA derivatives in treatment of atopic dermatitis. It took a bit of time, but in the end we published a paper we can all be proud of. I wish you a lot of luck with all the interesting research I am sure there is vet to come!

Lieve studenten die ik heb mogen begeleiden tijdens hun stage, Birgit, Noor, Lyan, Nathalie en Jari. Allemaal lieten jullie een enorm enthousiasme zien voor het onderzoek naar de AHR. Bedankt voor alle experimenten die jullie voor mij uitgevoerd hebben. Mede dankzij jullie hulp hebben we mooie resultaten kunnen publiceren. Ik wens jullie veel succes met jullie verdere loopbaan, maar ik weet zeker dat dat goed gaat komen!

Dear Prof. Dr. Annemiek van Spriel, Prof. dr. Dirk Jan Hijnen and Dr. Thomas **Haarmann-Stemmann,** Thank you for reading my thesis and your kind and positive feedback, I am looking forward to my defense and answering your questions! Also a thanks all members of my committee. I am looking forward to meeting you at my defense and the interesting discussion I am sure we will have.

Dan mijn lieve collega's van de pathologie, met in het bijzonder mijn collega's van de afdeling cytologie, Ruud, Anja, Judith, Brigit en Lin. Bedankt dat jullie de uitdaging aan durfde te gaan met iemand die misschien niet de juiste vooropleiding had, maar wel het nodige enthousiasme. Jullie hebben me met open arme ontvangen en ik kan me geen gezelligere werkplek wensen. Op hopelijk nog vele jaren samen met veel gelach, pauzegesprekken die soms het randje opzoeken en de nodige friet lunches (en vooruit, ook nog wat diagnostiek).

Ik ben enorm blij dat ik straks bij mijn verdediging de nodige girlpower achter me heb staan. Lieve paranimfen, bedankt dat jullie aan mijn zijde willen staan. Kim, je bent al sinds mijn studie een goede vriendin van me. Samen in de trein naar huis zijn er de nodige puzzels doorgevlogen. In het prille begin van mijn PhD heb je nog een stage bij ons gelopen op de afdeling dermatologie en konden we samen lachen (en soms klagen over) de experimenten van de dag. We zijn al weer heel wat jaren vriendinnen en ik wil je bedanken dat je al die tijd een luisterend oor hebt geboden over niet alleen hoe het ging met mijn thesis (ook al was het antwoord daarop soms "vraag maar niet"), maar ook over alles wat er in het leven speelt. Je bent altijd even enthousiast om wat te regelen om te gaan doen en ik hoop dat we in de toekomst nog veel gezellige dagen als vriendinnen mogen doorbrengen. Isa, miin liefste zusie. Over wat wii allemaal samen beleefd en meegemaakt hebben zou ik nog wel een boek kunnen schrijven. Hoewel we gua karakter niet meer hadden kunnen verschillen, hebben we het altijd enorm goed samen kunnen vinden. Samen naar de film, kledingadvies als ik zelf weer eens niet weet wat mij zou staan, of samen sparren over wat ons bezighoud, ik kan bij jou voor alles terecht. Het is voor mij dan ook extra speciaal dat je tijdens mijn verdediging achter me wil staan. En dat niet alleen, maar dat je ook binnenkort mijn getuige zal zijn. Je mag enorm trots zijn op de persoon die je geworden bent, want wat ben je daarin gegroeid. Ik wens je alle geluk straks met je nieuwe baan en je eerste eigen woning!

Wat mag ik me gelukkig prijzen met de rijkdom aan vrienden om me heen. Daarom noem ik niet iedereen bij naam, maar jullie zijn allemaal even speciaal voor mij. Lieve vrienden van **Plofkiep, NID maatschappij en de Meiden,** jullie zorgden altijd voor de nodige ontspanning. We gaan al jaren terug en hebben in die tijd het nodige wel en wee met elkaar meegemaakt. Bedankt voor het altijd luisterende oor, de steun als het allemaal wat minder ging maar vooral ook de lol die we met elkaar hebben. Het is zeker nooit saai met elkaar en we gaan in de toekomst nog genoeg mooie dingen met elkaar meemaken!

Lieve **pap** en **mam**, wat ben ik jullie enorm dankbaar dat jullie me gevormd hebben tot de persoon die ik nu ben. Jullie hebben ons altijd ondersteund in de keuzes die we maakten en boden altijd een luisterend oor en advies als we dat nodig hadden. Maar jullie waren ook mijn stok achter de deur als ik weer eens wat te lang liet liggen. Mijn 'komt goed, rustig aan' mentaliteit zal jullie geregeld op de zenuwen gewerkt hebben, maar dat jullie nu trots op me zijn weet ik zeker. Wat hebben we samen een hoop meegemaakt, en we gaan ook zeker nog genoeg mooie dingen samen beleven! Want een warmer gezin kan ik me niet wensen.

Lieve oma, jij bent er waarschijnlijk nog enthousiaster over dat je naar mijn verdediging kan gaan dan ikzelf. En wat ben ik blij dat je erbij zal zijn! Je bent een enorm sterke vrouw die altijd in is voor gezelligheid. Bedankt dat we altijd kind bij jou aan huis kunnen zijn, gezellig kunnen kletsen en koffiedrinken. Je staat altijd klaar om iedereen te helpen, en daar mogen we ons gelukkig mee prijzen.

Lieve opa en oma Heerde en opa Thei (†), helaas kunnen jullie niet meer bij mijn verdediging aanwezig zijn. Maar dat jullie trots zouden zijn geweest weet ik zeker.

Lieve schoonfamilie, Mart, Annie, Tom, Dorien, Paul, Suzanne, Mees, Caro, Juliette, Lucas, wat ben ik bij jullie in een warm gezin terecht gekomen. Altijd tijd voor koffie, een lach en een luisterend oor. Binnenkort kan ik jullie officieel mijn schoonfamilie noemen en wat ben ik daar trots op!

Ik kreeg van mijn ouders de opdracht mee om de honden niet voor hen in het dankwoord te noemen, dus ik doe het maar daarna. Lieve Bottas en Scotty, bedankt voor jullie eeuwige (soms snurkende) aanwezigheid bij mij op de bank als het baasie weer eens moest schrijven.

Allerliefste Marc, wat mag ik me gelukkig prijzen dat ik jou mijn partner mag noemen. We waren al jaren vrienden, maar wie had gedacht dat we zo goed bij elkaar zouden passen? Ik ken niemand die op zoveel punten dezelfde mening heeft als ik en die misschien wel net zo eigenwijs is. We matchen soms misschien wel iets te goed, van het alles last minute regelen tot het overal net te laat zijn (hopelijk niet bij mijn verdediging, we doen ons best zullen we maar zeggen). Bedankt dat je er altijd voor me bent, en mijn stok achter de deur bent geweest voor het schrijven van dit boekje, ook al is daar de nodige tijd in gaan zitten. Bij jou kan ik altijd terecht als ik mijn verhaal kwijt moet of voor een (soms iets te) flauwe grap. Samen hebben we het elke dag enorm naar ons zin en ik ben er trots op dat ik jou binnenkort mijn man mag noemen. Op nog vele mooie jaren samen, maar ons kennende gaat dat helemaal goed komen!

Bedankt aan iedereen die aan mijn zijde heeft gewandeld tijdens dit avontuur. Op nog vele mooie momenten samen!

Curriculum vitae

Noa Johanna Maria van den Brink was born in Venray on the 25th of January, 1996. She grew up first in Horst and later in Hegelsom. She finished her high school at the Dendron College in Horst in 2013.

She started her bachelor's in medical biology at the Radboud University Nijmegen in 2013, during which she also attended the Honours Academy. During her bachelor she focused on understanding the biology of the human body and diseases, and the molecular mechanisms underlying various biological processes. She performed an internship at the RIMLS under supervision of Dr. Huiging Zhou studying the role of p63 and its mutations in human keratinocytes. Noa graduated her bachelor in 2016.

After her bachelor, Noa started her master in medical epigenomics at the Radboud University Nijmegen in 2016. She studied the genomic and epigenomic processes and pathways underlying health and the development and disease. She performed two internships as part of this study. Her first master internship was at the RIMLS, under supervision of Dr. Richard Bartfai, during which she focused on investigating the gametocyte stage of malaria. Her second internship was at the department of dermatology at the Radboudumc, under supervision of Dr. Jos Smits. She optimized the technologies to use CRISPR/Cas9 to modify the genome of keratinocytes. Noa graduated her master in 2018.

Noa continued with a PhD fellowship at the department of Dermatology under the supervision of Prof. Dr. Ellen van den Bogaard, Dr. Jos Smits and Dr. Patrick Zeeuwen, which resulted in this thesis. During her PhD, Noa supervised several bachelor and master students during their internship, presented her research at both national and international conferences and was awarded a travel grant to present her work at the World AHR meeting in State College, Pennsylvania (USA).

After her PhD trajectory, Noa pursued a career with a closer involvement in patient care. She now works at the pathology department of VieCuri Venlo as a cytotechnologist. Noa lives together with her partner Marc and their dog Bottas in Castenray.

PhD portfolio of Noa Johanna Maria van den Brink

Department: Experimental Dermatology

PhD period: 11/2018-10/2025

PhD supervisor: Prof. Dr. E.H.J. van den Bogaard

PhD co-supervisors: Dr. Ing. J.P.H. Smits, Dr. P.L.J.M. Zeeuwen

Training activities	Hours
Courses	
Meet the expert - CRISPR/cas9 (2018)	2.00
 RIMLS - Introduction course "In the lead of my PhD" (2019) 	15.00
Radboudumc - Scientific integrity (2021)	20.00
Illustrator workshop (2021) PON	3.00
Workshop project supervision (2022)	12.00
Team science - pilot (2022)	12.00
• RU - The Art of Finishing Up (2022)	10.00
Seminars • Dutch Dermatology Day Nijmegen (2019)	10.00
Conferences	
NVED (2019, poster presentation)	20.00
PhD retreat (2019, poster presentation)	20.00
SFB829 symposium, Cologne meets Cornell and Nijmegen, Cologne, Germany (2019)	10.00
NVED (2020, poster presentation)	20.00
PhD retreat (2020, poster presentation)	10.00
• ESDR (2021, poster presentation)	40.00
PhD retreat (2021, poster presentation)	10.00
New Frontiers Symposium (2021)	20.00
AHR symposium (2022, poster presentation)	40.00
PhD retreat (2022, oral presentation)	20.00
• ESDR (2022, poster presentation)	40.00
Other	
Organizing RRR inflammatory diseases (2019)	15.00
Weekly labmeeting (2019 - 2022)	312.00
Weekly journalclub (2019 - 2022)	208.00
• RRR inflammatory diseases (2022)	3.00
Teaching activities	
Lecturing	
Teaching BMW course project supervision (2021)	4.00
Supervision of internships / other	
Supervision master student (2019)	84.00
Supervision bachelor student (2019)	42.00
Meet the PhD (2020)	20.00
Literature review supervision (2021)	15.00
Supervision bachelor internship (2021)	42.00
Supervision master student (2021)	84.00
Supervision BMW project proposal (2022)	50.00
Supervision bachelor student (BMS) (2022)	70.00
Total	1283.00

List of publications

Related to this thesis

Rikken G, Smith KJ, **van den Brink NJM**, Smits JPH, Gowda K, Alnemri A, Kuzu GE, Murray IA, Lin JM, Smits JGA, van Vlijmen-Willems IM, Amin SG, Perdew GH, van den Bogaard EH. Lead optimization of aryl hydrocarbon receptor ligands for treatment of inflammatory skin disorders. Biochem Pharmacol. 2023 Feb;208:115400. doi: 10.1016/j.bcp.2022.115400.

Rikken G, **van den Brink NJM**, van Vlijmen-Willems IMJJ, van Erp PEJ, Pettersson L, Smits JPH, van den Bogaard EH. Carboxamide Derivatives Are Potential Therapeutic AHR Ligands for Restoring IL-4 Mediated Repression of Epidermal Differentiation Proteins. Int J Mol Sci. 2022 Feb 4;23(3):1773. doi: 10.3390/ijms23031773.

Smits JPH, **van den Brink NJM**, Meesters LD, Hamdaoui H, Niehues H, Jansen PAM, van Vlijmen-Willems IMJJ, Rodijk-Olthuis D, Evrard C, Poumay Y, van Geel M, Hendriks WJAJ, Schalkwijk J, Zeeuwen PLJM, van den Bogaard EH. Investigations into the FLG Null Phenotype: Showcasing the Methodology for CRISPR/Cas9 Editing of Human Keratinocytes. J Invest Dermatol. 2023 Aug;143(8):1520-1528.e5. doi: 10.1016/j.jid.2023.02.021.

Smits JPH*, Qu J*, Pardow F, **van den Brink NJM**, Rodijk-Olthuis D, van Vlijmen-Willems IMJJ, van Heeringen SJ, Zeeuwen PLJM, Schalkwijk J, Zhou H, van den Bogaard EH. The aryl hydrocarbon receptor regulates epidermal differentiation through transient activation of TFAP2A. 2024 Sep;144(9):2013-2028.e2. doi: 10.1016/j.jid.2024.01.030. * shared first authorship

van den Brink NJM*, Pardow F*, Meesters LD, van Vlijmen-Willems I, Rodijk-Olthuis D, Niehues H, Jansen PAM, Roelofs SH, Brewer MG, van den Bogaard EH, Smits JPH. Electrical Impedance Spectroscopy Quantifies Skin Barrier Function in Organotypic In Vitro Epidermis Models. J Invest Dermatol. 2024 Apr 19:S0022-202X(24)00293-8. doi: 10.1016/j.jid.2024.03.038. * shared first authorship

Unrelated to this thesis

Smits JPH, Ederveen THA, Rikken G, **van den Brink NJM**, van Vlijmen-Willems IMJJ, Boekhorst J, Kamsteeg M, Schalkwijk J, van Hijum SAFT, Zeeuwen PLJM, van den Bogaard EH. Targeting the Cutaneous Microbiota in Atopic Dermatitis by Coal Tar via AHR-Dependent Induction of Antimicrobial Peptides. J Invest Dermatol. 2020 Feb;140(2):415-424.e10. doi: 10.1016/j.jid.2019.06.142.

Schaap MJ, Bruins FM, van den Brink NJM, Orro K, Groenewoud HMM, de Jong EMGJ, van den Bogaard EH, Seyger MMB. Challenges in Noninvasive Skin Biomarker Measurements in Daily Practice: A Longitudinal Study on Skin Surface Protein Detection by the Transdermal Analysis Patch in Pediatric Psoriasis. Skin Pharmacol Physiol. 2022;35(6):319-327. doi: 10.1159/000527258.



